UNIVERSITY OF NAIROBI

# GEOLOGICAL SETTING AND MINERALIZATION OF IRON ORE, RARE EARTH ELEMENTS, AND ASSOCIATED METALS IN KITHIORI AREA OF MARIMANTI, THARAKA NITHI COUNTY, KENYA.

BY

WAWERU MICHAEL KARANJA
REGISTRATION NUMBER: I56/69440/2013

A Dissertation submitted for examination in partial fulfillment of the requirements for award of the Degree of Master of Science in Geology, (Mineral Exploration) of the University of Nairobi

2020

# DECLARATION

I declare that this thesis is my original work and has not been submitted elsewhere for examination, award of a degree or publication. Where other people's work or my work has been used, this has been properly acknowledged and referenced in accordance with the University of Nairobi's requirements.

Signature: _____ Date:_____

**WAWERU MICHAEL KARANJA**

**I56/69440/2013**

Department of Geology

School of Physical Sciences

The University of Nairobi.

This Dissertation is submitted for examination with our approval as Supervisors:

[Signature] [Date]

**Dr. Daniel W. Ichang'i:** _____ _____

The Chairman, Department of Geology,

The University of Nairobi,

P. O. BOX: 30197 - 00100,

Nairobi, Kenya.

# UNIVERSITY OF NAIROBI

## DECLARATION OF ORIGINALITY FORM

This form must be completed and signed for all works submitted to the University for Examination.

| | |
|---|---|
| **Name of Student:** | Michael Karanja Waweru |
| **Registration Number:** | I56/69440/2013 |
| **College:** | Biological and Physical Sciences |
| **Faculty/School/Institute:** | School of Physical Sciences |
| **Department:** | Geology |
| **Course Name:** | Master of Science in Geology. Specialization: Mineral Exploration |
| **Title of Work:** | Geological Setting and Mineralization of Iron Ore, Rare Earth Elements and Associated Metals in Kithiori Area of Marimanti, Tharaka Nithi County, Kenya. |

**DECLARATION**

1. I understand what Plagiarism is and I am aware of the University's policy in this regard.
2. I declare that this *dissertation* (thesis, project, essay, assignment, paper, report, etc.) is my original work and has not been submitted elsewhere for examination, award of a degree or publication. Where other people's work or my work has been used, this has properly been acknowledged and referenced in accordance with the University of Nairobi's requirements.
3. I have not sought or used the services of any professional agencies to produce this work.
4. I have not allowed, and shall not allow anyone to copy my work to pass it off as his/her work.
5. I understand that any false claim in respect of this work shall result in disciplinary action, in accordance with University Plagiarism Policy.

Signature: _____

Date: _____

## DEDICATION

This thesis is dedicated to my lovely family: my parents – mother and father, Jane Njeri Muiruri, and Geol. Waweru Wangomi Wakaranja respectively, my brother and sisters – Steve Muiruri Waweru, Maureen Wanjeri Waweru, and Irene Wanja Waweru. Special dedication to my lovely son Lyon-Daley Waweru Keys and my lovely fiancee Joan Muthithi Njuguna.

Finally, I wish to dedicate this thesis to my supervisor Dr. Daniel. W. Ichang'i (Chairman, Department of Geology, University of Nairobi) and Mr. John M. Waita (Head of Mineral Exploration, Ministry of Petroleum and Mining, Kenya).

## ACKNOWLEDGEMENT

The completion of this thesis and the M.Sc. Course in general would not have been possible without the support of various people who were with me through the entire journey.

First and foremost, I am grateful to God Almighty for the divine grace, enablement, and patience to complete this thesis. Without His divine intervention and provision, this project would not have been completed. After seven years of the M.Sc. course and through various challenges, it is vital to give all the Glory to Jesus Christ my (our) Lord and Saviour for seeing me through to the end.

I sincerely appreciate my supervisor Dr. Daniel W. Ichang'i the Chairman, Department of Geology, University of Nairobi. You have patiently but firmly molded me in my academic journey in the time I have been under your supervision. You constantly pushed me to keep moving towards the finish line and I will forever be grateful.

I am very grateful to Mr. John Waita from the Ministry of Petroleum and Mining, Kenya, who took time off his busy schedule to travel with me to the study area and walked with me through the entire phase of the project. Your mentorship, guidance, and words of encouragement are highly appreciated.

Many thanks to Mr. Samuel Mbiga who was very helpful when I called on him at all times. I want to appreciate all staff from the Ministry of Petroleum and Mining at Madini House, Industrial Area, Kenya. My regular trips there have paid off.

I wish to thank my parents Geologist Waweru Wangomi Wakaranja and Mrs. Jane Njeri Muiruri, my siblings, Maureen Wanjeri Waweru, Irene Wanja Waweru, and Steve Muiruri Waweru for their support and prayers.

I categorically want to acknowledge my lovely son Lyon-Daley Waweru Keys and my lovely fiancee Joan Muthithi Njuguna for enduring my absence. You have been steady and reliable pillars and I can confirm that words are fully limited to describe your respective roles in my life throughout the entire project. All this for you two. Cheers to many more successful projects ahead.

May God bless you and all the other people who were part of this journey.

## ABSTRACT

The study area is located in Marimanti area in Tharaka Nithi County, Kenya, and it is bound by the following coordinates: 00° 10’ 50” S – 00° 09’ 10” S and 37° 58’ 20” E – 37° 40’ 00” E. The area is also located within the Neo-Proterozoic Mozambique Mobile Belt. The research was conducted with the main aim of understanding the structural, mineralogical, and geological setting of the iron ore deposits, rare earth elements, and associated metals in the Kithiori area. The study was also conducted to investigate the relationship between the iron ore deposits, REE, associated metals, and the host rock units trying to ascertain the nature and modes of occurrence in relation to alteration processes and the effects of structural developments.

X-Ray Diffraction, X-Ray Fluorescence, and Petrographical analysis were used. Sample preparation for the three methods was conducted at the Ministry of Petroleum and Mining - Kenya, and the analysis of the latter was done at the University of Nairobi petrological laboratory at the Department of Geology.

The findings of this study indicate that iron ore is centrally confined and is associated with pyroxenite rocks. The study reports polymetallic ores such as pyrophanite ($Mn_{0.5}$ $Ni_{0.5}$ $O_3$ Ti.), magnesioferrite ($Fe_2$ Mg $O_4$), cuprospinel ($Cu_{0.86}$ $Fe_{2.14}$ $O_4$), ilmenite ($Fe_{1.1}$ $O_3$ $Ti_{0.9}$), magnetite ($Fe_3$ $O_4$), and Franklinite ($Al_{0.028}$ $Fe_{1.91}$ $Mg_{0.035}$ $Mn_{0.426}$ $O_4$ $Zn_{0.602}$) among others, occurring in varying quantities. It should also be noted that rare mineral species have been identified in considerable quantities. These rare minerals include osbornite ($N_4$ $Ti_4$ - 16.8%) which is mostly considered extraterrestrial with very few known natural terrestrial occurrences the world over. Other rare minerals include moissanite – 28% and brunogeierite 16.6% among others all of which are in excess of 15% of the analyzed samples. From the structural perspective, it is noted that pyroxene pegmatites play an important role in the mineralization of iron ore through various hypotheses that have been presented in the report.

Geologically, the area is dominated by gabbro, anorthosite, and dolerite containing plagioclase feldspars ranging from 70% to 93%. These rocks appear to have intruded into the host rock. The study has categorized the anorthosites into two main suites based on their physical properties, Type 1 Kithiori Anorthositic Suite, and Type 2 Kithiori Anothorsitic Suite. The study has outlined various hypothetical modes of formation for the gabbroic rocks. A unique combination of anorthite and albite in one sample has been identified, reported, and recorded in the report. The report further indicates that multifaceted magmatism processes such as

fractionation, elemental incompatibility, and filter pressing played a crucial role in the geology of the area.

Elemental studies have also been carried out. The findings show that a decrease in Ca, Si, Al, and Na is accompanied by an increase in Fe and Ti from the gabbroic rocks to the ores. It is important to note the presence of Rare Earth Elements (REEs) such as Nd, Ce, Gd, Dy, Ho, Tm, La, Yb, Sc, and Y among others. Platinum Group Elements (PGEs) such as Pt, Pd, and Rh have been reported. Various theories for the occurrence of these elements have been enumerated in this study report some of which allude to the discordant properties of the constituent elements in the respective rock units.

With great interest, the presence of hydrothermal activity indicator minerals in various samples is noted. These minerals (and their respective percentages in the samples) include Sellaite (30%), Klockmannite (10%), Permingeatite (1.2% and 1.0%), Sphene (8.3% and 1.9%), Hawleyite (4.9%) among others. These minerals together with some of the associated structures suggest a strong presence of hydrothermal action having taken place in the study area. This phenomenon has been likened to various other areas of similar geology and mineralization for ease of comparison and inference in regards to the occurrence of iron ore and other associated elements and metals in the area.

Bearing the scope of the study, several recommendations have been fronted with the aim of getting the complete narrative of the mineralogical and structural transformation, the economic viability of the iron ore, REE, and other metals.

## TABLE OF CONTENTS

## LIST OF FIGURES

## LIST OF TABLES

## LIST OF ABBREVIATIONS, ACRONYMS, AND SYMBOLS

| | | |
|---|---|---|
| BIF | ..... | Banded Iron Formation |
| DD MM SS | ..... | Degrees Minutes and Seconds |
| ENE | ..... | East North East |
| GPS | ..... | Global Positioning System |
| HREEs | ..... | Heavy Rare Earth Elements |
| KMD | ..... | Kenya Meteorological Department |
| KNBS | ..... | Kenya National Bureau of Statistics |
| LMC | ..... | Layered Mafic Complexes |
| LREEs | ..... | Light Rare Earth Elements |
| NE | ..... | North East |
| NW | ..... | North West |
| OBP | ..... | Observation Point |
| OND | ..... | October, November, December |
| PGE | ..... | Platinum Group Elements |
| PPL | ..... | Plane Polarized Light |
| PT | ..... | Pressure - Temperature |
| QAPF | ..... | Quartz, Alkali Feldspar, Plagioclase, Feldspathoid (Foid) |
| REEs | ..... | Rare Earth Elements |
| SMP | ..... | Sampling Point |
| UTM | ..... | Universal Transverse Mercator |
| VMS | ..... | Volcanogenic Massive Sulphide |
| XPL | ..... | X-Polarized Light |
| XRD | ..... | X-Ray Diffraction |
| XRF | ..... | X-Ray Fluorescence |

### ABBREVIATIONS

| | | |
|---|---|---|
| Ma. | ..... | Millions of Years |

### SYMBOLS

| | | |
|---|---|---|
| β | ..... | Beta |
| θ | ..... | Theta |

# CHAPTER 1 INTRODUCTION

This dissertation aims to unravel the geological, structural, and mineralogical setting of iron ore, rare earth elements, and metals in the Kithiori area of Marimanti, Tharaka Nithi County. The objectives of the study have been met through comprehensive field studies and analysis of the samples collected. The project report has been categorized into five chapters.

This chapter presents the statement of the problem outlining what the study seeks to address. The chapter further presents the justification as to why carrying out the study is important and in the process showing the significance of the study. The chapter also presents the main objective and the specific objectives of the study. Finally, this chapter gives a comprehensive description of the study area. This includes the location, mode of transport and communication, land use, land resources and vegetation cover, climate, physiography and drainage, population, soils, surface, and groundwater resources.

## 1.1 Statement of the Problem

The Kithiori area in Marimanti, Tharaka Nithi County is part of the greater Mozambique Mobile Belt. This belt has been studied partially by previous researchers and very little has been recorded and published about the study area. For a holistic perspective of the Belt, there is certainly a need to carry out more studies in Kithiori using the latest technologies so as to have a clear understanding of the structural, mineralogical, and geological setting.

Apart from the above, there is very clear evidence of small-scale mining activities that had been ongoing in the area but all mining activities had been cut short and all that was left were many abandoned quarries. In more than the ten (10) the mining sites encountered during the field study, there was not even a single activity that was ongoing. This was because the small-scale miners only had basic knowledge of iron ore occurrence hence very low productivity which ended in premature termination of extraction, discouraging results and very minimal financial returns. This study looks to unravel pertinent issues in regards to the geological setting and mineralization in the area, to enable better mining methods and better financial returns for the locals and/or future investors.

## 1.2 Justification and Significance of the Research

- Kenya aims to be a middle-class economy by the year 2030 according to the economic pillar of the Vision 2030. The country has known and unknown mineral and fossil fuel

resources that ought to be tapped in order to realize these ambitious targets. Mineral inference has been done in various parts of the country creating the need to, among other things, grow and develop the local mining sector in order to reduce foreign expenditure on raw materials.

- Industrial rocks, minerals, and metals are vitally important in industrialization. To realize national development strategies such as the Big 4 Agenda, Kenya needs large supplies of raw materials. The manufacturing sector and the technology industries are all dependent on the mining industry. The construction industry for instance will need adequate aggregate, metallic and nonmetallic minerals. Health, which is also one of the key pillars of the Government's Big 4 Agenda, requires lots of supplies some of which are from the mining sector.
- To actualize this, preliminary surveys, detailed exploration, and valuation must be done to prove that minerals exist and in economically viable quantities for exploitation.

## 1.3 Objectives

The study has been guided by various goals in order to understand the geological, structural, and mineralization setting in Kithiori. The study's main focus is on iron ore but the report will also give an account of the rare earth elements and other associated metals. These have been described below as the main objective and specific objectives.

### 1.3.1 Main Objective

The main objective of the study is to give an understanding of the structural, mineralogical, and geological setting of the Kithiori iron ore, rare earth elements, and associated metals.

### 1.3.2 Specific Objectives

i. To investigate the petrology and mineralogy of the host rocks in the study area with a key focus on iron ore, rare earth elements, and associated metals.
ii. To outline the minor and major structural features and infer their effects on mineralization.
iii. To investigate the geochemical composition of the rock units in the study area.

## 1.4 Geographical Setting of the Study Area

To appreciate and get acquainted with the study area, this section presents a comprehensive description of the location, mode of transport and communication in the area, land use, climate, drainage, physiography, soil, population, and water resources.

### 1.4.1 Location

The study area, Kithiori, is located in Marimanti Ward in Tharaka Constituency of Tharaka Nithi County, Figure 1.1. The County is one of the 47 Counties in Kenya and is located in the central part of the country, about 230 kilometers North-East of Nairobi. The County is bordered by Meru County [North], Kitui County [South East], Embu County [South], Kirinyaga County [South East], and Nyeri County [East].

The County is bounded by the coordinates:

- Latitude: 00° 07’ and 00° 26’ South and
- Longitude: 37° 19’ and 37° 46’ East.

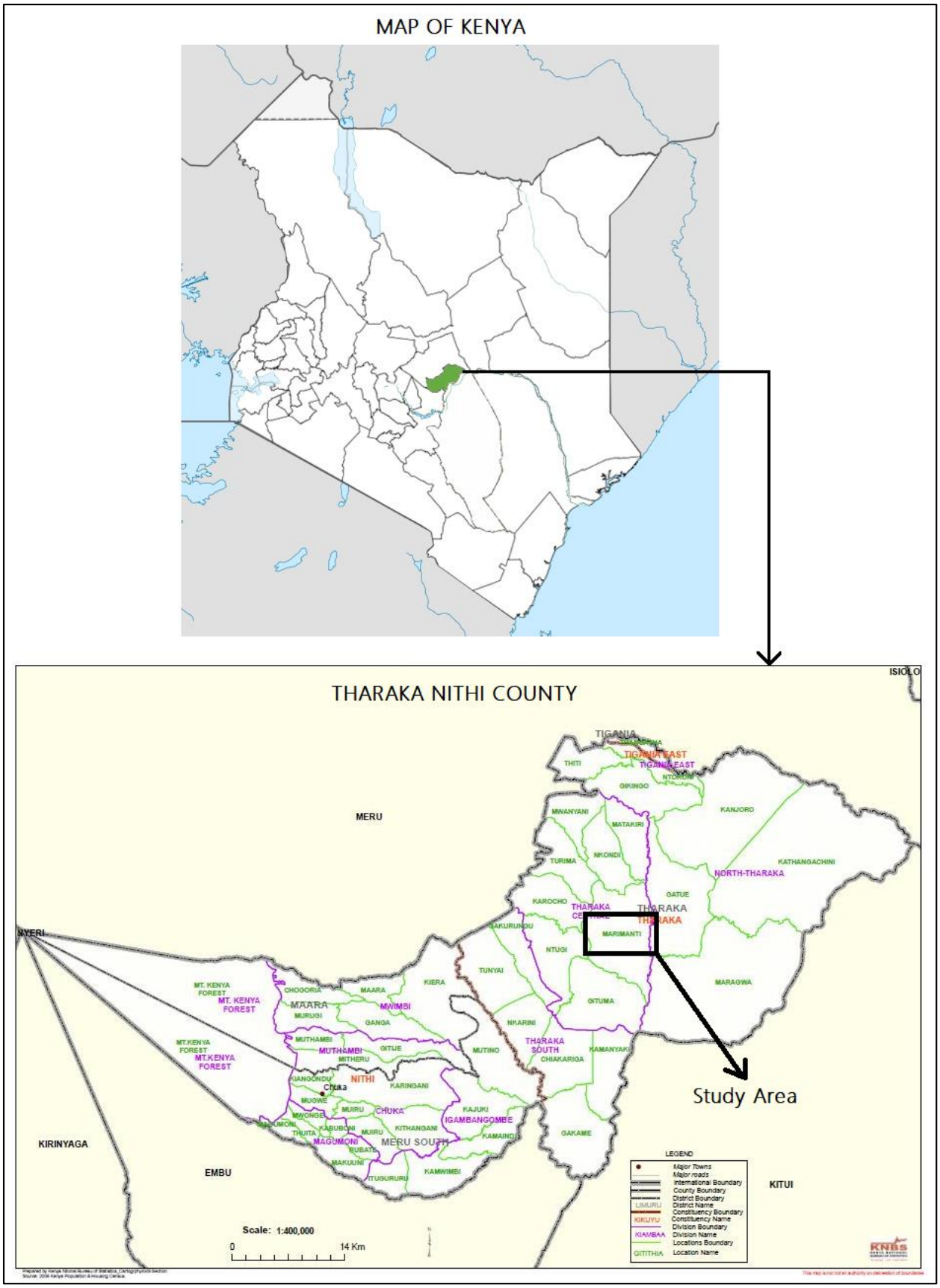


Figure 1.1 Map showing the location of the study area within Tharaka Nithi County, Kenya.

The County has a total area of 2,564.4 square kilometers. The study area of Kithiori is 7.5 kilometers South West of the Marimanti shopping center off the Marimanti – Chiakariga Road, 19.5 kilometers North North East of Chiakariga shopping center, and 30 kilometers North East of Kathwana County Headquarters.

Kithiori is located on topographical map 122/2 of the Survey of Kenya and Report Number 17 of the Geological Survey of Kenya. The study area is part of the Neo - Proterozoic Mozambique Mobile Belt which stretches from Egypt through to Mozambique in a North-South trend.

### 1.4.2 Transport and Communication

The study area can easily be accessed by road network. The tarmac along Chiakariga – Kathwana road, is 12 kilometers long. The Chiakariga – Marimanti road has only 2 kilometers of tarmac [from Chiakariga – towards Marimanti], and the rest of the drive to the study area is on an all-weather road. Sections of Marimanti shopping center have bitumen cover which does not go beyond the center. The entire drive from Marimanti town to the Kithiori area is along an all-weather road which, during the field visit, was newly graded.

The study area is covered by mobile network and internet connection, though in some sections, the connectivity is poor.

### 1.4.3 Land Use, Land Resources, and Vegetation Cover

The key land uses in the study area revolve around crop farming, animal herding, apiculture, and small scale mining. All the mining sites in the study area had been abandoned at the time of the fieldwork. The main crops grown in the area are maize, beans, green grams, among others most of which are for domestic use. Crop farming is done both on the slopes of the hills and at the foot of the hills and is rain-fed. Other activities done in the study area include small scale sand harvesting and rock crushing for ballast.

Largely, the study area is covered by dense thickets, thorny shrubs, and forested areas. Deforestation was noted and with huge concern, as the locals cut down trees and bushes for either charcoal-burning or to create room for crop farming. Regionally, forest cover in the County includes Ntugi Forest [South West of the study area] and Kijege forests [some kilometers South of the study area].

### 1.4.4 Climate

Regionally, the altitude generally decreases eastwards from the Mt. Kenya region to the midland areas of Tharaka Nithi. The high altitude areas experience reliable rainfall compared to the mid-altitude and lower altitude regions. The peak of Ntugi Hill, South West of the study area, for example, is cool due to the influence of the Ntugi Forest. The County experiences bimodal rainfall, October to December (short rains) whereas the long rains fall between April and June. The area was classified to have "Below Average Rainfall" for the period October to December 2020. However, and despite the below-average rainfall, the area was expected to receive storms and flash floods, (KMD, 2020).

The study area is hot and semi-arid. Temperatures range between 22°C to 40°C during cold and hot seasons respectively. The study area receives about 500mm of rainfall every year, with the highly raised areas receiving more rainfall.

### 1.4.5 Physiography and Drainage

The volcanic activities of the Mt. Kenya area have greatly influenced the topography of the study area and areas within its proximity. Regionally, Rivers such as Ruguti, Nithi, Thuuci, Maara, and Tungu originate from Mt. Kenya Forest and traverse the county as tributaries of Tana River. Some of the rivers are in the primary stage of river development and have "V-Shaped" valleys.

The drainage of the area is dendritic and this can be seen in Figure 1.2 below and the topographical map 122/2, with main rivers flowing towards the southeast. River Thingithu is one of the major permanent rivers that flows through the study area. Others are stream-size rivers and are mostly seasonal. The Ntugi Hill which is South West of the study area has the highest altitude. The highest elevation in the study area is about 685 meters above sea level and the lowest at 570 meters above sea level. The area is very hilly whereas some sections are low-lying areas. The hilly areas are prone to soil erosion and this has been worsened by land degradation activities such as logging activities and uncontrolled agriculture.

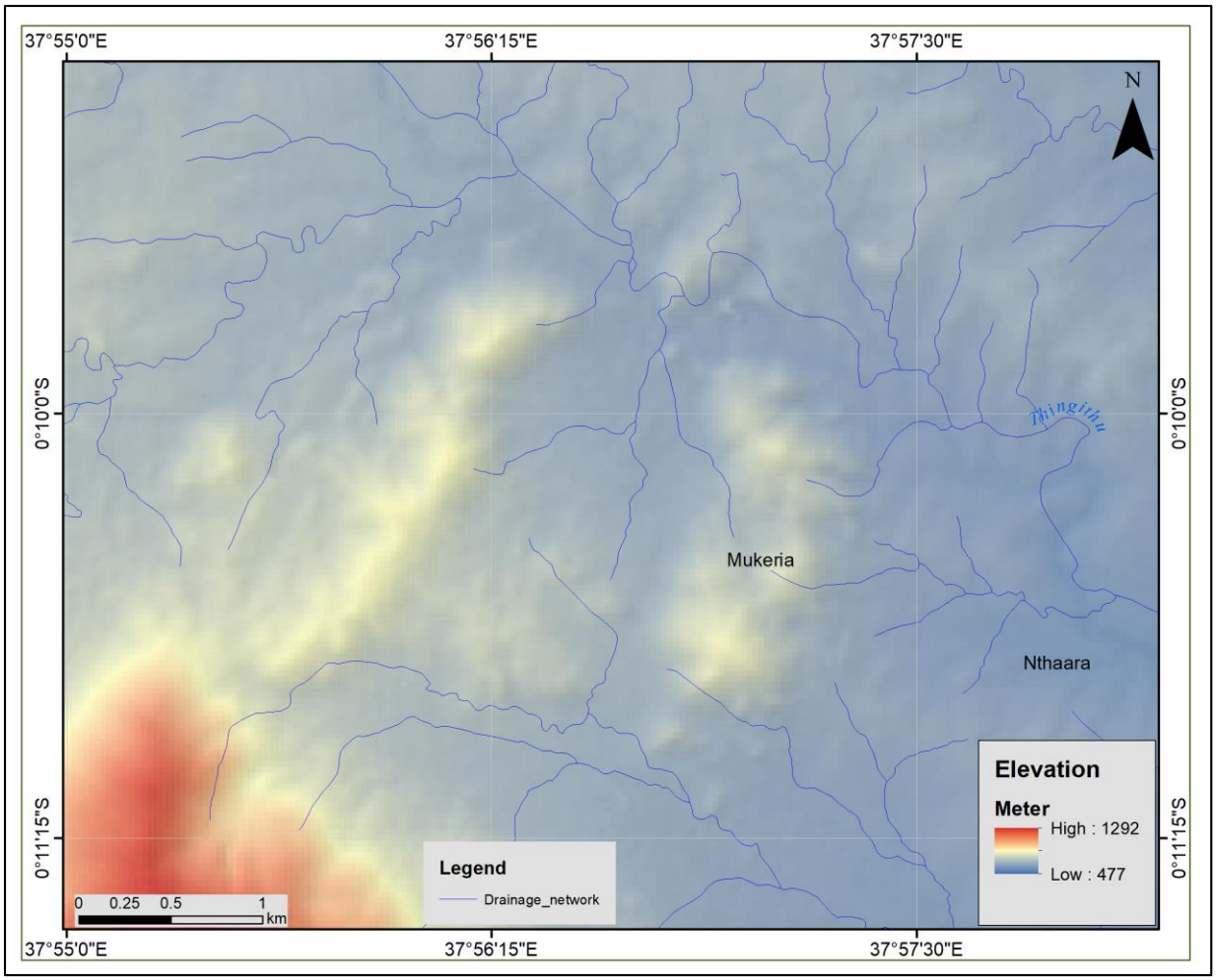


Figure 1.2: Drainage map of the study area.

### 1.4.6 Population

Tharaka Nithi County had a population of about 365,330 people in 2009 whereas in 2019 the population census was 393,177 people with an estimation of 3.6 persons per household and 153 people per square kilometer. As of 2019, the male population was 193,764 [49%] and that of the female populace was 199,406 [51%], (Kenya National Bureau of Statistics [KNBS], 2019).

The population density in the area is determined by the general climatic condition, soil fertility, setting, etc. Based on county urbanization, the rural-urban county estimates for Tharaka Nithi were, 93.4% of the locals in the county live in rural areas and 6.6% in the urban areas. The study area is in a rural setting, (KNBS, 2019).

### 1.4.7 Soils

The area of study is moderately covered by exposed rock units. The soil cover is thin in some sections of the area compared to others. Some soils are brownish – reddish and some areas are covered by sandy soils.

Soils in some sections are covered by pebbles and boulders of iron ore all over the surface. Due to various factors, the loose topsoil is washed away into rivers and streams during erosion, which is of high prevalence. Erosion is mostly caused by overexploitation of land resources through human activities such as agriculture. There are insufficient erosion prevention measures that have been put in place by locals who are practicing farming on hill slopes. This leaves the land more exposed to erosion. Gullies and sedimentation into rivers are some of the effects of erosion noted in the study area.

### 1.4.8 Surface Water and Groundwater Resources

The County has a considerable number of surface water resources such as rivers, streams, and water pans. These rivers create great potential for farming and power generation and are tributaries of the River Tana. Much of the rainwater largely goes to waste as most of it is not harvested. The County also has considerable groundwater resources in form of boreholes and springs. Despite the number of water resources, the county continues to be subject to periodic drought and food insecurity. Little use is made of the water resources for domestic use and irrigation.

A large population does not have access to water in their immediate neighborhood, forcing some of them to walk for several minutes or hours to fetch water from the rivers, drilled boreholes, or water pans. Several areas just outside the study area have boreholes that were drilled by the county government to benefit the local communities.

## 1.5 Dissertation Layout

This dissertation is subdivided into five main chapters as follows:

**Chapter One:** This chapter outlines the statement of the problem, justification, and significance of the research. The main objective and specific objectives are also described in this chapter. It also gives a comprehensive description of the study area and this includes; location, mode of transport and communication, land use, resources and vegetation cover, climate, physiography and drainage, population, soils, surface, and groundwater resources.

**Chapter Two:** The chapter presents the literature review in relation to the topic and gives an account of the global overview of iron and ferroalloy metal production narrowing down to the Kenya perspective. The chapter also describes in detail the theoretical perspective of two of the main rock units encountered in the study area.

**Chapter Three:** This chapter presents the materials and methods used to achieve the aforementioned objectives. Challenges faced during the research have also been recorded.

**Chapter Four:** This chapter presents the field observations and a comprehensive outline of the geochemistry, mineralogy, and petrology based on microscopic, XRD, and XRF analysis. The Chapter also presents the geological map of the study area, structural geology of the area highlighting the major and minor structures identified. The chapter also attempts to highlight the possible nature of occurrence for these structures. Finally, the chapter presents the discussion of the results.

**Chapter Five:** This chapter presents the conclusions and gives several recommendations.

Chapters one to five have been structured in a way that they fully address the main aim and the specific objectives of the study.

# CHAPTER 2 LITERATURE REVIEW

This chapter presents a review of the available information regarding the title both from a general perspective and specific to the area of study. The chapter has been segmented as follows: a global overview of iron and ferro-alloy metals, iron ore occurrence in Kenya, types of iron ore-bearing minerals, modes of formation of iron ore, and background of common rock units in the study area.

## 2.1 Global Overview of Iron and Ferro Alloy Metals

Minerals are the lifeblood of any economy. According to (Reichl *et. al.*, 2018), world mining production was 16.9 Billion metric tons in 2016, 11.3 Billion metric tons in 2000, and 9.7 Billion metric tons in 1985. Of the 16.9 billion metric tons in 2016, 9.5% (1.6 Billion metric tons) comprised of Iron, Ferro-Alloy Metals.

Of the 1.6 billion metric tons, 1.5 Billion metric tons represent iron production in 2016 and this represents a growth of 15.70% from 2012. The rest represents Cr, Co, Mn, Mo, Ni, Nb, Ta, Ti, V, and W, Table 2.1 below. The growth trajection is gradual and looks to increase even further with the continued exploration and production globally.

Table 2.1: World Production of Iron and Ferro-Alloy Metals in 2016 in Metric Tonnes

| | | | |
|---|---|---|---|
| Iron (Fe) | 1,575,123,716 | Cobalt (Co) | 126,234 |
| Manganese (Mn) | 15,414,509 | Niobium (Nb) | 91,827 |
| Chromium (Cr) | 13,092,060 | Tungsten (W) | 85,789 |
| Titanium (Ti) | 6,877,550 | Vanadium (V) | 85,729 |
| Nickel (Ni) | 1,953,503 | Tantalum (Ta) | 1,694 |
| Molybdenum (Mo) | 279,309 | | |

In 2016, developed countries produced 605 million metric tons, developing countries produced 849 million metric tonnes, least developed countries produced 13 million metric tonnes and transition countries produced 107 million metric tonnes, (Reichl *et. al.*, 2018). Kenya is listed in the developing countries category. The importance of iron ore is emphasized by the fact that millions of tons of steel are consumed annually around the world, with China leading at 45% in 2017 according to a report published by Deloitte on, an overview of the steel and iron ore market, 2018, (Deloitte CIS Research Centre, 2019).

World iron resources are estimated to be greater than 800 billion tons of crude ore containing more than 230 billion tons of iron, (U.S. Geological Survey, 2020). Iron ore is arguably the most important resource that is shaping the global economy, second to oil and gas.

## 2.2 Iron Ore Occurrence in Kenya

Iron ore dominates the study area in various proportions and sizes. Before comprehensively analyzing the occurrences in the study area, this section gives a brief overview of the occurrences elsewhere in the country based on previous studies.

Iron ore in Kenya occurs in the forms of oxides, sulfides, or carbonates. Marimanti in Tharaka Nithi County, Ikutha in Kitui County, Bukura in Kakamega County, Uyoma in Siaya County, Samia in Busia County, Wanjala mines in Taita – Taveta County, Ishiara in Mbeere, Baragoi in Samburu County are known to have the iron ore deposits. The Nyanzian Group of rocks are frequently associated with the rocks of the goldfield formation, (Pulfrey and Walsh, 1969).

Deposits of iron ore exist in south Machakos and they occur in hematite – magnetite schists and magnetite segregations. Ilmenite also exists near Malindi and clay ironstones at the Coast, VMS deposits (pyrite and pyrrhotite), and banded ironstones in Nyanza, (Pulfrey and Walsh, 1969). They continue to state that in 1965, iron ore containing 5 – 15 % $TiO_2$ (based on grab sample) was discovered in Marimanti.

(Ichang'i, 1990) notes that some rocks of the Nyanzian Group in Western Kenya occur as Banded Iron Formations (BIFs) which occur within felsic and mafic rocks. In his report, he also notes that parts of the larger Kisii District have occurrences of BIF, as had been mapped by (Huddleston, 1951) and (Shackleton, 1946). The Greenstone Belt and sections of Migori contain BIFs. Macalda Mines also contain BIFs which could be auriferous (Ichang'i, 1990).

In tertiary rocks of the Nyanzian and Kavirondian Groups, (Huddleston, 1959) suggests the occurrence of iron ores as accessory minerals. This is as reported from the Kakamega Diorites, Dolerites, Andesitic Tuffs, Basalts, Maragoli Granites, which have traces of iron ores as accessory minerals. (Pulfrey, 1936) reports of 41%, 48%, and 62% of iron within the Samia ironstone. He suggested that the ore could be of economic importance having mapped the resource laterally, further suggesting that the resource could be impersistent with depth. (Ichang'i, 1983), studied the Mbesa and Bukura area in western Kenya and the study reported

that $FeS_2$ (pyrite) was hydrothermally influenced with waters of metamorphic and magmatic origin such as the Mumias Granite which is adjacent.

(Matheson, 1966), notes numerous stains of iron minerals on the cavities of quartzite outcrops. Analysis of the samples indicates a presence of about 2% to 7% of $Fe_2O_3$. He recommended further studies to ascertain the vertical extent of the possible iron mineralization.

(Abuga *et al.*, 2013) conducted a geological and geophysical survey in the Kimachia area of Tigania in Meru County to ascertain the source of iron ore in the area. Their study was able to locate iron ore (magnetite) in the hilly areas of the study area. Two forms were noted, some of fist-size boulders whereas others were of fine-grain nature and smaller in size. Based on the geophysical analysis, the study suggests a vertical extension of the deposit. (Bett *et al.*, 2019) conducted research on the quality of iron ore in Tharaka Nithi and Samia. In their findings, they report that iron composition in the Marimanti area is between 41% and 57%.

## 2.3 Types of Iron Bearing Minerals

Iron ore is a rock mass that, when subjected to various processes and procedures produces the element iron which can be extracted economically. Iron is denoted as (Fe) in the periodic table of elements (atomic number 26 and atomic mass of 55.845) and it is one of the common widely distributed elements on the earth's crust, making it one of the most abundant elements on the earth's crust.

Iron exists in two common forms, ferric iron denoted as ($Fe^{3+}$) or iron (III) oxide, and ferrous iron denoted as ($Fe^{2+}$) or iron (II) oxide. Ferrous combines readily with silicates to form different kinds of minerals. The ferric type is the most stable form of (Fe) in air and is selective to particular silicates and the excess is stable as hematite. There are various species of iron oxide minerals which comprise mainly of oxygen-iron combinations. To illustrate this, Table 2.2 lists some of the common oxides of iron known to occur. Likewise, iron is known to occur in sulfide form and these complexes have been presented in Table 2.3 below.

Table 2.2: Types of Iron Ores: Oxides.

| **Name** | **Formula** | **Name** | **Formula** |
|---|---|---|---|
| Magnetite | $Fe_3O_4$ | Ilmenite | $FeTiO_3$ |
| Hematite | $Fe_2O_3$ | Wustite | FeO |
| Limonite | $Fe_2O_3.3H_2O$ | Maghemite | ($Fe_2O_3$, $\gamma$-$Fe_2O_3$) |
| Akaganéite | Fe3+O(OH,Cl) | Feroxyhyte | $(Fe3+)_2O_3.0.5H_2O$ |
| Fougèrite | Fe2+4Fe3+2(OH)12[CO3]·$3H_2O$ | Lepidocrocite | FeO(OH) |
| Bernalite | $Fe(OH)_3$ | Schwertmannite | $Fe_8O_8(OH)_6(SO_4).nH_2O$ |
| Goethite | (FeO(OH) | Ferrihydrite | $(Fe3+)_2O_3.0.5H_2O$ |

Table 2.3 Types of Iron Ores: Sulphides

| **Name** | **Formula** | **Name** | **Formula** |
|---|---|---|---|
| Pyrrhotite | FeS | Troilite | FeS |
| Marcasite | $FeS_2$ | Pyrite | $FeS_2$ |
| Greigite | $Fe_3S_4$ | Mackinawite | (Fe, Ni)$S_{0.9}$ |

## 2.4 Modes of Formation of Iron Ore

To make any iron ore a viable ore, the iron content has to be about 30% on average. Most iron ore deposits are known to have an occurrence in:

i. Banded Iron Formations.
ii. Magmatic environments. Kiruna and Bushveld in Sweden and South Africa respectively are common examples.
iii. Hydrothermal environments. Buhwa in Zimbabwe is one of the examples.
iv. Metasomatic skarns, residual deposits, and oolitic ironstones such as Minette in Europe and Clinton in the USA.

## 2.5 Background of Common Rock Units in the Study Area

### 2.5.1 Gabbroic Rocks

The area is noted to be heavily dominated by gabbro as had been reported by (Schoeman, 1951) and therefore a brief description is given below to contextualize. Gabbro is an intrusive igneous rock that originates from magmas that cool slowly. It is to be noted that the term gabbro has been used in a broad sense and the specific gabbroic rocks have been distinguished based on

their mineral composition and/or texture. The study area is dominated by gabbroic rocks which are crosscut by mafic dykes of doleritic nature.

The gabbro samples collected during the fieldwork exercise appear in various forms and contain various proportions of mafic, intermediate, and felsic minerals. Some of the outcrops appear coarse-grained whereas some are medium-grained with allotriomorphic texture indicating simultaneous growth of minerals present in the rock. Generally, the rocks seem not to contain considerable quantities of quartz signifying the cooling environment of the magmas from which the rocks originated.

In the larger sense, and according to the QAPF diagram Figure 2.1, gabbroic rocks contain considerable quantities of feldspars in the plagioclase series, i.e. from pure albite – $NaAlSi_3O_8$ (Ab) to pure Anorthite $CaAl_2Si_2O_8$ (An). Other mid-range plagioclase feldspars that are found in gabbro rocks include oligoclase, andesine, labradorite, and bytownite. The plagioclase series minerals have been noted in the gabbro units from the study area as indicated by the XRD results. Chemically, gabbros also contain pyroxene minerals; either clinopyroxene (which are dominant) or orthopyroxene minerals which are rare in the area.

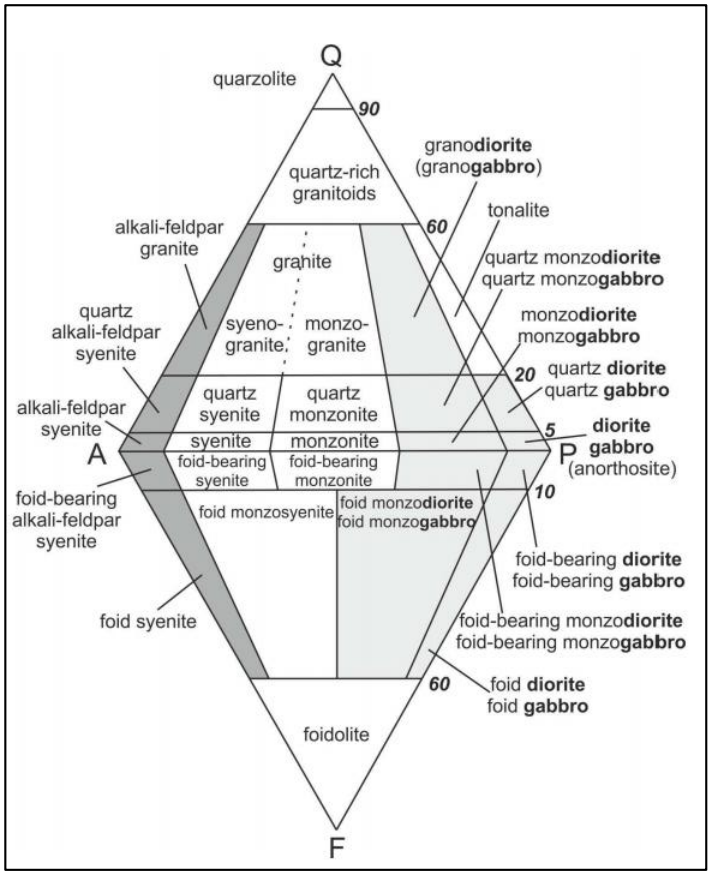


Figure 2.1: QAPF Diagram based on Streckeisen, 1976.

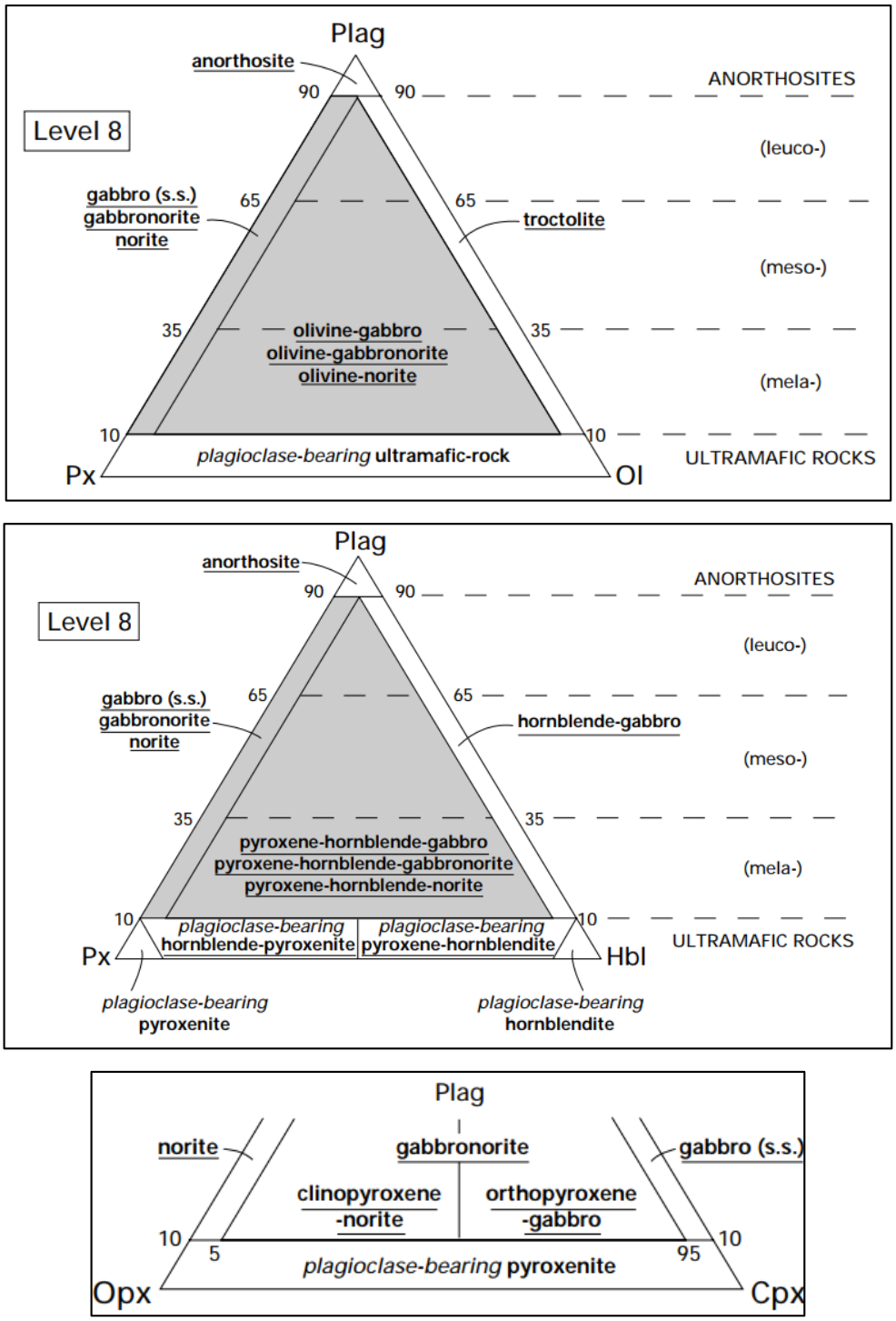


Figure 2.2: Triangular diagrams for the classification and nomenclature of gabbroic rocks based on the proportions of plagioclase (Plag), pyroxene (Px), olivine, (Ol), clinopyroxene (Cpx), and hornblende (Hbl), (after Streckeisen, 1976).

### 2.5.2 Anorthositic Rocks

(Streckeisen, 1976) recommended that anorthosites be defined by having more than 90% plagioclase. Six types of anorthosites have been discussed by (Ashwal, 2010). A brief

description of these types has been given below, so as to relate to what may have taken place in the study area.

**a) Archean Anorthosites**

The Archean Anorthosites are rare and their occurrences are minimal. The Archean craton of Western Greenland and Superior Province in Canada are examples. These intrusions are composed mainly of cumulate layers of anorthosite, leucogabbro, gabbro, and ultramafic rocks, and mostly occur as intrusions (Polat *et al.*, 2018). These two examples are located close to major tectonic boundaries separating different plates, in some instances, along subduction zones. The crystals are up to about 30 centimeters in diameter, displaying megacrystic textures. The Greenland Anorthosites are known to contain corundum and traces of iron in the Fiskenaesset complex, (Yakymchuk and Szilas, 2018). Other mineral occurrences in the Fiskenaesset anorthosite complexes include chromite, Platinum Group Elements, V-Ti bearing magnetite and ilmenite, (Stendal and Secher, 2011), (Rollinson *et al.*, 2010), and (Sørensen *et al.*, 2016). All these aforementioned minerals occur in Kithiori in varying concentrations. The Superior Province in Canada is the largest Archean Craton in the world, (Percival *et al.*, 2012). Several researchers have written about the economic geology in the Superior Province in Canada, (Ashwal *et al.*, 1983), (Ashwal, 1993), (Hartlaub *et al.*, 2005), and (Zhou *et al.*, 2016). Iron ore features prominently in these studies and some cases, similar situations to the Marimanti area.

**b) Proterozoic Anorthosites**

The Proterozoic types are the most abundant types of anorthositic rocks according to various researchers. The sizes of these types of anorthosites vary, to as big a size as a batholith, (Ashwal, 2010). Plagioclase, pyroxene, olivine, iron and titanium oxides, and apatite are known to exist in these types of rocks. Compared to the Archean type, Proterozoic Anorthosites show their distinct texture and chemical composition.

The Proterozoic Anorthositic massif occurs in the Grenville Province in Canada. In the Adirondack Mountains, for example, they are associated with leuconorite, leucogabbro, gabbroic anorthosite, and anorthositic gabbro. The Fe-Ti oxide-bearing rocks occur towards the border. (Ashwal, 1993) described the possible hypothesis for the massif type anorthosites to form from magma.

Another example of Proterozoic Anorthosite is the Kunene Intrusive Complex from the South West of Angola through to the North West of Namibia, (Gleißner, 2010). They are one of the largest Proterozoic anorthosite massif-type exposures in the world and they comprise of pyroxene as well as olivine-bearing lithologies. These rocks are known to contain Fe-Ti ore, Ilmenite, Vanadium, Phosphorus, Apatite, Olivine, Graphite, REE, and hercynite, (Villanova-de-Benavent *et al.*, 2017). They report that the Kunene Intrusive Complex consistent with the mineralogies of Fe – Ti – V could be Labradorite-type anorthosite.

**c) Layered Mafic Complexes**

The ages of these rocks range between 23Ma to 4,000Ma, (Ashwal, 2010) and have smaller grain sizes compared to the Proterozoic and Archean Anorthosites. The Anorthosites appear in layered units, together with mafics, in most cases horizontally placed. Stillwater Complex, Montana USA, is an example of a Layered Mafic Complex but a small section of it shows the layering, where a majority of the complex is uniform, except for some rocks which show igneous lineation for feldspar (plagioclase) and pyroxene (augite).

Stillwater is known to have PGE, Cr and V. Stillwater chromites represent about 80% of the identified chromium reserves in the United States, (McCallum, 2012). Plagioclase composition in the Layered Mafic Complexes can be varied. (Streckeisen, 1976) noted that the Anorthosites of the Bushveld Complex and Stillwater contain labradorite and bytownite. (Maier *et al.*, 2016) noted that layering in the Bushveld Complex formed through a combination of magmatic and structural processes. They note that Anorthosites of the Merensky Reef contain pockets of pyroxenites which contain iron. The Bushveld Complex is known to contain several other deposits of economic value.

**d) Anorthosites of Oceanic Settings**

(Ashwal, 2010) records that Anorthosites occurring in oceanic settings and those found in LMC are almost similar. The major difference is the manner of occurrence. (Ashwal, 1993) records the presence of trace amounts of Fe – Ti in these kinds of set up. Mid Oceanic Ridges are perfect examples of where these types of Anorthosites can be found.

(Stroup, 1981) describes rock occurrences, structures, and tectonics in the Cayman Trough at the floor of the Caribbean Sea and notes the occurrence of clinopyroxenes, orthopyroxenes, and iron minerals in the rocks.

### e) Anorthosite Inclusions in Other Rock Types

An example of this type of anorthosite is within diabase rocks in the Beaver Bay Complex in Minnesota, USA. The anorthositic inclusions occur as xenoliths. In some scenarios, the anorthosites are minor accumulates from the parent magma, (Ashwal, 2010). (Miller and Chandler, 1997) record iron enrichment in anorthositic inclusions.

Based on the analysis of the samples by use of XRD, some samples are almost entirely composed of plagioclase feldspars and highly deficient in other oxide content. These include sample 10 and sample 11 from SMP-10 and SMP-11 respectively. From the above six types, it is easier to relate the type of occurrences for the anorthosite rocks in the study area.

# CHAPTER 3 MATERIALS AND METHODS

Chapter three outlines the materials and the methods used to address the main objective and the specific objectives of the study. More details have been given on how the field study was conducted, the procedures and methods used for analysis.

## 3.1 Description of the Materials and Methods Used

To fulfill the study objectives mentioned above, several methods and materials were used as indicated below.

### 3.1.1 Desktop Studies

Desktop studies played a crucial role during the research. Many publications such as reports, maps, books, theses/dissertations, statistics, and journals were reviewed, for related settings locally and internationally. These have been referenced accordingly. Another purpose for conducting desktop studies was to strategize on the best approach to fulfill the objectives of the study.

### 3.1.2 Fieldwork Studies

In December 2018, a detailed field study was carried out in the Kithiori area measuring about 18 square kilometers. The following activities were done during this period to address the study objectives.

The study area was traversed on foot, Figure 3.1, noting various physical and structural features. Rock samples were collected throughout the traverse sites within the area. The samples were described by identifying macroscopic features/structures and field names allocated to each sample and the related rock units. All coordinates of the observation points were recorded using UTM and DD MM SS units. Every waypoint was given a unique number with the prefix; “SMP” meaning sampling point or “OBP” meaning observation point. Elevation readings were also recorded to compare the different levels above sea level.

For structural geology, various features were noted and recorded. These include rock and associated orientation of the fabric. Dykes, lineations, folds, and other structures, [micro and macro structures] were recorded.

The following tools/equipment were carried for use during the fieldwork exercise: Tape measure, masking tape, laptop, compass, phone to take pictures, Garmin Geographical Positioning System, sample bags, a geological hammer, dilute HCL, notebook, and pencil.

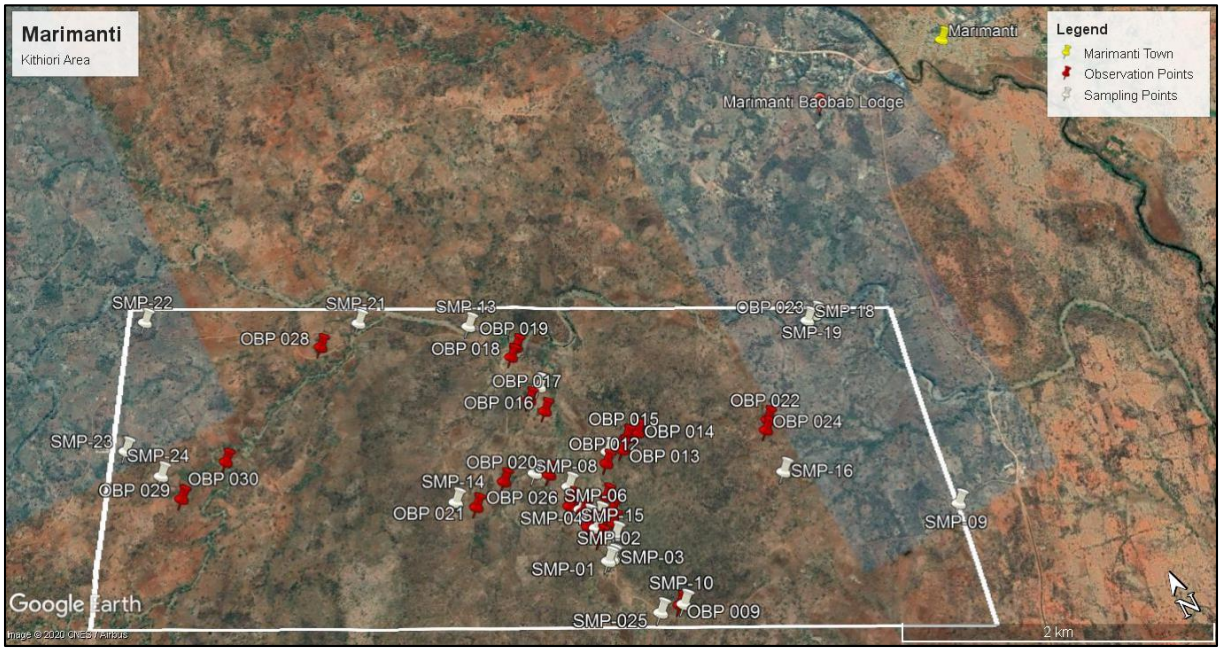


Figure 3.1: Map showing the sampling points and the observation points in the study area.

A total of 54 sites were mapped either as observation points or sampling points, Figure 3.1, and in these 54 sites, a total of 25 samples were collected in duplicate including samples of purple prismatic amethyst crystals from SMP-13. Samples were not collected at every site either because of the degree of weathering, very poor exposure, inaccessibility, or hostility from the local community making it a challenge to adhere strictly to the grid sampling that had been planned prior. Where samples were not collected, these have been tagged under the prefix [OBP – Observation Point]. A majority of samples collected were fresh whereas some were moderately weathered. Where samples were collected, this has been indicated under the prefix [SMP – Sampling Point]. These samples were labeled and packed in the field storage bags. Sections of the study area had kunkar limestone which fizzled with the acid that was poured on them. The outcrops barely fizzled showing little or lack of carbonates. Rock sections were prepared from some of the samples collected. A detailed analysis of the rock sections has been made in subsequent chapters.

### 3.1.3 Generation of a Geological Map

Coordinates were recorded using a Garmin GPS. A total of 54 sites were mapped, Figure 3.1, and their respective coordinates recorded. Whilst traversing through the study area, geological

features, and rock units were noted. The coordinates were used to develop a geological map. This was done in two ways, first, a freehand map developed as the field study was ongoing, and second a digitized map developed using ArcGIS 10.3 software, as an adaptation of the freehand geological map.

### 3.1.4 Rock Section Making Procedure

Rock sections were developed from fresh rock samples as follows:

i. The sample was cut using a blade saw machine to the required size according to the hardness of the sample.
ii. The sample was then ground using carborundum, starting with a coarser grinding plate (Grade 80). This was used for removing the sole lines from the samples. Other grades used were Grade 100, Grade 120, Grade 150, Grade 2F, Grade 600, and 1000. With the increasing grade, there was a gradual increase towards fine texture.
iii. Afterwards, the specimen was mounted on a glass slide. Canada balsam was smeared on the glass slide then left for 5 minutes. Later on, the specimen was mounted and left for 2 hours. The grinding procedure was repeated using the scale on the side of the glass that the specimen was mounted. The final product was 30 microns to allow light to pass through for analysis by a microscope.
iv. A coverslip was put on to prevent contamination of the sample. Canada balsam was prepared then the coverslip was attached to the sample and all bubbles were removed. The specimen was later washed with methylated spirit to remove the excess reagents used. The section was then washed with ordinary water and labeled.
v. Rock section analysis was done at the University of Nairobi, Department of Geology.

The rock sections were prepared at the Madini House, Ministry of Petroleum and Mining, Kenya. Note: *the thickness of the slides has influenced the anomalous coloration of some of the rock sections.*

### 3.1.5 Geochemical Analysis

#### a) X-Ray Diffraction (XRD) Analysis

The X-Ray Diffraction is used for analyzing solid and powdered material through a diffracted pattern developed when an electron oscillates in an alternating electromagnetic field of the same frequency as in the field. The diffracted beam is

composed of scattered rays which reinforce one another; both constructive and destructive interferences play a greater role in analyzing elemental proportions in a sample.

Samples collected from different locations within the Kithiori area were pulverized and crushed into porter form and put in the XRD for mineralogical identification and analysis. The quartering system was used to select the right proportion and the best representation.

The procedure used to prepare the samples is as follows:

i. The samples were dried and later pulverized into powder.
ii. The samples were put into a sample cap.
iii. The samples were loaded into the sample holder and mounted.
iv. The samples were each loaded into the machine and analyzed.
v. Once the diffraction pattern was obtained, the diffraction pattern was analyzed using a software known as *Diffract Eva*, to obtain qualitative and quantitative mineral phases present and other lattice parameters.

A Brucker Phaser D2 from the Ministry of Petroleum and Mining, Madini House, Kenya was used to conduct the XRD analysis for representative samples. Apart from the quartering system used for quality purposes and reliability of the data, control samples were prepared for repeat experiments to confirm that similar results, to a high confidence level, would be generated by the machine. The equipment was calibrated to internationally accepted standards as per the manufacturer's certificate of calibration. *It is important to note that the XRD machine was unable to identify some of the minerals it analyzed and quantified. In the report, these have been indicated as "—unidentified". However, efforts were made to identify some of the unidentified species.*

**b) X-Ray Fluorescence (XRF)**

Like the XRD analysis, XRF analysis was conducted at the Ministry of Petroleum and Mining, Madini House, Nairobi, Kenya, for representative samples. XRF Bruker machine was used for this analysis to ascertain oxide and elemental concentration levels which were given in percentage units. The equipment was calibrated to internationally accepted standards as per the Bruker certificate of calibration.

## 3.2 Limitations and Key Challenges

Though the objectives of the study were realized, many challenges and limitations were experienced during the exercise, however, efforts were done to address or minimize their impacts on the results. The following are some of the challenges experienced:

i. Financial constraints: A lot of money was required for various purposes. The biggest demands were on financing the field study and sample analysis. Many efforts were made and this challenge was addressed. For example, not all samples were analyzed but based on the macroscopic similarities, a representative sample was analyzed.

ii. Analysis: Based on the limitations of the XRD equipment, some of the minerals were not identified even having been quantified by the same equipment. Efforts were made to find the internationally accepted names of the minerals but to no success for some. In the XRD tables, these minerals have been noted as *unidentified.*

iii. Field Study:

   a. Accessibility: Some areas were completely inaccessible due to poor infrastructural network. Some of these areas were traversed on foot, and this helped to some extent.

   b. Community hostility: the community is well aware of the value of the deposits in the area. In as much as the researcher managed to inform the local administration of the planned field study and also got a local guide, there was resistance in some areas. This resulted in the area being partially covered especially in private property where the locals own extensive parcels of land. Coupled with their hostility, traversing sections of the study area were hampered.

# CHAPTER 4 RESULTS AND DISCUSSION

This chapter comprehensively presents the results of the study for each of the following: mineralogy and petrology, XRD, XRF, and structural geology accompanied by the respective discussion points.

## 4.1 Mineralogy and Petrology

This section describes the mineralogy and petrology of the rock units in the study area, as analyzed through microscopy and X-Ray Diffraction (XRD). The samples were prepared at the Ministry of Mining and Petroleum's Madini Centre in Nairobi and they were analyzed at the University of Nairobi. Rock sections were studied under plane-polarized and crossed polarized light; microphotographs of mineralogical textures (rock sections). X-Ray Diffractometer was used for the mineralogical identification and analysis of samples.

The following rocks were identified and studied: Iron Ore, Generic Gabbro, Anorthosite, Dolerite, Iron Ore, Quartzofeldspathic Gneisses & Pegmatites, quartzites, among others.

### 4.1.1 Gabbro

Based on the analysis of the samples by use of XRD, some samples are dominated by plagioclase feldspars between 79.2% to 87.8%. These include: Samples 01, 15, 16, 21 and 22 from respective sampling points SMP-01, SMP-15, SMP-16, SMP-21 and SMP-22. The XRD analysis shows that the major and minor minerals vary from sample to sample. From a macroscopic observation, the rock unit mapped at observation point OBP 003 is wholly similar to the sample collected at sampling point SMP-01 and has therefore been categorized as a gabbro, backed by the laboratory analysis as shown below.

i. **Results of Sample No. 01**

As per the field observations, the insitu outcrop is massive. It has a phaneritic texture and has gray-black colored minerals, (varied shades of gray in some cases) in mm-size due to the slow cooling of the parental magma occurring as an intrusive. The rock weathers to red-brown soils which were stained with black pigments. Figure 4.1 below shows a cut section of sample 01 which was collected in fresh form from observation point SMP-01. The fracture in Figure 4.1

indicates external force (stress/strain) within the area. The insitu outcrop showed strained zones trending in the NS direction.

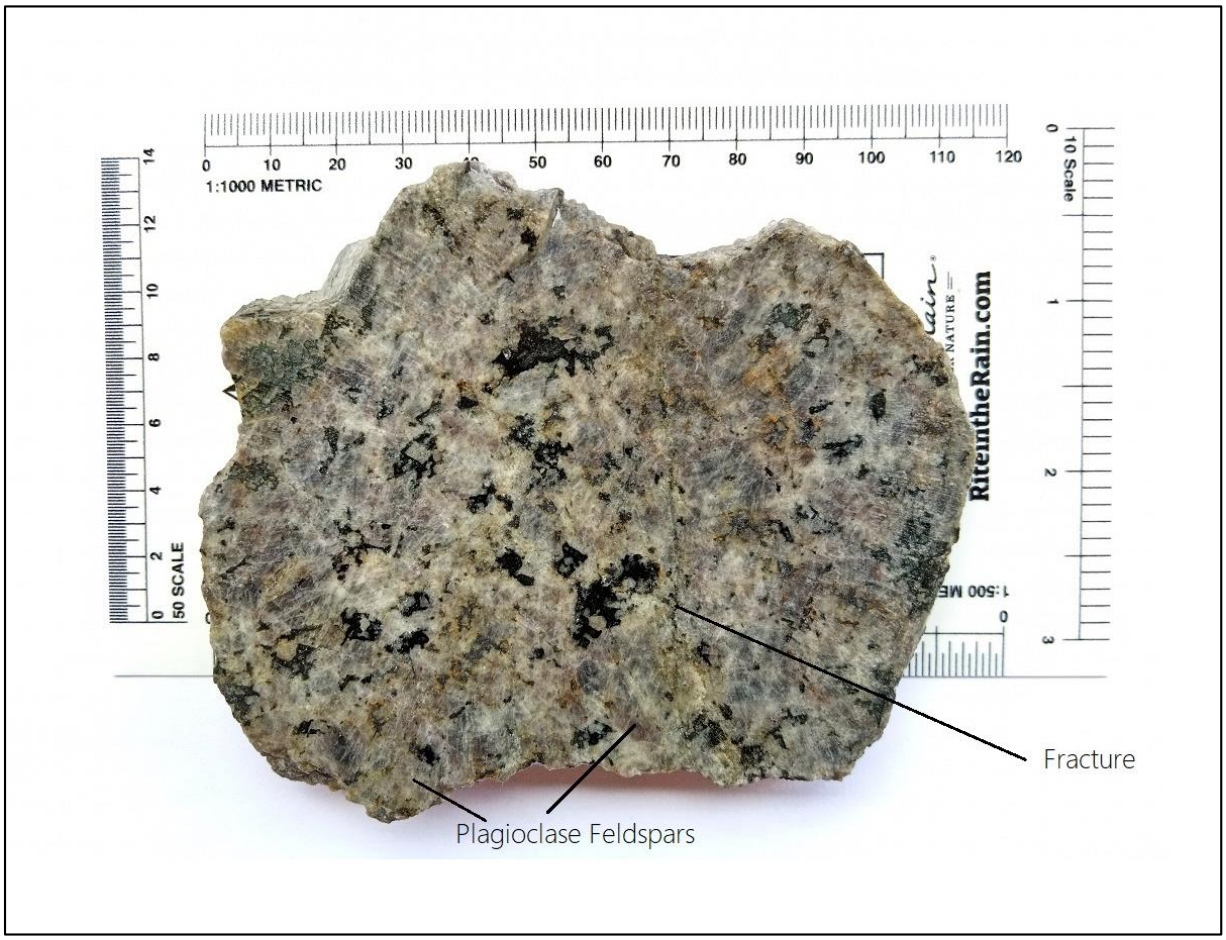


Figure 4.1: Sample 01 of gabbro collected at SMP-01, coordinate: 0°10'38.30"S | 37°56'39.40"E.

**Mineralogy:** SMP-01 was subjected to XRD analysis and this shows that the rock is heavily dominated by the plagioclase feldspars; Oligoclase and Labradorite which make up 87.80% of the unit as shown in Table 4.1 below. The presence of these two feldspars, as with other feldspar series minerals, is an indication of different chemical and physical properties. Other minerals such as Oxyfluorides, Calcium Uranium Fluoride, Barium Vanadium Trisulfide, and other trace minerals constitute the remaining 12.20%. By virtue of the dominance by these plagioclase feldspar minerals, the rock has been dubbed a leucogabbro.

Table 4.1: XRD analysis of sample 01

| Compound Name | Formula | Percentage |
|---|---|---|
| Labradorite | $Al_{1.46}\ Ca_{0.347}\ Na_{0.685}\ O_8\ Si_{2.54}$ | 44.8 % |
| Oligoclase | $Al_{1.277}\ Ca_{0.277}\ Na_{0.723}\ O_8\ Si_{2.723}$ | 43.0 % |
| Calcium uranium fluoride | $Ca_{0.925}\ F_{2.15}\ U_{0.075}$ | 7.1 % |
| Oxyfluoride of Cesium, Manganese & Molybdenum | $Cs\ F_3\ Mn\ Mo\ O_3$ | 3.5 % |
| Barium vanadium trisulfide | $Ba\ S_3\ V$ | 0.9 % |
| *-unidentified* | $Cd\ Cu_2\ Se_4\ Sn$ | 0.6 % |
| *--unidentified* | $Au_5\ Zn_8$ | 0.1 % |
| **Total** | | **100.0%** |

The X-Ray Diffraction patterns and spread have been shown in Figure 4.2. The pie chart in Figure 4.3 presents the mineral species representation differently for ease of correlation as recorded in the XRD machine. The pattern below is a summation of the respective diffraction patterns produced by individual species in the gabbro, at SMP-01. The minerals that have been presented in Figure 4.2 are a result of d-spacings that result in patterns / unique "fingerprints" of the mineral species in the gabbro. Plagioclase feldspars exhibit the most peaks and counts giving a clear indication of their dominance in gabbro at SMP-01.

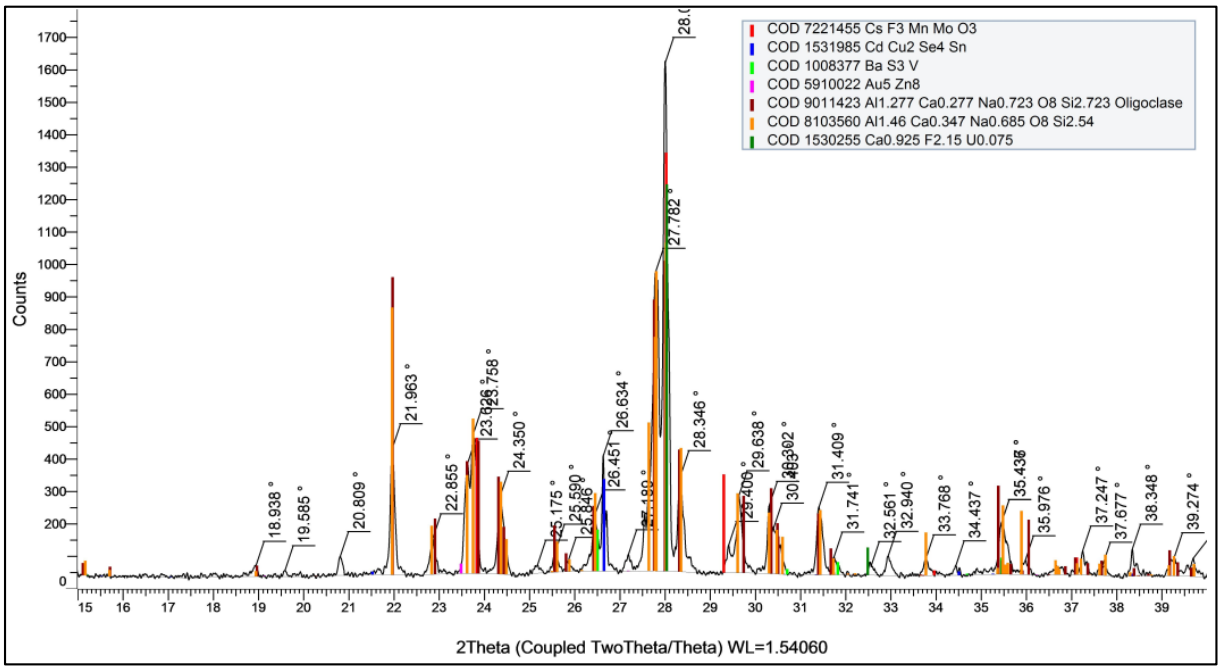


Figure 4.2: X-Ray Diffraction pattern of sample 01 from SMP-01 showing the presence of plagioclase feldspars and other accessory minerals.

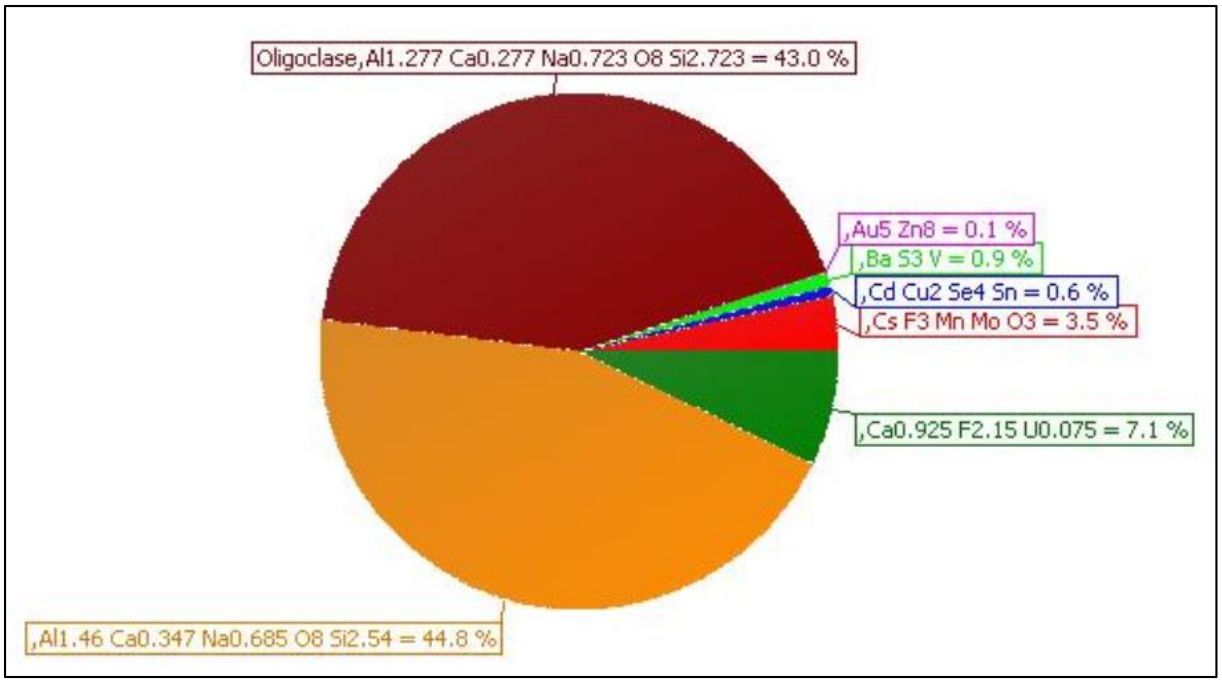


Figure 4.3: Pie chart diagram showing the percentage of the constituent minerals in sample 01.

**Petrography:** In the rock section, sample 01 shows plagioclase group minerals oligoclase and labradorite. The minerals appear to contain elongated laths exhibiting parallel lamellae. Lone polysynthetic albite twinning and carlsbad twinning is very well developed and this is evident in both sets of the feldspar minerals. The third type of twining (pericline twinning) is seen as the lamellae cut the albite twins in a normal fashion. Pericline twinning, though is not pronounced as the other forms of twinning, is noted. In the rock section, some twin lamellae appear bent, and this is as a result of plastic deformation occasioned by the intrusive structures. In Figure 4.4, there is a clear show of this by the microveinlet which appears to have a “fore” and a “tail” which is intruding into plagioclase feldspars, causing the latter to exhibit funnel-like shape and the development of a microfracture. The bending of these twinned zones shows evidence of secondary deformation on the rock. Optically, the plagioclase crystals show varied extinction properties. The extinction is also occasioned by sharp composition breaks from the feldspar (which is the majority mineral) and other accessory minerals.

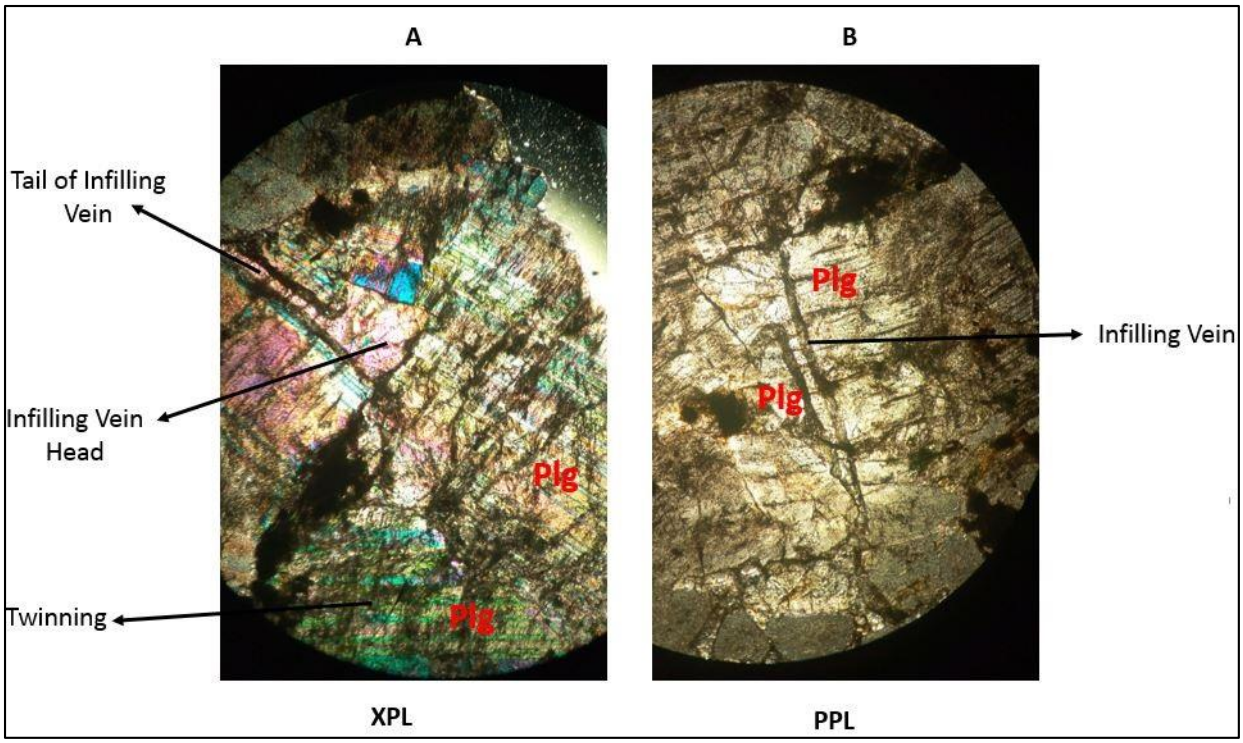


Figure 4.4: Microphotograph of sample 01, showing twinning patterns and microveinlet infilling, displacing plagioclase feldspar sets. Plg: Plagioclase. Magnification X100.

ii. **Results of Sample No. 15**

Sample 15 was collected from a roadside cutting at SMP-15 and it was flanked by a fine-grained dyke of about 2m in width. The unit is coarse-grained – medium, mafic, compact and it was sampled for analysis. The results have been presented below.


Figure 4.5: Hand specimen of sample 15 of gabbro at SMP-15 at coordinate: 0°10'34.40"S | 37°56'43.00"E.

**Mineralogy:** XRD analysis shows that close to 80% of the rock is composed of the plagioclase feldspar Labradorite. Sample 15 also contains various mineral species in significant quantities, such as Klockmannite (10%), Nitratine (3.5%), and some which were unidentified. The Klockmannite mineral is of hydrothermal origin, (Spieth, 2019) and its presence would suggest one of the possible processes that contributed to the occurrence of the gabbro.

Table 4.2: XRD analysis of sample 15

| **Compound Name** | **Formula** | **Percentage** |
|---|---|---|
| Labradorite | $Al_{0.81}\ Ca_{0.325}\ Na_{0.16}\ O_4\ Si_{1.19}$ | 79.2 % |
| Klockmannite | Cu Se | 10.0 % |
| Nitratine | N Na $O_3$ | 3.5 % |
| *-unidentified* | Cr $F_4$ Sr | 2.6 % |
| *-unidentified* | $F_6$ V Zr | 2.1 % |
| *-unidentified* | Cs Cu $F_6$ Mn | 1.1 % |
| Germanium Tin Antimony Telluride | $Ge_{0.75}\ Sb_2\ Sn_{0.25}\ Te_4$ | 0.9 % |
| *-unidentified* | $N_2$ Ni $Sr_2$ | 0.5 % |
| Krasnogorite | $O_3$ W | 0.2 % |
| **Total** | | **100.1%** |

The X-Ray Diffraction patterns and spread have been shown in Figure 4.6 and Figure 4.7 as recorded in the XRD machine, each mineral species presenting a unique pattern. A majority of the peaks on the 2θ axis are those of Labradorite and from the patterns, it is clear why the mineral takes up a huge percentage of the mineral species in the rock. Klockmannite on the other hand exhibits various angles between the transmitted and the reflected beams on the 2θ axis. Both Labradorite and Klockmannite add up to about 90% of the gabbro unit. The rest of the peaks are as a result of the other minerals such as Krasnogorite, Nitratine, and others which comprise about 10%.

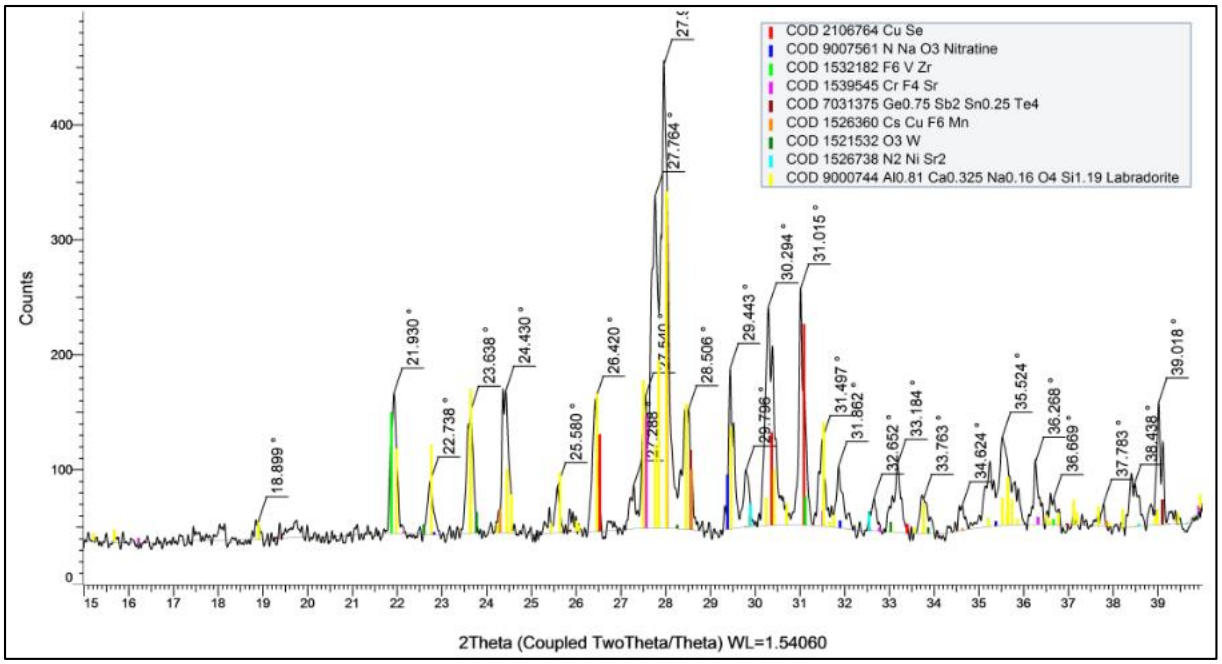


Figure 4.6: X-Ray Diffraction pattern of sample 15 from SMP-15 showing the presence of Labradorite and other accessory minerals.

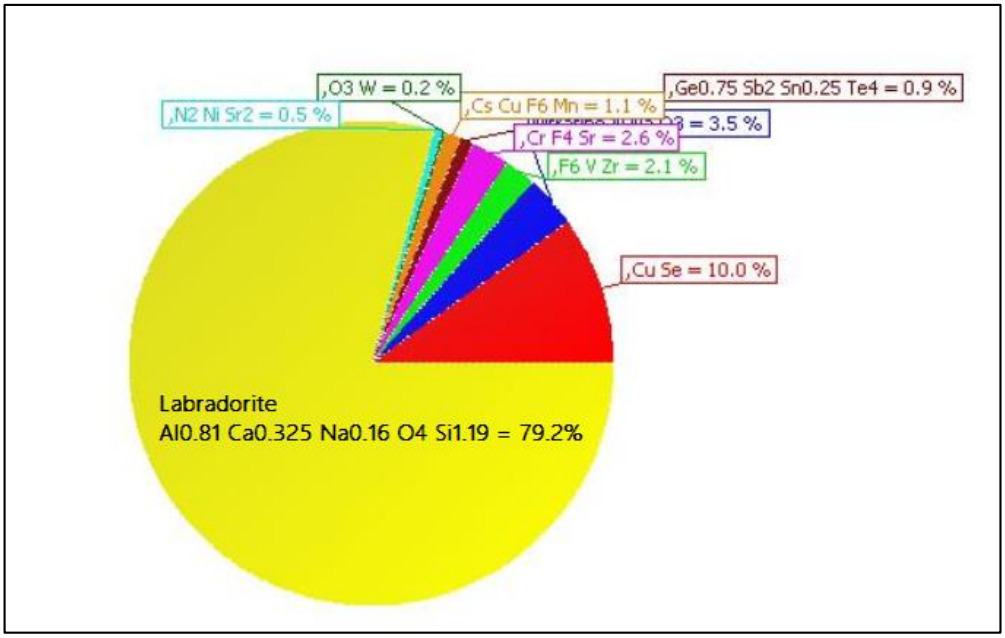


Figure 4.7: Pie Chart diagram showing the percentage of each mineral in sample 15 from SMP-15.

### iii. **Results of Sample No. 16**

Sampling Point SMP-16 where sample 16 was collected was located next to an abandoned mine. The outcrop was poorly exposed but samples collected indicate a medium - coarse-

grained rock unit, Figure 4.8. It appeared to be dark grayish and weathers to reddish-brown soils. The host rocks are minimally mineralized.


Figure 4.8: Hand specimen sample 16 at SMP-16 at coordinate: 0°10'39.20"S | 37°57'20.70"E.

**Mineralogy:** XRD analysis shows that the rock is heavily dominated by the plagioclase feldspars; Oligoclase and Labradorite which make up 85.60% of the rock. Minerals such as Fluoro-Pargasite, Sphaerobismoite, and others tally the rest of the percentage. Fluoro-Pargasite, a member of the pargasite group, is also a member of the amphibole group. This mineral makes up slightly over 12% of the mineral quantities in sample 16, which is the second most abundant species after the plagioclase feldspars and this is a significant amount. Fluoro-Pargasite forms through metasomatic processes, (Oberti *et al.*, 2010). On the other hand, Sphaerobismoite, an oxide mineral of Bismuth, comprises close to 1.0% of the rock unit. The rock is a leucogabbro based on the high quantity of plagioclase minerals such as labradorite and oligoclase.

Table 4.3: XRD analysis of sample 16

| **Compound Name** | **Formula** | **Percentage** |
|---|---|---|
| Labradorite | $Al_{1.46}\ Ca_{0.347}\ Na_{0.685}\ O_8\ Si_{2.54}$ | 45.9 % |
| Oligoclase | $Al_{1.277}\ Ca_{0.277}\ Na_{0.723}\ O_8\ Si_{2.723}$ | 39.7 % |
| Fluoro - Pargasite | $Ca_{1.8}\ F_2\ Ga_{1.28}\ Mg_{4.82}\ Na_{0.46}\ O_{22}\ Si_{7.04}$ | 12.1 % |
| Sphaerobismoite | $Bi_2\ O_3$ | 0.9 % |
| *-unidentified* | $Nd\ Rh_2\ Si_2$ | 0.4 % |
| *-unidentified* | $Ba\ F_6\ Pd\ Sr$ | 0.3 % |
| *-unidentified* | $Bi_2\ Hf_2\ O_7$ | 0.2 % |
| *-unidentified* | $Bi\ Li_{2.44}\ Zr_{0.14}$ | 0.2 % |
| *-unidentified* | $Ag_2\ Ho$ | 0.2 % |
| *-unidentified* | $Hf\ O_3\ Sr$ | 0.1 % |
| *-unidentified* | $Bi\ La\ O\ Pb\ S_3$ | 0.1 % |
| **Total** | | **100.1%** |

The X-Ray Diffraction pattern in Figure 4.9 below shows the domination of plagioclase feldspars and pargasite peaks with Labradorite showing the most peaks followed by Oligoclase then pargasite. The three comprise about 97.70% of the gabbro rock unit as clearly demonstrated by the pie chart representation in Figure 4.10 below.

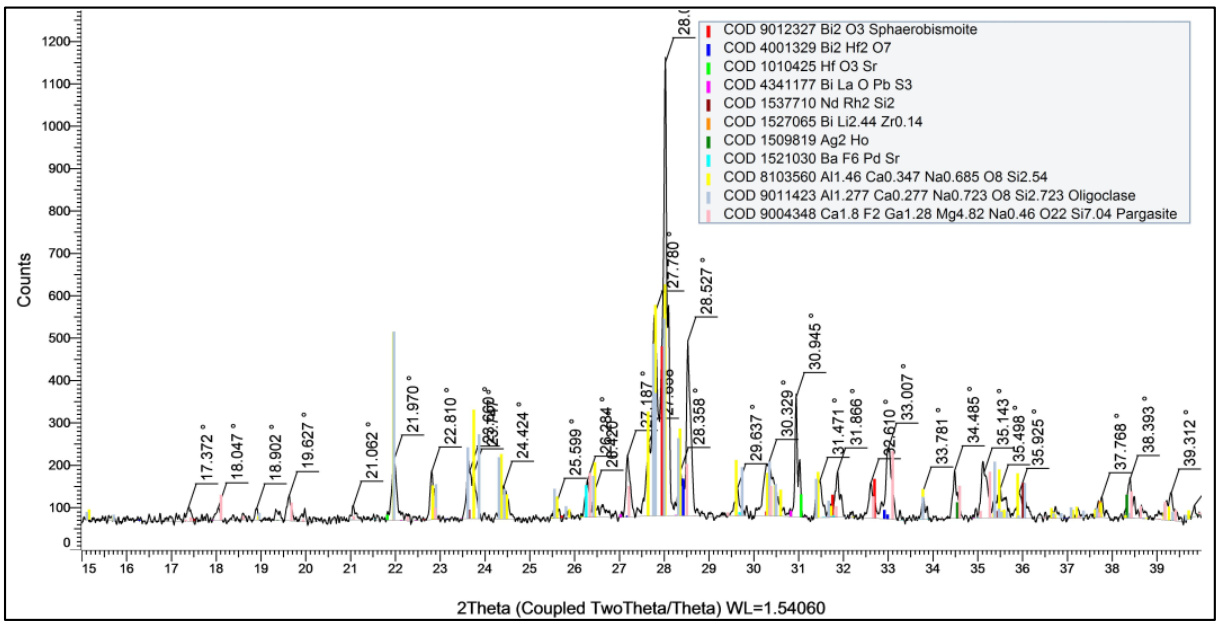


Figure 4.9: X-Ray Diffraction pattern of sample 16 showing the presence of plagioclase feldspars and other accessory minerals.

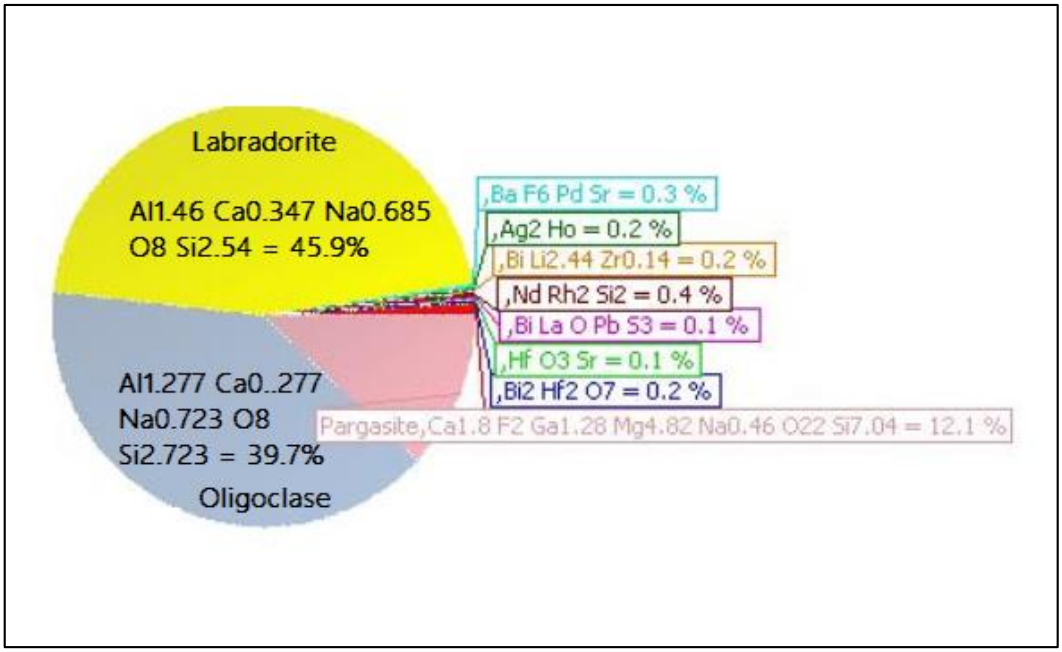


Figure 4.10: Pie Chart diagram showing the percentage of each mineral in sample 16.

### iv. **Results of Sample No. 21**

Sampling point SMP-21 was mapped along a dry river bed of a tributary of River Thingithu. The outcrop was massive and had ductile shear structures. Quartz geodes and mafic lenses were noted on the outcrop. Kunkar limestone was present and it cemented rounded debris. This rock unit shows xenolithic pressure shadows both in hand specimen and in the massive insitu outcrop, Figure 4.11. Mineral grains in the unit also appear elongated and some are slightly aligned to a specific direction. Shiny bronze-like micaceous flakes characterize the rock. Sample 21 was collected for analysis and results have been presented below.

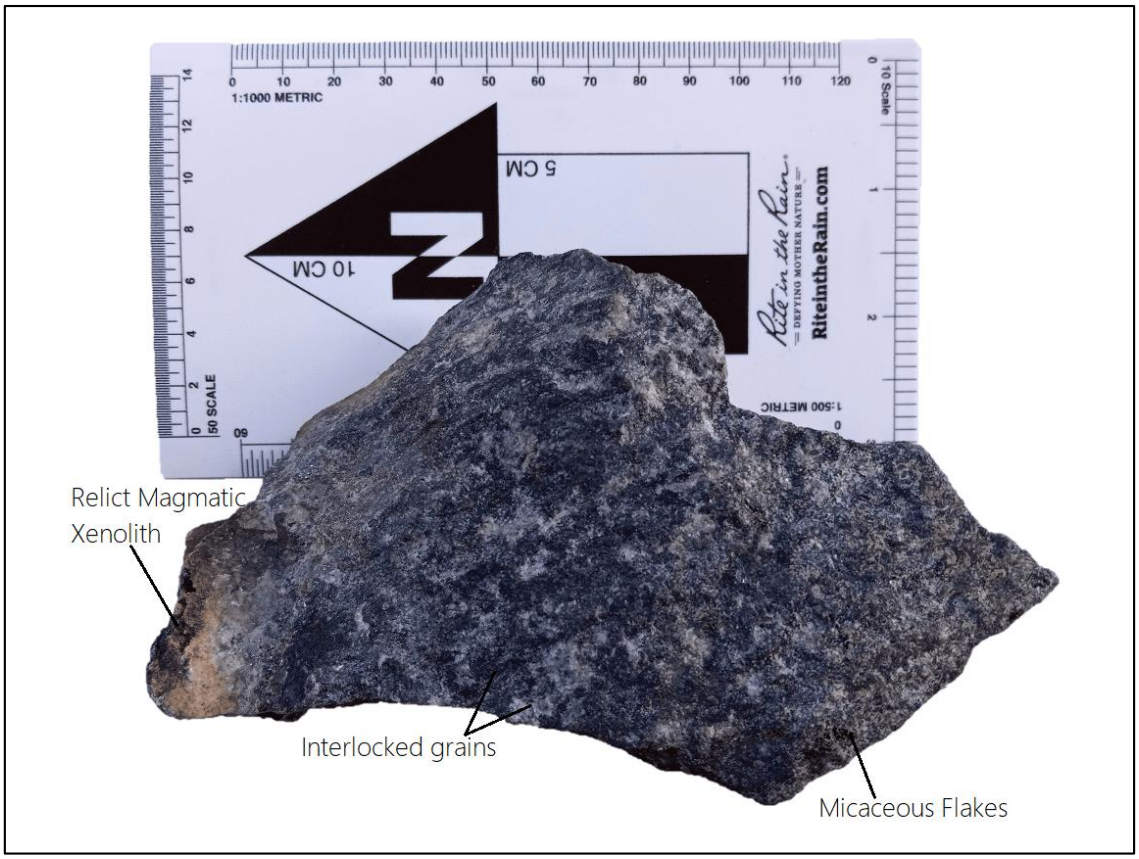


Figure 4.11: Hand specimen sample of gabbro at SMP-21 at coordinate: 00° 09' 28.20"S | 37°56'14.70"E.

**Mineralogy:** Sample 21 XRD analytics show that the rock unit is dominated by minerals from the Na – Ca plagioclase feldspar series in the form of Anorthite (An: 90%-100% / Ab: 0%-10%), Oligoclase (Ab: 90%-70% / An: 10%-30%) and Albite (Ab: 90%-100% / An: 0%-10%) which cumulatively tally to 85.40%. This dominance is a clear indication of differences in the chemical and physical properties of the constituent plagioclase feldspar minerals. It is particularly interesting to note the simultaneous occurrence of plagioclase end-member series minerals albite and anorthite on the same sample as it is well known from the Bowens Reaction Series that the formation temperature for calcium-rich plagioclase is higher than that of sodium-rich minerals.

Table 4.4: XRD analysis of sample 21

| **Compound Name** | **Formula** | **Percentage** |
|---|---|---|
| Oligoclase | $Al_{1.277}\ Ca_{0.277}\ Na_{0.723}\ O_8\ Si_{2.723}$ | 35.5 % |
| Albite | $Al\ Na\ O_8\ Si_3$ | 26.6 % |
| Anorthite Sodian | $Al_{1.52}\ Ca_{0.52}\ Na_{0.48}\ O_8\ Si_{2.48}$ | 23.3 % |
| Copper Arsenide Selenide | As Cu Se | 4.9 % |
| Quartz | $O_2\ Si$ | 3.6 % |
| Mercury Tellurium | Hg Te | 1.4 % |
| Beryllium Fluoride | $Be\ F_2$ | 1.2 % |
| Magnesite | $C\ Cd_{0.45}\ Mg_{0.55}\ O_3$ | 0.9 % |
| Praseodymium Zinc Arsenide | $As_5\ Pr_4\ Zn_{1.68}$ | 0.9 % |
| --*unidentified* | $Ce_{0.24}\ Co_2\ O_{5.91}\ Sr_{2.76}$ | 0.7 % |
| Thallium Antimony Telluride | $Sb\ Te_2\ Tl$ | 0.5 % |
| Diytterbium Palladium Hexagermanide | $Ge_6\ Pd\ Yb_2$ | 0.3 % |
| Gadolinium Nickel | Gd Ni | 0.2 % |
| **Total** | | **100.0 %** |

The X-Ray Diffraction patterns and spread have been shown in Figure 4.12 below as recorded in the XRD machine. Anorthite Sodian, Albite, and Oligoclase peaks are well visible from the spreads of the 2θ angles, their respective peaks, and respective color codes. This has also been indicated in the pie chart, Figure 4.13.

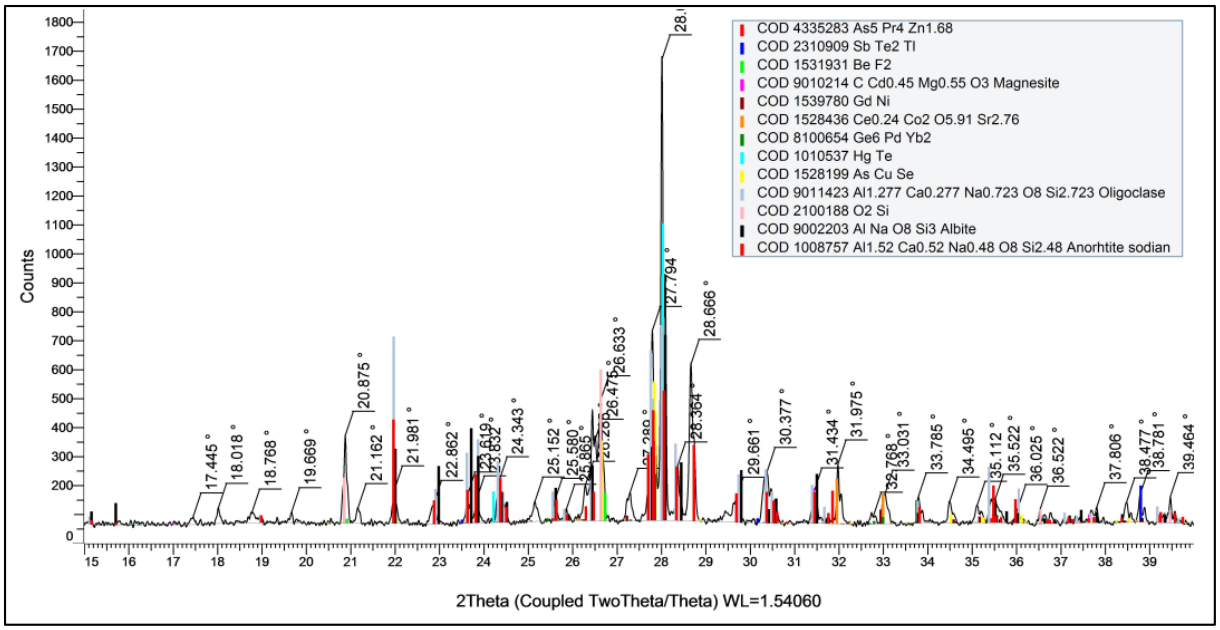


Figure 4.12: X-Ray Diffraction pattern of sample 21 showing the presence of feldspars and other accessory minerals.

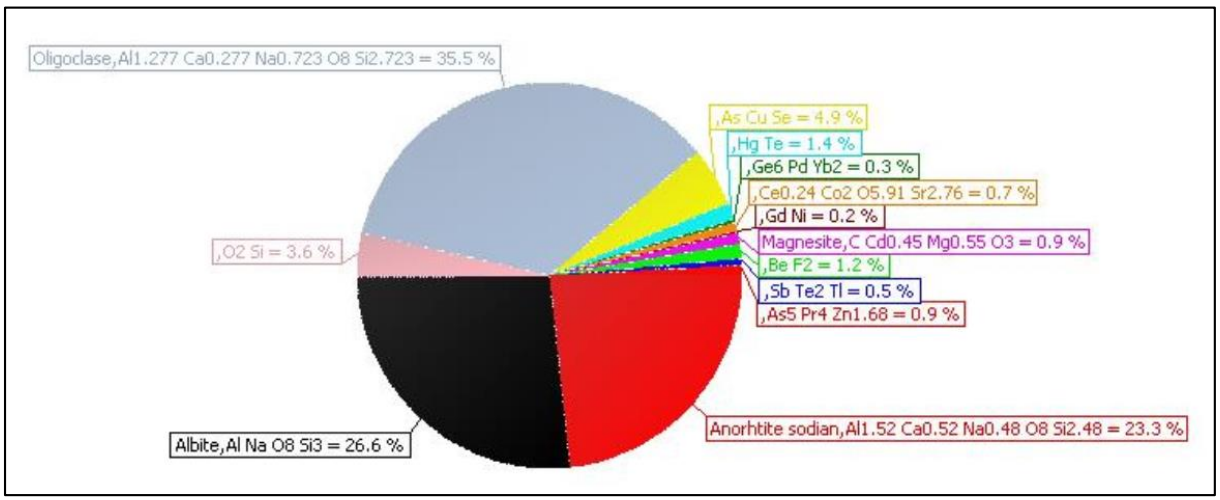


Figure 4.13: Pie Chart showing the percentage of each mineral in sample number 21.

### v. **Results of Sample No. 22**

Sample 22 was collected from a massive outcrop at the sampling point SMP-22, Figure 4.14. The rock unit weathers through physical means as well as biological means. Exfoliation is most notable in the figure below. The rock unit has been crisscrossed by millimeter size veins. The outcrop and the entire area is not mineralized. The rock unit is coarse-grained and a representative sample was collected for analysis, Figure 4.15. The rock did not appear to have quartz grains from a macroscopic perspective and this was confirmed via analysis of the sample.

Figure 4.14 Massive gabbro outcrop mapped at SMP-22


Figure 4.15: Hand specimen sample of gabbro at sampling point SMP-22 at coordinate: 00° 09' 06.70"S | 37° 55' 33.80"E.

**Mineralogy:** XRD analysis shows that the rock is heavily dominated by Oligoclase and Anorthite which make up 82.10% of the rock. Vihorlatite is a mineral from the tetradymite group and occurs in association with quartz mineral species, (Skála *et al.*, 2007). Reference is made to the XRD analysis where this is an exemption i.e. the analyzed sample does not show any mineralization of quartz, Table 4.5. The quantity of hurlbutite is also notable in the results below in addition to being a hydrothermal signature mineral, (Mrose, 1952).

Table 4.5: XRD analysis of sample 22

| **Compound Name** | **Formula** | **Percentage** |
|---|---|---|
| Oligoclase | $Al_{1.277}\,Ca_{0.277}\,Na_{0.723}\,O_8\,Si_{2.723}$ | 45.8 % |
| Anorthite sodian | $Al_{1.52}\,Ca_{0.52}\,Na_{0.48}\,O_8\,Si_{2.48}$ | 36.3 % |
| Titanite | $Al\,Ca\,F\,O_4\,Si$ | 8.3 % |
| Hurlbutite | $Be_2\,Ca\,O_8\,P_2$ | 6.9 % |
| Nantokite | $Cl\,Cu$ | 2.3 % |
| Vihorlatite | $Bi_{21.68}\,S_{1.7}\,Se_{15.3}\,Te_{6.32}$ | 0.5 % |
| **Total** | | **100.1 %** |

The X-Ray Diffraction pattern for sample 22 has been shown in Figure 4.16 whereas the spread has been presented in Figure 4.17 as recorded in the XRD machine. 2θ peaks of Oligoclase 45.8% and Anorthite Sodian 36.3% have been indicated in the figure below and as seen, both plagioclase minerals have the theta angles spread along the entire spectrum signifying their dominance in the gabbro. Peaks of the other mineral species are not as pronounced as the plagioclase peaks. In the pie chart, it is well clear that the plagioclase species take up 82.10% with oligoclase alone being close to 50%.

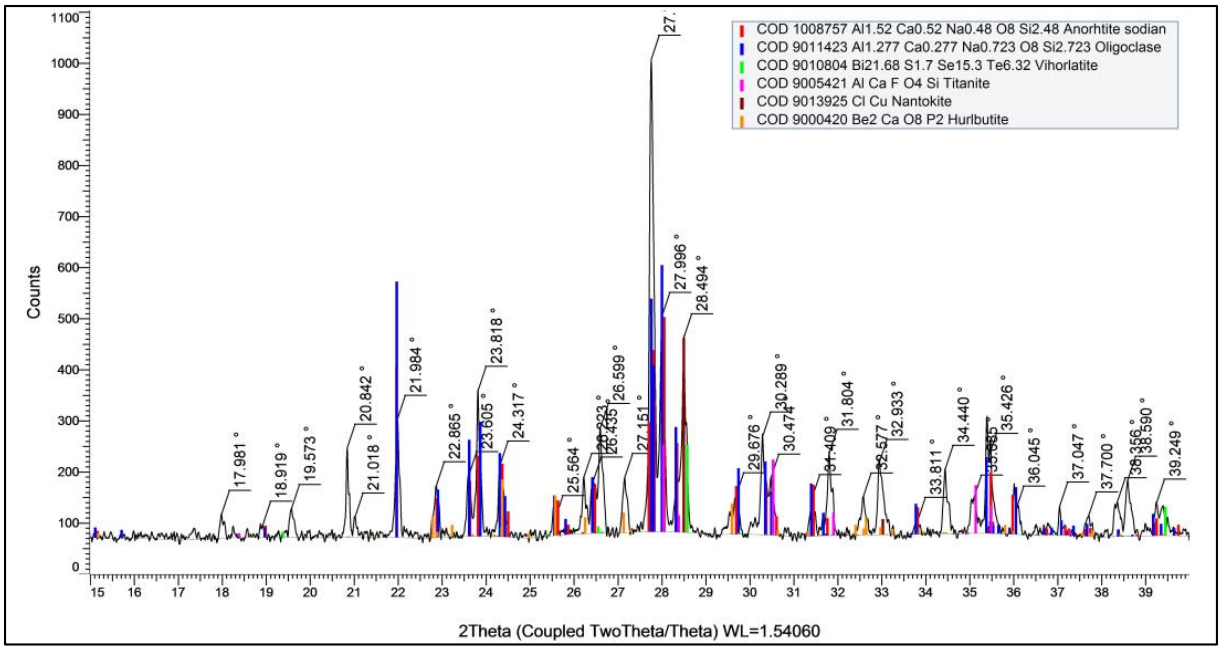


Figure 4.16: X-Ray Diffraction pattern of sample 22 showing the presence of plagioclase feldspars and other accessory minerals.

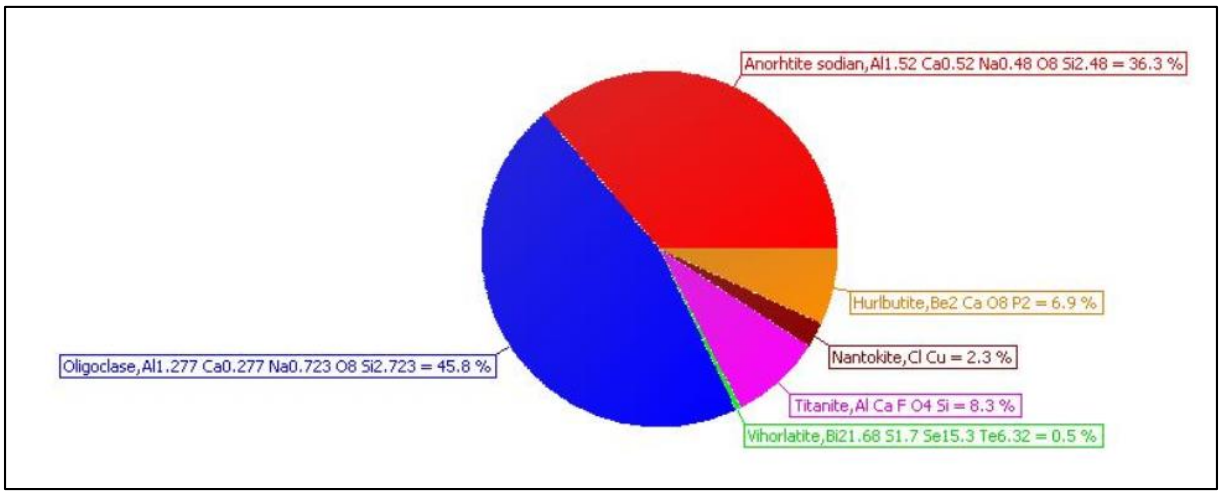


Figure 4.17: Pie Chart diagram showing the percentage of each mineral in sample 22.

### 4.1.2 Anorthositic Gabbro

(Streckeisen, 1976) recommended that anorthosites be defined by having more than 90% plagioclase. Based on this definition, the following results are presented.

i. **Results of Sample No. 10**

Macroscopically, sample 10 collected from sampling point SMP-10 and the unit mapped at observation point OBP 028 have been likened and sample 10 was analyzed, Figure 4.18. The sampling point SMP-10 was located by the roadside, a few kilometers from sampling point

SMP-09. The rock appeared to contain grains that had undergone mylonitization. There appeared to be fracturing in the area as well. This appeared to be a boundary of various rock units. The rock was mafic, medium to coarse-grained, and compact.

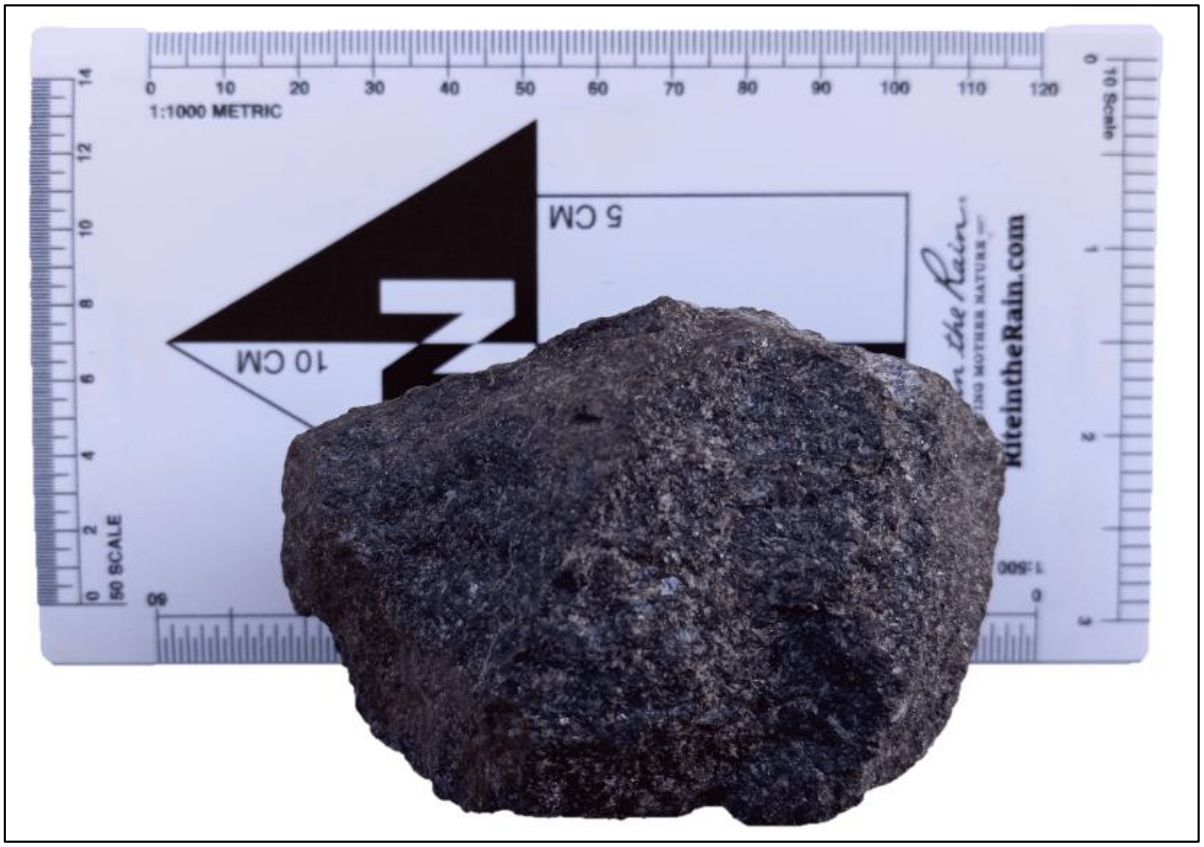


Figure 4.18: Hand specimen sample of anorthosite at sampling point SMP-10, coordinate: 00° 10' 53.00"S | 37° 56' 49.10"E.

**Mineralogy:** XRD analysis shows that the rock is heavily dominated by plagioclase feldspars; Andesine (An: 35%-50% & Ab: 70%-50%), Labradorite (An: 50%-70% & Ab: 50%-30%) and Anorthite (An: 90%-100% & Ab: 10%-00%) which make up 92.30% of the rock. Other minerals such as Nantokite, Minium, titanite, and other accessory minerals constitute the remaining 7.70%. It is observed that various mineral species in sample 10 have been recorded in other samples in varying quantities. Nantokite was noted in sample 22 in almost similar quantity (2.4% in sample 10 vis a vis 2.3% in sample 22). Titanite and anorthite are the other mineral species recorded in sample 22. The oxide of bismuth, (sphaerobismoite) occurring in sample 10 was also recorded in sample 16.

Table 4.6: XRD analysis of sample 10

| **Compound Name** | **Formula** | **Percentage** |
|---|---|---|
| Andesine | $Al_{0.735}\ Ca_{0.24}\ Na_{0.26}\ O_4\ Si_{1.265}$ | 34.5 % |
| Labradorite | $Al_{0.81}\ Ca_{0.325}\ Na_{0.16}\ O_4\ Si_{1.19}$ | 30.6 % |
| Anorthite sodian | $Al_{1.52}\ Ca_{0.52}\ Na_{0.48}\ O_8\ Si_{2.48}$ | 27.2 % |
| Nantokite | Cl Cu | 2.4 % |
| Titanite | Ca $O_5$ Si Ti | 1.9 % |
| Caesium nickel hexafluorovanadate (III) | Cs $F_6$ Ni V | 1.1 % |
| Yttrium strontium cobalt oxide | Co $O_{2.69}\ Sr_{0.8}\ Y_{0.2}$ | 1.0 % |
| Sphaerobismoite | $Bi_2\ O_3$ | 0.9 % |
| Praseodymium Telluride | $Pr_3\ Te_4$ | 0.3 % |
| Minium | $O_4\ Pb_3$ | 0.1 % |
| Copper gallium holmium | $Cu_{0.2}\ Ga_{1.8}$ Ho | 0.1 % |
| **Total** | | **100.1%** |

The X-Ray Diffraction pattern showing the respective peaks have been presented in Figure 4.19 whereas Figure 4.20 presents the same as a pie chart as recorded in the XRD machine. As noted elsewhere in the report, plagioclase feldspars present various 2θ angles with respective counts across the axis.

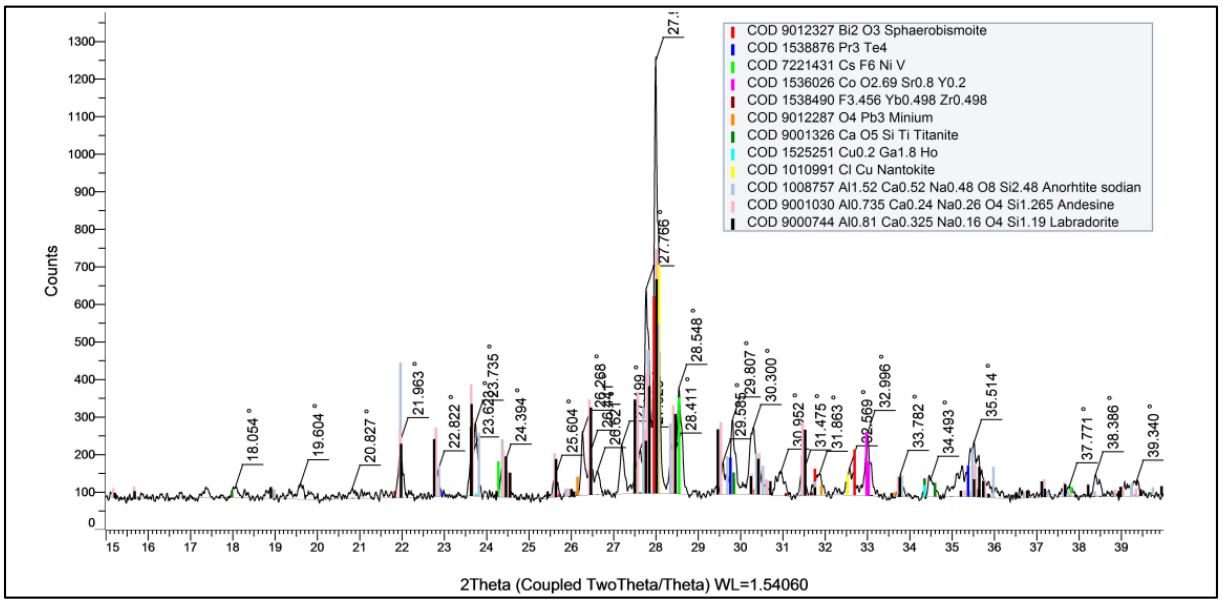


Figure 4.19: X-Ray Diffraction pattern of sample 10 showing the presence of plagioclase feldspars and other accessory minerals.

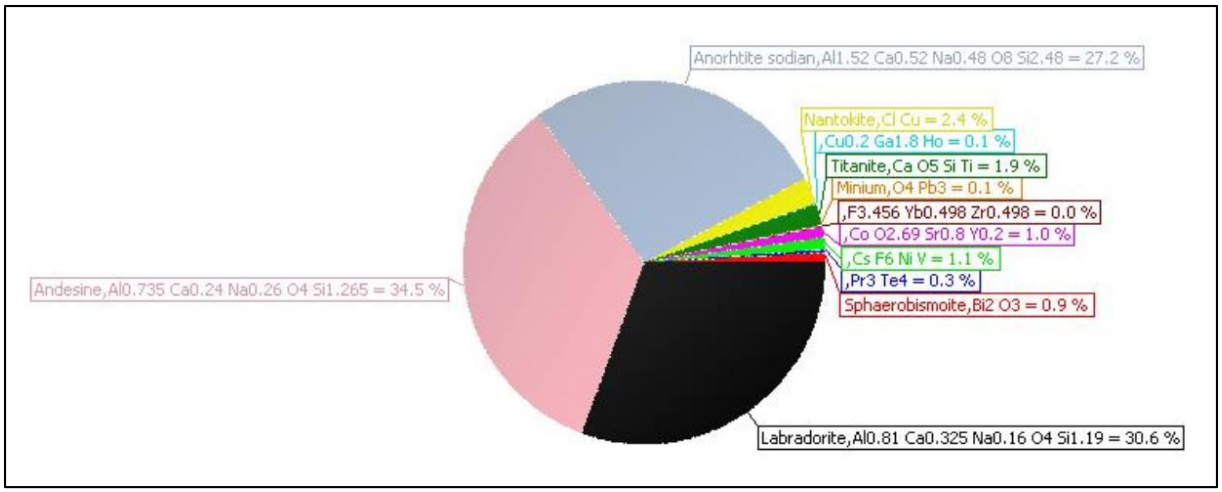


Figure 4.20: Pie Chart diagram showing the percentage of each mineral in sample 10.

**Petrography:** Figure 4.21 below shows the rock section for sample 10 in magnification 100X. Albite twinning of Plagioclase which is the most dominant mineral is notable. The rock appears coarse-grained from the rock section. Parallel striae cleavage is evident from the plagioclase feldspars. Concentric zoning is evident in a matrix of plagioclase feldspar. This has been shown in Figure 4.21a. Olivine and diamond-shaped titanite have been indicated in Figure 4.21c and Figure 4.21d. The zoning phenomena suggests different growth conditions potentially due to fractional setting. The dominance of plagioclase feldspars in the rock section and the matrix further suggests that the rock is an anorthositic gabbro.

Also, crystals of mafic minerals are embayed into the plagioclase feldspar crystals showing a clear change in environment for crystal growth. This is evident from the rock section in Figure 4.21 below where opaque minerals grow into the plagioclase feldspar crystals through processes that could be synonymous with hydrothermal processes common for sphene. Titanite (Sphene) observed in the rock section is highly pleochroic. It takes a diamond-like shape and is yellowish in XPL. Yttrium is a common rare earth element associated with sphene. Yttrium is one of the elements identified from the XRD analysis.

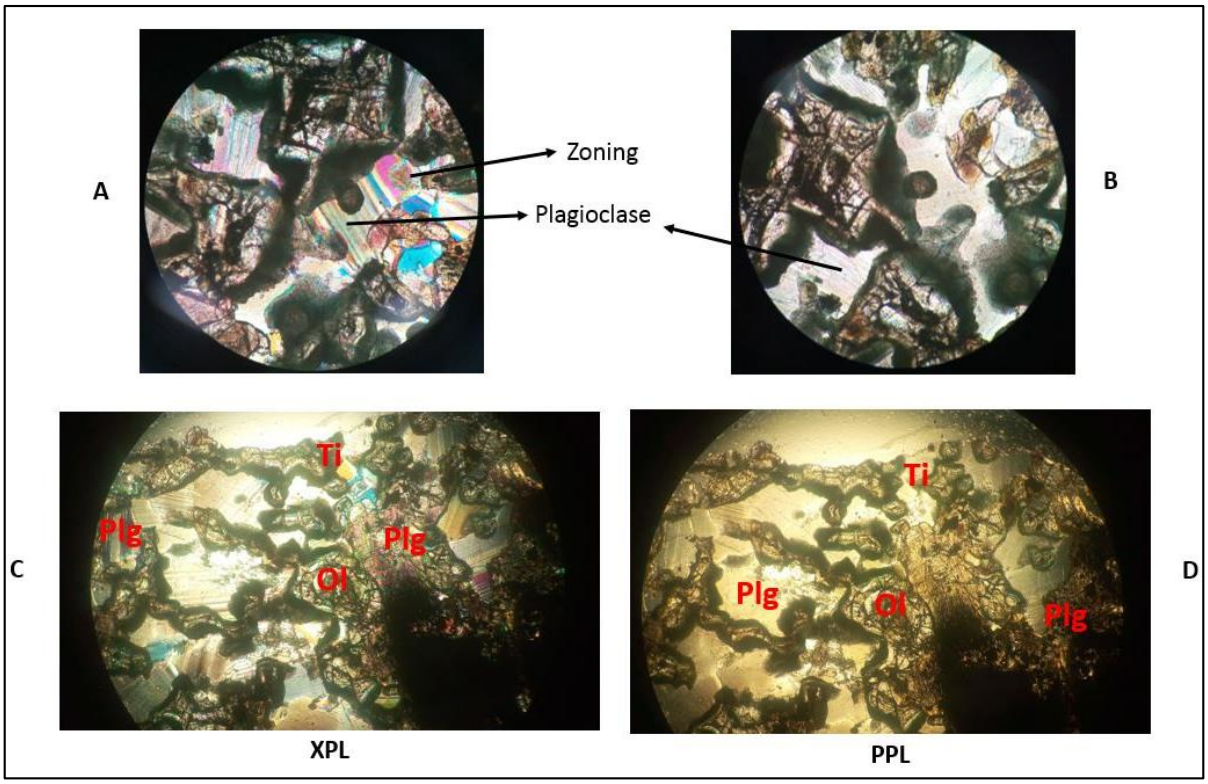


Figure 4.21: Sample 10 in rock section, showing the dominance of plagioclase feldspars. Ti: Titanite, Plg: Plagioclase, Ol: Olivine.

### ii. **Results of Sample No. 11**

Sample 11 was collected along a small stream at sampling point SMP-11. It had intermediate coloration, contained feldspar minerals and it was coarse-grained. Kunkar limestone was present and this could have implied tectonism of some sorts. The area had some shear zones trending North-South and a minor fold whose peak was millimeter size. A keen focus on the grain displacement showed evidence of sinistral movement. Sample 11 was collected for analysis. Figure 4.22 presents a fresh cut sample giving more detail of the rock unit.

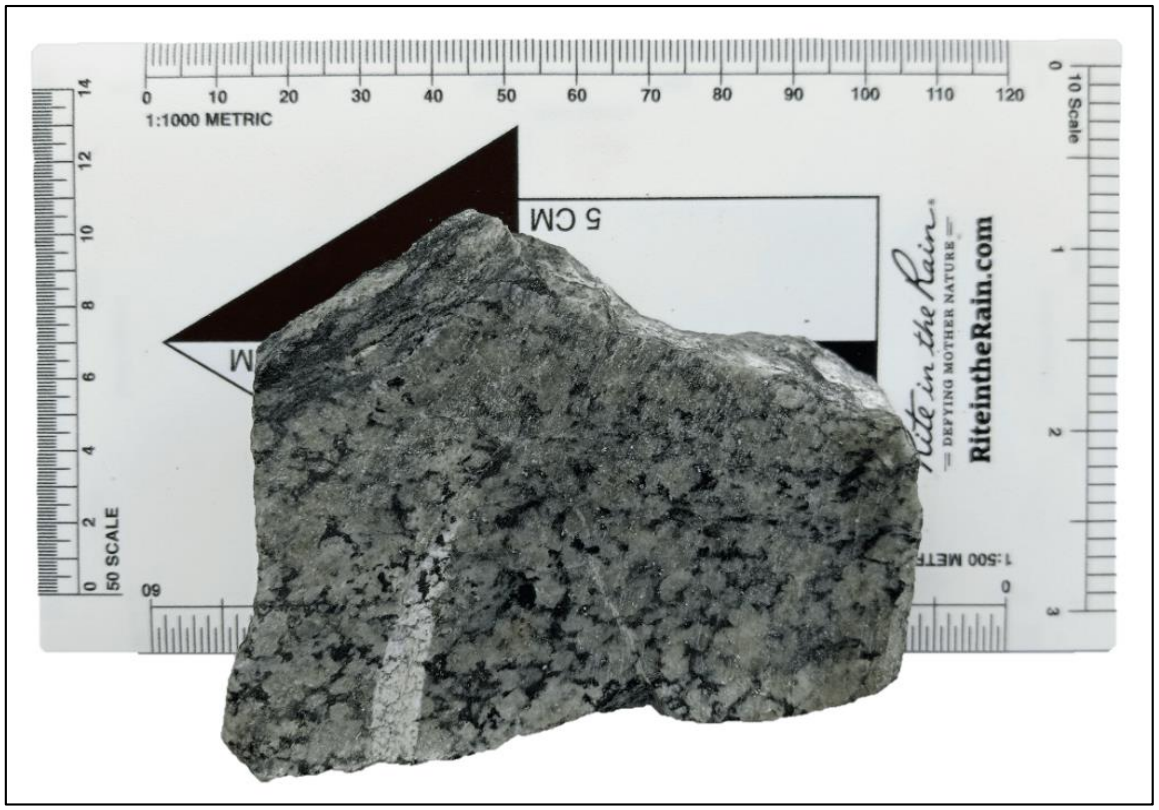


Figure 4.22: Hand specimen sample 11 of anorthositic gabbro at sampling point SMP-11 at coordinate: 00° 10' 18.30" S | 37° 56' 49.80" E.

**Mineralogy:** Sample 11 XRD analytics show that Anorthite, Bytownite, and Albite cumulatively comprise 93.8% of the mineral species in the rock qualifying the rock to be a leucogabbro with a color index of M < 10, Table 4.7. Referring to the Bowens Reaction Series and the liquidus/solidus curves for the Plagioclase feldspars, the Ca Plagioclase Feldspars are the first to crystalize. In this case, Bytownite and Anorthite seem to have crystallized first depleting the magma of Ca. This leaves the magma with more alkali metals. Albite which is the third most abundant mineral in the sample may have crystalized last, among the plagioclase feldspars. Of interest to note is the presence of berlinite, an indicator mineral, for formation under high temperatures, (Bogdan and Herta, 2007). The presence of berlinite and the Ca-rich plagioclases suggest high formation temperatures during rock formation followed by a change in the conditions of formation.

Table 4.7: XRD analysis of sample 11

| **Compound Name** | **Formula** | **Percentage** |
|---|---|---|
| Bytownite | $Al_{7.76}\ Ca_{3.44}\ Na_{0.56}\ O_{32}\ Si_{8.24}$ | 36.3% |
| Anorthite | $Al_2\ Ca\ O_8\ Si_2$ | 30.0% |
| Albite | $Al\ Na\ O_8\ Si_3$ | 27.5% |
| Oxyfluorides of Cesium, Manganese, and Molybdenum | $Cs\ F_3\ Mn\ Mo\ O_3$ | 2.9% |
| Lanthanum manganese nickel | $La\ Mn_{0.5}\ Ni_{4.5}$ | 1.1% |
| Berlinite | $Al\ O_4\ P$ | 1.0% |
| Tribarium diiron(III) pentaoxide dichloride | $Ba_3\ Cl_2\ Fe_2\ O_5$ | 0.5% |
| Distrontium copper tellurate | $Cu\ O_6\ Sr_2\ Te$ | 0.4% |
| Uranium cerium oxide | $Ce_{0.368}\ O_{8.937}\ U_{3.632}$ | 0.2% |
| **Total** | | **99.9%** |

The X-Ray Diffraction patterns for sample 11 have been presented in Figure 4.23 where 2θ angles for the plagioclase feldspars and the accessories have been presented together with their respective counts. Dominance by the feldspar series is notable from the patterns. The pie chart presented under Figure 4.24 as recorded in the XRD machine shows that sample 11 is nearly monomineralic as far as plagioclase feldspars are concerned.

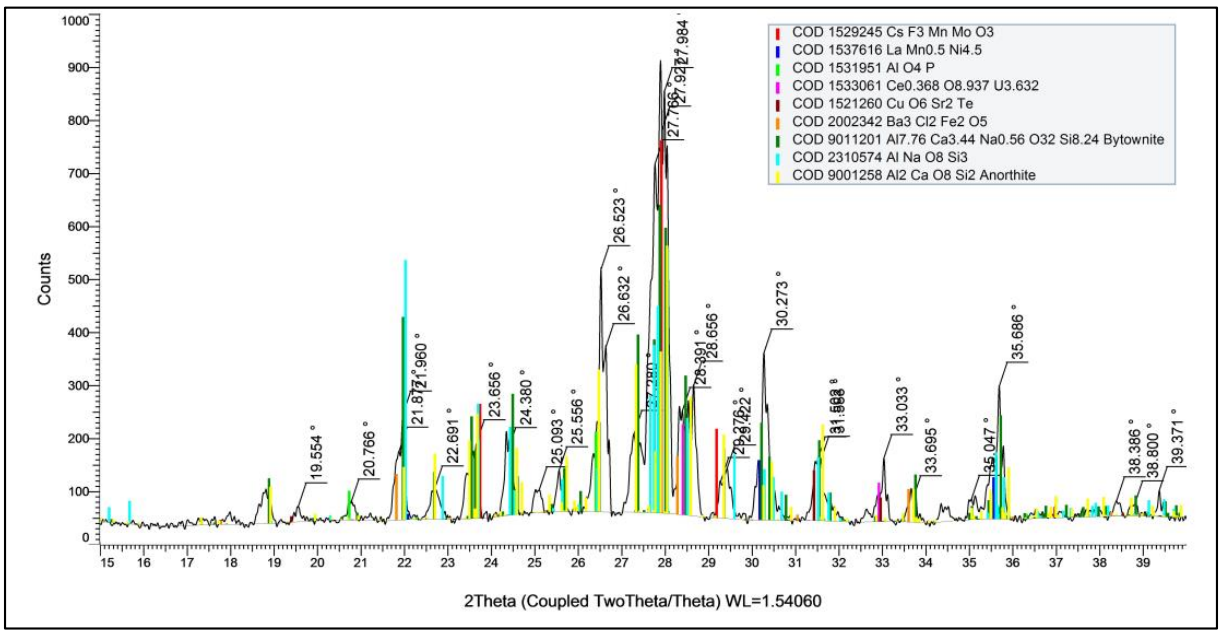


Figure 4.23: X-Ray Diffraction pattern of sample 11 showing the presence of plagioclase feldspars and other accessory minerals.

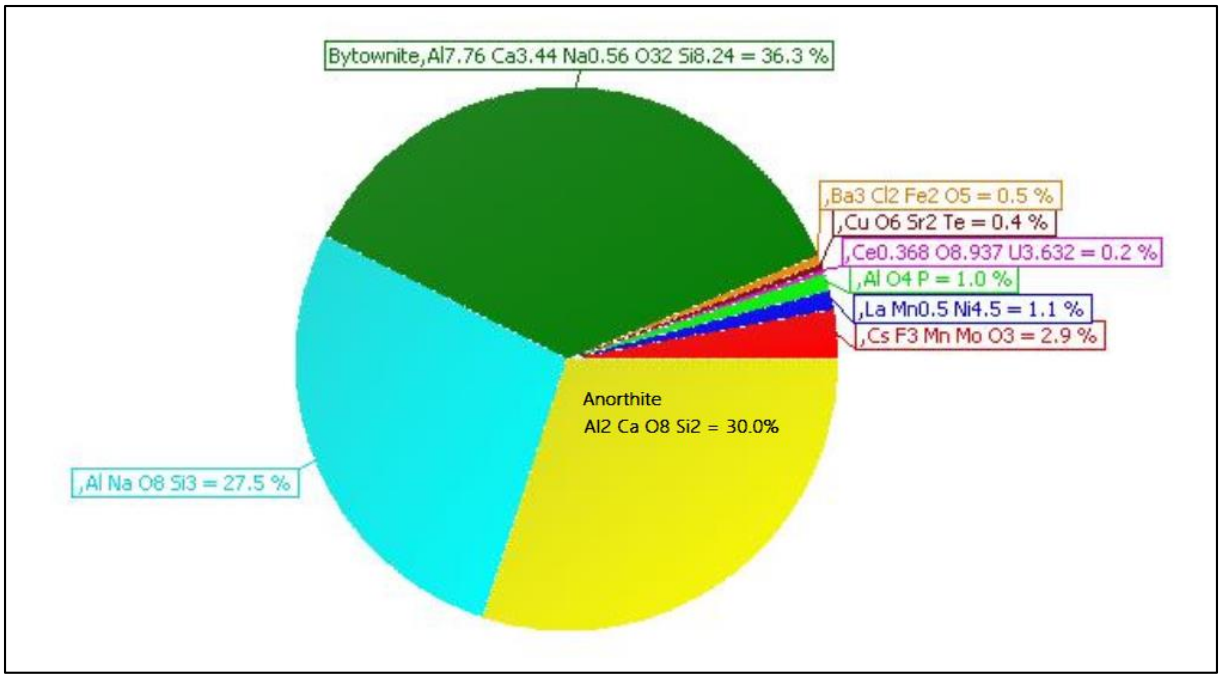


Figure 4.24: Pie Chart showing the percentage of each mineral in sample 11.

**Two Main Forms of Anorthositic Gabbro in the Marimanti Area**

Several rock types from the study area qualify to be Anorthosites based on (Streckeisen, 1976). Field occurrences and nature of rock fabric suggest the rocks to the Proterozoic Type of Anothorsites. The rocks typically lack the descriptive features of the other types of Anorthosites. However, mineral occurrences also suggest that the rocks could be layered mafics. Refer to the section on the review of anorthosite occurrences.

The anorthosite rock samples collected are in a variety of shades. From the macroscopic analysis of the samples, two distinctive shades are observed, a more mafic rock and an intermediate to felsic rock. Both rocks are nearly monomineralic as has been presented for samples 10 and 11. The rocks are very fresh with very little to no alteration. They are medium-grained to coarse-grained and are compact.

The first type which is more mafic can be distinguished through its texture. The rock is medium grained and compact. XRD analysis of the rock also shows the dominance of plagioclase feldspars (anorthite sodian, labradorite, and andesine) up to 92.30%. The second type, which is the felsic to intermediate gabbroic rock appears coarse-grained and has a cumulus texture. Further analysis of the rocks using XRD shows rocks that are heavily dominated by plagioclase feldspars (anorthite, bytownite, and albite), up to 93.80% composition. Based on this, the two

units have been classified as Type 1 Kithiori Anorthositic Suite (dark-colored) and Type 2 Kithiori Anorthositic Suite (light-colored).

### 4.1.3 Dolerite / Microgabbro

Doleritic rocks, alternatively known as diabase or microgabbro dominantly crosscut the study area as mafic, medium to fine-grained dykes. The mineral grains of the dolerite dykes were visible from the view of a hand lens. They exhibit ophitic texture. The grain sizes compared to typical gabbro show that they formed from a different process. A majority of the dykes mapped were massive and fresh. There were exceptions of various dykes that appeared weathered especially those that were exposed along road-side cuttings. The dykes are of various sizes, ranging from millimeter size to tens of meters wide. Some dolerite rocks contain small acicular white-colored phenocrysts. Figure 4.25 below shows the contact between dolerite and its host gabbro. The contacts are very sharp in the majority of exposures.

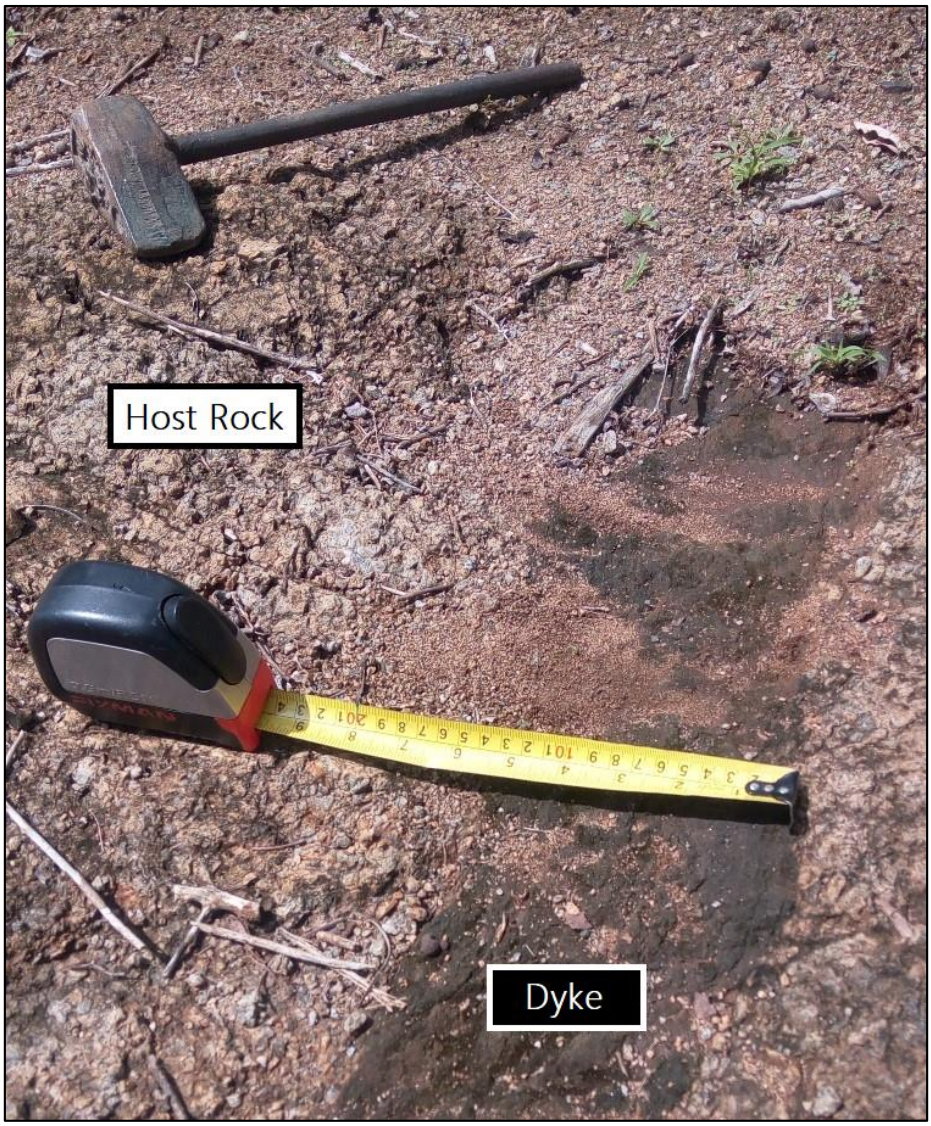


Figure 4.25: Contact between a dolerite dyke and the host gabbro at SMP-01. The mafic dyke is 13cm in width.

In several observation points, the dykes were seen to criss-cross the host rocks in a discordant fashion both in mineralized areas and non-mineralized areas. Observation point OBP 026 is one such example where the dykes cut through the mineralized pyroxenite host rocks in the process leaving sharp boundaries, Figure 4.26, with kunkar limestone developed along the boundaries of the two rocks. In the image below, the local community had excavated the mineralized areas on the flanks of the dolerite dyke. These dykes were mapped in 24 sites within the study area. This represents just under half of the sites visited showing the dominance of the dykes in the study area.

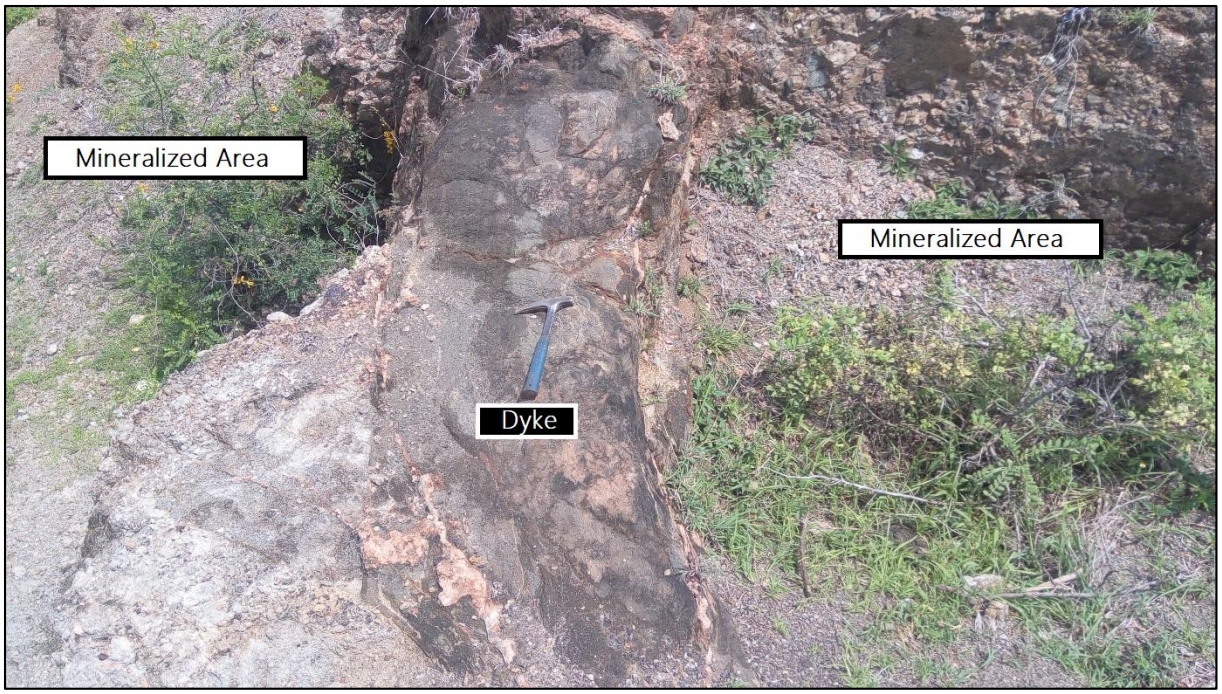


Figure 4.26: Contact between a dolerite dyke and a mineralized pyroxenite rock at observation point OBP 026.

**XRD Analysis of Dolerite Dykes: Results of Sample No. 23**

All dolerite dykes resembled each other from a macroscopic perspective i.e of grain size and color and therefore only sample 23, Figure 4.29, was analyzed. At sampling point SMP-23 the dyke mapped was massive (about 50 meters wide), Figure 4.30, medium to fine-grained and mafic. Minimal kunkar limestone was noted. There was no iron ore mineralization recorded at this observation point. The soils appeared reddish brown.

**Mineralogy:** SMP-23 XRD analytics show that Oligoclase forms 83.4% of the mineral species in the rock, Table 4.8. About 5% of the rock is iron beryllium silicate – danalite. Other accessory minerals form about 12% of the rocks' minerals.

Table 4.8: XRD analysis of sample 23

| **Compound Name** | **Formula** | **Percentage** |
|---|---|---|
| Oligoclase | $Al_{1.277}\ Ca_{0.277}\ Na_{0.723}\ O_8\ Si_{2.723}$ | 83.4 % |
| Danalite | $Be_6\ Fe_8\ O_{24}\ S_2\ Si_6$ | 4.9 % |
| Nickel Scandium | $Ni_5\ Sc$ | 4.4 % |
| Bismuth Titanium Oxide | $Bi_{7.68}\ O_{12.16}\ Ti_{0.32}$ | 2.1 % |
| Silver Barium Germanium | $Ag_3\ Ba_4\ Ge_{20}$ | 2.0 % |
| Thulium Boride Carbide | $C2\ B_2\ Tm$ | 1.2 % |
| Sn-Doped GST Mineral (Germanium Antimony Telluride) | $Ge_{0.5}\ Sb_2\ Sn_{0.5}\ Te_4$ | 0.9 % |
| Tellurium | Te | 0.6 % |
| --*unidentified* | Eu Ga Sn | 0.5 % |
| **Total** | | **100.0%** |

The X-Ray Diffraction patterns and pie chart for sample 23 have been presented in Figure 4.27 and Figure 4.28 as recorded by the XRD machine. Being the majority in the sample, Oligoclase (An: 10% - 30% & Ab: 90% - 70%) shows the most peaks on the 2θ axis and at the same time the respective counts along the y-axis. Of key interest is the element - Te and mineral - danalite both of which are hydrothermal activity indicator minerals. In the pie chart, it is seen that oligoclase dominates the mineral composition of the dolerite rock unit. This inference is made for the other dolerite dykes mapped in the study area.

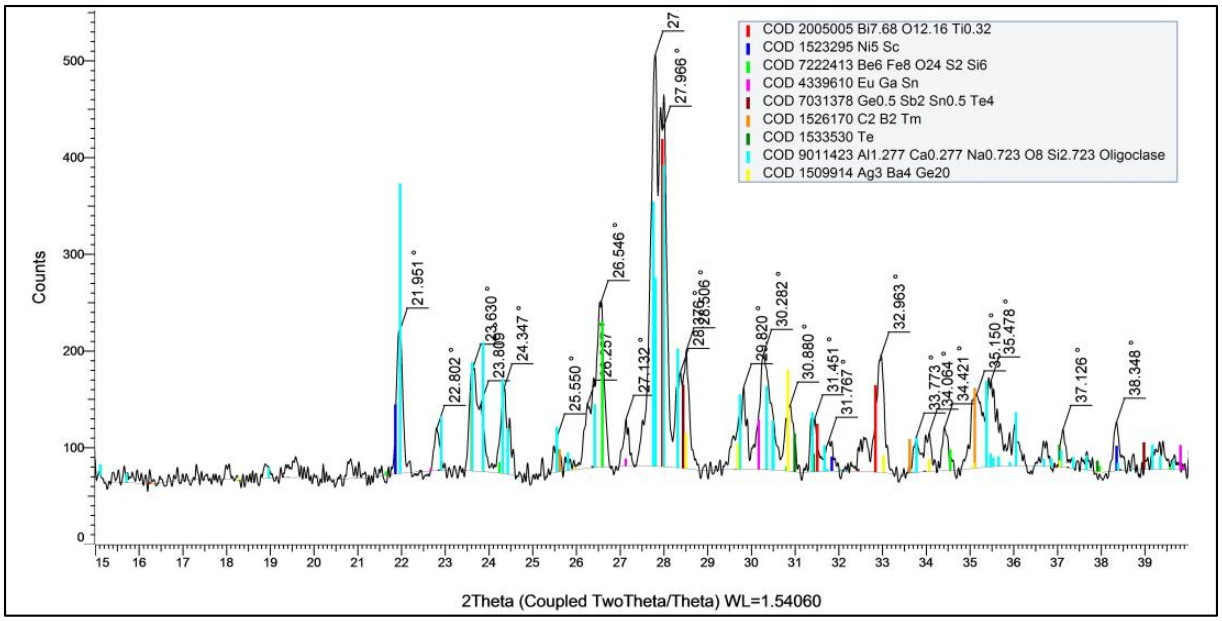


Figure 4.27: X-Ray Diffraction pattern of sample 23 showing the dominant mineral oligoclase feldspar and other accessory minerals.

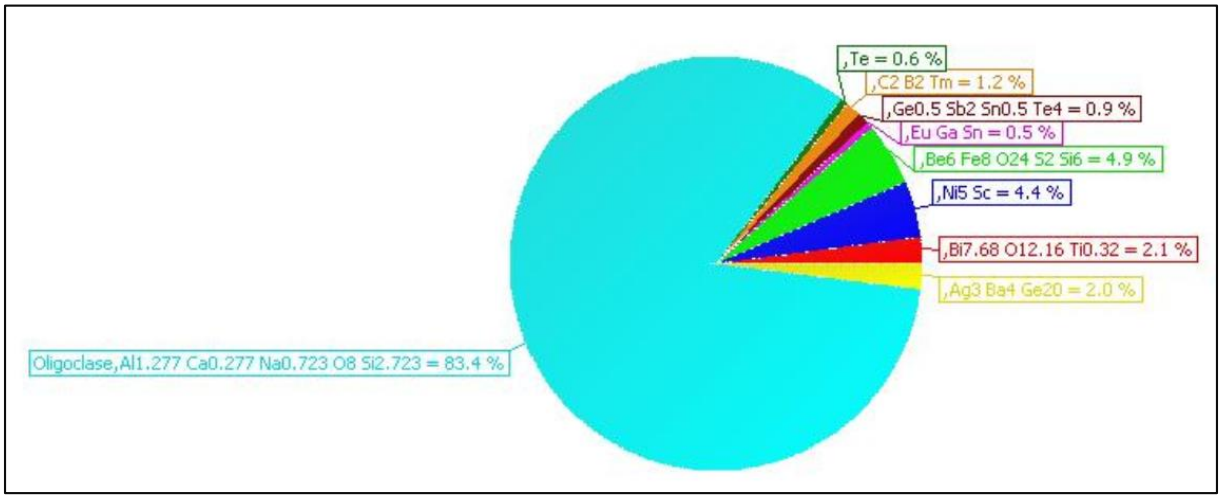


Figure 4.28: Pie Chart showing the percentage of each mineral in sample 23.

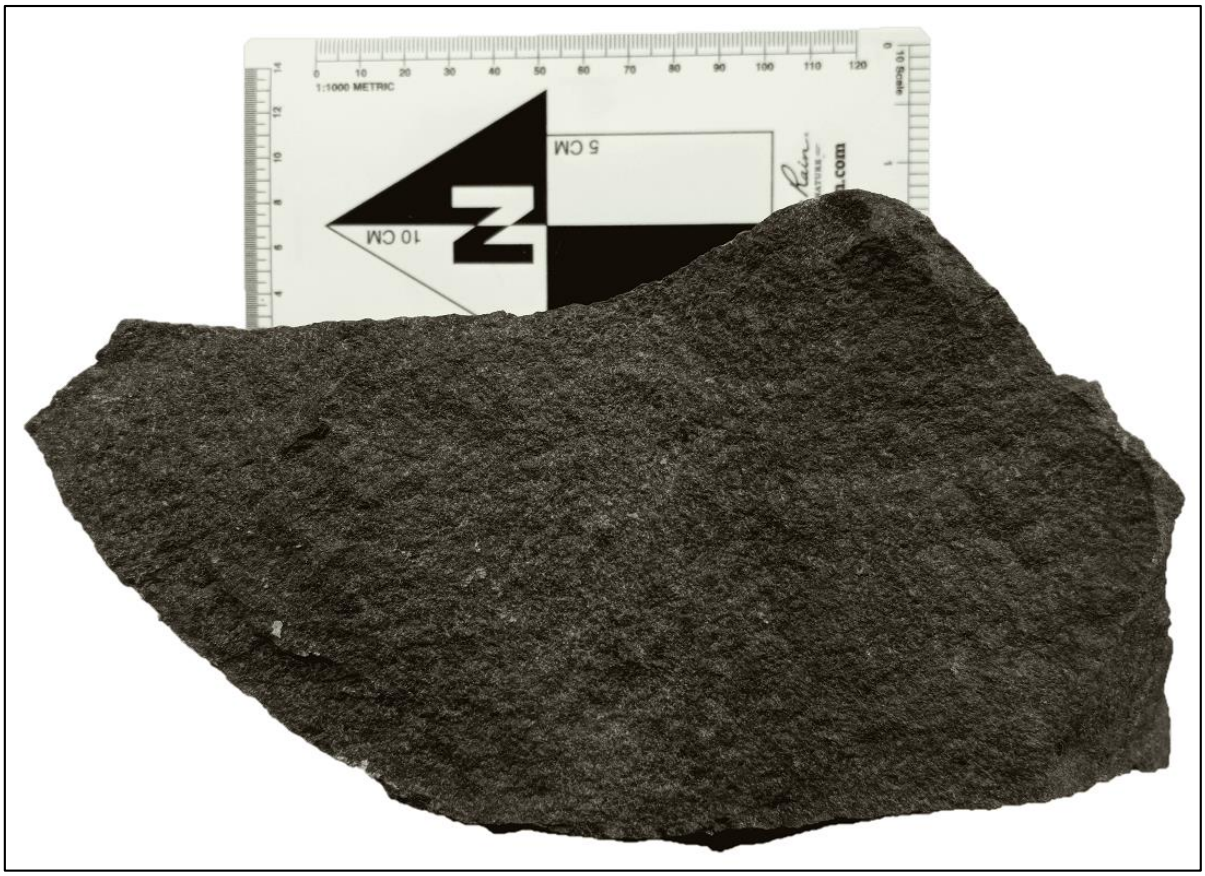


Figure 4.29: Hand specimen sample 23 of dolerite dyke at sampling point SMP-23 at coordinate: 00° 09' 31.00" S | 37° 55' 19.90" E.

Figure 4.30: Sampling point SMP-23 - dolerite massive dyke.

Posing as the scale, Figure 4.30, is the author of the report, Geologist Michael Karanja. The dolerite dykes which are about 50 meters wide (measured) contain danalite which is a common mineral in hydrothermal environments.

**Petrography of Sample 23**

In the rock section, Figure 4.31, the dolerite dykes display elongated lath-shaped crystals of plagioclase feldspars under mag. 40X. There are various accessory minerals noted through petrological studies some of which are opaque. Some of the accessory minerals are olivine and iron oxides. Also, very evident is a microfracture as indicated in the photomicrograph below signifying strain/stress processes.

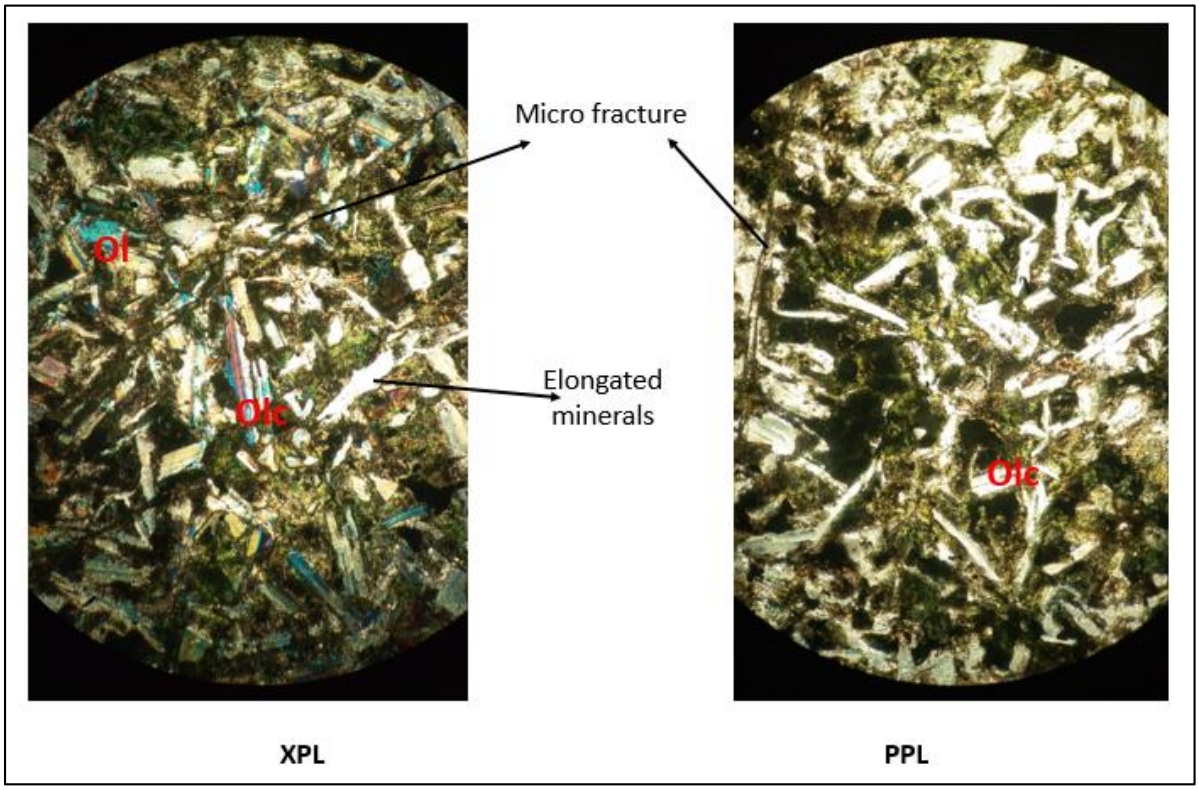


Figure 4.31: Sample 23 in rock section. Ol; Olivine, Olc; Oligoclase

### 4.1.4 Iron Ore

Several sections of the study area have occurrences of iron ore which appear as black/brown boulders or varied sizes. The iron ore pebbles are dense and some are of euhedral to subhedral, Figure 4.32, shapes with a dull metallic lustre. Several sections of the study area have heaps of ore from shallow mining sites dug up by the local community.


Figure 4.32: Hand specimen sample 02 of the iron ore at sampling point SMP-02 at coordinate: 0°10'38.20"S | 37°56'40.20"E.

Iron Ore deposits were noted in the following points: SMP-02, SMP-03, OBP 001, SMP-04, SMP-05, SMP-06, SMP-07, SMP-08, OBP-12, SMP-12, SMP-13, SMP-14 and SMP-17. One of the major outcomes of this study is to present the field relation between iron ore and the host rocks. Figure 4.33 shows this by presenting a boundary between a pyroxenite pegmatite and the iron ore. The pyroxenite pegmatite measured was 26cm in width and it was discordant. At the same observation point, the iron ore occurred as disseminated deposits within the pyroxenite in mm-size pebbles.

Figure 4.33: Contact zone between a mineralized pyroxenite and the iron ore at observation point OBP 012.

**XRD Analysis of the Iron Ores**

A majority of the iron ore deposits resembled each other from a macroscopic analysis. The samples that have been analyzed were selected based on spatial distribution to get much detail from a spatial perspective.

**i. Results of Sample No. 03**

From sample 03, Figure 4.34, attention is drawn to the black colorations which are intergrowths of iron ore inside the pyroxenite rocks. The outcrop appeared very coarse with reddish-brown and gray coloration. Some grains appeared tabular, others were yellowish and appeared shiny. The host rock is susceptible to weathering giving rise to soils with black pigments. Some of the minerals are tabular. This is a classic example showing the dissemination of iron ore in a pyroxenite host rock. Sample 03 was collected from sampling point SMP-03.

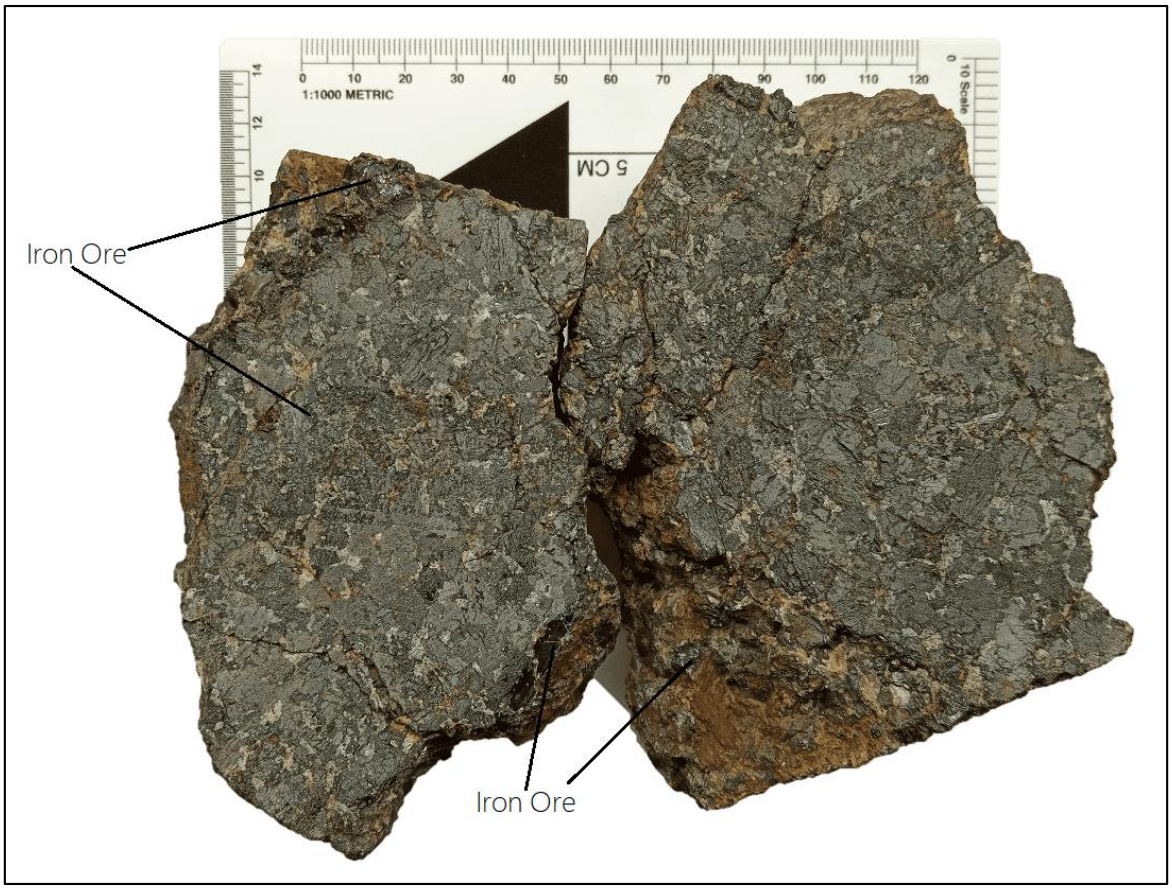


Figure 4.34: Hand specimen sample 03 of iron ore at sampling point SMP-03 at coordinate: 00° 10' 38.20" S | 37° 56' 40.50" E.

**Mineralogy:** XRD analysis shows that sections of the rock are heavily dominated by oxides of titanium and iron which tally up to 99.4% and the Coloradoite mineral 0.5% as an inclusion, Table 4.9. Of all the minerals, Pyrophanite is of the highest percentage, close to 27%. Sample 03 is coarse-grained with a porphyritic texture and with gray, black, and brown coloration of iron ore.

Table 4.9: XRD analysis of sample 03

| **Compound Name** | **Formula** | **Percentage** |
|---|---|---|
| Pyrophanite | $Mn_{0.5}$ $Ni_{0.5}$ $O_3$ Ti | 26.5 % |
| Magnesioferrite | $Fe_2$ Mg $O_4$ | 21.9 % |
| Tausonite | $Ca_{0.4}$ $O_3$ $Sr_{0.6}$ Ti | 18.6 % |
| Cuprospinel | $Cu_{0.86}$ $Fe_{2.14}$ $O_4$ | 17.8 % |
| Chromite | $Cr_2$ Fe $O_4$ | 14.6 % |
| Coloradoite | Hg Te | 0.5 % |
| **Total** | | **99.9%** |

The X-Ray Diffraction patterns and spread have been shown in Figure 4.35 and Figure 4.36 as recorded in the XRD machine.

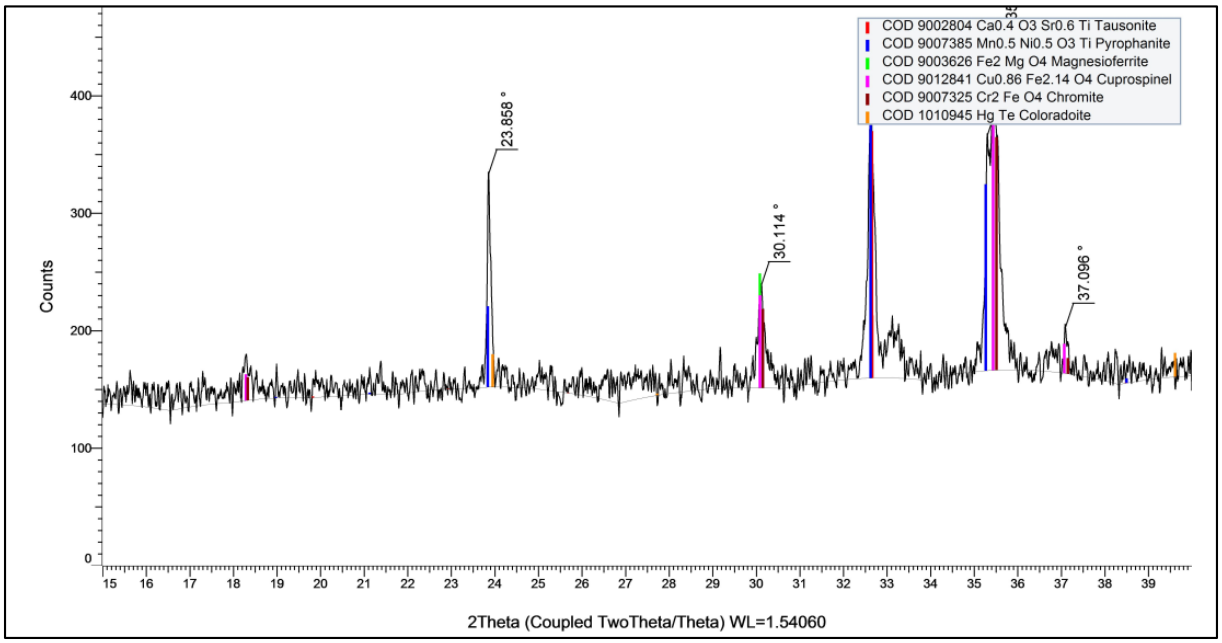


Figure 4.35: X-Ray Diffraction pattern of sample 03 showing the presence of titanium/iron oxide minerals in the ore sample.

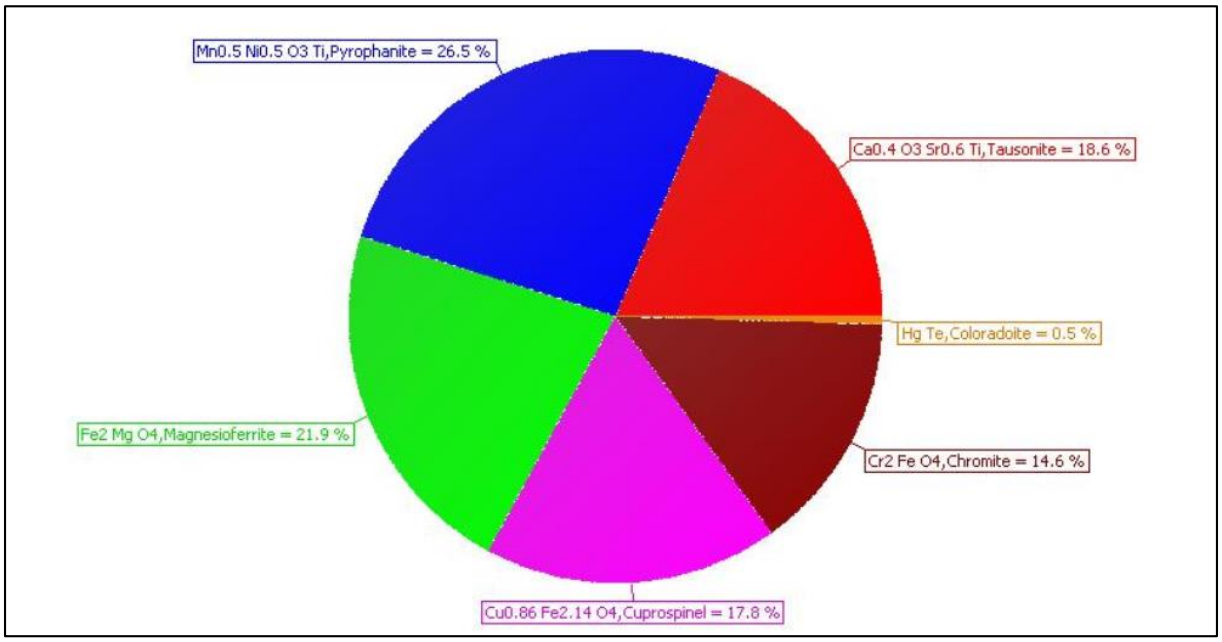


Figure 4.36: Pie Chart diagram showing the percentage of each mineral in sample 03 from sampling point SMP-03.

### ii. Results of Sample No. 05

Sample 05, Figure 4.37, was collected from a mining site, at sampling point SMP-05. Several mining sites were scattered in the vicinity of this sampling point. Also, several holes drilled by

the Directorate of the Geological Survey at the Ministry of Petroleum and Mining were seen in the area. The holes drilled were sited through ground magnetics but the results were not available for input in this report. There was a mafic dyke mapped at the area cutting across the units.

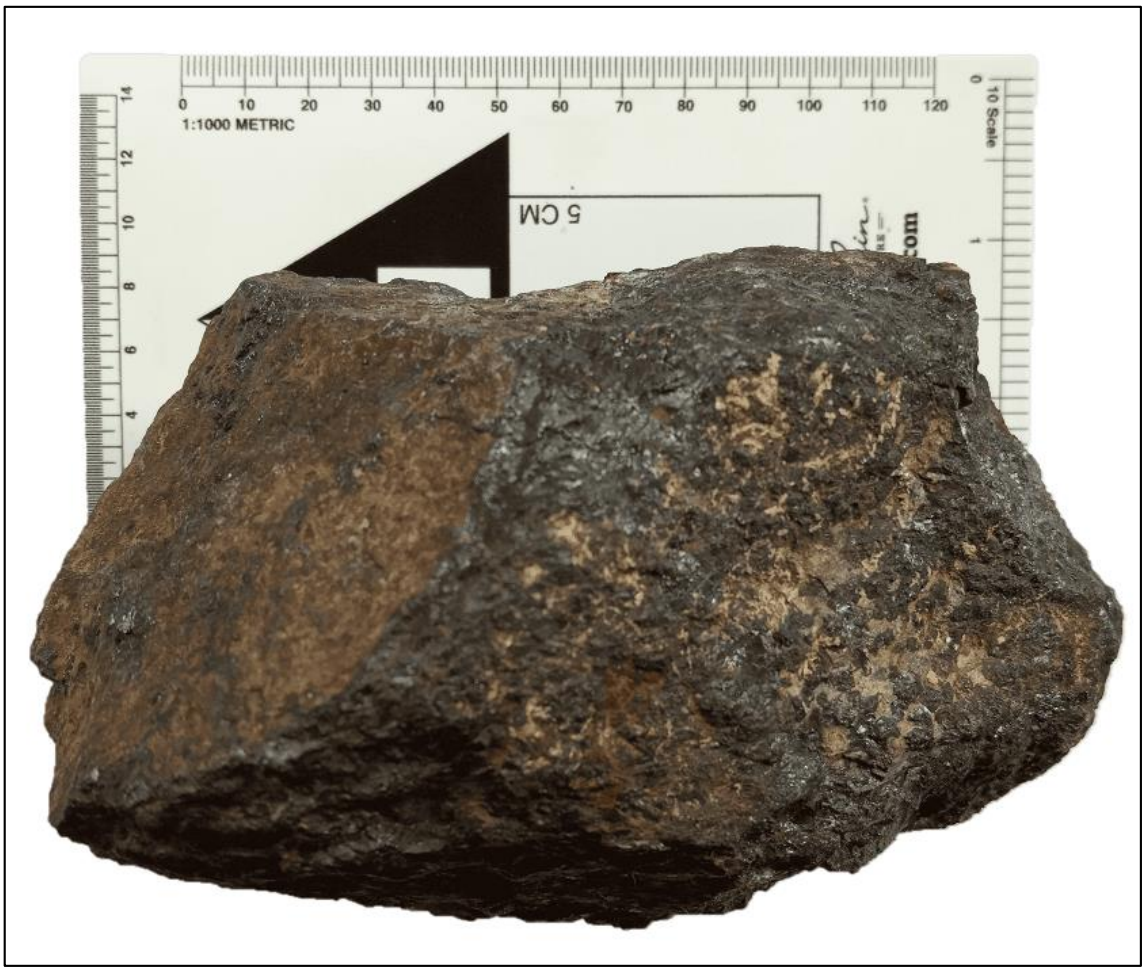


Figure 4.37: Hand specimen sample 05 an iron ore at sampling point SMP-05 at coordinate: 00° 10' 28.60" S | 37° 56' 39.50" E.

Mineralogy: Sample 05 XRD analytics, Table 4.10, show that iron and titanium bearing minerals comprise 93.8% of the ore sample. The ore is very compact and very dense and occurs in juxtaposition with the pyroxenite rocks.

Table 4.10: XRD analysis of sample 05

| **Compound Name** | **Formula** | **Percentage** |
|---|---|---|
| Magnetite | $Fe_3 O_4$ | 18.2 % |
| Ilmenite Species | $Fe_{1.1} O_3 Ti_{0.9}$ | 25.9 % |
| Ilmenite | $Fe O_3 Ti$ | 5.5 % |
| Lithium Zinc Iron Oxide | $Fe_{2.05} Li_{0.05} O_4 Zn_{0.9}$ | 18.7 % |
| Iron Silicate | $Fe_{2.719} O_4 Si_{0.289}$ | 11.3 % |
| Magnesium Tin Iron(III) Oxide | $Fe_{1.6} Mg_{1.2} O_4 Sn_{0.2}$ | 10.8 % |
| Copper Germanium Lanthanum | Cu Ge La | 6.0 % |
| Franklinite | $Al_{0.028} Fe_{1.91} Mg_{0.035} Mn_{0.426} O_4 Zn_{0.602}$ | 3.4 % |
| Cuprite | $Cu_2 O$ | 0.2 % |
| Ytterbium(Ii) Diindium Sulfide | $In_2 S_4 Yb_2$ | 0.1 % |
| **Total** | | **100.1%** |

The X-Ray Diffraction patterns and spread have been shown in Figure 4.38 and Figure 4.39 as recorded in the XRD machine.

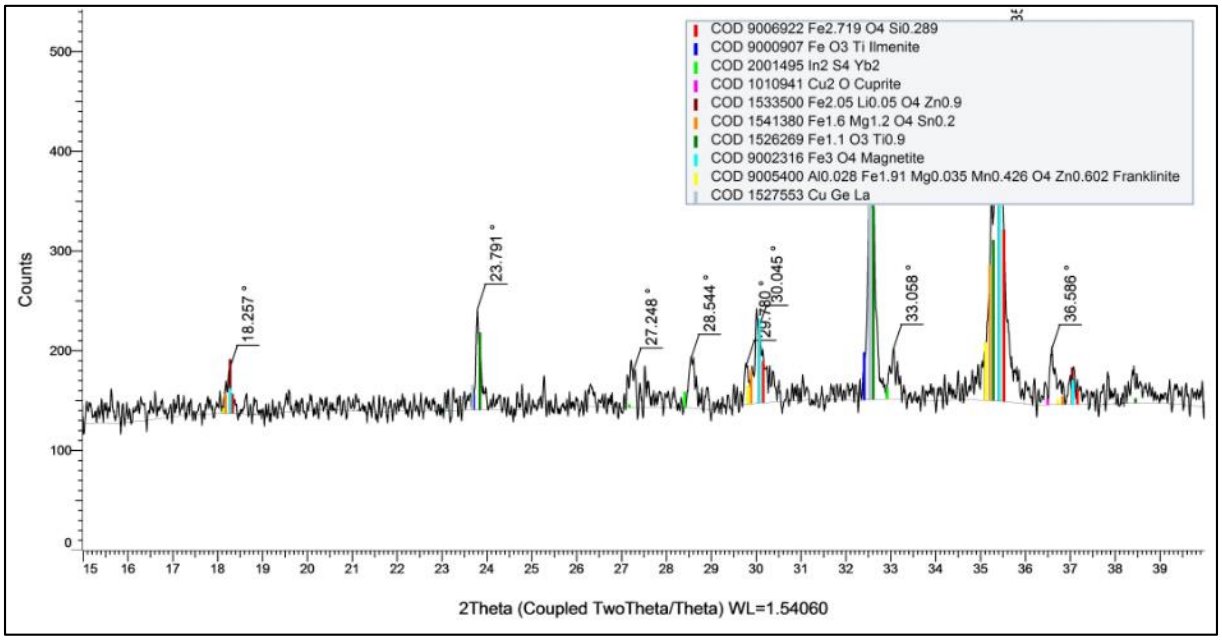


Figure 4.38: X-Ray Diffraction pattern of sample 05 showing the presence of iron - titanium minerals in the ore sample.

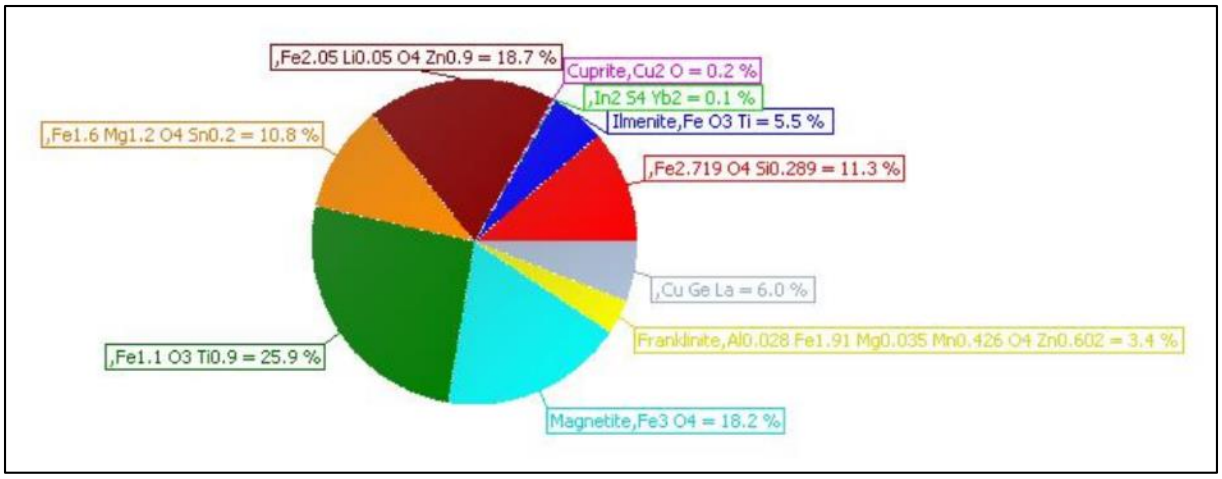


Figure 4.39: Pie Chart diagram showing the percentage of each mineral in Sample 05

### iii. Results of Sample No. 06

Sample 06, Figure 4.40, was collected from a heap of ore which had been piled up by the local small scale miners. The ore is dense, compact, has dark gray and dark brown coloration, and exhibits a dull metallic lustre.

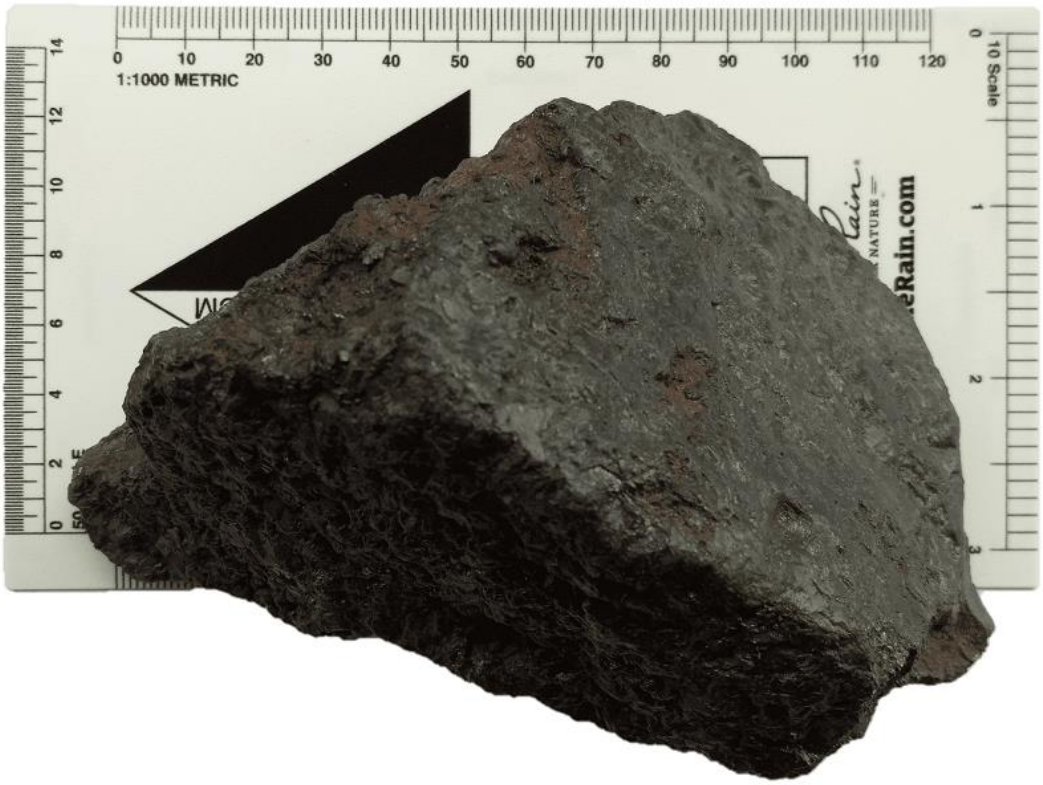


Figure 4.40: Hand specimen of sample 06 collected at sampling point SMP-06 at coordinate: 00° 10' 29.20"S | 37° 56' 41.80"E.

The XRD analysis shows that the ore has considerable quantities of iron – titanium bearing minerals totaling up to about 76.2% of the ore, Table 4.11. There are interesting and considerable quantities of minerals such as pyrophanite, osbornite, magnesioferrite, stishovite, and tricalcium aluminate. (Zaccarini *et. al.*, 2004) have described pyrophanite as a rare and rich species of the ilmenite group that can occur in hydrothermal environments containing manganese. On account of being a rare ilmenite species, the fact that pyrophanite has been reported in many of the analyzed ore samples is an interesting finding in this study.

(Rajendran and Nasir, 2014) take note of the occurrence of significant ore deposits in mafic-ultramafic series referring to magnesioferrite and other ores mentioning hydrothermal environments and serpentinization as possible modes of occurrence. Osbornite is of significant interest to the study area given that it is known to be a mineral of extraterrestrial origin and very rarely does it have a terrestrial origin (Dobrzhinetskaya *et al.*, 2009). In their study, (Dobrzhinetskaya *et al.*, 2014) concluded that Nitrogen in Osbornite has its origins from the mantle and that it combined with Titanium to form Osbornite. With this background, the occurrence of osbornite in Kithiori is of great importance given the rarity of the mineral in terrestrial settings.

Finally, sample 06 XRD analysis shows the occurrence of the highest pressure polymorph of $SiO_2$ in the form of Stishovite (Ross *et al.*, 1990). Its occurrence indicates the environment of origin of the iron ore. Table 4.11 below presents a summary of these minerals and their respective percentages.

Table 4.11: XRD analysis of sample 06

| **Compound Name** | **Formula** | **Percentage** |
|---|---|---|
| Pyrophanite | $Mn_{0.5}\ Ni_{0.5}\ O_3\ Ti$ | 30.0 % |
| Magnesioferrite | $Fe_2\ Mg\ O_4$ | 29.4 % |
| Osbornite | $N_4\ Ti_4$ | 16.8 % |
| Stishovite | $Si\ O_2$ | 13.2 % |
| Tricalcium Aluminate | $Al_2\ Ca_3\ O_6$ | 10.6 % |
| **Total** | | **100.0%** |

The X-Ray Diffraction peak patterns, Figure 4.41, of Pyrophanite, Osbornite, Stishovite, Tricalcium aluminate, and magnesioferrite together with their respective spreads, Figure 4.42, have been presented as recorded in the XRD machine.

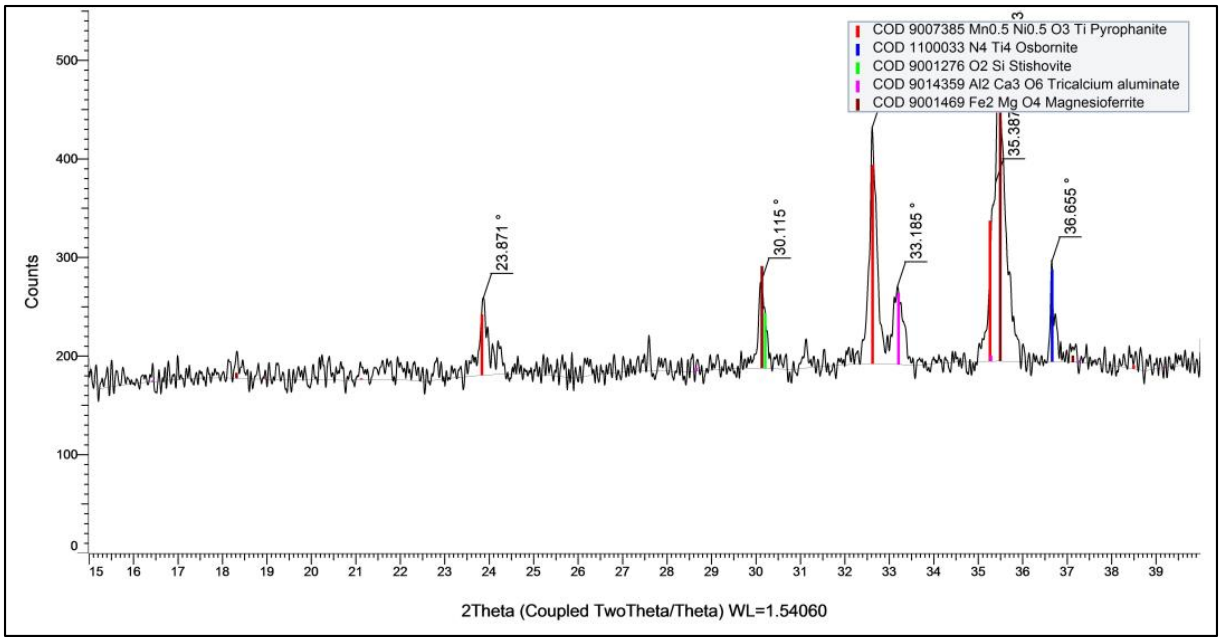


Figure 4.41: X-Ray Diffraction pattern showing the mineral species in ore sample 06.

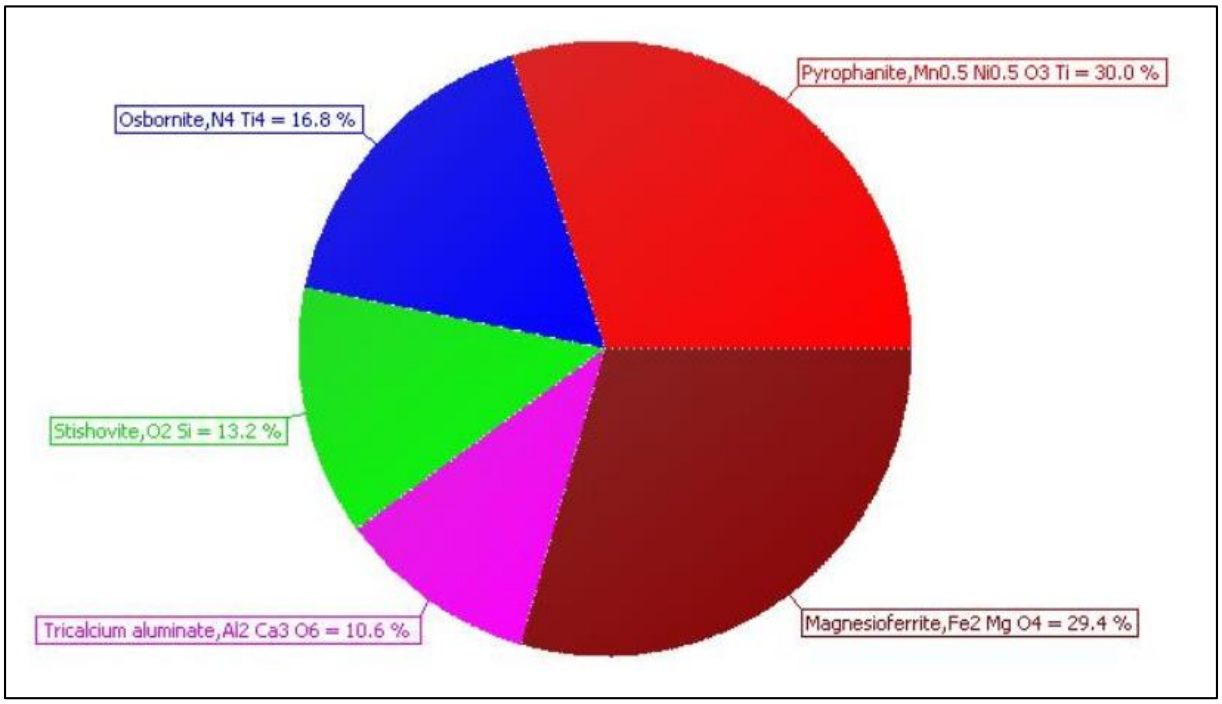


Figure 4.42: Pie Chart diagram showing the percentage of each mineral in sample 06 from SMP-06.

### iv. Results of Sample No. 08

Sample 08 was collected at the sampling point SMP-08 in an abandoned mine site. The ore is compact, resistant to weathering, dense and it occurs in dark gray coloration. Some of the ore boulders occur in euhedral shapes, Figure 4.43.


Figure 4.43: Hand specimen sample of ore at SMP-08 at coordinate: 00° 10' 20.90"S | 37° 56' 39.10"E.

**Mineralogy:** XRD analysis shows that the ore has varying quantities of Ti / Fe / Mn bearing minerals. There are considerable quantities of Pyrophanite which comprise 36.2% of the ore, possibly similar occurrence phenomena as the pyrophanite in sample 06. Analysis of sample 08 exhibited a fairly high concentration of rare earth elements such as Neodymium, Cerium, Lanthanum, and Praseodymium all in the mineral - Loparite. The complex minerals tally to about 76.5% of the rock whereas 23.5% is a rare earth mineral as presented in Table 4.12.

Table 4.12: XRD analysis of sample 08

| **Categorization** | **Compound Name** | **Formula** | **Percentage** |
|---|---|---|---|
| Complex Mineral | Pyrophanite | $Mn_{0.5}\ Ni_{0.5}\ O_3\ Ti$ | 36.2 % |
| | Magnesioferrite | $Fe_2\ Mg\ O_4$ | 17.5 % |
| | Brunogeierite | $Fe_2\ Ge\ O_4$ | 16.6 % |
| REE dominated | Loparite-(Ce) | $Ca_{0.13}\ Ce_{0.18}\ La_{0.09}\ Na_{0.46}\ Nb_{0.13}\ Nd_{0.05}\ O_3\ Pr_{0.02}\ Sr_{0.05}\ Ti_{0.87}$ | 23.5 % |
| Complex Mineral | Bixbyite C | $Fe\ Mn\ O_3$ | 6.2 % |
| | **Total** | | **100.0%** |

Loparite-(Ce) is a form of a Perovskite mineral that is commonly formed through magmatic processes and also common in some hydrothermal processes. Perovskite is resistant to weathering, (Castillo-Oliver *et al.*, 2016) high temperature, (Gralik *et al.*, 2014), occurs in silica deficient parental magma. Brunogeierite is a rare germanate from the spinel group (Welch *et al.*, 2001). The significant occurrence based on the XRD analysis is worth taking note of. Bixbyite on the other hand is an uncommon mineral and it comprises 6.2% of the minerals in sample 16. (Gutzmer and Beukes, 1997) suggest the occurrence of Bixbyite mineral to be through metasomatism and hydrothermal activities among other processes. The X-Ray Diffraction patterns and spread have been presented in Figure 4.44 and Figure 4.45 as recorded in the XRD machine. The x-axis and the y-axis presented show the 2θ peaks and counts of the respective minerals respectively.

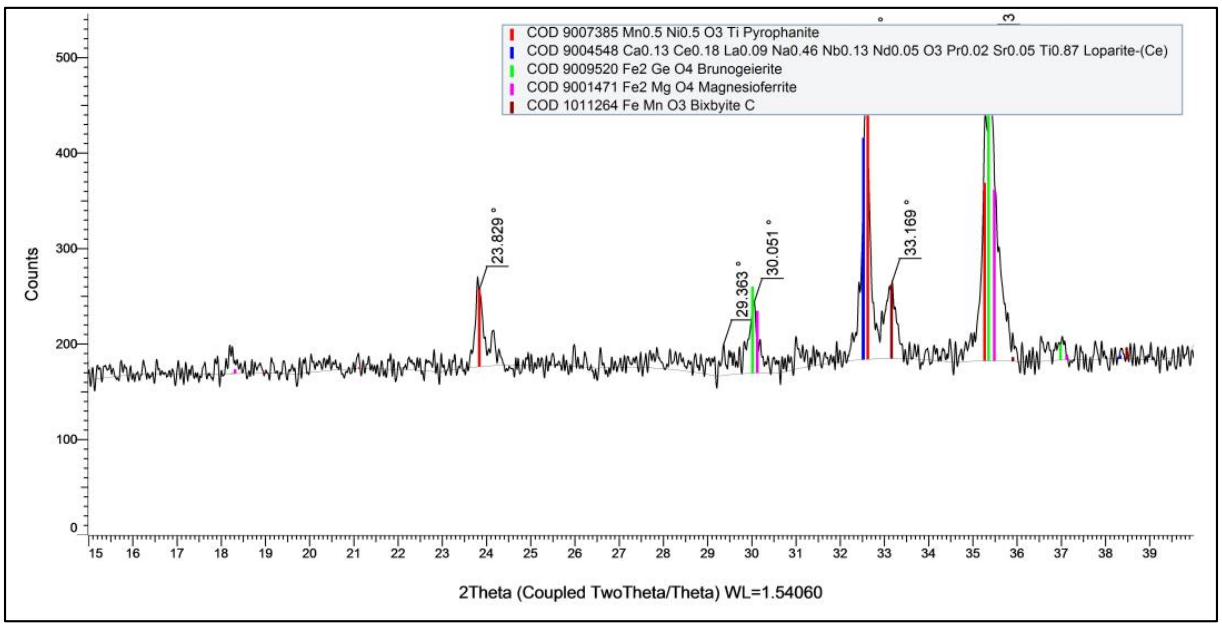


Figure 4.44: X-Ray Diffraction pattern showing the mineral species in ore sample 08.

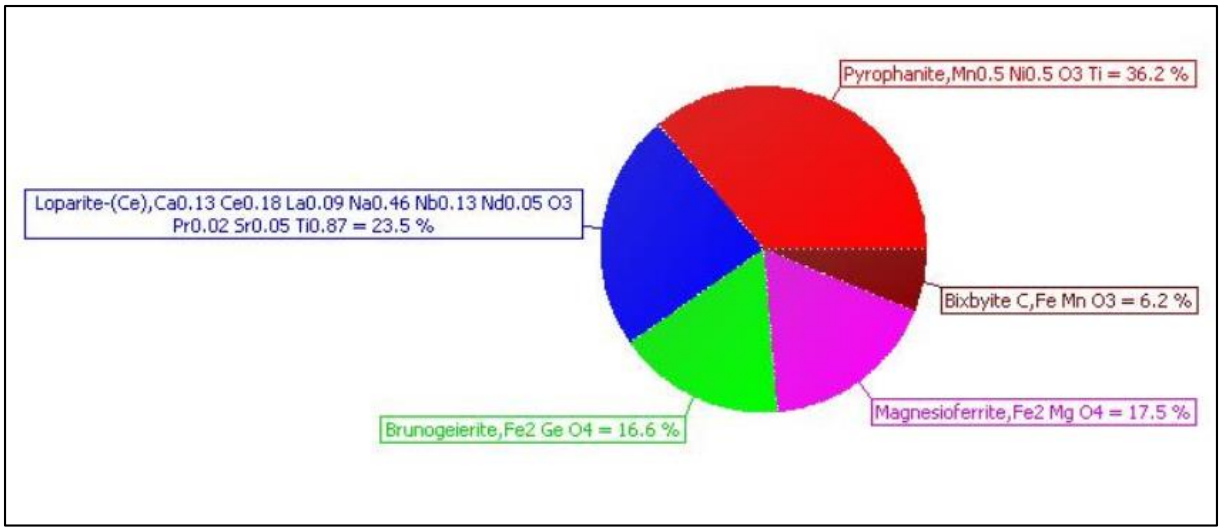


Figure 4.45: Pie Chart diagram showing the percentage of each mineral in sample 08.

### v. Results of Sample No. 12

Observation points OBP 016, OBP 017, and sampling point SMP-12 were mapped inside the Kithiori Primary School. The area was highly mineralized and most of the ores were covered by soils, the only visible ores were from nearby mining sites which had been abandoned at the time of the field study. Several heaps of ore were noted adjacent to the aforementioned mining sites. Pyroxene bearing rocks were seen as well demonstrating the association of the ores and pyroxene bearing rocks. A representative sample from sampling point SMP-12 was collected for analysis. The samples collected were dense and had brown to dark brown coloration, Figure 4.46.


Figure 4.46: Hand specimen sample of ore at SMP-12 at coordinate: 00° 09' 59.00"S | 37° 56' 43.20"E.

XRD analysis shows that sample 12 has considerable quantities of ilmenite totaling up to about 73.4% of the ore, iron-bearing minerals totaling 78.80%, titanium bearing minerals totaling 88.80% whereas iron – titanium bearing minerals totaling to 94.20%, Table 4.13. Praseodymium bearing mineral makes up just under 6.0% of the analyzed sample.

Table 4.13: XRD analysis of sample 12

| **Percentage** | **Compound Name** | **Formula** | **Percentage** |
|---|---|---|---|
| Principal Minerals (73.4%) | Ilmenite Species 2 | $Fe_{1.1}\ O_3\ Ti_{0.9}$ | 40.6 % |
| | Ilmenite Species 1 | $Fe_{1.2}\ O_3\ Ti_{0.8}$ | 32.8 % |
| Complex Minerals (20.8%) | --*unidentified* | $Ti_{0.89}\ V_{0.11}$ | 15.4 % |
| REE Compound Mineral (5.9 %) | Cadmium praseodymium | $Cd_2\ Pr$ | 5.9 % |
| Complex Minerals (20.8%) | Iron platinum | $Fe_{0.5}\ Pt_{0.5}$ | 5.4 % |
| | **Total** | | **100.1%** |

The X-Ray Diffraction patterns showing the respective peaks and count have been presented in Figure 4.47 whereas the respective spreads have been presented in Figure 4.48 as recorded by the XRD machine.

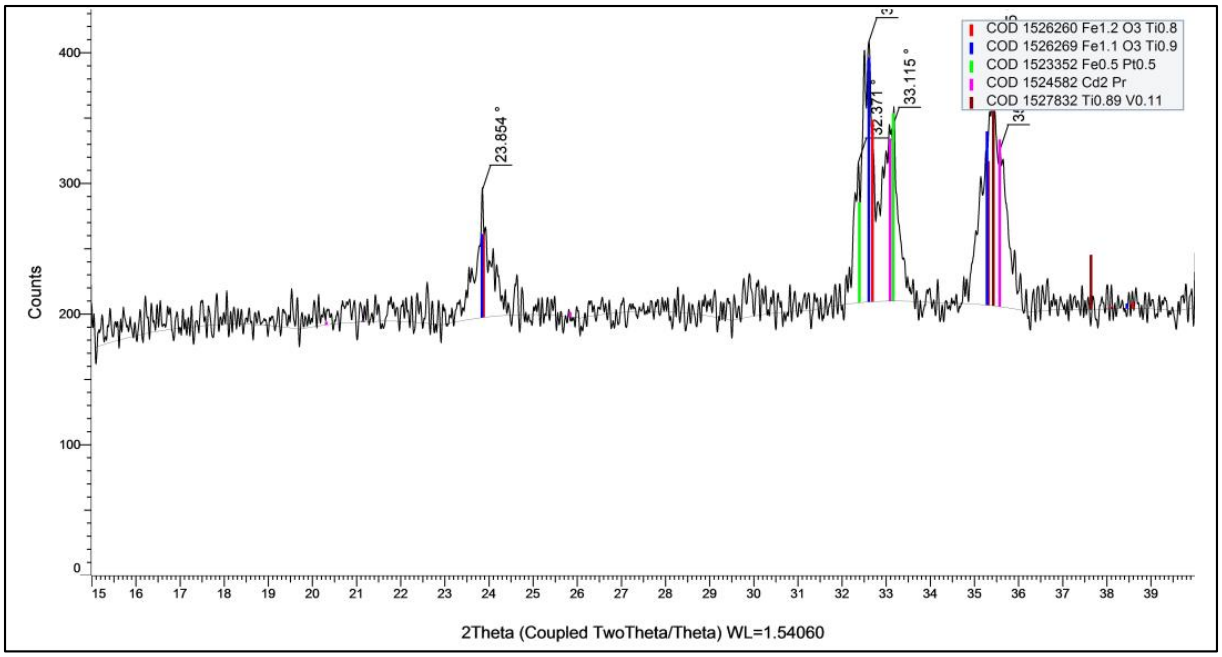


Figure 4.47: X-Ray Diffraction pattern showing the mineral species in ore sample 12.

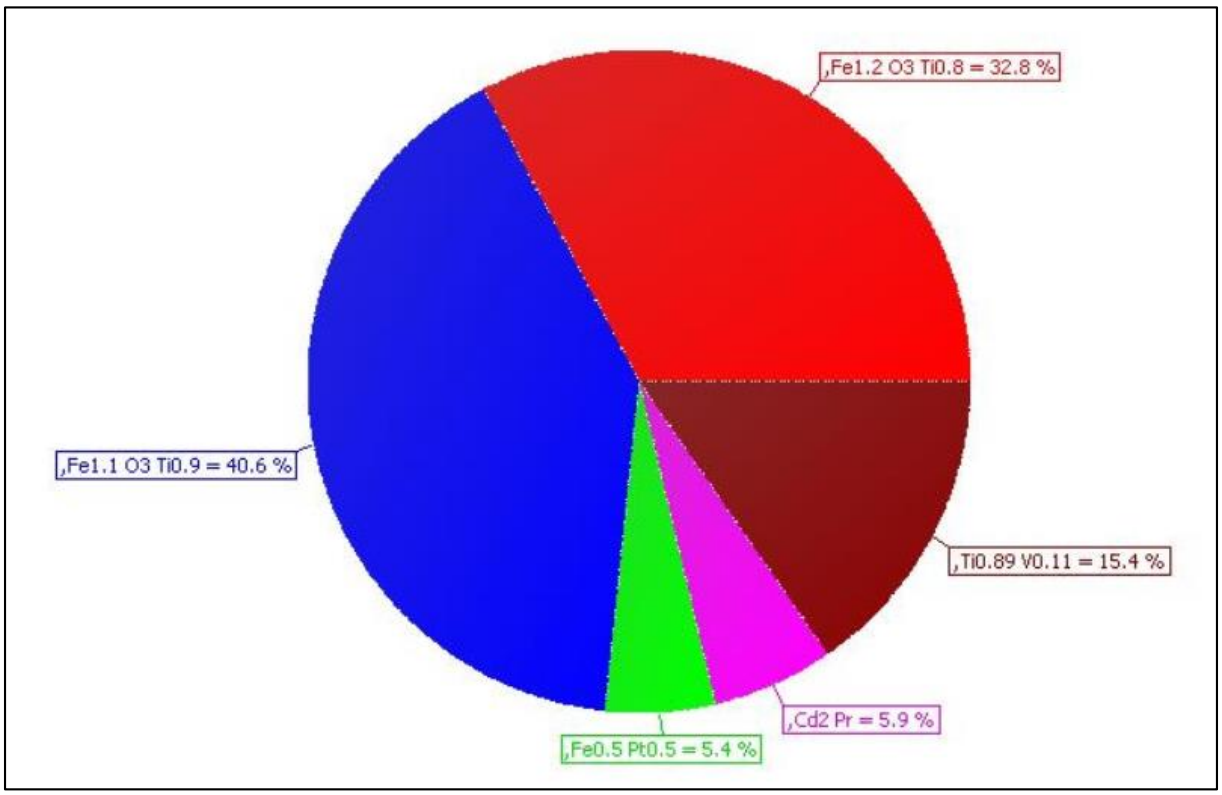


Figure 4.48: Pie Chart diagram showing the percentage of each mineral in sample 12.

### vi. Results of Sample No. 13

The iron ore at the sampling point SMP-13 was sampled at a roadside cutting. The red-brown soils on the surface were seen to contain pebbles of ore, in millimeter size. At the same point,

quartz pegmatites were noted and they contained amethyst crystals, Figure 4.50 and Figure 4.51. A few meters away, an abandoned quarry was mapped, but the exposure of outcrops was poor. The soils in the entire area are covered by millimeter-sized iron ore pebbles which are not susceptible to weathering, Figure 4.52Figure 4.52. Sample 13, Figure 4.49, which is compact, dark brown, and has a dull metallic lustre was collected for analysis.


Figure 4.49: Hand specimen sample 13 at coordinate: 00° 09' 40.00" S | 37° 56' 35.60" E.

**Mineralogy:** XRD analysis shows that the rock is heavily dominated by titanium – iron-rich minerals such as ilmenite, ecandrewsite, magnesioferrite, titanomagnetite, and achavalite which tally up to 92.40%, and the silica mineral stishovite 7.60%. Of the 92.40%, ilmenite is highest, comprising close to 30%. Together with ilmenite, magnesioferrite and stishovite have extensively been discussed in samples 05, 06, and 08 collected from SMP-05, SMP-06, and SMP-08 respectively. (Mitchell and LIferovich, 2004) have described Ecandrewsite as a rare isostructure of ilmenite and this possibly infers their coexistence in sample 13. (Matthews *et al.*, 2016) report of only three iron selenide phases known to exist, one of them is the β-phase achavalite. Table 4.14 presents a summary of the XRD analysis of sample 13 showing the percentages of each of the mineral species.

Table 4.14: XRD analysis of sample 13

| **Compound Name** | **Formula** | **Percentage** |
|---|---|---|
| Ilmenite | $Fe\ O_3\ Ti$ | 28.7 % |
| Ecandrewsite | $Mn_{0.3}\ O_3\ Ti\ Zn_{0.7}$ | 23.9 % |
| Magnesioferrite | $Fe_2\ Mg\ O_4$ | 18.9 % |
| Titanomagnetite | $Fe_{2.75}\ O_4\ Ti_{0.25}$ | 15.4 % |
| Stishovite | $O_2\ Si$ | 7.6 % |
| Achavalite | $Fe\ S_{0.5}\ Se_{0.5}$ | 5.5 % |
| **Total** | | **100%** |

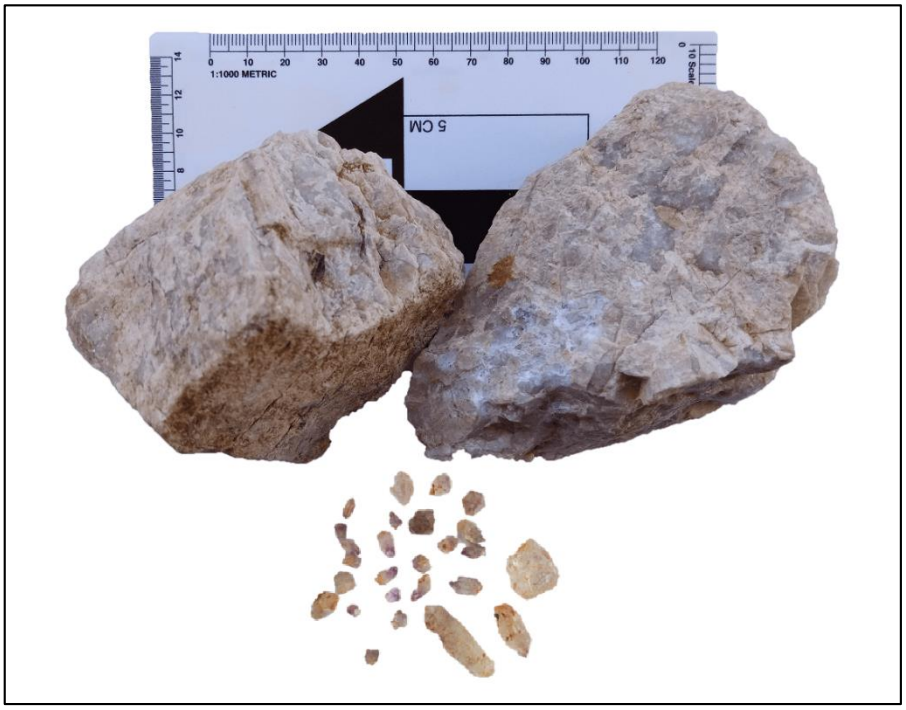


Figure 4.50 Prismatic amethyst crystals and the corresponding pegmatite rock units at SMP-13


Figure 4.51 Natural occurring environment of the prismatic amethyst crystals within the quartzite

Figure 4.52: The ore deposit at SMP-13 occurs close to mineralized quartz veins bearing moderately colored prismatic amethyst crystals.

The X-Ray Diffraction patterns and spread have been shown in Figure 4.53 and Figure 4.54 as recorded in the XRD machine.

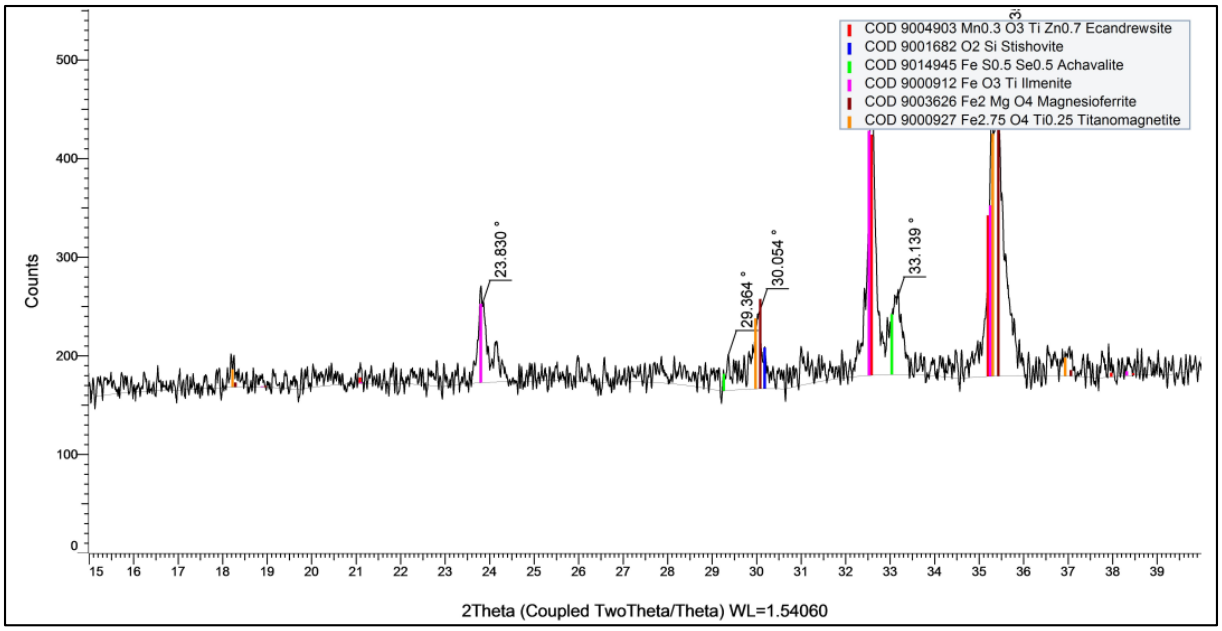


Figure 4.53: X-Ray Diffraction pattern of sample 13 showing the presence of titanium – iron-bearing minerals in the ore.

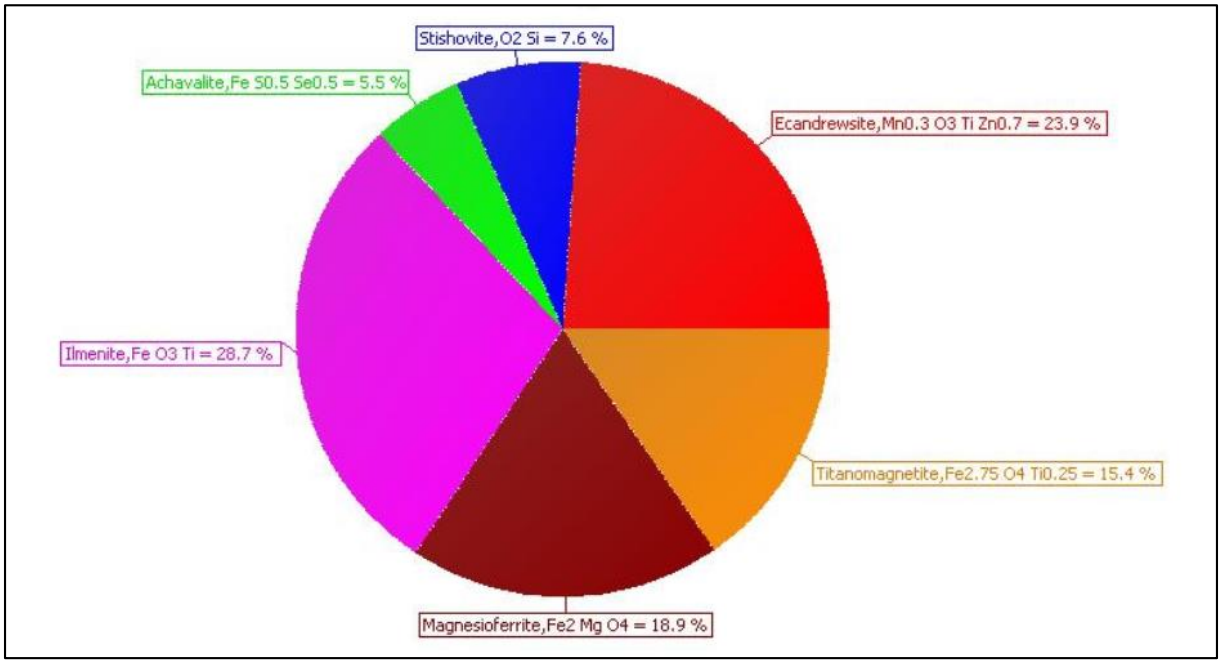


Figure 4.54: Pie Chart diagram showing the percentage of each mineral in sample 13.

### vii. Results of Sample No. 17

The sampling point SMP-17 was mapped next to an abandoned mine. The host outcrop was poorly exposed. It appeared grayish-green in color and weathered to reddish-brown soils. Quartz pebbles and the host rocks were minimally mineralized. The iron ores in the sampling

point were sampled for analysis, Figure 4.55. The ores were dark brown to dark gray, compact and resistant to weathering.

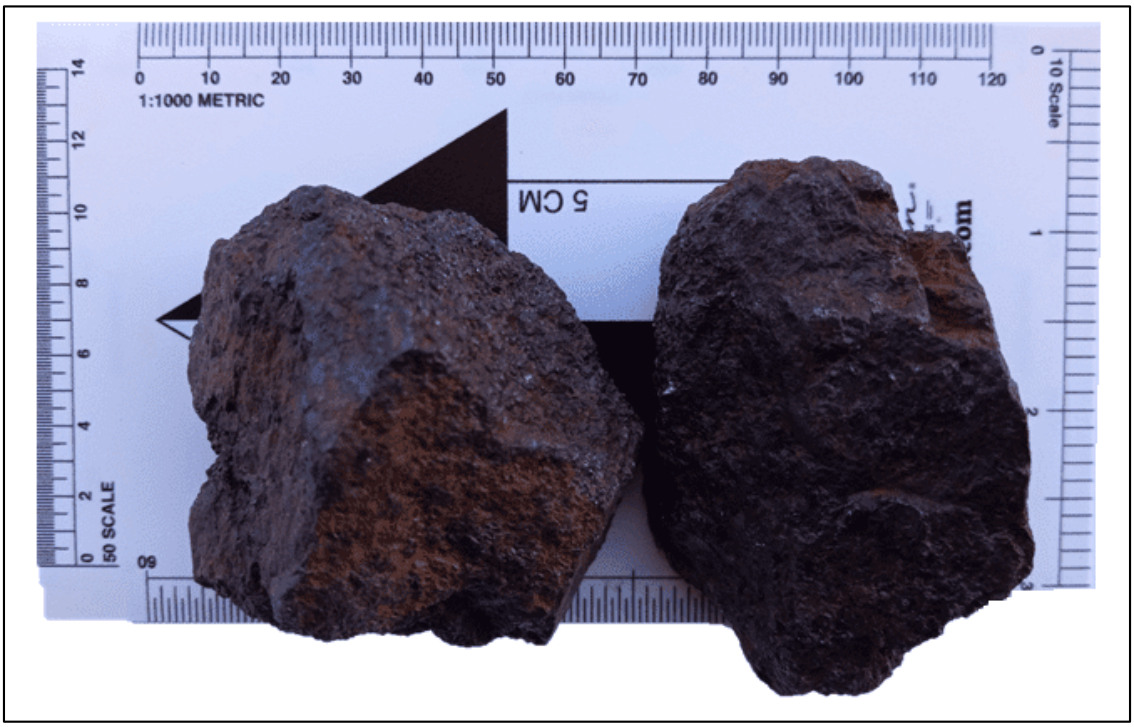


Figure 4.55: Hand specimen sample at sampling point SMP-17 at coordinate: 00° 10' 39.20" S | 37° 57' 20.70" E.

**Mineralogy:** XRD analysis shows that the ore has varying quantities of Ti / Fe / Mn bearing minerals which add up to about 65% in the form of pyrophanite, ecandrewsite, bixbyite, and hematite. As presented earlier in the report, these minerals have common occurrences among the iron ores sampled and analyzed. Of special interest, is the significant presence of Moissanite 3C which is about 28% of the mineralogy of the ore. (Schmidt *et al.*, 2014) describe moissanite as a mineral most commonly found in ultrabasic settings. Further, Moissanite has occasionally been likened to diamond based on its hardness of 9.5 and potentially similar environments of formation. Arsenolamprite at 7% is also significant for a little known mineral which has been likened to arsenic. Table 4.15 presents a summary of the minerals analyzed from the sample.

Table 4.15: XRD analysis of sample 17

| **Percentage** | **Compound Name** | **Formula** | **Percentage** |
|---|---|---|---|
| Moissanite 3C (28%) | Moissanite 3C | Si C | 28.0 % |
| Complex Minerals (38.4%) | Pyrophanite | $Mn_{0.5}$ $Ni_{0.5}$ $O_3$ Ti | 21.6 % |
| | Ecandrewsite | $Mn_{0.3}$ $O_3$ Ti $Zn_{0.7}$ | 16.8 % |
| Principal Mineral (14.5%) | Hematite | $Fe_2$ $O_3$ | 14.5 % |
| Complex Minerals (19.1%) | Bixbyite C | Fe Mn $O_3$ | 12.0 % |
| | Arsenolamprite | As | 7.1 % |
| | **Total** | | **100.0%** |

The X-Ray Diffraction patterns and spread have been shown in Figure 4.56 and Figure 4.57 as recorded in the XRD machine.

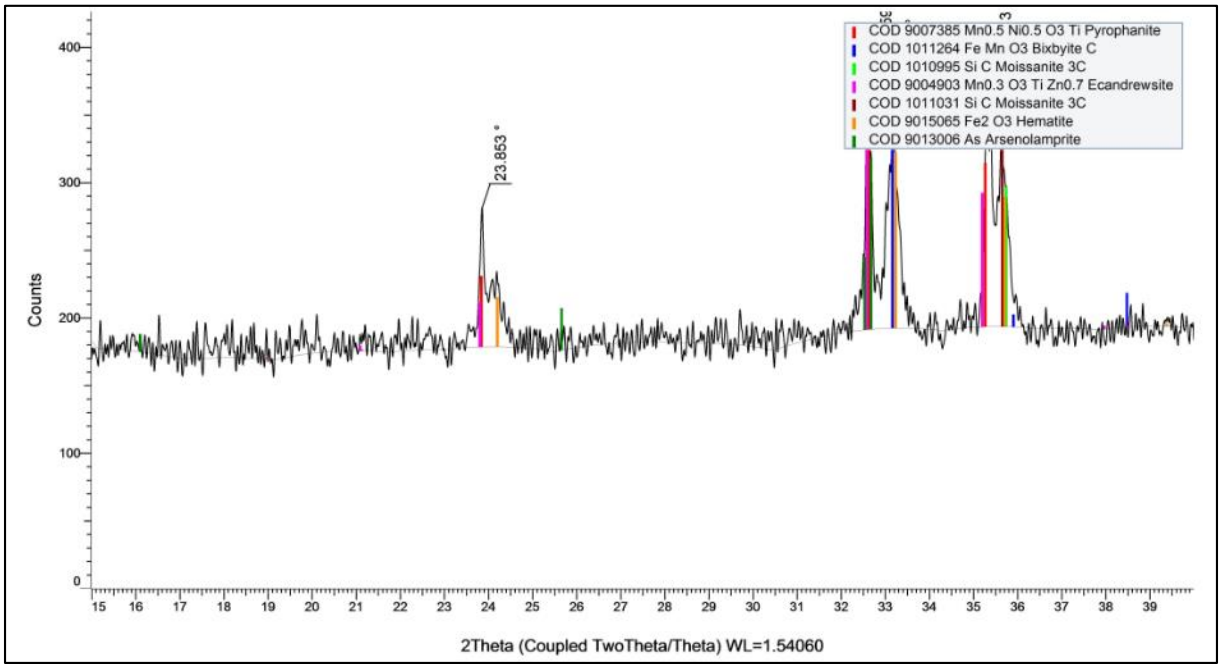


Figure 4.56: X-Ray Diffraction pattern showing the mineral species in ore sample 17.

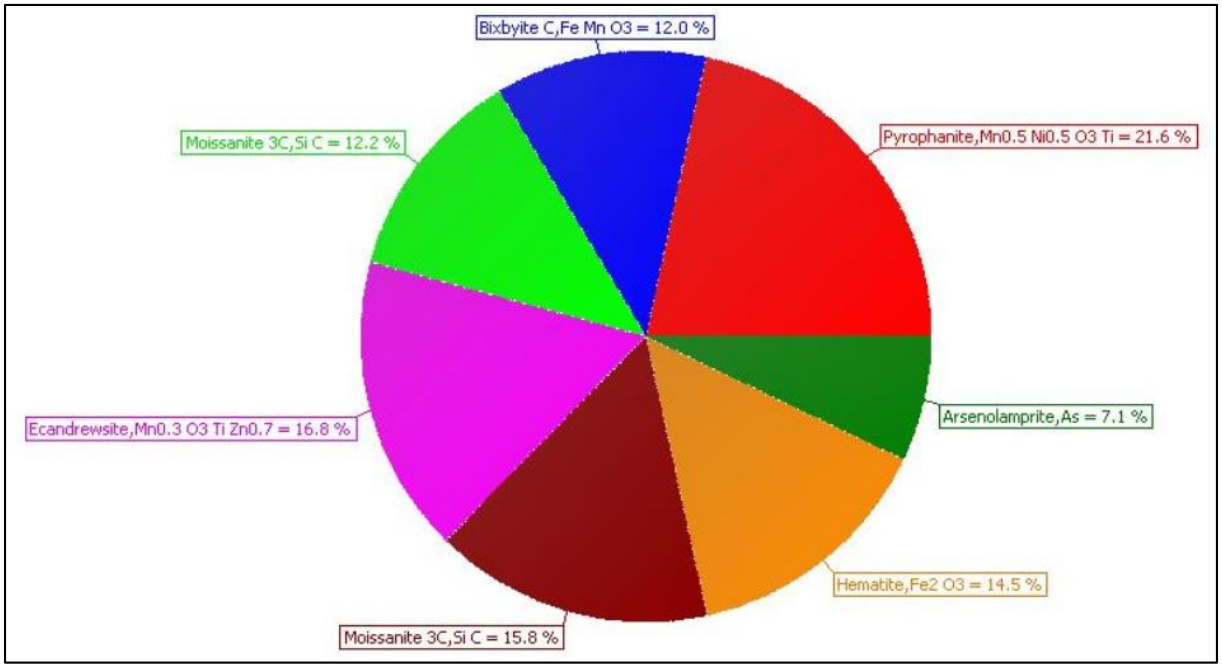


Figure 4.57: Pie Chart diagram showing the percentage of each mineral in sample 17.

Table 4.16 below presents a summary of all the analyzed samples of iron ore. These are samples 03, 05, 06, 08, 12, 13, and 17.

Table 4.16: XRD Summary of the Iron Ores

| **Sample 03** | | |
|---|---|---|
| **Compound Name** | **Formula** | **Percentage** |
| Pyrophanite | $Mn_{0.5}$ $Ni_{0.5}$ $O_3$ Ti | 26.5 % |
| Magnesioferrite | $Fe_2$ Mg $O_4$ | 21.9 % |
| Tausonite | $Ca_{0.4}$ $O_3$ $Sr_{0.6}$ Ti | 18.6 % |
| Cuprospinel | $Cu_{0.86}$ $Fe_{2.14}$ $O_4$ | 17.8 % |
| Chromite | $Cr_2$ Fe $O_4$ | 14.6 % |
| Coloradoite | Hg Te | 0.5 % |

| Sample 05 | | |
|---|---|---|
| **Compound Name** | **Formula** | **Percentage** |
| Ilmenite Species | $Fe_{1.1}$ $O_3$ $Ti_{0.9}$ | 25.9 % |
| Lithium Zinc Iron Oxide | $Fe_{2.05}$ $Li_{0.05}$ $O_4$ $Zn_{0.9}$ | 18.7 % |
| Magnetite | $Fe_3$ $O_4$ | 18.2 % |
| Iron Silicate | $Fe_{2.719}$ $O_4$ $Si_{0.289}$ | 11.3 % |
| Magnesium Tin Iron(III) Oxide | $Fe_{1.6}$ $Mg_{1.2}$ $O_4$ $Sn_{0.2}$ | 10.8 % |
| Copper Germanium Lanthanum | Cu Ge La | 6.0 % |
| Ilmenite | Fe $O_3$ Ti | 5.5 % |
| Franklinite | $Al_{0.028}$ $Fe_{1.91}$ $Mg_{0.035}$ $Mn_{0.426}$ $O_4$ $Zn_{0.602}$ | 3.4 % |
| Cuprite | $Cu_2$ O | 0.2 % |
| Ytterbium(Ii) Diindium Sulfide | $In_2$ $S_4$ $Yb_2$ | 0.1 % |
| **Sample 06** | | |
| **Compound Name** | **Formula** | **Percentage** |
| Pyrophanite | $Mn_{0.5}$ $Ni_{0.5}$ $O_3$ Ti | 30.0 % |
| Magnesioferrite | $Fe_2$ Mg $O_4$ | 29.4 % |
| Osbornite | $N_4$ $Ti_4$ | 16.8 % |
| Stishovite | Si $O_2$ | 13.2 % |
| Tricalcium Aluminate | $Al_2$ $Ca_3$ $O_6$ | 10.6 % |
| **Sample 08** | | |
| **Compound Name** | **Formula** | **Percentage** |
| Pyrophanite | $Mn_{0.5}$ $Ni_{0.5}$ $O_3$ Ti | 36.2 % |
| Loparite-(Ce) | $Ca_{0.13}$ $Ce_{0.18}$ $La_{0.09}$ $Na_{0.46}$ $Nb_{0.13}$ $Nd_{0.05}$ $O_3$ $Pr_{0.02}$ $Sr_{0.05}$ $Ti_{0.87}$ | 23.5 % |
| Magnesioferrite | $Fe_2$ Mg $O_4$ | 17.5 % |
| Brunogeierite | $Fe_2$ Ge $O_4$ | 16.6 % |
| Bixbyite C | Fe Mn $O_3$ | 6.2 % |

| Sample 12 | | |
|---|---|---|
| **Compound Name** | **Formula** | **Percentage** |
| Ilmenite Species | $Fe_{1.1}$ $O_3$ $Ti_{0.9}$ | 40.6 % |
| Ilmenite Species | $Fe_{1.2}$ $O_3$ $Ti_{0.8}$ | 32.8 % |
| --*unidentified* | $Ti_{0.89}$ $V_{0.11}$ | 15.4 % |
| Iron platinum | $Fe_{0.5}$ $Pt_{0.5}$ | 5.4 % |
| Cadmium praseodymium | $Cd_2$ Pr | 5.9 % |
| **Sample 13** | | |
| **Compound Name** | **Formula** | **Percentage** |
| Ilmenite | Fe $O_3$ Ti | 28.7 % |
| Ecandrewsite | $Mn_{0.3}$ $O_3$ Ti $Zn_{0.7}$ | 23.9 % |
| Magnesioferrite | $Fe_2$ Mg $O_4$ | 18.9 % |
| Titanomagnetite | $Fe_{2.75}$ $O_4$ $Ti_{0.25}$ | 15.4 % |
| Stishovite | $O_2$ Si | 7.6 % |
| Achavalite | Fe $S_{0.5}$ $Se_{0.5}$ | 5.5 % |
| **Sample 17** | | |
| **Compound Name** | **Formula** | **Percentage** |
| Moissanite 3C | Si C | 28.0 % |
| Pyrophanite | $Mn_{0.5}$ $Ni_{0.5}$ $O_3$ Ti | 21.6 % |
| Ecandrewsite | $Mn_{0.3}$ $O_3$ Ti $Zn_{0.7}$ | 16.8 % |
| Hematite | $Fe_2$ $O_3$ | 14.5 % |
| Bixbyite | Fe Mn $O_3$ | 12.0 % |
| Arsenolamprite | As | 7.1 % |

### 4.1.5 Ferro-Gabbro

The Ferro-gabbro rock, sampled from SMP-20, is one of the unique rocks that showed a classic transition into an iron ore through alteration. The area was heavily stained by ore pebbles of millimeter size and heavily weathered host rock. The pebbles were dense, coarse-grained, and are poorly exposed. A sample was collected for analysis and from the XRD analysis, it is noted that there is a considerable amount of pyroxene mineral - diopside whereas the composition of the unit also comprises of iron dominated mineral species, Table 4.17. As mentioned elsewhere in the report, the mineral permingeatite, a product of hydrothermal alteration is recorded in the analysis.

Table 4.17: XRD analysis of sample 20

| **Compound Name** | **Formula** | **Percentage** |
|---|---|---|
| Diopside | $Ca\ Fe_{0.26}\ Mg_{0.74}\ O_6\ Si_2$ | 43.2 % |
| Silver Gallium Sulfide | $Ag\ Ga\ S_2$ | 18.8 % |
| Chromium Chalcogenide Spinel | $Cr_{1.37}\ Se_{0.75}\ Te_{1.25}$ | 9.1 % |
| Cobalt Copper Praseodymium | $Co_{2.5}\ Cu_{2.5}\ Pr$ | 7.1 % |
| Sphalerite | $Fe_{0.11}\ S_{0.99}\ Zn_{0.9}$ | 7.1 % |
| Lanthanum Strontium Barium Manganese Oxide | $Ba_{0.2}\ La_{0.02}\ Mn\ O_3\ Sr_{0.78}$ | 6.0 % |
| Lanthanum Barium Calcium Copper Oxide | $Ba\ Ca\ Cu_3\ La\ O_{7.06}$ | 2.7 % |
| Lutetium Silicide | $Lu\ Si_{1.8}$ | 2.6 % |
| Disamarium Trioxide | $O_3\ Sm_2$ | 2.2 % |
| Permingeatite | $Cu_3\ Sb\ Se_4$ | 1.2 % |
| **Total** | | **100.0%** |

### 4.1.6 Pyroxenite

Several sections of the study area have occurrences of rocks rich in pyroxene minerals such as diopside and augite with no occurrence of quartz. The units appear striated and greenish which are moderate to strongly altered. The rocks have distinct lines of weakness and have a dull metallic lustre. In some cases, the pyroxenite appears as pegmatites of varying widths, Figure 4.58.

Figure 4.58: Sections of the study area have pyroxene rich rocks which occur as pegmatites cutting through the mineralization, observation point OBP 012.

The pyroxenite units were mapped in the following points: OBP 001, SMP-04, OBP 012, OBP 013, and OBP 026. Key interest is drawn to observation point OBP 013, a hill with an elevation of 648 meters. The rock units on this hill are monomineralic and have a high degree of weathering, through physical, biological, and chemical processes. The pyroxenite weathers to brownish soils.

Sampling point SMP-04 was located next to an ore mining site. This was a heap of millimeter size iron ore. Pebbles appeared euhedral. Two samples were collected. One was a sample of ore and another one for the host rock which looked monominerallic, Figure 4.59, but mineralized. The soil in the entire area had very many pebbles of iron ore.


Figure 4.59: Hand specimen sample of ore at sampling point SMP-04 at coordinate: 00° 10' 31.20" S | 37° 56' 40.30" E.

**XRD Analysis of Pyroxenite**

The pyroxenites occur in the form of dykes and some cases as segregations. All the pyroxene samples collected resembled each other from a macroscopic perspective. Sample 04, Figure 4.59, was analyzed and the results have been presented below.

i. **Results of Sample No. 04**

**Mineralogy:** XRD analysis of sample 04 from SMP-04 shows that the rock is dominated by clinopyroxene minerals diopside ferrian and augite up to 86.40% with the other minerals such as platinum oxide, antimony vanadate among others comprising 13.60%. Table 4.18 presents a summary of the minerals as analyzed during XRD analysis.

Table 4.18: XRD analysis of sample 04

| **Compound Name** | **Formula** | **Percentage** |
|---|---|---|
| Augite | $Al_{0.7}$ Ca $Fe_{0.2}$ $Mg_{0.6}$ $O_6$ $Si_{1.5}$ | 50.3 % |
| Diopside-Ferrian | Ca $Fe_{0.194}$ $Mg_{0.906}$ $O_6$ $Si_{1.9}$ | 36.1 % |
| Antimony Vanadate | $O_4$ Sb V | 4.6 % |
| Dilanthanum Dioxide Telluride | $La_2$ $O_2$ Te | 3.0 % |
| Silver Antimony Telluride | Ag Sb $Te_2$ | 2.3 % |
| Cerium Carbide Indide | C $Ce_3$ In | 1.7 % |
| Platinum Oxide | O Pt | 1.1 % |
| Chalcogenide Stannite | $Cu_{2.2}$ $Se_{3.9}$ Sn $Te_{0.1}$ $Zn_{0.78}$ | 0.9 % |
| **Total** | | **100%** |

The X-Ray Diffraction patterns and spread for sample 04 have been shown in Figure 4.60 and Figure 4.61 as recorded in the XRD machine.

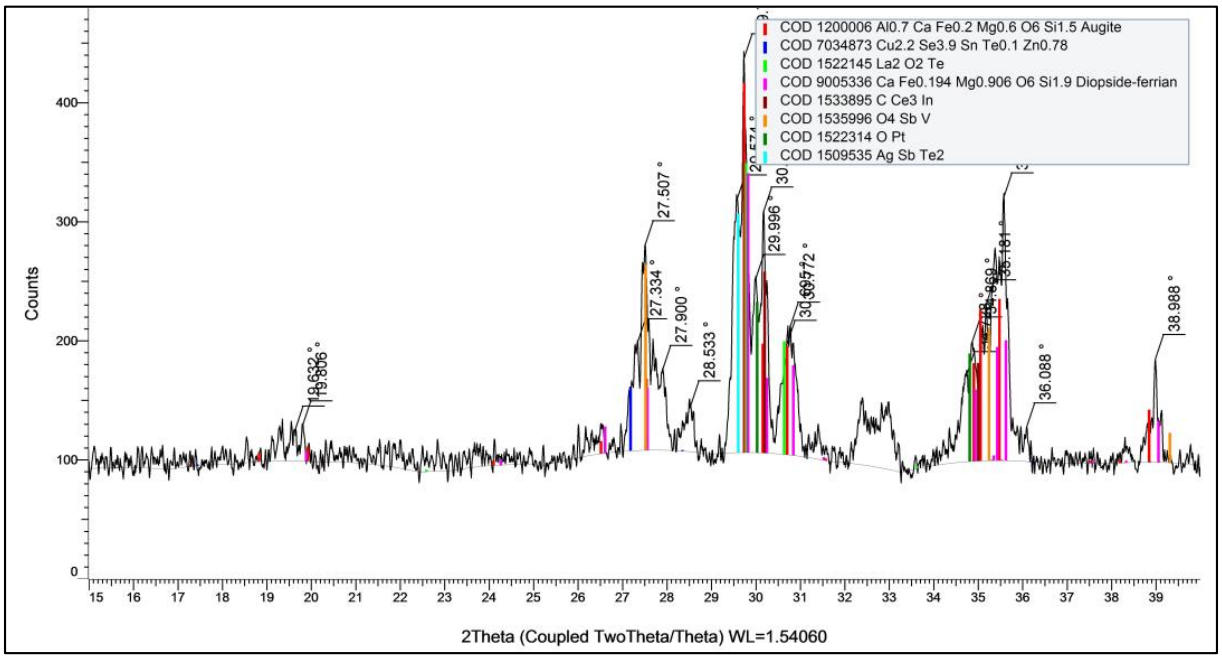


Figure 4.60: X-Ray Diffraction pattern showing the presence of pyroxene minerals in sample 04.

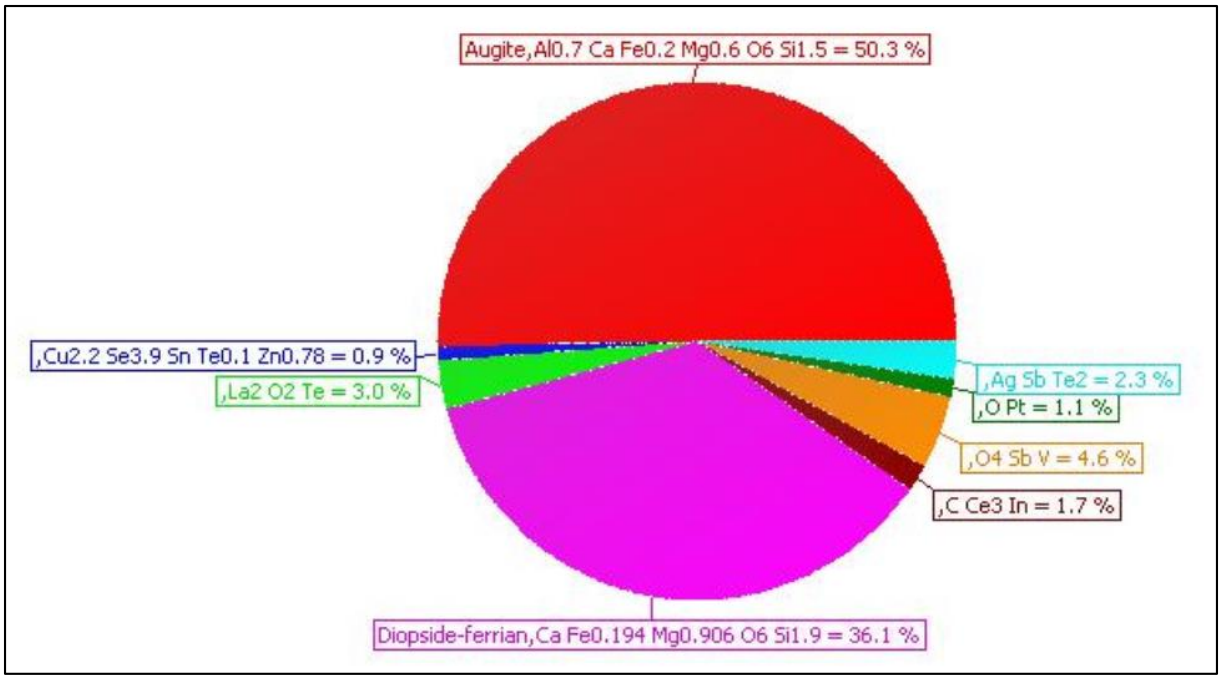


Figure 4.61: Pie Chart diagram showing the percentage of each mineral in sample 04.

### 4.1.7 Quartzofeldspathic Pegmatite

#### i. Results of Sample No. 18

A sample of the quartzofeldspathic pegmatite Figure 4.62 was collected from the sampling point SMP-18 from a massively exposed outcrop along the bank of River Thingithu. The pegmatite has metamorphic fabric Figure 4.62 (a) and is seen to have intruded into the host rocks based on the law of superposition. The pegmatite is coarse-grained and appears to contain substantial quantities of biotite crystals Figure 4.62 (b). From a macroscopic perspective, feldspars and quartz are the principal constituents of the rock. The pegmatite was observed at coordinate: 00° 10' 13.10" S | 37° 57' 41.90" E.

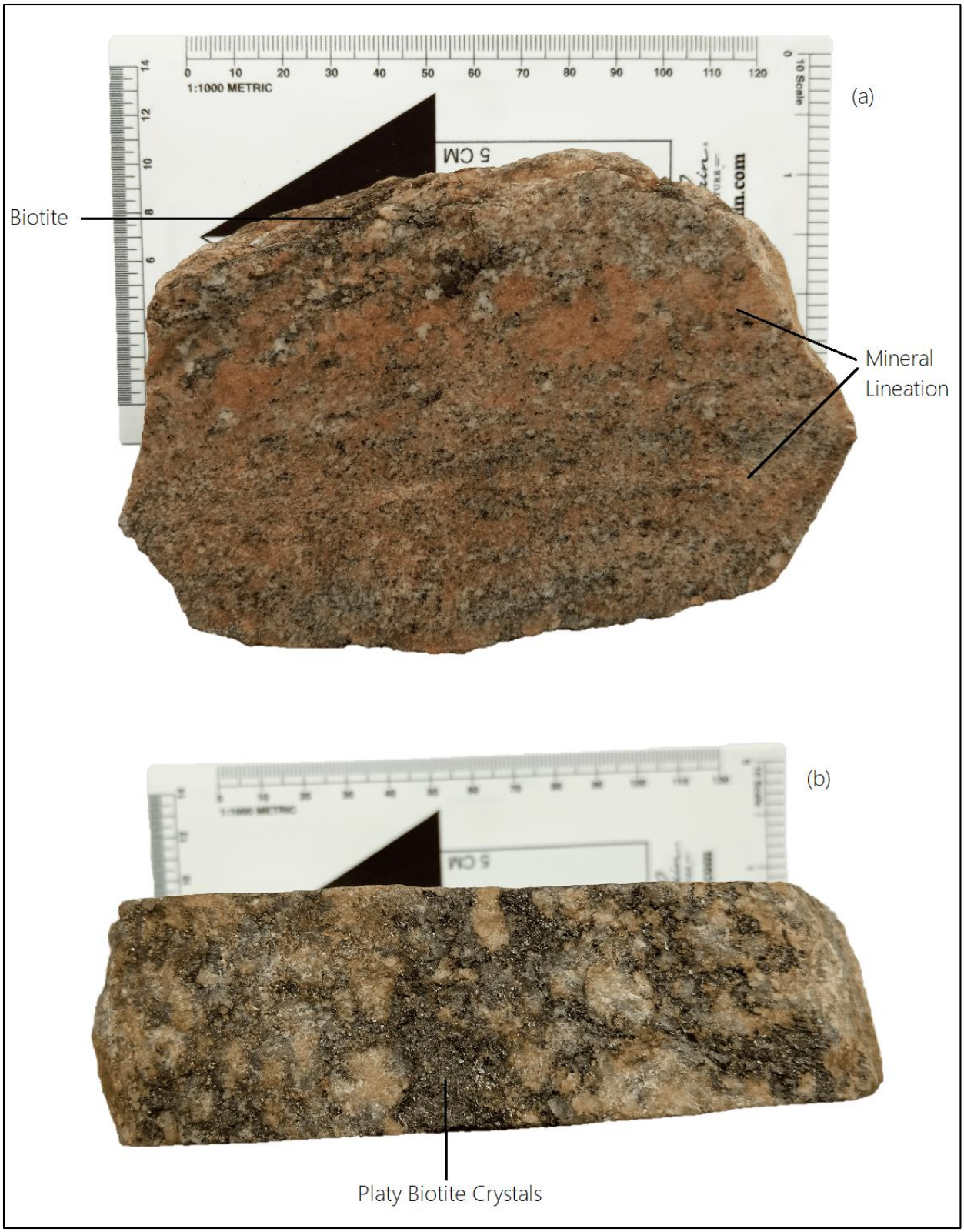


Figure 4.62: Hand specimen sample of the pegmatite at sampling point SMP-18

Kunkar limestone appears on the edges of the pegmatite inferring possible shearing processes on the planes of the pegmatite and the gabbroic rocks, Figure 4.63. This suggests heterogeneous

subsurface pressures and heat which gave the pegmatite some metamorphic fabric. The direction of the shear stress is not apparent due to the lack of clear apophysis on the pegmatite.

In theory, the source of the pegmatite would be inferred to anatectic sources. The basis for this argument is that the area is principally dominated by gabbro rocks which generally appear to be intrusive and discordant. The action of the gabbroic intrusions may have resulted in localized contact metamorphism which may have caused partial melting of deep-seated host rocks. The melts may have made their way up the fractures to form the pegmatitic rocks.

Figure 4.63: Discordant Quartzofeldsparthic Pegmatite at sampling point SMP-18

Joints were recorded, trending 310 degrees and 320 degrees. The rocks were of varied grain sizes. Dykes were noted and they were either mafic or felsic with kunkar limestone noted at the contact zone of the two units. Table 4.19 presents a summary of the XRD analysis showing the percentages of the mineral species i.e indicating that the rock is dominated by feldspars and quartz adding up to 99.30%.

Table 4.19: XRD analysis of Quartzofeldspathic Pegmatite, sample 18

| **Compound Name** | **Formula** | **Percentage** |
|---|---|---|
| K-Feldspar | Al K $O_8$ $Si_3$ | 52.5 % |
| Quartz | $O_2$ Si | 46.8 % |
| Strontium Telluride | Sr Te | 0.7 % |
| **Total** | | **100.0%** |

The X-Ray Diffraction patterns and spread have been presented in Figure 4.64 and Figure 4.65 as recorded in the XRD machine. As has been presented, feldspar and quartz minerals take a majority of the mineral representation of the sample. At 0.7% the presence of Tellurium suggests the possibility of having had hydrothermal influence in the formation of the rock.

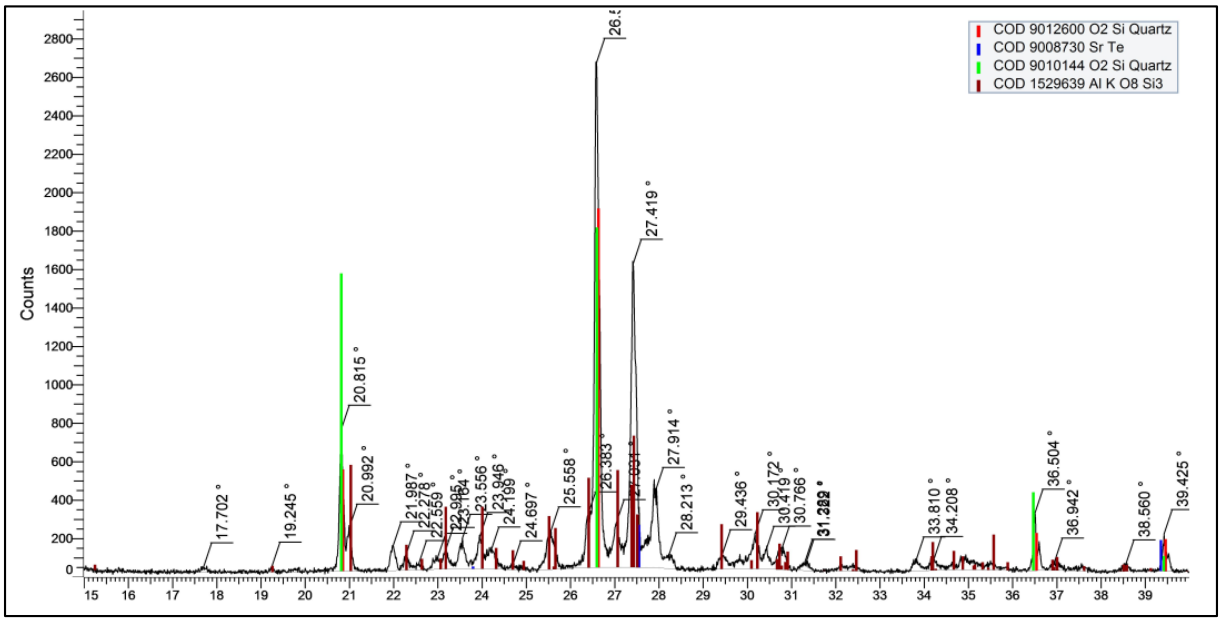


Figure 4.64: X-Ray Diffraction pattern showing the presence of quartz and feldspar minerals in sample 18.

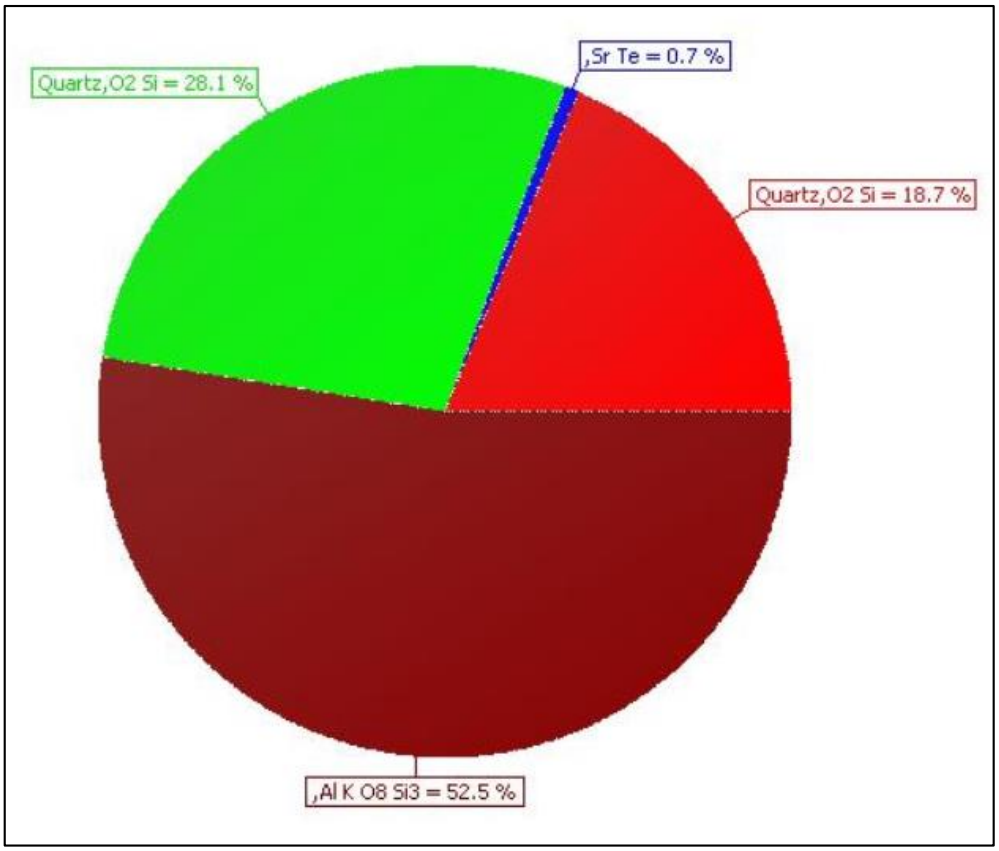


Figure 4.65: Pie Chart diagram showing the percentage of each mineral in sample 18.

**Petrography:** Figure 4.66 below shows the rock section for sample 18, mag. 40X. Quartz and K-Feldspar form the principal minerals of the rock totaling up to 99.30% according to XRD analysis. From a macroscopic point of view, biotite is visible and this is the same for the rock section. Notable accessory minerals include Strontium Telluride, Tourmaline, and Chromium. In the rock section, twinning is displayed for the feldspars as well as showing cleavage on the same. The sample appears coarse in the rock section. Concentric zoning is evident in a matrix of plagioclase feldspar and this suggests different growth conditions such as different growth environments.

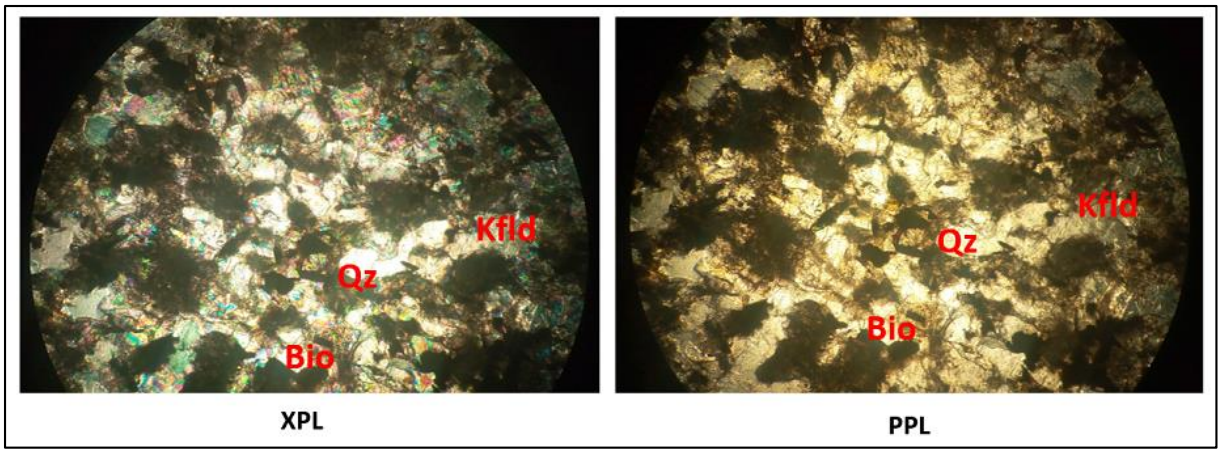


Figure 4.66: Sample 18 in rock section, showing the minerals present in the quartzofeldspathic pegmatite, Qz; Quartz, Kfld; K Feldspar, Bio; Biotite.

ii. **Results of Sample No. 19.**

Sample 19 was collected from a massively exposed outcrop along the banks of River Thingithu at sampling point SMP-19, Figure 4.67. The rock appears heavily sheared with quartz/sellaite crystals aligned to the direction of less stress. Comparably, the mineral components on sample 18 and sample 19 from a macroscopic point of view do not show significant variation. However, from the XRD analysis, the two units show their mineralogical diversity but what is common is the occurrence of feldspar and quartz minerals.

Figure 4.67: Sampling at observation point SMP-19 along the banks of River Thingithu


Figure 4.68: Hand Specimen of sample 19

The area was not mineralized and had considerable quantities of kunkar limestone. The recorded outcrops trend East North East. XRD analysis of sample 19 shows that the rock is dominated by feldspars, quartz, sellaite which make up close to 90% of the rock. Table 4.20 presents a summary of the XRD analysis showing the respective percentages of the mineral species in the sample.

Table 4.20: XRD analysis of Quartzofeldspathic Pegmatite, sample 19

| **Compound Name** | **Formula** | **Percentage** |
|---|---|---|
| Albite | $Al\ Na\ O_8\ Si_3$ | 32.3 % |
| Sellaite | $F_2\ Mg$ | 30.0 % |
| Quartz | $O_2\ Si$ | 27.1 % |
| Hawleyite | $Cd\ S$ | 4.9 % |
| Caesium Stannide | $Cs_8\ Sn_{44}$ | 2.9 % |
| Lead Tin Telluride | $Pb\ Sn\ Te_2$ | 1.8 % |
| Permingeatite | $Cu_3\ Sb\ Se_4$ | 1.0 % |
| **Total** | | **100.0%** |

The X-Ray Diffraction patterns and spread have been presented in Figure 4.69 and Figure 4.70 as recorded in the XRD machine. The x-axis shows the 2 theta angles whereas the y-axis shows the counts of the respective mineral species.

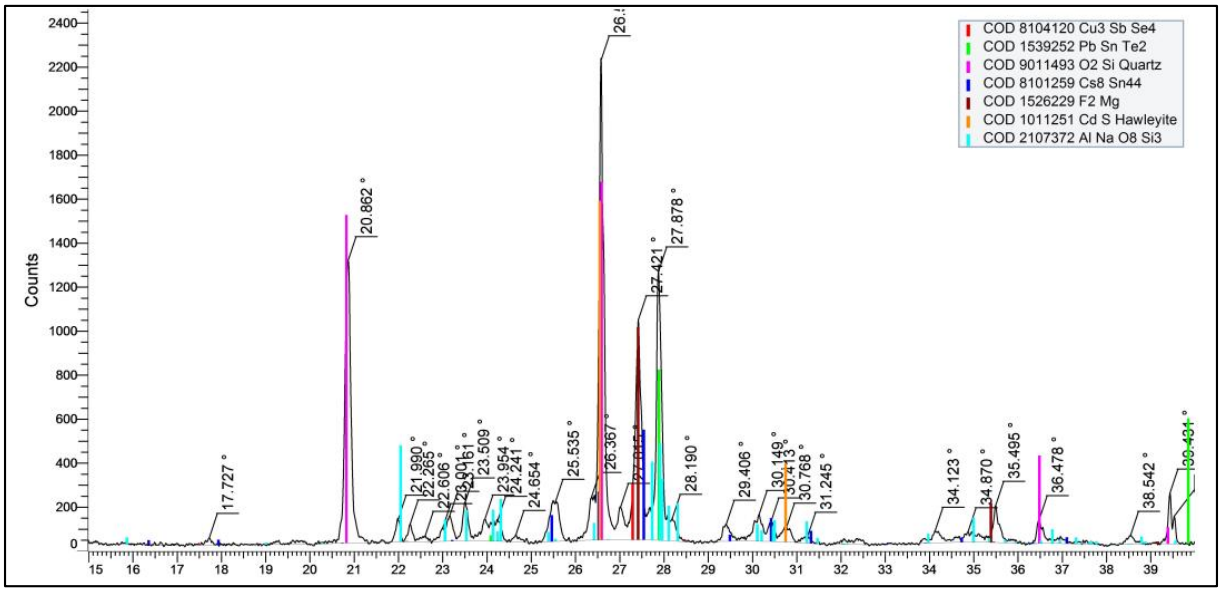


Figure 4.69: X-Ray Diffraction pattern showing the mineral species in sample 19

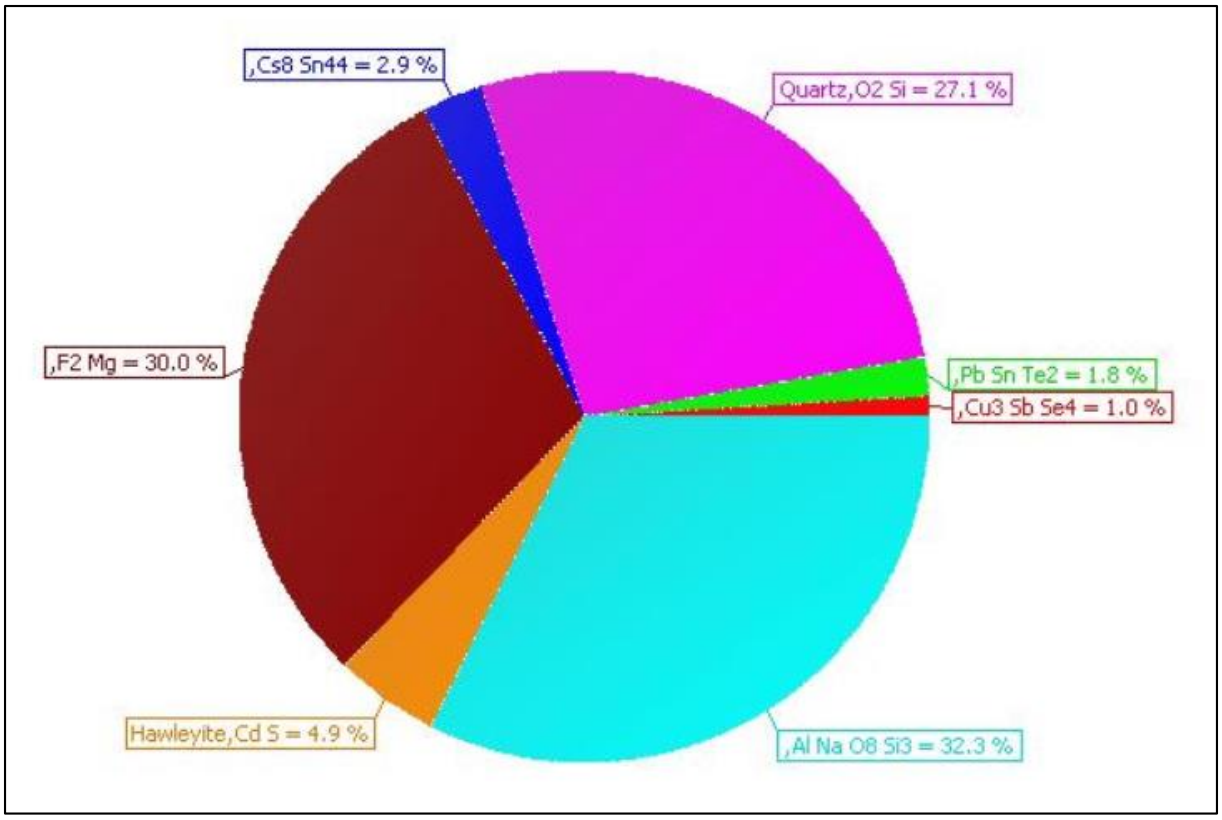


Figure 4.70: Pie Chart diagram showing the spread percentage of each mineral in sample 19.

**Petrography:** Figure 4.71 below shows the rock section for sample 19 which also shows the presence of various minerals that form from hydrothermal processes under magnification of 40X. This is inferred by the presence of Sellaite, (Pfaff *et al.*, 2012), Permingeatite, and the Sulphide mineral Hawleyite. To support this hypothesis, the rock has pronounced metamorphic fabric as seen through the lineation of some of the crystals. Based on the Bowens Reaction Series, Albite forms under intermediate temperatures which correlates well with the formation conditions of Permingeatite. Biotite crystals are also visible in the hand specimen.

Locally, sampling points SMP-18 and SMP-19 are almost in the same linear orientation as SMP-09. Analysis of sample 09 shows the presence of Caminite and Fizelyite, which form under hydrothermal conditions.

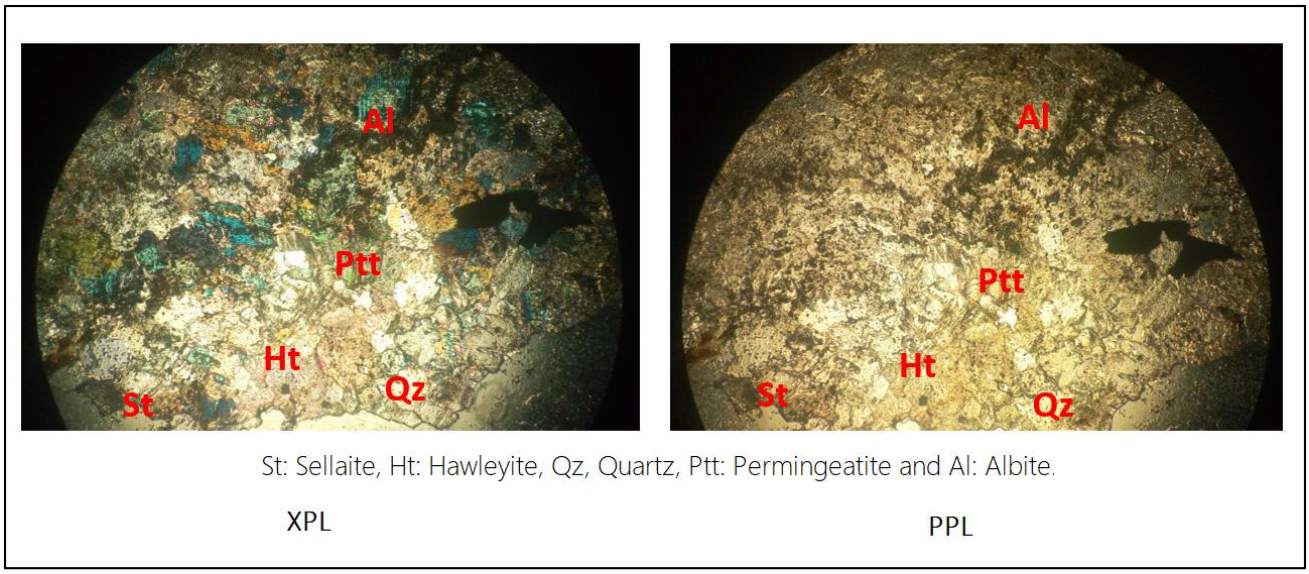


Figure 4.71: Sample 19 in rock section, showing the minerals present in the pegmatite.

### 4.1.8 Quartzofeldspathic Gneiss

**Results of Sample No. 09.** The quartzofeldspathic gneiss sample, Figure 4.72, was collected at the sampling point SMP-09 about 4 kilometers away from the study area. This was marked as a control center to indicate the occurrences just outside the boundaries of the study area. The rock unit mapped was massive, pinkish, and contained considerable amounts of quartz and feldspar grains. The rock was very coarse and was encountered along the road as a cutting, under coordinates: 00° 11' 2.00" S | 37° 57' 49.90" E. The soils in the area had scattered pebbles of quartz. The quartz grains in the sample appeared elongated with a preference towards the direction of less stress, Figure 4.72. Monitoring was also done some kilometers away from observation point SMP-09 and the rock unit mapped was consistent with SMP-09.

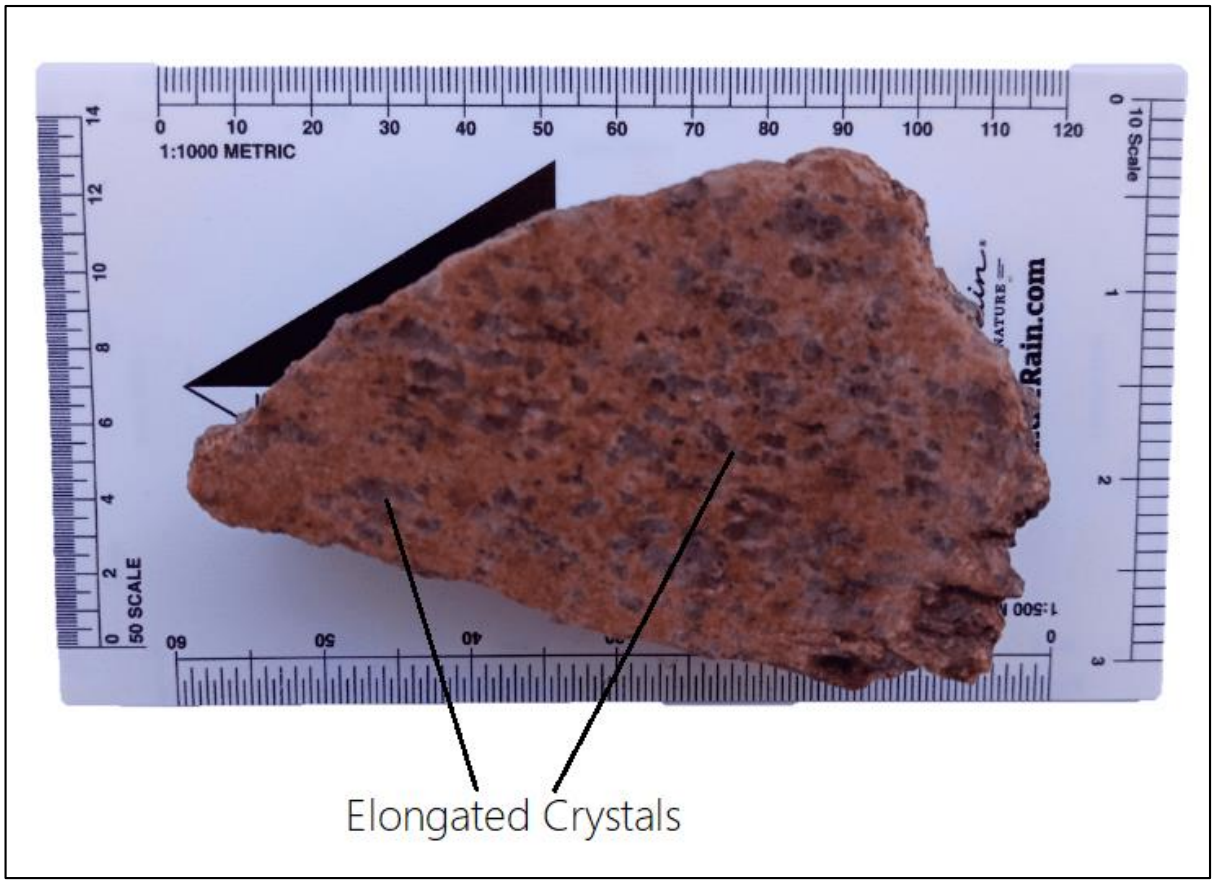


Figure 4.72 Sample 09 collected at the sampling point SMP-09 as a control sample.

From the XRD analysis, it has been presented that sample 09 comprises a wide range of mineral species from the feldspar group (microcline and albite), sulfide group (fizelyite), silica group (quartz), sulfate group, and the oxide group. (Schmidt *et al.*, 2019) report of abundant caminite occurrences in hydrothermal systems in the research work for the Terceira rift. 16.60% of the sample analyzed is comprised of caminite which would imply that hydrothermal processes may have affected the formation of the quartzofeldspathic gneisses. Fizelyite comprising 2.7% of the sample minerals has been reported by (Sugaki *et al.*, 1983) as a mineral of hydrothermal origin. Table 4.21 presents a summary of the mineral species in sample 09 following XRD analysis.

Table 4.21: XRD analysis of Quartzofeldspathic Gneiss

| **Compound Name** | **Formula** | **Percentage** |
|---|---|---|
| Albite | $Al\ Na\ O_8\ Si_3$ | 27.8 % |
| Quartz | $O_2\ Si$ | 21.2 % |
| Microcline | $Al_{1.03}\ K_{0.986}\ Na_{0.014}\ O_8\ Si_{2.97}$ | 19.9 % |
| Caminite | $H_2\ Mg_3\ O_{10}\ S_2$ | 16.6 % |
| Chrysoberyl | $Al_{1.98}\ Be\ Cr_{0.02}\ O_4$ | 11.9 % |
| Fizelyite | $Ag_{1.486}\ Pb_{3.436}\ S_{12}\ Sb_{5.215}$ | 2.7 % |
| **Total** | | **100.1%** |

Figure 4.73 below presents the 2θ peaks for the respective mineral species in sample 09. This has been complemented by the pie chart spread of the same, in Figure 4.74 as recorded in the XRD machine.

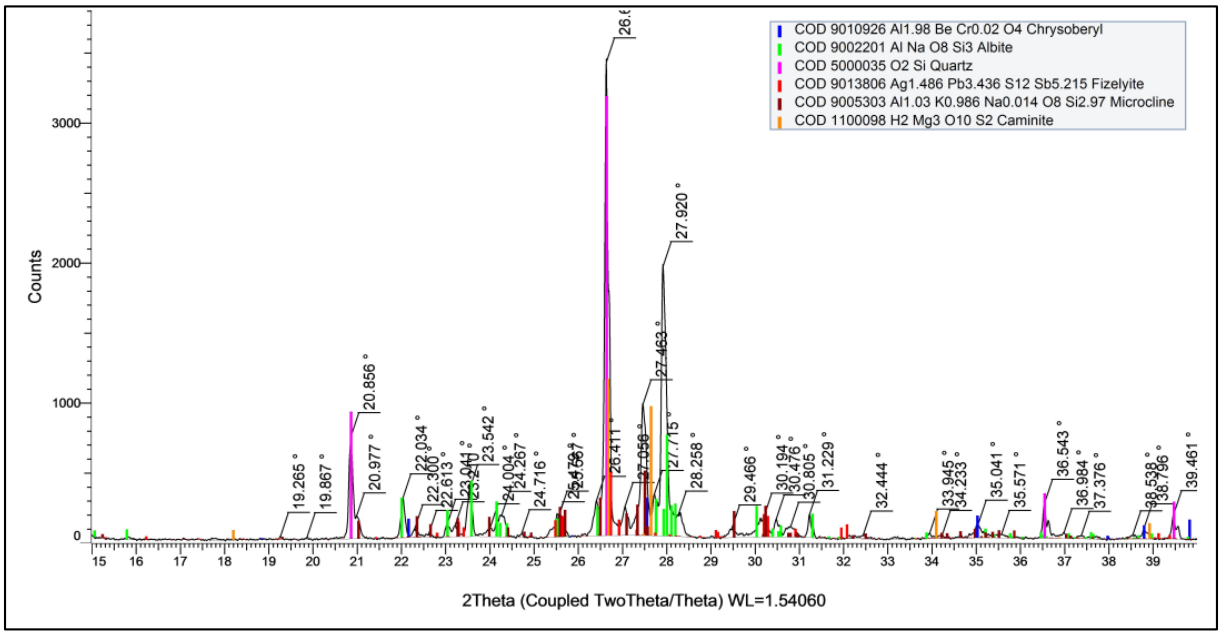


Figure 4.73: X-Ray Diffraction pattern showing the constituent minerals in sample 09

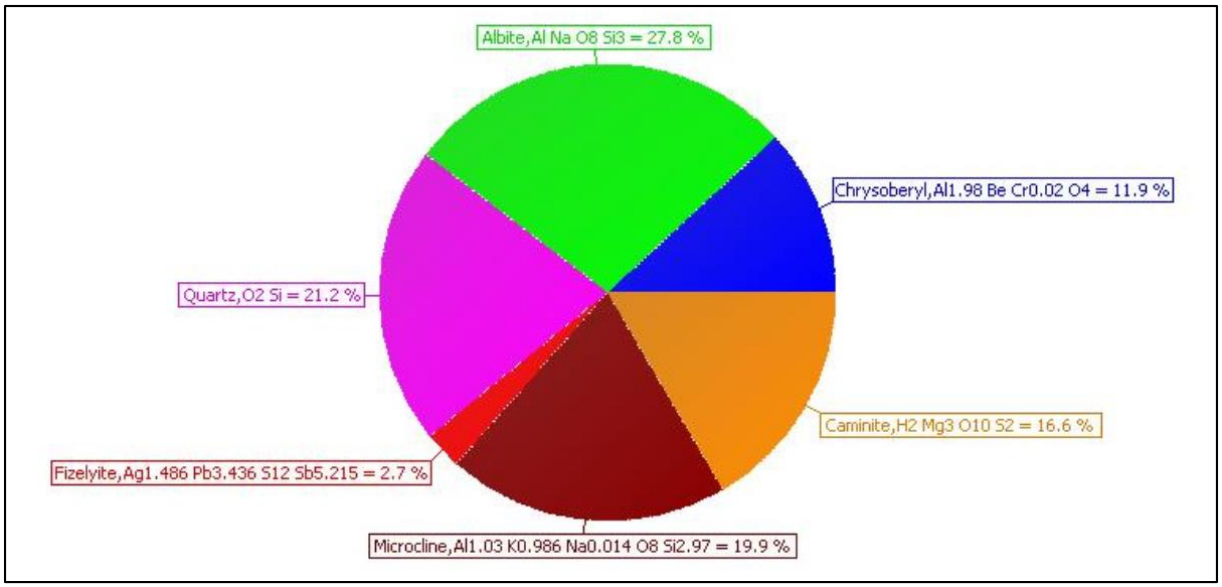


Figure 4.74: Pie Chart diagram showing the percentage of each mineral in sample 09.

### 4.1.9 Quartzite

Several sections of the study area have massive to intermediate occurrences of quartzite. In several observation points, the quartzite was intertwined with the iron ore occurrences. In several sections, quartzite occurs as pegmatites. Important to note the size and nature of the quartzite at sampling point SMP-14 (00° 10' 13.00" S | 37° 56' 16.90" E) where the outcrop is massive and occurs as an extensive hill – about 50 meters wide at the peak, Figure 4.75, where some of the crystals are up to 50cm long. Sections of the quartzite units are mineralized as shown in Figure 4.76.

Figure 4.75: Massive outcrop of quartzite, the peak of a hill.

Figure 4.76: Mineralized sample 14 of quartzite collected from coordinate: 00° 10' 13.00" S | 37° 56' 16.90" E.

**Results of Sample No. 14.** XRD analysis done on sample 14 shows that the rock is heavily dominated by Manganese Selenide, Berlinite, and Quartz as presented in Table 4.22. Berlinite forms a crucial part of the phosphate suite present in the quartzite outcrop. It is an isostructural mineral that occurs as a high temperature hydrothermal/metasomatic mineral, (Onac and White, 2003). This infers the nature of occurrence and processes that may have had a role in the secondary composition in the quartzite outcrop.

Table 4.22: XRD analysis of the Quartzite Unit, sample 14

| **Compound Name** | **Formula** | **Percentage** |
|---|---|---|
| Quartz | $O_2$ Si | 46.6 % |
| Berlinite | Al $O_4$ P | 27.9 % |
| Manganese Selenide | Mn Se | 25.6 % |
| **Total** | | **100.1%** |

The X-Ray Diffraction patterns and spread have been shown in Figure 4.77 and Figure 4.78 as recorded in the XRD machine.

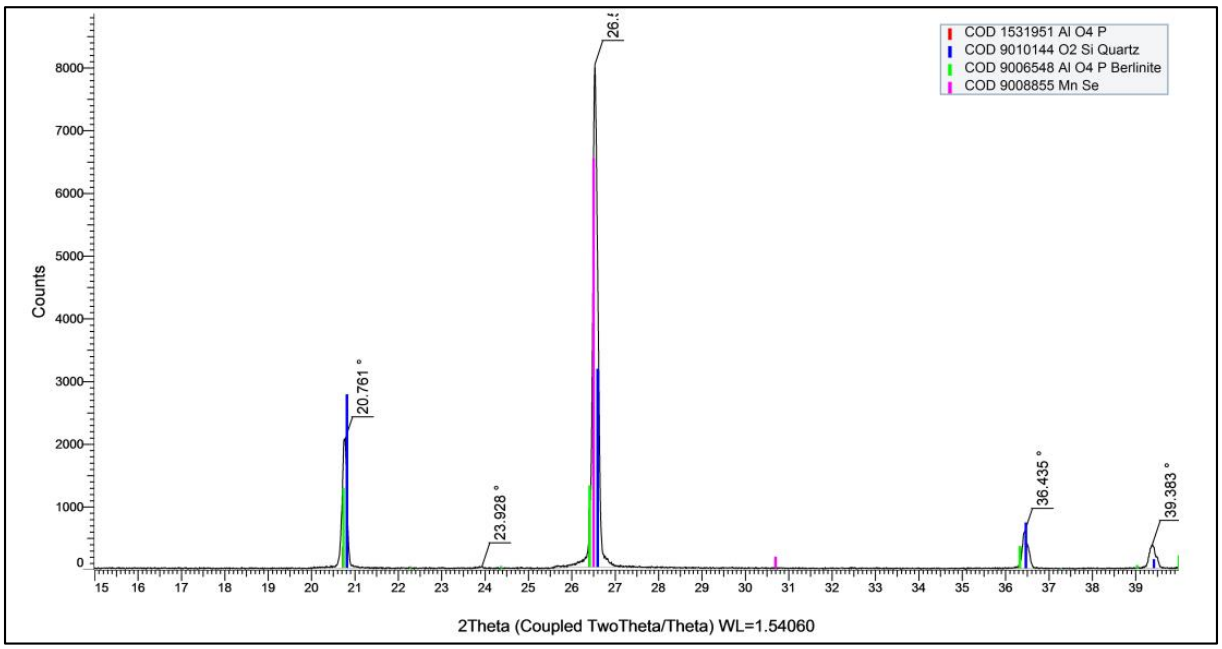


Figure 4.77: X-Ray Diffraction pattern of sample 14.

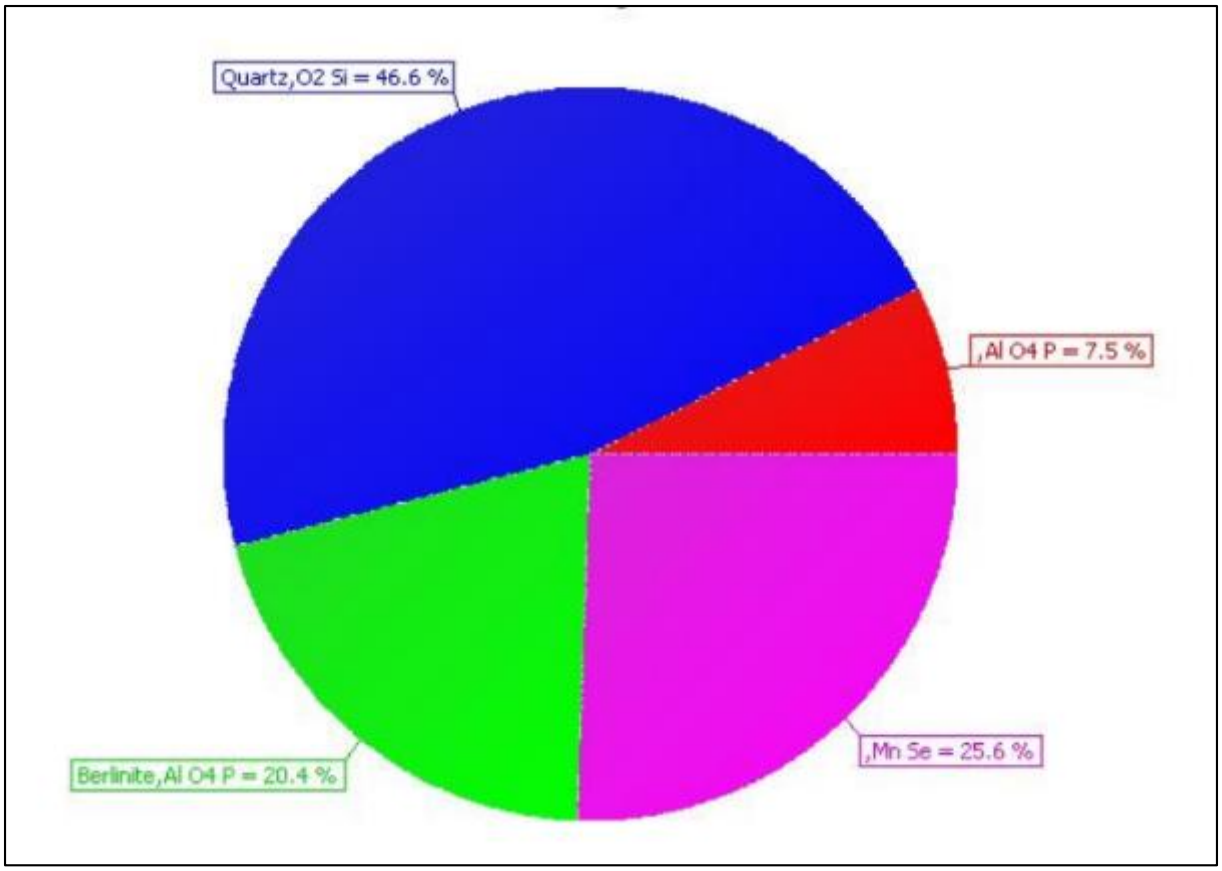


Figure 4.78: Pie Chart diagram showing the percentage of each mineral in sample 14.

Sampling point SMP-13 is another notable area where occurrences of quartz pegmatite were mapped. The quartzite pegmatites have minor occurrences of biotite crystals, gemstones such as amethyst, Figure 4.50. Sample 13 was collected from coordinate: 00° 09' 40.00" S | 37° 56' 35.60" E.

At sampling point SMP-13, the iron ore deposit occurs near mineralized quartz veins bearing moderately colored prismatic amethyst crystals Figure 4.52 and Figure 4.51. The growth of prismatic amethyst crystals suggests a peculiar environment. These new conditions may be through irradiation which influences the tonation of the amethyst crystals or the development of different zoned colors through the acquisition of trace impurities such as iron on quartz crystals, (Lameiras *et al.*, 2009). Iron ore is common in this area and may have played a role in the color tonation of the amethyst.

### 4.1.10 Quartz Diorite

**Results of Sample No. 24.** Sample 24 was collected from a massive outcrop under the coordinates 00° 09' 39.20" S | 37° 55' 24.40" E at SMP-24. The sample is coarse-grained and it contains minute crystals of reddish garnet.


Figure 4.79: Hand specimen of sample 24 from sampling point SMP-24.

**Mineralogy:** XRD analysis of sample 24 shows that the rock is dominated by feldspars and Silica Oxides adding up to 98.30%. (Berry *et al.*, 1985) indicate an almost 1:1 ratio of iron and nickel in argentopentlandite, a hydrothermal mineral. Cristobalite is a high-temperature signature mineral and a polymorph of the silica group. Its presence together with that of Silver bearing pentlandite associate the rock with high-temperature formation environments. Table 4.23 presents a summary of the XRD analysis for sample 24.

Table 4.23: XRD analysis of the Quartz Diorite, sample 24

| **Compound Name** | **Formula** | **Percentage** |
|---|---|---|
| Anorthite sodian | $Al_{1.52}\ Ca_{0.52}\ Na_{0.48}\ O_8\ Si_{2.48}$ | 69.3 % |
| Quartz | $O_2\ Si$ | 20.7 % |
| Cristobalite | $O_2\ Si$ | 8.3 % |
| Argentopentlandite | $Ag\ Fe_{4.8}\ Ni_{3.2}\ S_8$ | 1.7 % |
| **Total** | | **100.0%** |

The X-Ray Diffraction patterns and spread have been shown in Figure 4.80 and Figure 4.81 as recorded in the XRD machine. Anorthite sodian is seen to have the most 2θ angles, together with quartz.

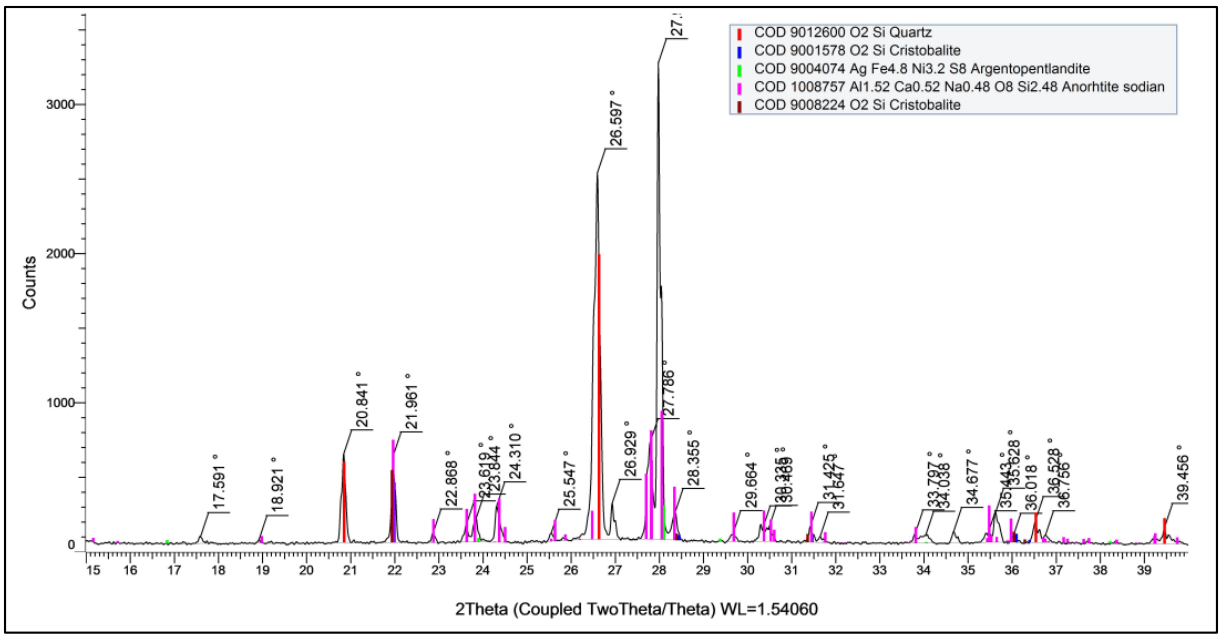


Figure 4.80: X-Ray Diffraction pattern showing the presence of Silica minerals and feldspar in sample 24.

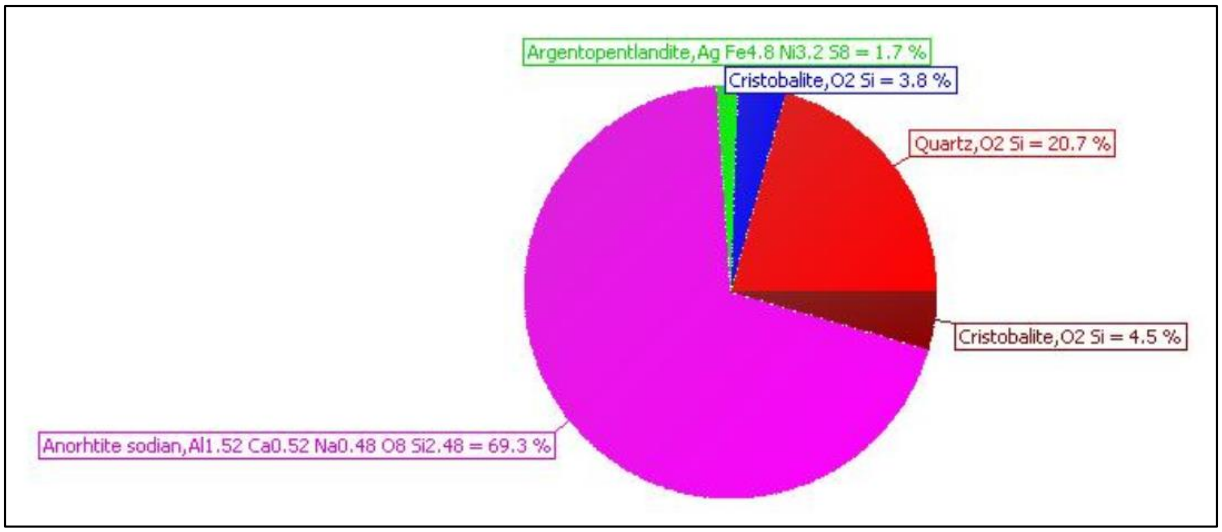


Figure 4.81: Pie Chart diagram showing the percentage of each mineral in sample 24.

**Petrography:** Figure 4.82 shows the rock section for sample 24 under magnification 40X. Silica minerals and Feldspar form the principal minerals of the rock totaling up to 98.30% according to XRD analysis. From a macroscopic point of view, biotite (bt) is visible and this is the same for the rock section. Notable accessory minerals include garnet (Gt), argentopentlandite (Ape), and other opaque minerals. The garnet crystal appears reddish-brown and this could be inferred as concentrations of iron content in the garnet. Almandine, from the pyralspite group of garnets, is the likeliest of the garnet minerals occurring in the study area. The elongated crystal as can be seen in the plane polarised rock section, the characteristic deep red color, and its association with plagioclase gives the best indication that the mineral, which is an iron aluminium silicate mineral, ($Fe_3Al_2[SiO_4]_3$), is almandine. (Harangi *et al.*, 2001) give possible phenomena for the occurrence of the almandine garnet in various igneous settings.

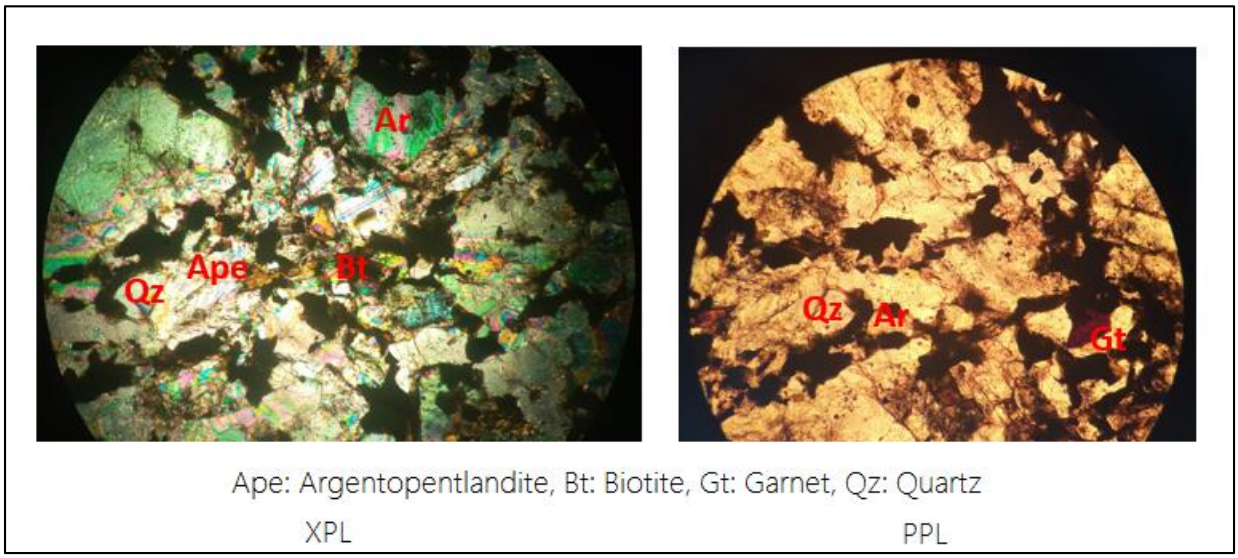


Figure 4.82: Sample 24 in rock section, showing the minerals present in the quartz diorite.

## 4.2 Geological Map of the Study Area

Based on the field observations, detailed petrographic studies, and XRD analysis, the following geological map of the study area was developed, Figure 4.83. As can be noted, the area is heavily dominated by feldspar rich rock units such as gabbro, anorthosites, and dolerites as well as pyroxene rich rock units (pyroxenite). The intrusives occur in juxtaposition with the iron ore mineralization in lumpsum, disseminated and stain (minimal) quantities. From West to East, the area is zoned as follows: gabbroic rock units, pyroxenites (both crisscrossed by the dolerite dykes), and iron ores followed by metamorphosed rock units.

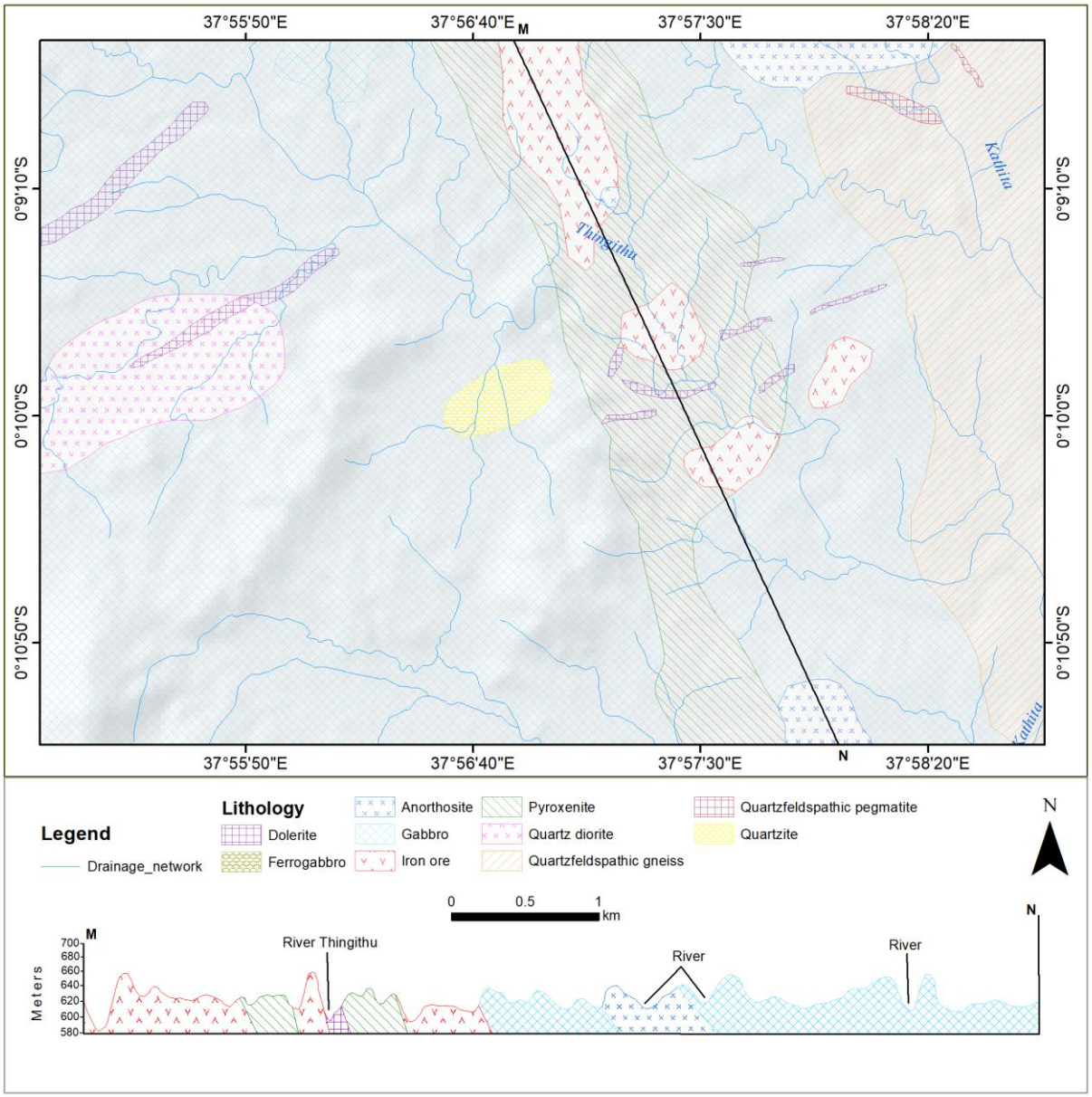


Figure 4.83: Geological map of the Kithiori area indicating the rock units, their distribution, and associations.

## 4.3 Structural Geology

The study area is characterized by various structural features some of which have contributed to the mineralization and occurrence of the subject ore deposit. The structural features vary in terms of size and shape as indicated below.

### 4.3.1 Dykes

Massive dykes are seen crisscrossing rock units in the study area. The dykes vary in size, from about 5 - 10 centimeters close to about 50 meters. Megascopically, the dykes appear fine to medium-grained, very compact, and mafic. Figure 4.84 below shows a 15-centimeter mafic dyke trending 270° in the East-West direction. The different features/structures show multi-episodal processes and going by the law of cross-cutting relationships, the dykes are younger than the host rocks and also younger than some of the joints.

In several discordant units, most of which are the mafic dykes, veinlets separate the dyke and the host gabbroic rock. The development of the veinlets may be as a result of the newly developed lines of weakness that may have formed voids within which quartz-rich veins developed. Observation point OBP 010, Figure 4.85, is one such example.

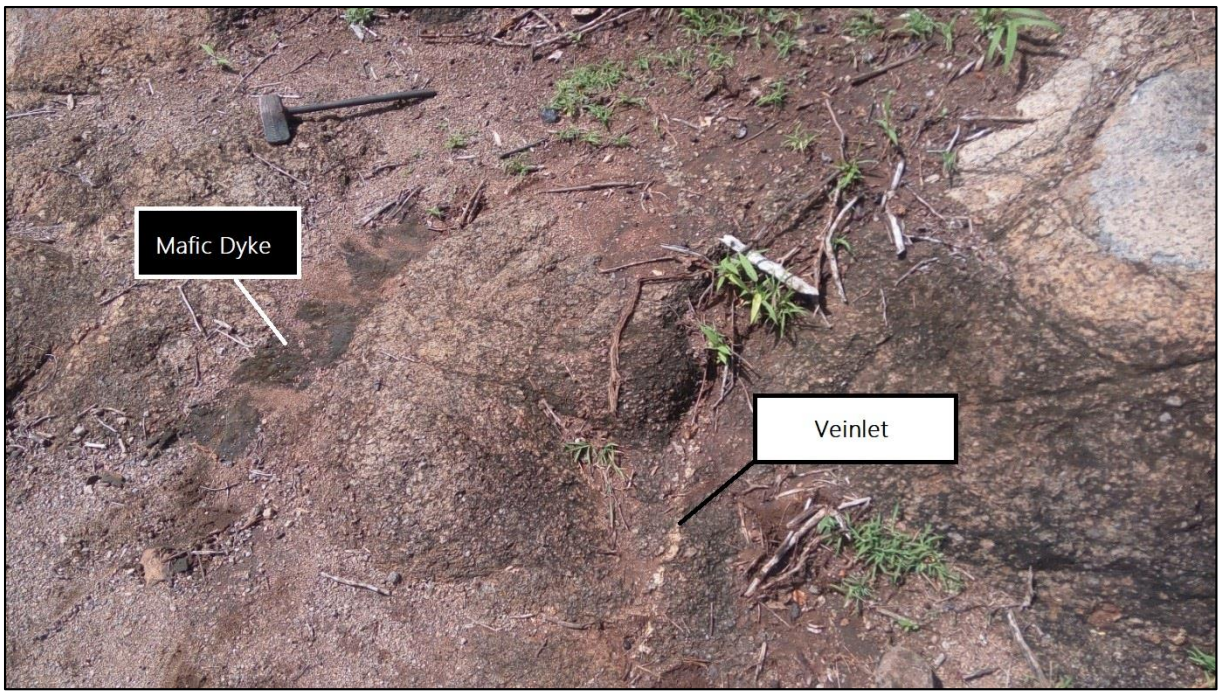


Figure 4.84: Microgabbro co-occurring with millimeter size felsic veinlets at SMP-01.


Figure 4.85: Contact zone between a mafic dyke and the host rock, OBP 010

The mafic dyke appears susceptible to weathering in several sections, especially when exposed to agents of weathering. The general trend of the dykes is shown below. It is observed that in some sections of the study area, OBP 022, dykes occur with the abundance of quartz pebbles.

Figure 4.86 presents the orientations for dyke trends mapped in the study area. As indicated in the rose diagram, a majority of the dykes take the NW – NE orientation from 18 measurements.

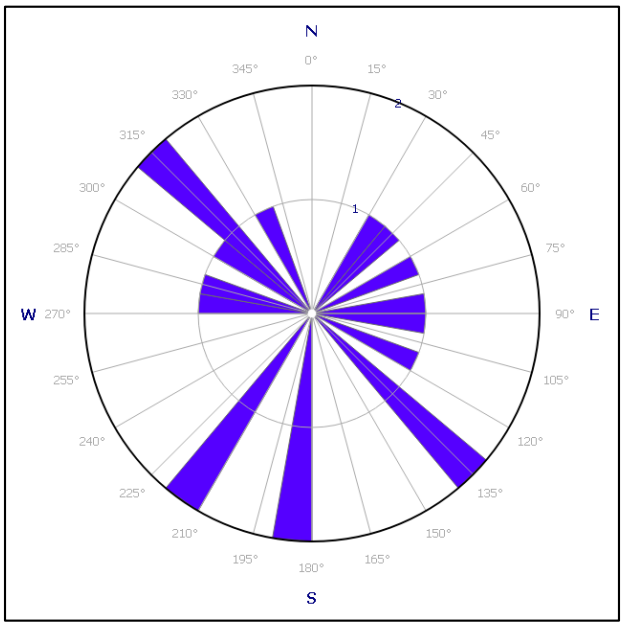


Figure 4.86: Rose Diagram for the dyke trends

### 4.3.2 Veinlets

Most veinlets are felsic, they are dominated by plagioclase feldspars/ quartz and they occur within the gabbroic units and dolerites. The widths of the veinlets range from a few millimeters to a couple of centimeters in width. Despite their limited occurrence, their development has important implications for processes of melt emplacement and evolution. Several hypotheses have been proposed by (Niu *et al.*, 2002) – fractional crystalization, (Dick *et al.*, 2000) – melt to wall rock reaction and immiscibility as possible ways for the formation of the felsic veinlets. Figure 4.85 shows the proximity of the felsic veinlets and a microgabbroic unit which have a cross-cutting relationship. This phenomenon was also observed in the rock section for sample 01. Similar occurrences were noted at observation point OBP 005.

As mentioned elsewhere in the report, felsic veins occur at sampling point SMP-13 with mineralization of moderately colored prismatic amethyst crystals. At the same site, iron mineralization is evident. Biotite crystals occur in the area as well.

### 4.3.3 Relict Magmatic Xenoliths

Relict igneous magmatic signatures in the host gabbro unit at sampling point SMP-21, Figure 4.87, are relatively common, mostly signifying that deformation may not have been holistic and this allowed them to "survive". The xenoliths form sigmoidal structures. Adjacent to the mafic xenoliths are crystalized quartz grains that form within fractures in the rock.

Figure 4.87: Xenoliths imply ductile deformation (dextral shearing) may have taken place.

The gabbro units in sampling point SMP-21 are variably deformed following impacts from indiscriminate heterogeneous strain distribution and metamorphic-like action acting on them.

### 4.3.4 Lineation

Mineral lineation in the area is evident through the alignment of minerals in a preferred direction. The lineation structures are poorly developed in the study area and notably, boudins and mineral lineations in rock units are seen in areas adjacent to metamorphic-like terrains. The presence of boudin structures for example is evidence of non-linear stress as recorded by (Hudleston and Lan, 1995).

One example of the typical mineral lineation is recorded at observation point OBP 023 where the lineation is plunged at 55°W, Figure 4.88.


Figure 4.88: Mineral lineation as recorded at observation point OBP 023.

Generally speaking, lineation is not as pronounced as would be expected for metamorphic terrains. Where present, they are very minimal and occur in micro-scale.

### 4.3.5 Joints and Fractures

Sections of the study area have been cut across by networks of joints that show little or no displacement. Some of the joints seem to have been infilled by molten material that constitutes a network of veins. The extensive hill at sampling point SMP-10, Figure 4.90, exhibits parallel

joints developed in a conspicuous manner dipping at 55°. The direction and parallelism of the joints infer the uniformity of stress acting on the rocks in the area.

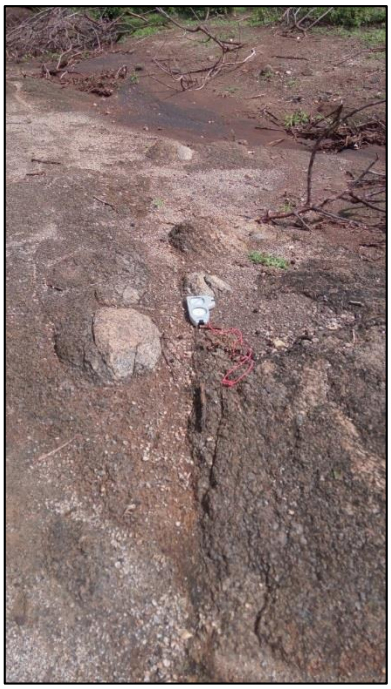

Figure 4.89: Image from sampling point SMP-01 shows a joint structure.

Importantly, several units exhibit rocks that have undergone brittle fracture in a general E-W direction. A road cutting at sampling point SMP-10, Figure 4.90, shows that the hill is multi-lithologic as per the descriptions of the units elsewhere in this report. It is the same hill that has several occurrences of rare earth elements of varying quantities.


Figure 4.90: SMP-10 - 3 meter wide anorthositic gabbro boulders of centimeter-sized diameter have been fractured and dipped

Figure 4.91 presents the orientations for the joint trends mapped in the study area. As indicated in the rose diagram, a majority of the joints trend between the NW and NE direction.

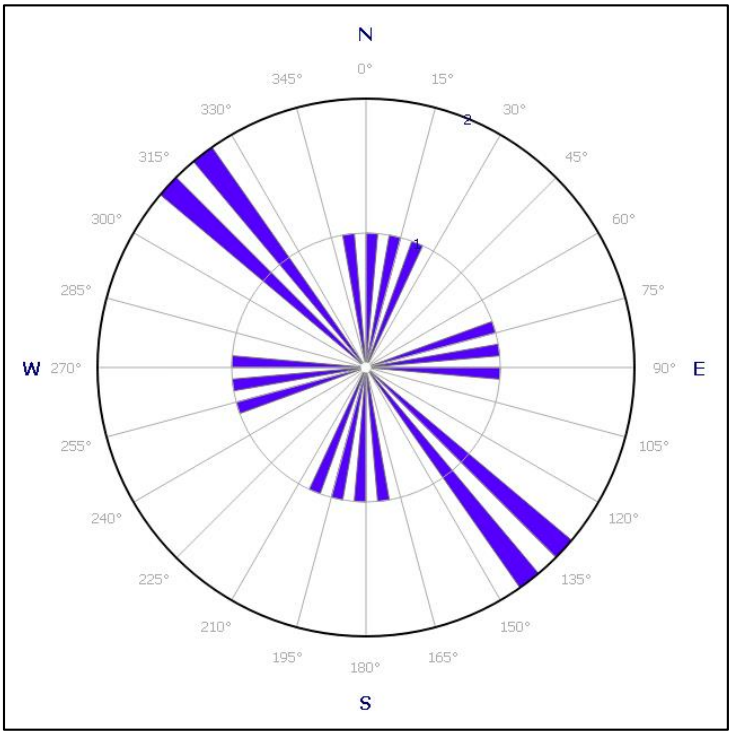


Figure 4.91: Rose Diagram for the joint orientations

### 4.3.6 Folds

Folds are some of the notable structures mappable in the study area. The folds are minor and localized. One easily recognizable fold was mapped at observation point SMP-11 as shown in Figure 4.92. The folds have weakly defined and poorly reserved lineation to allow any structural analysis. Figure 4.93 indicates minor folds associated with gabbro which could be of ophiolitic nature at SMP-21.

Figure 4.92: Figure showing a compositional fold which has a combination of leucocratic and mafic minerals.

Figure 4.93: Sampling point SMP-21 manifests discrete strained zones as minor folds producing, multi-oriented, cross-grained random fabric in gabbro.

### 4.3.7 Shear Zones

It is evident in various sections of the study area that millimeter size to centimeter size shear zones occur. Some of the shearing planes are infilled indicating ductile movement. Sampling point SMP-01, Figure 4.94, is an example, where ductile movement is in the North-South direction.

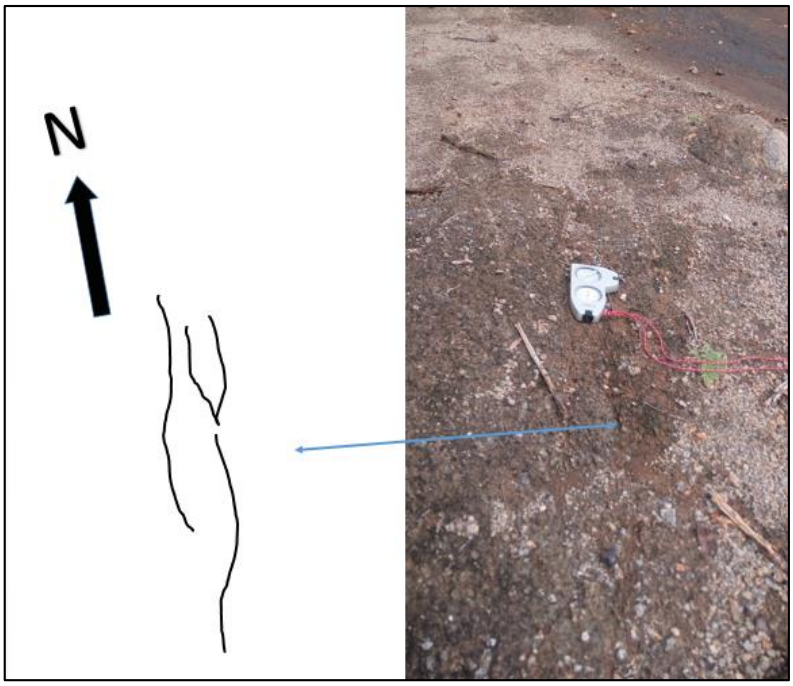


Figure 4.94: Shearing plane at SMP-01 trending in the N-S direction

At the Nineveh center, observation point OBP 018, kunkar limestone cements a shear zone which marks a contact zone/boundary between the microgabbro and a pyroxene pegmatite. Grain deformation coupled with boudin shaped and elongated crystals is due to the shear stress. The sinistral movement is observed for the general section close to observation point SMP-11 as indicated in Figure 4.95. This could be inferred as a localized deformation pattern. In sections of the fault zones, kunkar limestone is developed as a further indication of tectonic movement in the area. Shearing could have created more room/vacuum for infilling by the mafic dykes. Pyroxene pegmatites bearing minute Fe – Ti – V mineralization have also developed in the shear zones.


Figure 4.95: SMP-11 showing tensional forces that influenced the formation of a minor sinistral shear pattern

At the observation point OBP 023 a shear zone occurs between two gabbros. The contact/shear zone has been in-filled by quartz veins of millimeter size trending in the East North-East direction.

## 4.4 Geochemistry

This section outlines the comprehensive geochemical analysis based on XRF studies. Elemental analysis has been presented and discussed. The section also gives an insight into the possible magmatic origin discerning the difference in lithologies.

### 4.4.1 Major and Minor Elements

The major and minor elements in the rocks were analyzed using the X-Ray Fluorescence method. The Bruker equipment used was from the Ministry of Petroleum and Mining, Kenya. The results are as shown in Table 4.24 below. Quantities have been expressed in weight percent (wt. %) for a total of 25 samples.

Table 4.24: Chemical analysis through XRF for the samples collected in the study area in wt%

| | | SMP-01 | SMP-02 | SMP-03 | SMP-04 | SMP--5 | SMP-06 | SMP-07 | SMP-08 | SMP-09 | SMP-10 | SMP-25 | SMP-11 | SMP-12 |
|---|---|---|---|---|---|---|---|---|---|---|---|---|---|---|
| | **Rock Type** | Gabbro | Iron Ore | Iron Ore | Pyroxenite | Iron Ore | Iron Ore | Iron Ore | Iron Ore | Qfd Gneiss | An. Gabbro | Gabbro | An. Gabbro | Iron Ore |
| **Major Elements** | | | | | | | | | | | | | | |
| | **$SiO_2$** | 56.687 | 16.669 | 8.728 | 48.350 | 20.289 | 7.205 | 6.754 | 6.241 | 79.043 | 47.699 | 55.121 | 52.135 | 7.541 |
| | **$Al_2O_3$** | 23.780 | 6.346 | 10.313 | 4.269 | 6.576 | 8.488 | 8.098 | 7.184 | 12.613 | 15.964 | 3.047 | 27.166 | 8.230 |
| | **CaO** | 13.952 | 14.146 | 0.599 | 18.773 | 5.772 | 0.444 | 0.266 | 0.382 | 0.839 | 12.893 | 14.413 | 15.064 | 1.466 |
| | **MgO** | 0.000 | 0.000 | 0.000 | 12.310 | 6.184 | 0.000 | 0.000 | 0.000 | 0.000 | 7.804 | 15.496 | 1.963 | 0.000 |
| | **$K_2O$** | 0.595 | 0.968 | 0.141 | 0.069 | 0.058 | 0.170 | 0.145 | 0.178 | 5.246 | 0.242 | 0.147 | 0.108 | 0.145 |
| | **$P_2O_5$** | 0.309 | 0.104 | 0.000 | 0.120 | 0.000 | 0.000 | 0.000 | 0.000 | 0.056 | 0.570 | 0.071 | 0.068 | 0.470 |
| | **Fe** | 3.21 | 56.892 | 55.468 | 13.318 | 43.489 | 57.871 | 56.347 | 59.186 | 1.078 | 12.018 | 10.004 | 2.524 | 57.057 |
| | **Ti** | 0.558 | 3.046 | 22.869 | 1.807 | 16.110 | 23.908 | 26.497 | 24.904 | 0.134 | 1.332 | 0.662 | 0.187 | 23.630 |
| **Total** | | **99.991** | **99.875** | **99.911** | **99.995** | **99.926** | **99.885** | **99.907** | **99.903** | **99.990** | **99.978** | **99.992** | **99.992** | **99.917** |
| **Minor Elements** | | | | | | | | | | | | | | |
| | **S** | 0.188 | 0.213 | 0.072 | 0.156 | 0.058 | 0.002 | 0.110 | 0.164 | 0.308 | 0.484 | 0.165 | 0.119 | 0.000 |
| | **Cl** | 0.510 | 0.482 | 0.354 | 0.417 | 0.374 | 0.310 | 0.364 | 0.444 | 0.556 | 0.479 | 0.478 | 0.514 | 0.335 |
| | **V** | 0.000 | 0.071 | 0.198 | 0.027 | 0.179 | 0.299 | 0.230 | 0.093 | 0.000 | 0.042 | 0.032 | 0.002 | 0.012 |
| | **Cr** | 0.014 | 0.000 | 0.000 | 0.000 | 0.000 | 0.000 | 0.000 | 0.000 | 0.028 | 0.000 | 0.063 | 0.028 | 0.000 |
| | **Mn** | 0.059 | 0.523 | 0.330 | 0.328 | 0.340 | 0.344 | 0.313 | 0.284 | 0.070 | 0.324 | 0.245 | 0.031 | 0.273 |
| | **Co** | 0.000 | 0.252 | 0.602 | 0.000 | 0.342 | 0.618 | 0.592 | 0.625 | 0.000 | 0.001 | 0.000 | 0.000 | 0.596 |
| | **Ni** | 0.004 | 0.034 | 0.064 | 0.018 | 0.055 | 0.071 | 0.055 | 0.061 | 0.000 | 0.017 | 0.021 | 0.003 | 0.029 |
| | **Cu** | 0.004 | 0.011 | 0.020 | 0.010 | 0.019 | 0.000 | 0.023 | 0.013 | 0.002 | 0.023 | 0.011 | 0.006 | 0.019 |
| | **Zn** | 0.005 | 0.017 | 0.128 | 0.013 | 0.065 | 0.127 | 0.095 | 0.112 | 0.000 | 0.015 | 0.010 | 0.002 | 0.073 |
| | **As** | 0.000 | 0.000 | 0.000 | 0.002 | 0.000 | 0.000 | 0.000 | 0.000 | 0.000 | 0.000 | 0.000 | 0.000 | 0.000 |
| | **Rb** | 0.000 | 0.012 | 0.011 | 0.000 | 0.007 | 0.014 | 0.010 | 0.011 | 0.010 | 0.000 | 0.000 | 0.000 | 0.014 |
| | **Sr** | 0.103 | 0.053 | 0.000 | 0.003 | 0.000 | 0.000 | 0.000 | 0.000 | 0.000 | 0.062 | 0.004 | 0.063 | 0.000 |
| | **Zr** | 0.013 | 0.036 | 0.014 | 0.005 | 0.009 | 0.014 | 0.008 | 0.021 | 0.007 | 0.009 | 0.002 | 0.009 | 0.027 |

| | | SMP 13 | SMP 14 | SMP 15 | SMP 16 | SMP 17 | SMP 18 | SMP 19 | SMP 20 | SMP 21 | SMP 22 | SMP 23 | SMP 24 |
|---|---|---|---|---|---|---|---|---|---|---|---|---|---|
| | **Rock Type** | Iron Ore | Quartzite | Gabbro | Gabbro | Iron Ore | Qtz. Pegmatite | Qtz. Pegmatite | Ferro Gabbro | Gabbro | Gabbro | Dolerite | Qtz. Diorite |
| **Major Elements** | | | | | | | | | | | | | |
| | **SiO2** | 4.483 | 79.884 | 50.017 | 50.213 | 7.425 | 75.336 | 77.264 | 44.752 | 56.221 | 53.055 | 52.336 | 72.184 |
| | **Al2O3** | 6.725 | 0.216 | 20.076 | 17.352 | 5.965 | 13.944 | 12.314 | 9.892 | 16.232 | 14.409 | 14.832 | 14.524 |
| | **CaO** | 0.346 | 0.738 | 14.844 | 12.632 | 0.201 | 0.921 | 0.883 | 11.691 | 12.516 | 12.347 | 10.526 | 4.266 |
| | **MgO** | 0.000 | 0.000 | 7.486 | 6.285 | 0.000 | 0.000 | 0.000 | 6.518 | 3.835 | 3.576 | 8.929 | 0.000 |
| | **K2O** | 0.156 | 0.037 | 0.118 | 0.343 | 0.154 | 7.120 | 6.878 | 0.094 | 0.725 | 0.784 | 1.210 | 2.186 |
| | **P2O5** | 0.000 | 0.163 | 0.068 | 0.447 | 0.000 | 0.039 | 0.040 | 0.052 | 0.315 | 1.000 | 0.425 | 0.070 |
| | **Fe** | 58.593 | 10.122 | 6.148 | 10.574 | 62.711 | 1.241 | 1.387 | 20.557 | 8.277 | 11.932 | 9.289 | 4.712 |
| | **Ti** | 27.91 | 8.559 | 0.216 | 1.221 | 21.454 | 0.329 | 0.244 | 5.365 | 0.686 | 1.637 | 1.442 | 0.749 |
| **Total** | | **99.888** | **99.719** | **99.949** | **99.992** | **99.826** | **99.722** | **99.914** | **99.982** | **99.994** | **99.871** | **99.980** | **99.863** |
| **Minor and Trace Elements** | | | | | | | | | | | | | |
| | **S** | 0.085 | 0.000 | 0.217 | 0.096 | 0.069 | 0.168 | 0.285 | 0.137 | 0.239 | 0.142 | 0.216 | 0.277 |
| | **Cl** | 0.419 | 0.000 | 0.541 | 0.488 | 0.373 | 0.547 | 0.564 | 0.457 | 0.591 | 0.597 | 0.475 | 0.695 |
| | **V** | 0.134 | 0.000 | 0.001 | 0.018 | 0.335 | 0.000 | 0.000 | 0.040 | 0.018 | 0.009 | 0.000 | 0.000 |
| | **Cr** | 0.000 | 0.000 | 0.056 | 0.006 | 0.000 | 0.007 | 0.018 | 0.000 | 0.018 | 0.000 | 0.000 | 0.004 |
| | **Mn** | 0.277 | 0.235 | 0.121 | 0.200 | 0.394 | 0.008 | 0.011 | 0.340 | 0.173 | 0.231 | 0.141 | 0.083 |
| | **Co** | 0.528 | 0.010 | 0.000 | 0.000 | 0.550 | 0.000 | 0.000 | 0.000 | 0.000 | 0.000 | 0.000 | 0.000 |
| | **Ni** | 0.065 | 0.005 | 0.015 | 0.014 | 0.084 | 0.003 | 0.000 | 0.024 | 0.003 | 0.008 | 0.022 | 0.003 |
| | **Cu** | 0.000 | 0.005 | 0.008 | 0.020 | 0.044 | 0.003 | 0.000 | 0.023 | 0.005 | 0.006 | 0.010 | 0.005 |
| | **Zn** | 0.128 | 0.006 | 0.004 | 0.011 | 0.040 | 0.002 | 0.002 | 0.021 | 0.010 | 0.018 | 0.011 | 0.008 |
| | **As** | 0.000 | 0.000 | 0.000 | 0.001 | 0.000 | 0.001 | 0.000 | 0.000 | 0.001 | 0.001 | 0.000 | 0.001 |
| | **Rb** | 0.015 | 0.002 | 0.000 | 0.000 | 0.016 | 0.009 | 0.006 | 0.000 | 0.000 | 0.000 | 0.002 | 0.005 |
| | **Sr** | 0.000 | 0.000 | 0.006 | 0.053 | 0.000 | 0.035 | 0.006 | 0.011 | 0.086 | 0.101 | 0.089 | 0.068 |
| | **Zr** | 0.024 | 0.000 | 0.007 | 0.018 | 0.011 | 0.009 | 0.012 | 0.008 | 0.043 | 0.018 | 0.025 | 0.023 |

The Harker Diagrams below have been used to ascertain the similarity and the origin of the parent magma by comparing the oxides of major elements such as Ca, Mg, Al, P, and K against the oxide of Si. The XRF results indicated in the table above have been used to illustrate this to give a representative overview of the spread per rock unit. In the figures below, it is easy and important to note the clustering of ores, gabbroic, and metamorphosed rocks. An illustration has been given for each of the plots.

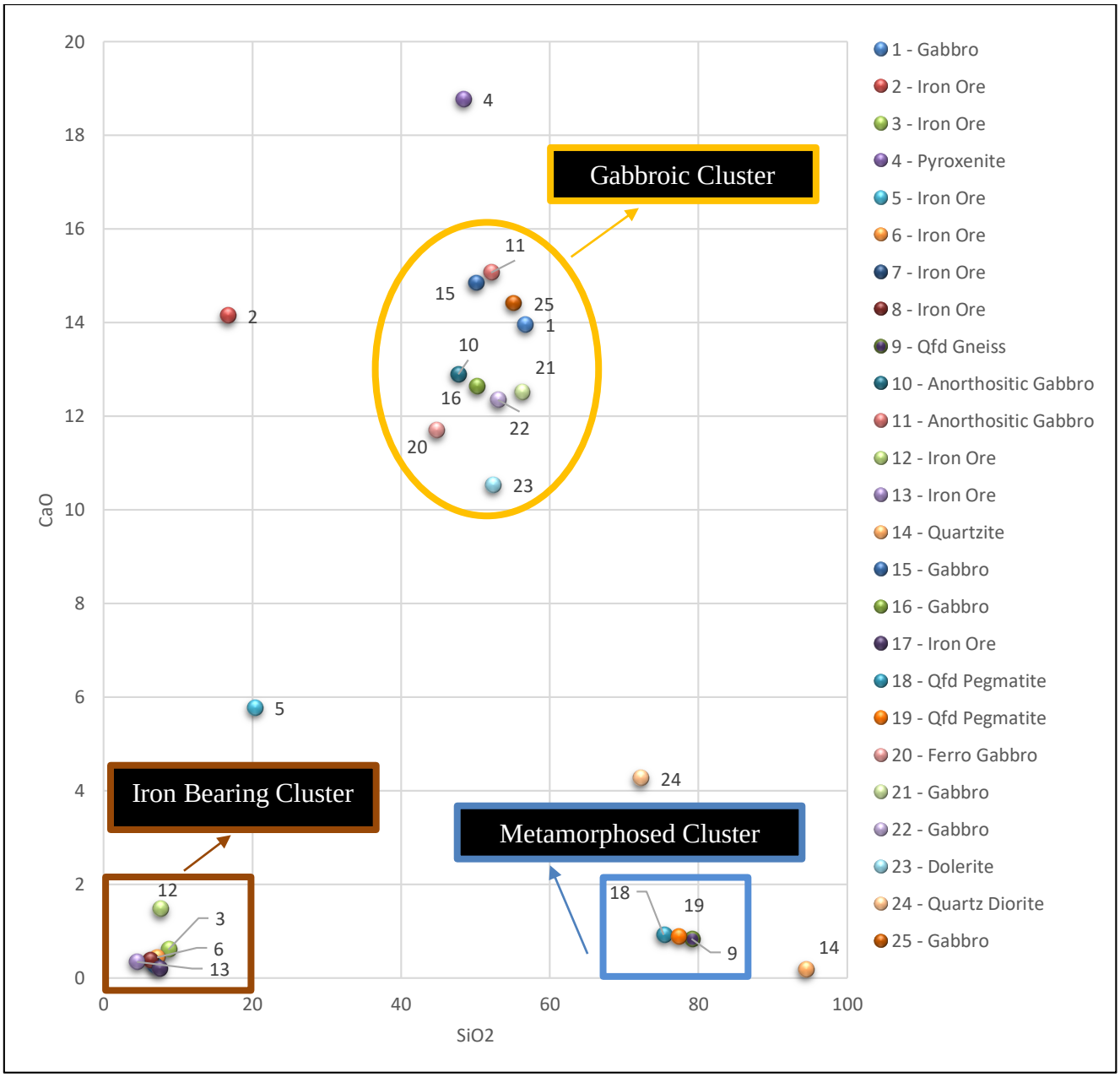


Figure 4.96: CaO vs $SiO_2$ Plot

In Figure 4.96 plot above, the clustering of ores, gabbroic rocks, and metamorphosed rocks is evident. The plot shows that the iron-bearing ores are different as three basic groups have been identified indicating ore categorization.

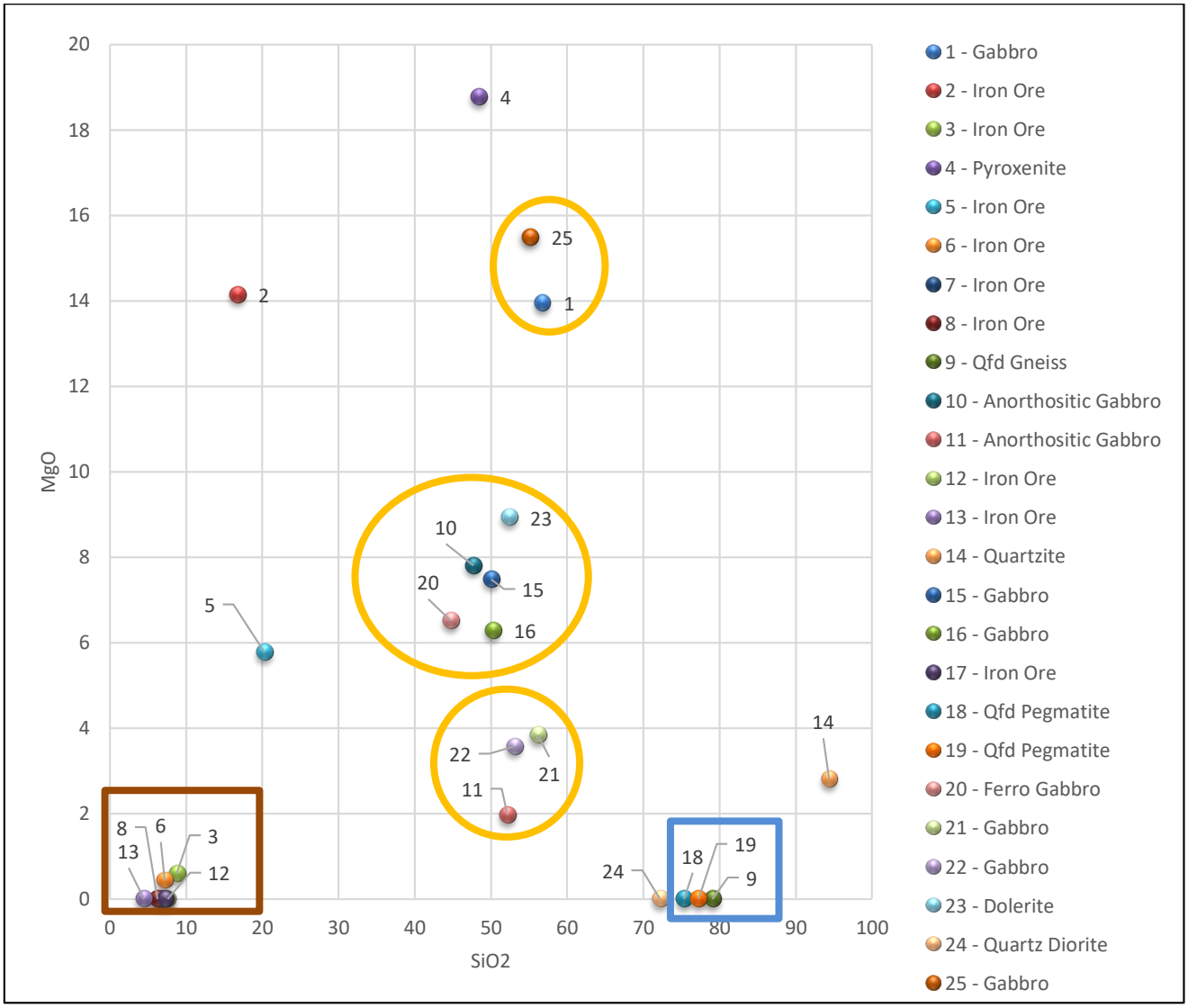


Figure 4.97: MgO vs $SiO_2$ Plot

Similarly, Figure 4.97 showing MgO vs $SiO_2$ plot, indicates three different clusters for the iron ore and three clusters for the gabbroic rocks. The clustering color coding is as in Figure 4.96. The metamorphosed cluster shows enrichment in silica content and this is consistent with Figure 4.96, petrography results, and XRD results. The iron ores show a deficiency in silica content and this again is consistent with the XRD and petrographic results.

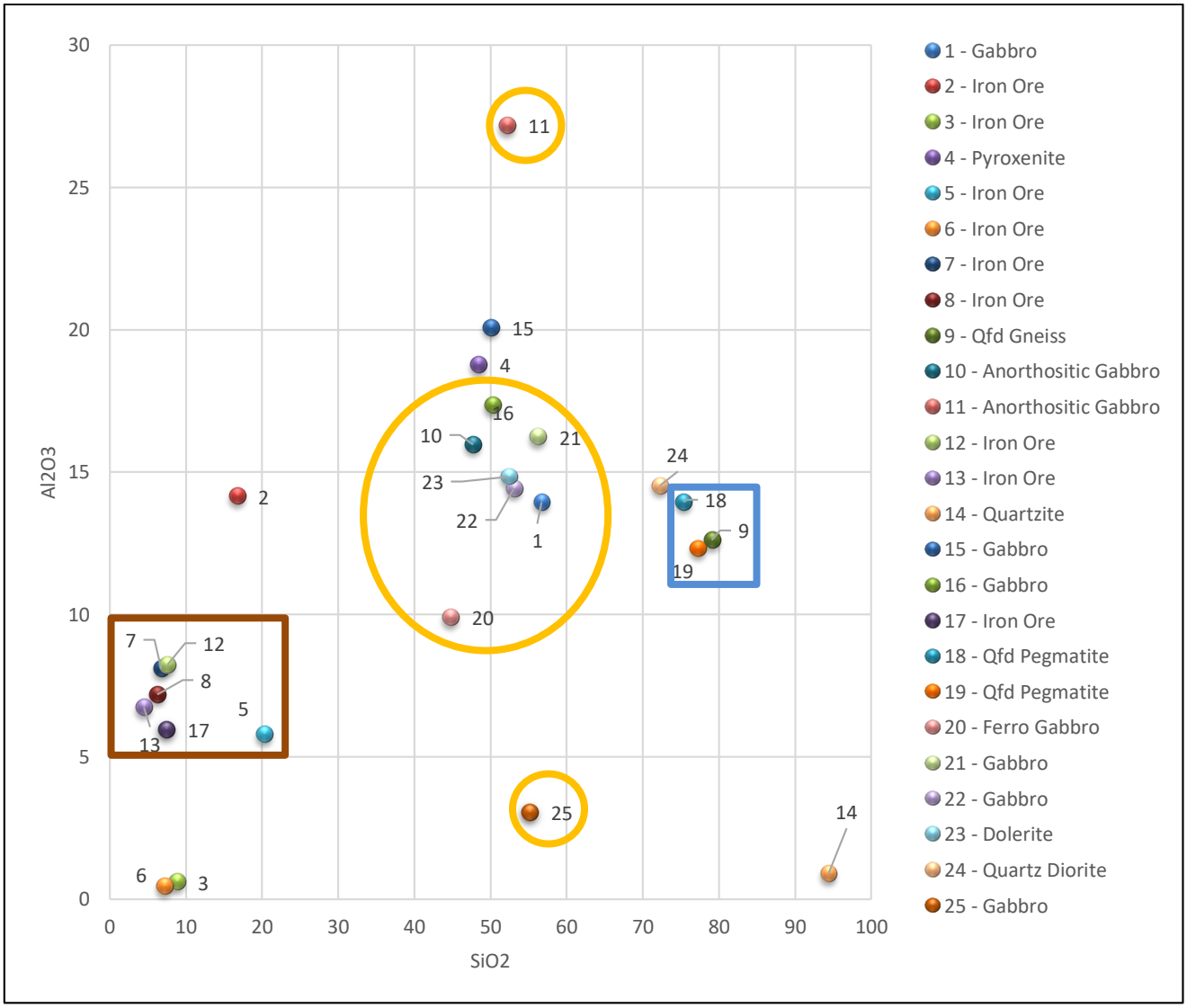


Figure 4.98: $Al_2O_3$ vs $SiO_2$ Plot

Figure 4.98 indicates three different clusters of gabbroic rock units and three clusters of iron ore occurrences. The clustering color coding is as in Figure 4.96. The quartzite sample, which is rich in silica is conspicuously located on the plot indicating Si enrichment. On the same plot, the metamorphosed samples indicate silica enrichment and considerable Al enrichment almost similar to the gabbroic units.

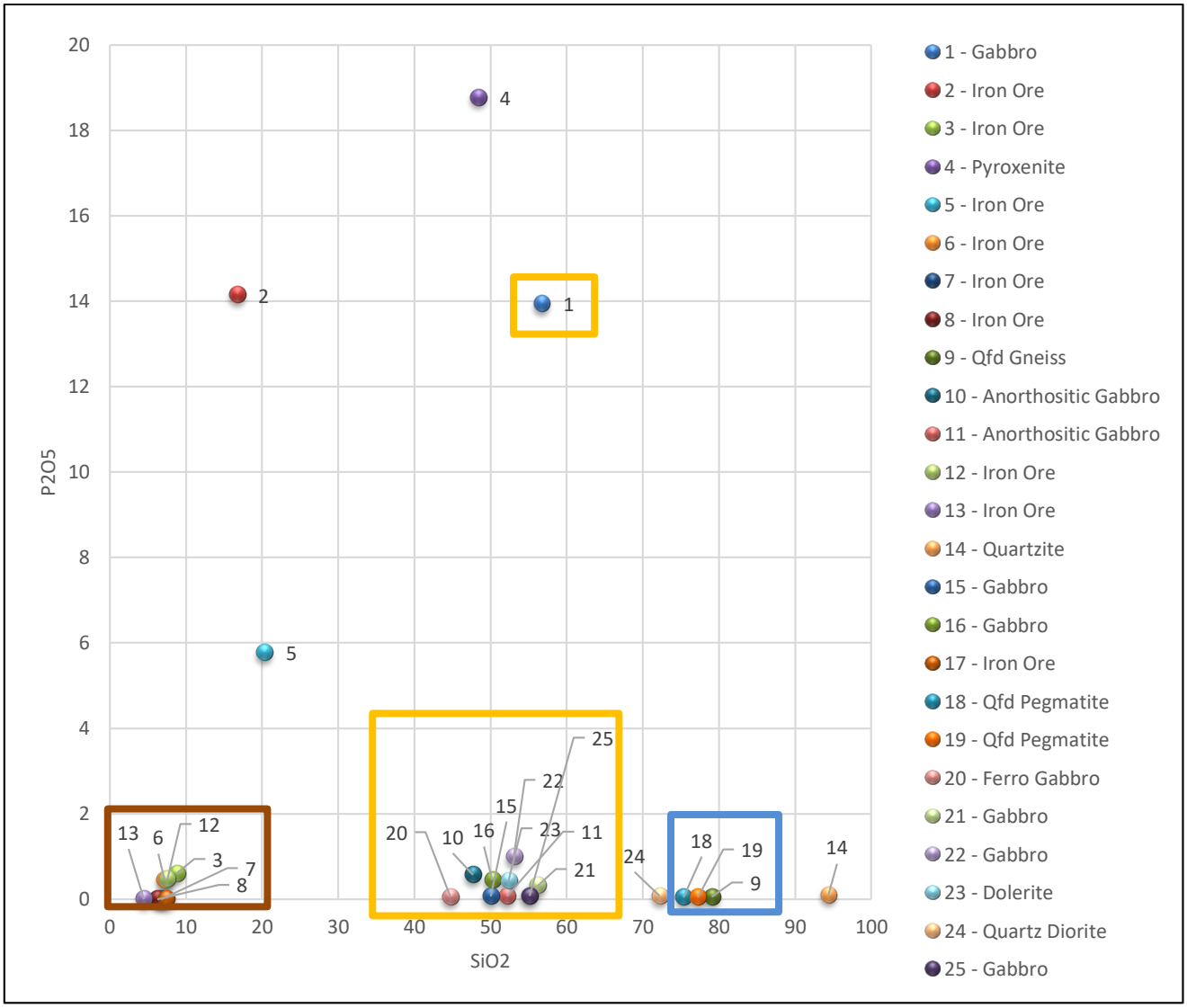


Figure 4.99: $P_2O_5$ vs $SiO_2$ Plot

The samples, as indicated in Figure 4.99, show a deficiency in phosphorus content. This is an exemption though, for some of the independent clusters. The clustering color coding is as in Figure 4.96.

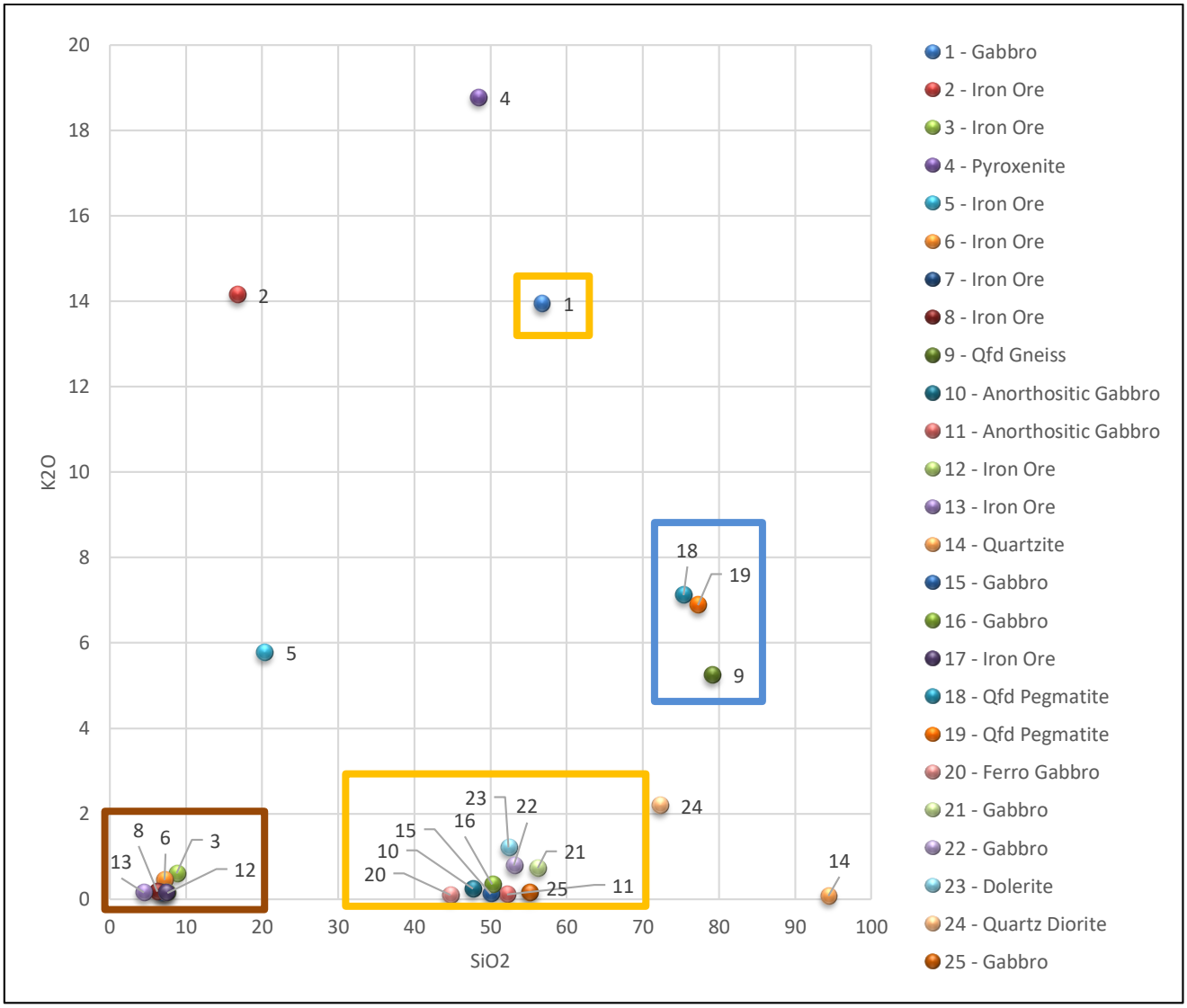


Figure 4.100: $K_2O$ vs $SiO_2$ Plot

Finally, the $K_2O$ vs $SiO_2$ plot indicates similar clusters with the evidence of additional clusters of the rock units. Gabbro, under this plot, shows 2 clusters. The iron ores indicate silica deficiency whereas, at the far end of the x-axis, quartzite indicates silica enrichment followed by the rock units with a metamorphic fabric and the gabbroic rocks. The clustering color coding is as in Figure 4.96.

From the above Harker diagrams, there is a slight variation in the trends and clustering for each of the combinations and this would suggest varied magmatic sources for the rock units. A similarity in trends would mean that the magmatic sources are the same.

### 4.4.2 Elemental Representation

The XRF results have also been used to plot the elemental representation curves for the sampling points for ease of comparison in regards to abundances, as illustrated in the section below. The elements have been plotted in weight percentage, representing 25 sites within the study area, Figure 4.101.

**Iron (1)**

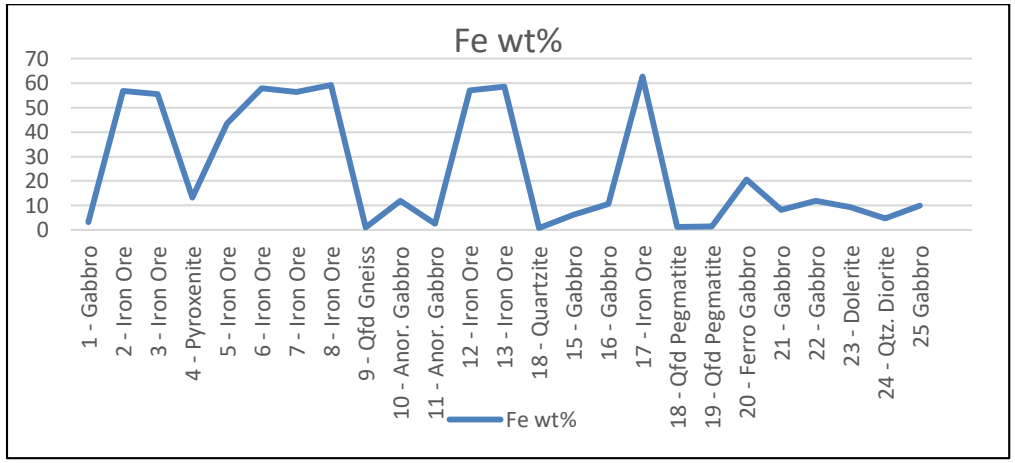


**Vanadium (2)**

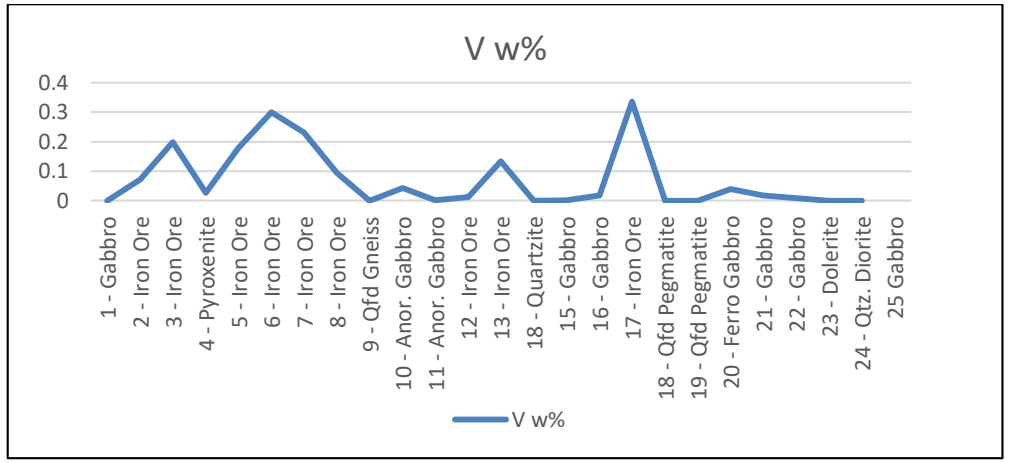


**Titanium (3)**

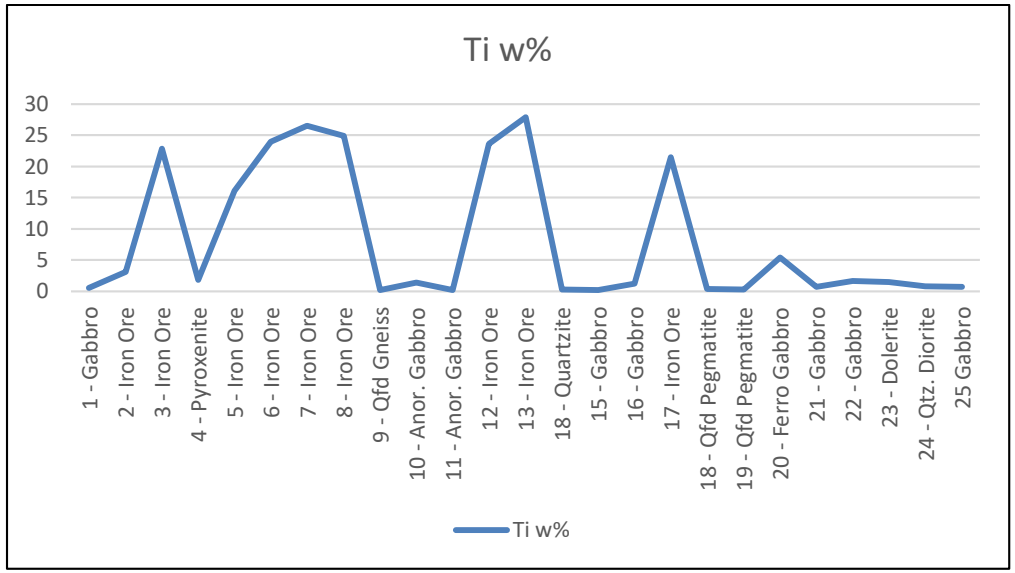


**Chromium (4)**

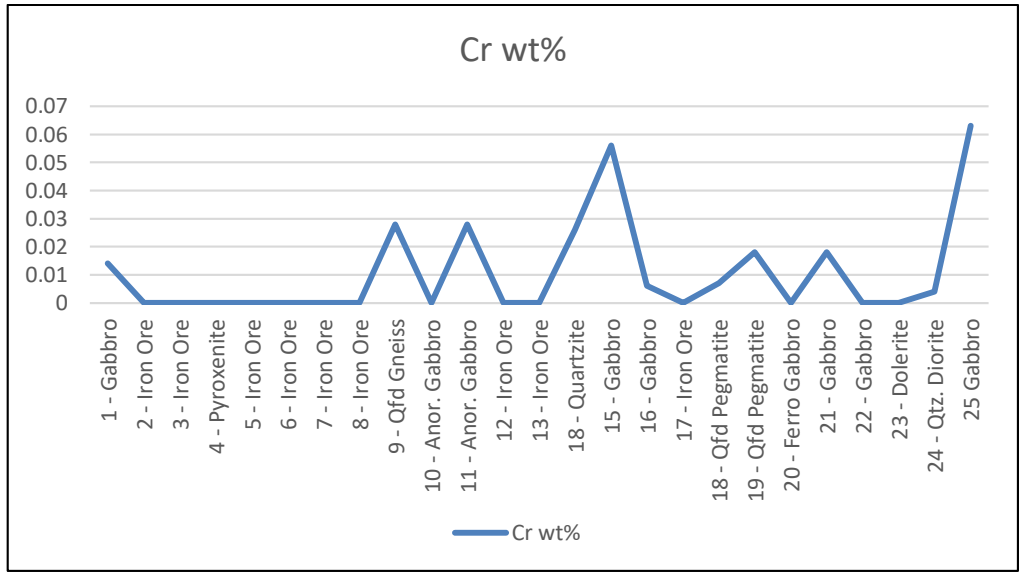

**Nickel (5)**

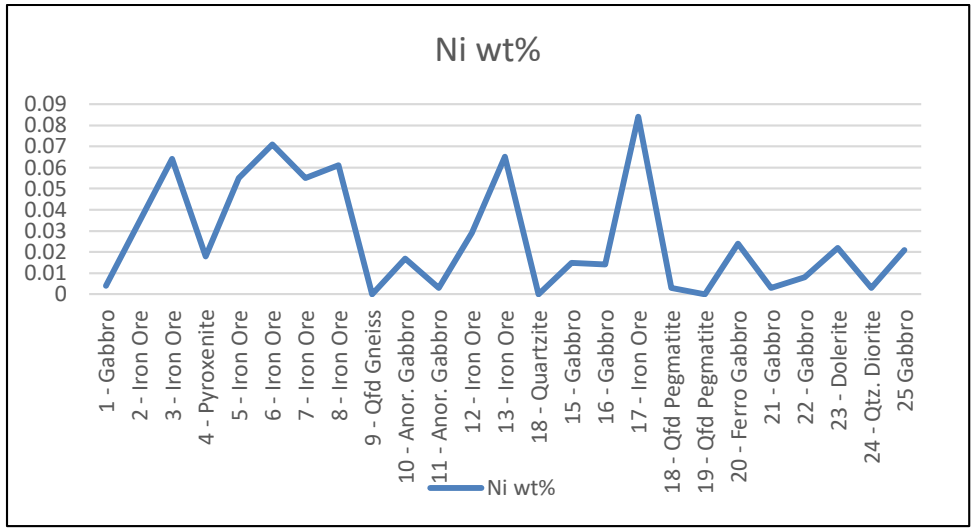


**Copper (6)**

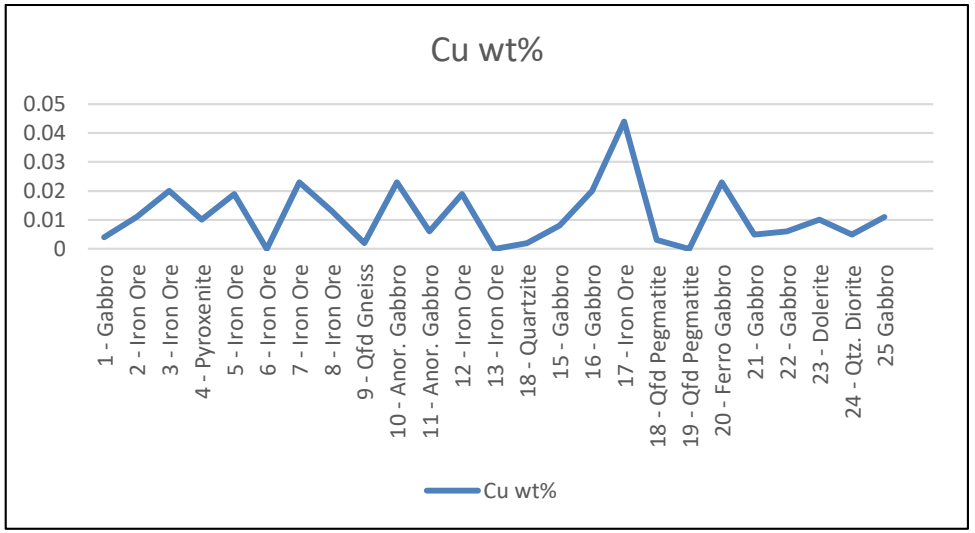


**Strontium (7)**

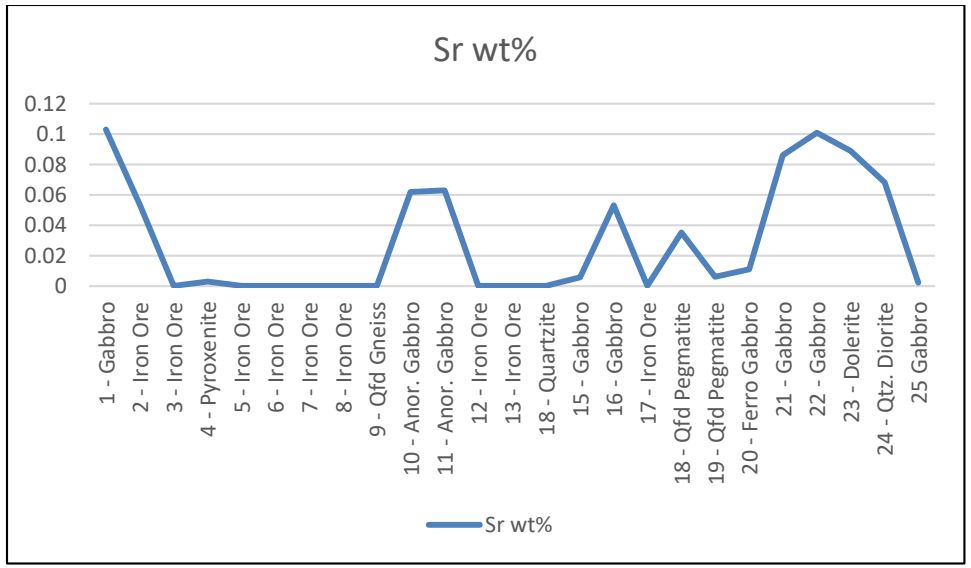


**Yttrium (8)**

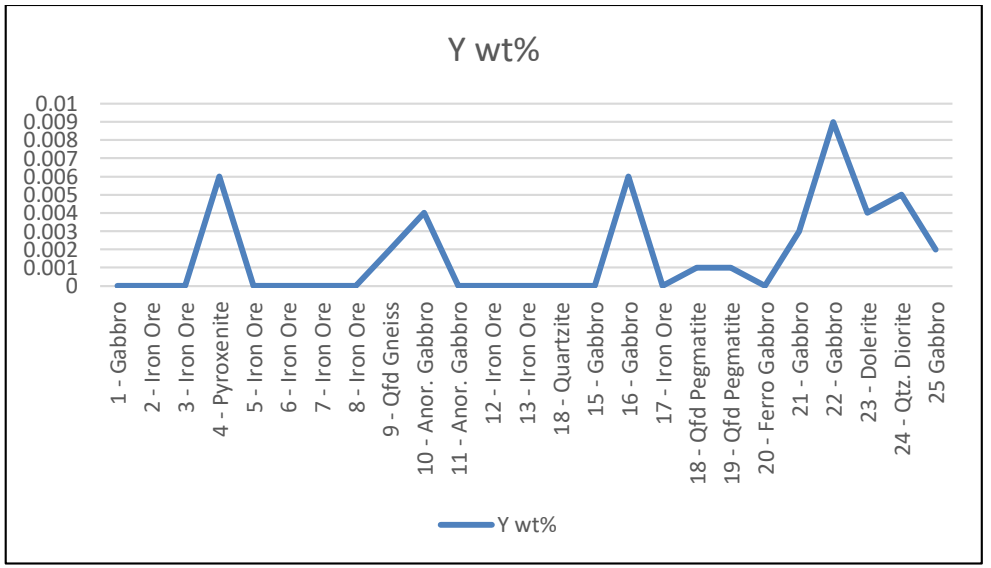

**Zirconium (9)**

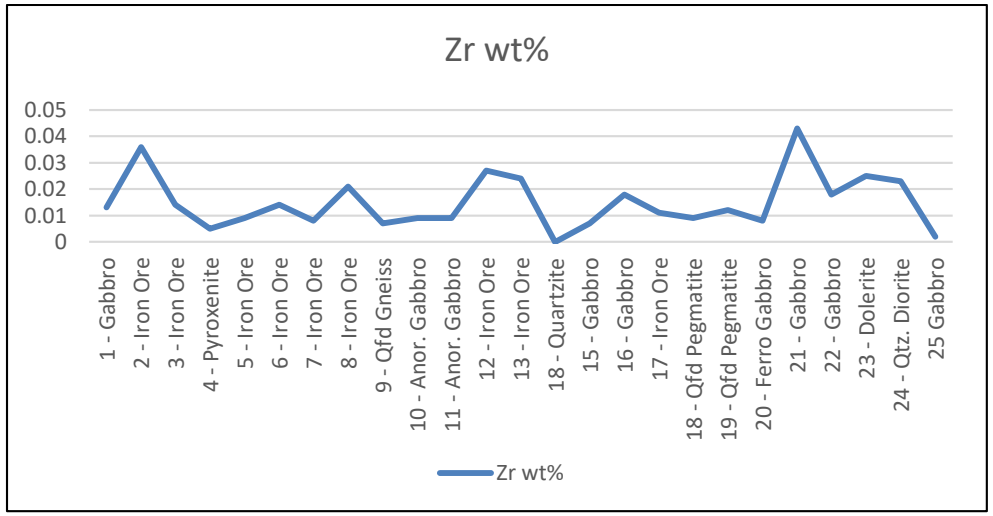


**Lead (10)**

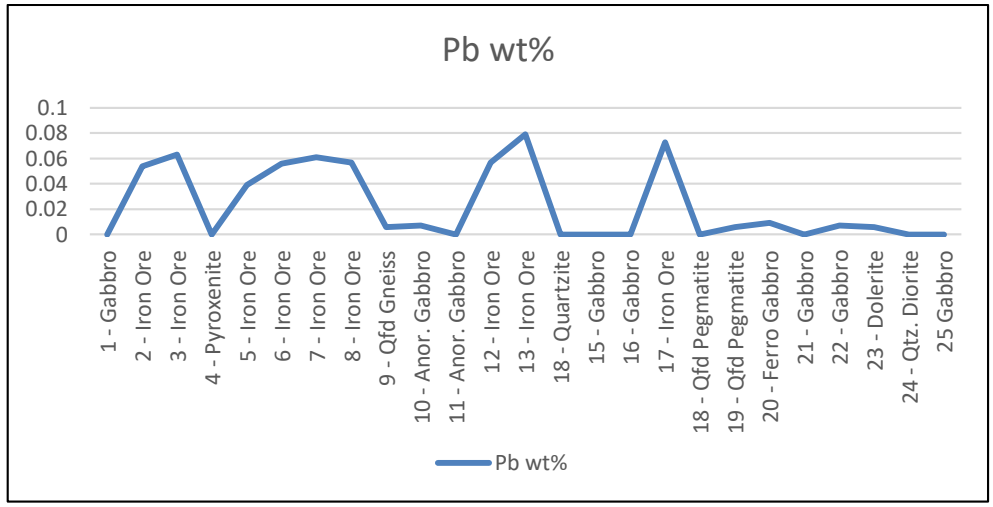


**Gold, Tungsten, Platinum, and Tantalum (11)**

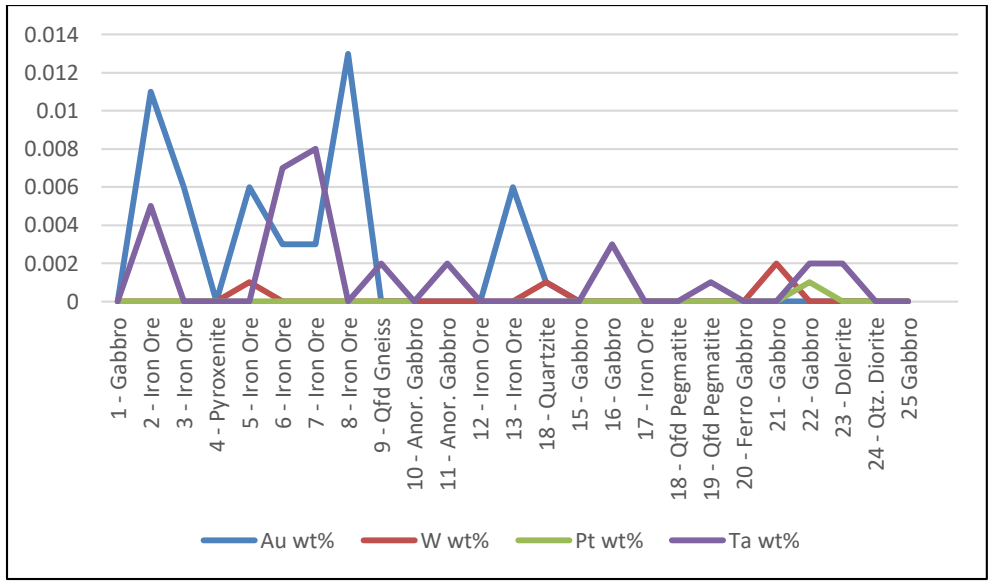


**Rubidium (12)**

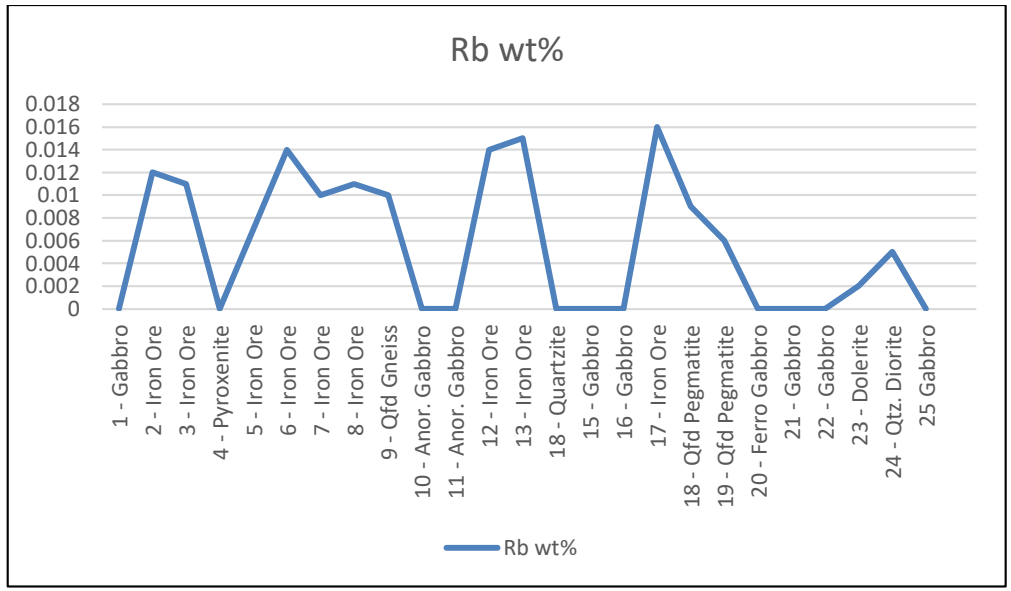

**Cobalt (13)**

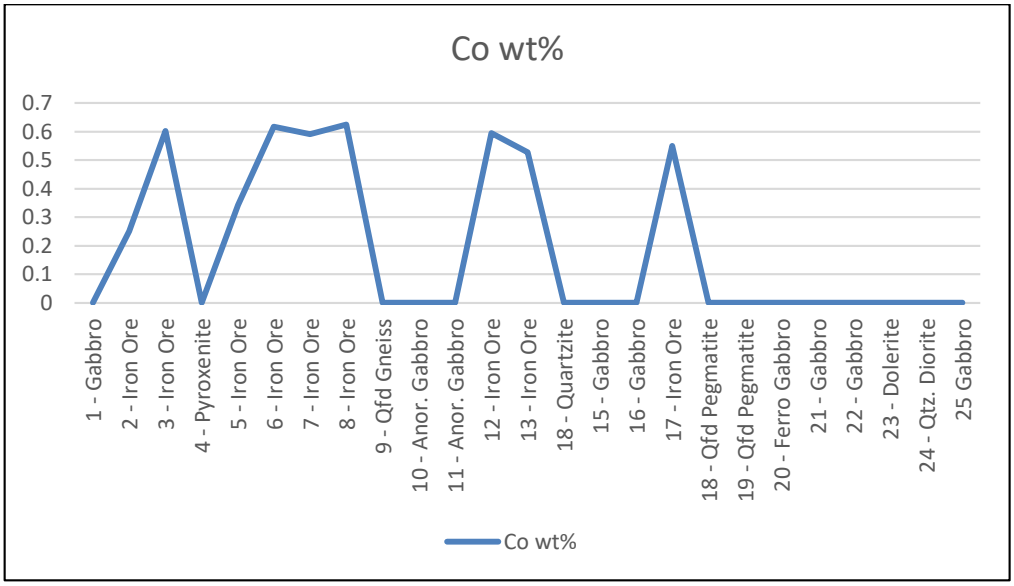


Figure 4.101: Plots illustrating the elemental representation with respect to the sampling points.

The XRF results have been used to plot the elemental representation for the sampling points, as illustrated in the diagrams. The elements have been plotted in weight percentage, representing 25 sites within the study area. The Platinum Group Metals are rare with only Pt occurring in minute quantities in sample 17 and sample 22. There is iron and titanium enrichment in all the ores as indicated in Figure 4.101 (1) and (3). By comparison, the iron ores contain more iron enrichment than titanium enrichment. Further, and in addition to Fe/Ti enrichment, the iron ores show enrichment in the following elements (Vanadium, Nickel, Copper, Lead, Rubidium, and Cobalt) compared to the gabbroic rocks where the gabbroic rocks indicate nil or close to zero enrichment for some of these elements. On the other hand, the gabbroic rocks show enrichment in the following elements with almost nil occurrence in the iron ores: Chromium and Strontium. There are indicative traces of gold in the iron ores warranting more investigative analytical studies for gold to ascertain the economic viability of the Au mineralization.

Attention is drawn to control station SMP-09 which shows nil or close to nil occurrences for the above elements. Iron, titanium, yttrium, copper, zirconium, lead, tantalum, rubidium, and chromium occur only in trace levels and as mentioned earlier, the minute quantities signify that the conditions at the study area were highly localized. Chromium concentration as presented in the results is low. This would give an inference of the origin of the parent rock as abyssopelagic whereas a high concentration of chromium would indicate subduction origins.

## 4.5 Discussion

It is noted that the Kithiori rock units and deposits are as a result of multi-phased magmatic evolution in form of deposition and crystallization, with some of the gabbroic rock units representing ultramafic portions of what indicates the ophiolitic suite, Figure 4.93. The area faced several episodes of secondary alteration through hydrothermal processes and structural modifications seen through features such as the cross-cutting discordant dykes. These processes had significant impacts on the formation of iron ore, gabbro, anorthosite, pyroxenite, diorite, and dolerite which constitute the geology of the area and a majority of these processes were highly localized

### 4.5.1 Mineralization of Iron Ore

It is imperative to note that close to half of the study area has varying concentrations of iron ore deposits. The occurrence and relation of the ore deposits with the structures and geology forms the basis of the objectives of this study. Two main hypotheses have been suggested as possible causes for the mineralization of the iron ore deposits, as follows:

During formation and crystallization, the minerals within the magma were dissimilar due to varied elemental properties. This variation led to fractionation which, when the magma began to cool, minerals associated with gabbro, anorthosite, dolerite, etc were expunged, at a cotectic, from the melts leaving behind magma richer in Fe – Mn – Ti concentration. Fe – Mn – Ti would be inferred to be incompatible with feldspars and pyroxene during magmatic setting, as alluded to by (Hoatson and Glaser, 1989). With this in mind, various conditions are seen to play an important role in the crystallization and mineralization of iron ore. (St. Clair, 1913) reports of ore deposits produced by magmatic segregation focussing on ores from Sudbury. In her research, (St.Clair, 1913) notes that the gabbroic units together with the iron ores of Sudbury occur as a result of magmatic differentiation.

What role does alteration play in the formation of iron ore, one may ask? There are numerous intergrowths of iron ore in and around pyroxene minerals, sample 03 from SMP-03 is an example. This has been noted at the edges of the pyroxene minerals within the pyroxenite rocks. It is commonly known that pyroxene minerals predate iron oxides but through alteration, the latter is formed. Magnetite and ilmenite are the dominant iron oxides and occasionally, titanium-iron oxides are seen to occur. In this hypothesis, it is postulated that mineralization took place under oxidation conditions.

Moreover, pockets of iron ore were noted and mapped in key sections of the study area, as disseminated occurrences. An example is given of sample SMP-14 where iron ore is noted to occur in a uniquely massive outcrop of quartzite, Figure 4.76. What would be the mode of formation of these minute occurrences of iron ore stains on the quartzite? Perhaps, during the formation of the quartzite, some chunks of Fe – Mn – Ti mineralization were confined as "Fe – Mn – Ti bubbles" and crystallized as xenocrysts. These disseminations are also noted in some other sites where iron ore is disseminated in gabbro and pyroxenite, with the latter representing a majority of the nature of the occurrence.

It is important to note that the above occurrences are exceptional and limited to a few sites and in small pockets. The bulk of the mineralization occurs in form of exclusive iron ore masses some of which have distinct euhedral shapes, Figure 4.32. The iron ore boulders were noted to be very dense compared to the intrusives further suggesting a unique mode of formation, such that the Fe – Mn – Ti-rich magma crystallized in isolation given that a majority of other elements had been isolated to form intrusives. This is qualified by the fact that the iron ores are characterized by rare earth elements which, like Fe – Mn – Ti, are incompatible. Comparatively, the intrusives have few rare earth elements.

Further to the above theories, crystallization of the culumates is hinged on two very critical parameters, temperature (T) and pressure (P). (T) in the sense that the incompatibility of the Fe – Mn – Ti elements and the mainstream intrusive elements played an important role in the fractional crystallization. Parameter (P) comes into play insinuating that the area of deposition may be either primary or secondary, i.e the environment of accumulation could be different from the location of deposition and crystallization. This means that either there was in situ crystallization where massive units of iron ore occur or there was mass and/or minor mobility due to pressure changes and pressure differences that caused the Fe – Mn – Ti-rich magma to crystalize elsewhere such as along fractures and faults. What has been noted in the study, is that some of the iron ore crystallizations were structurally controlled.

### 4.5.2 Evidence of hydrothermal/epithermal/metasomatic conditions

Various minerals in gabbro, pegmatites, and pyroxenes give a clear indication of the possibilities of having had hydrothermal/epithermal conditions and this influenced the nature and occurrence of rocks in the Marimanti area. Below are some of the minerals/elements which were observed and hence justify this argument:

**i. Mineral / Element Name: Tellurium (Te)**

Occurrence: SMP-03, SMP-04, SMP-10, SMP-11, SMP-15, SMP-18, SMP-19, SMP-20, SMP-21, SMP-22 and SMP-23

Discussion: In their work, (Paar *et al.*, 2005), have discussed Tellurium element as an epithermal mineral with occurrences in Argentina. (Iatan, 2009) reports of similar occurrences in Romania and (Hein *et al.*, 2003) have given an account of the global occurrence of tellurium-rich ferromanganese crusts and a model for the enrichment of tellurium. This could be true for the occurrence of Te in the study area.

Tellurium, a chalcogen, is noted to occur in some cases, in association with Selenium. This is the case in gabbro mentioned above and in anorthosites at SMP-10 and SMP-11. In their research on Tellurium, (Goldfarb *et al.*, 2017) allude to various processes that lead to the occurrence of this element. Hydrothermal/epithermal processes come across as one of the common processes. In their findings, Tellurium occurs in association with other elements such as copper and gold some of which are noted in the study area.

**ii. Mineral / Element Name: Titanite**

Occurrence: SMP-10, SMP-22

Discussion: Various writers have written about the occurrence of sphene (titanite) in pegmatitic and hydrothermal environments. Sphene, an accessory mineral has been noted in some of these environments by (Giere, 1992).

**iii. Mineral / Element Name: Klockmannite**

Occurrence: SMP-15

Discussion: (Spieth, 2019) notes that Klockmannite is of hydrothermal origin based on the nature of the occurrence. Klockmannite occurs in considerable quantities in SMP-15 at about 10%.

**iv. Mineral / Element Name: Sellaite**

Occurrence: SMP-19

Discussion: Based on research on the origin of this mineral, (Pfaff *et al.*, 2012) note $MgF_2$ forms under dynamic PT conditions of hydrothermal nature. At SMP-19, Sellaite quantities are rather high, at 30%.

**v. Mineral / Element Name: Permingeatite**

Occurrence: SMP-19

Discussion: Permingeatite has been noted in various locations worldwide such as in Czech as recorded by (Škácha *et al.*, 2017). In their research, this mineral occurs together with other selenides such as hakite and crookesite among others. Permingeatite is 1.0% at SMP-19.

**vi. Mineral / Element Name: Hawleyite**

Occurrence: SMP-19

Discussion: (Traill and Boyle, 1955) were among the first to write about the Hawleyite mineral. In their research journal, they describe the origin of this mineral as one that occurs as a secondary mineral having been deposited in veins and fractures. In the study area, the outcrop at SMP-19 is entirely a massive pegmatite with various characteristics of a hydrothermal setting. This mineral is just but one of the indicators that complement the aforementioned minerals as an inference for hydrothermal processes. Hawleyite is 4.9% at SMP-19.

**vii. Mineral / Element Name: Caminite**

Occurrence: SMP-09

Discussion: (Haymon and Kastner, 1986) have given a concise report on the occurrence of Caminite in hydrothermal conditions. (Schmidt *et al.*, 2019) also, report on the formation of Caminite through hydrothermal processes in the Terceira Rift of the Atlantic Ocean. Further, they state that Caminite is a rare mineral and occurs in special conditions and recharge areas of hydrothermal systems. At SMP-09, this mineral comprises about 16.6% of the sampled and analyzed rock.

**viii. Mineral / Element Name: Fizelyite**

Occurrence: SMP-09

Discussion: (Sugaki *et al.*, 1983) report on the geological study of the polymetallic ore deposits in the Potosi District, Bolivia. In their report, they note that five out of six mines within the Potosi District are hydrothermal deposits. Fizelyite is one of the many deposits mentioned in the report recorded to occur in this set up in close association with other polymetallic ore deposits of sulfur such as galena, sphalerite among others. The presence of fizelyite at SMP-09 is yet another example of a hydrothermal mineral that could infer the presence of hydrothermal processes.

**ix. Mineral / Element Name: Argentopentlandite**

Occurrence: SMP-24

Discussion: This Silver bearing pentlandite mineral has been referenced by various writers who note its occurrence in world-class mines such as Sudbury, Canada. (Ruano and Hach - Ali, 1996) in their journal, give a highlight of the occurrence of Argentopentlandite as a result of hydrothermal processes in Spain.

**x. Mineral / Element Name: Selenium**

Selenium is a common factor among the mineral species in some gabbro rocks. It has been used to deduce the nature of occurrence for gabbro units in the study area. (Stillings, 2017), indicates Selenium occurrences in hydrothermal and magmatic conditions for the formation of Se-rich minerals. She also associates Se with sulfides which it commonly substitutes in many mineral assemblages. (Stillings, 2017) outlines many modes of occurrence for Selenium and lists several other elements associated with its formation. The report takes note of related structures such as veins and stockworks as probable environments for the formation of Se-deposits. These structures have been hosted by various rocks of igneous origin, including gabbro. Another study carried out by (Koljonen, 1973) on the occurrence of Selenium in igneous rocks records Selenium occurrences in hydrothermal environments in Finland. Many of these deposits are structurally controlled, occurring in pegmatites, veins, and other structures of similar nature. Many similarities have been noted in the study area in the manner in which Selenium hosting minerals occur, in gabbro.

It is generally observed that a decrease in Calcium, Silica, Aluminium, and Sodium content is accompanied by an increment in Iron and Titanium content through the gabbroic rocks to the ores. The gabbro and the anorthosite rocks have a synonymous signature with respect to mineralogy only except the variations of the dominant mineral plagioclase feldspars and minute mafic mineral content. Some common phenomena are noted which give the inference of diverse processes and parameters that may have influenced the formation of the rocks, in addition to what has been discussed before.

i. The constituent mineral components in the two major units are a mixture of both albite and anorthite end series. The diversity of the feldspars within the An – Ab series depicts conditional changes with which the rock units were formed. The plagioclase feldspars are richer in the An content than in Ab content, i.e. labradorite and anorthite dominate

the units. An-rich minerals are known to form from high temperatures. This is commonly shown by solid-solution diagrams for example.

ii. The second trend that is evident in the petrographical studies is zoning in concentric nature. Zoning is common with the accessory minerals occurring within the plagioclase feldspars. In dolerite, anorthosite, and gabbro, zoning is clear and obvious and this could signify periodic magmatic replenishment.

iii. Embayment into the plagioclase feldspar crystals infers a clear change in the environment during crystal growth.

Geologically and of notable importance is that the dolerite dykes and gabbro have nearly full compositional equilibrium. It is important to point out that plagioclase feldspars range between 79.2% to 93.8% in the rocks, with minor and accessory minerals making up the rest of the percentage. It is also key to note that the crystal sizes and texture of these rocks are distinct. This begs the question, why are the dykes having smaller crystals compared to the host gabbro rocks? Would the two units have crystallized from different magmas? If this analogy is true, then there would generally be compositional variation. Would this be a unique hypothesis of the formation of different physical properties from the same parental melt?

(Anderson *et al.*, 1984), (Bea *et al.*, 2005) and (Pistone *et al.*, 2015) have described filter pressing and suggest that this could be the reason behind the different grain sizes and similar mineralogical composition as witnessed in the gabbro and dolerite dykes.

Worth taking note of is the deficiency of K-Feldspars in both the gabbro and the anorthosite. This shows that the melts from which the gabbro and the anorthosites formed were Ca-Na rich signifying high to intermediate temperatures of magmatic cooling. Their textures too are a function of the rate of cooling. Comparatively, elsewhere in this report, we take note of the fractional crystallization of Fe-rich magmas as a function of temperature reduction.

A few kilometers from the gabbroic units are the quartzofeldspathic gneisses which are K-Feldspar rich with sedimentary fabric. The formation of the gabbro and the gneisses are different as occasioned by the different species of feldspars.

The richness in Ca-rich pyroxenes resonates with the Ca-rich feldspars and this would signify comagmatism, the main difference being varied PT conditions. As noted in the results some pyroxenites such as SMP-04 contain significant amounts of Calcium Pyroxenes; Augite and Diopside. Aluminous augite constitutes about 50% of the pyroxene minerals in SMP-04

whereas diopside ferrian constitutes about 36% of the pyroxene minerals in the sample. In total, pyroxenes are about 86.4% of the rock sample. The pyroxenites occur in close juxtaposition with the gabbroic rocks and this could imply that the pyroxenites may have been comagmatic but under different PT conditions, (Sriramadas *et al*., 1969) on synthetic experiments.

### 4.5.3 Platinum Group Elements (PGEs)

It is noted that the following three PGEs occur in the study area based on XRD results: Platinum, Palladium, and Rhodium. These, have been noted to occur at SMP-04, SMP-12, SMP-16, and SMP-21, associated with iron ore and intrusives. Traces of Platinum are noted in samples SMP-17 and SMP-22.

Palladium is one of the regular occurring Platinum Group Elements in the gabbro series. (Zientek *et al.*, 2017) in their research on Platinum Group Metals, indicate that it can substitute for nickel in the mineral pentlandite. This mineral is seen to occur in sample SMP-24, though at this stage nickel has not yet been replaced. If this is the case, this inference may hold for the occurrences of Palladium at SMP-16 and SMP-21.

The PGE formation in the Bushveld Complex has been described by (Cawthorn *et al.*, 2002), (Cawthorn, 2010). The latter gives a highlight of findings by previous researchers. Two major hypotheses have been suggested as possible origins of the PGE associated minerals. Hypothesis (i) suggests an upward fluid infiltration where PGE and S-rich waters dissolved into the magma which was later recrystallized to form rocks. Hypothesis (ii) suggests downward accumulation of Platinum Group Elements which was followed by various magmatic enrichment processes. Both theories have their fair share of opinions and criticisms from subsequent researchers whereas others conducted more studies based on the previous studies. (Cawthorn, 2010) concludes that many episodes of magmatism played crucial roles in the PGE enrichment.

(Hoatson and Glaser, 1989) give various theories for the enrichment of PGE, some of which have been alluded to by other researchers. In this research, (Hoatson and Glaser, 1989) suggest possible fractional crystallization and filter pressing which have been mentioned elsewhere in this report. They also mention hydrothermal processes and incompatibility of some PGEs as possible ways of enrichment.

The major PGE complexes across the world have been studied extensively by many researchers over time. The study area on the other hand has very limited information on PGE and associated

minerals. This notwithstanding, several similarities have been drawn from the heavily researched complexes globally. Some of the similarities are on the nature of the occurrence of the rocks, the types of rocks, the nature of geological structures, the mineral occurrences among others. The preliminary inference is made that multi-phased episodes of magmatic action affected the study area resulting in the formation of the PGE.

### 4.5.4 Rare Earth Elements

The fifteen (15) elements of the lanthanide series are popularly known as Rare Earth Elements, (REEs), which includes both LREEs and HREEs. Two more elements, Scandium and Yttrium are regarded as REEs due to chemical similarities with the lanthanides. Of the seventeen (17) elements, eleven (11) are spread across the study area as mineral assemblages, in varying quantities and different rock types. Some of the REE assemblages have been listed below:

i. SMP-25 has the following seven lanthanides Neodymium, Cerium, Gadolinium, Dysprosium, Holmium, Thulium, and Lanthanum.
ii. SMP-08 has four REEs namely: Lanthanum, Cerium, Praseodymium and Neodymium.
iii. SMP-20 has the following four: Praseodymium, Samarium, Lutetium, and Lanthanum.
iv. SMP-21 has four: Cerium, Ytterbium, Praseodymium and Gadolinium

Other REEs are spread in other units in lesser quantities, i.e. one to three occurrences. Mineral assemblages bearing REEs in SMP-25 comprise 79.5% of the entire sample. This is a significant quantity of rare earth elements on a single sample. Of the analyzed samples, Lanthanum has 9 individual occurrences in mineral assemblages, Cerium has 8, Praseodymium has 5 whereas Gadolinium, Ytterbium, and Yttrium each have 4 occurrences as elements forming mineral species.

(Van Gosen *et al.*, 2017) have described the origin of the name “rare earth” elements showing that some REE are in actual fact more abundant than some of the well-known elements such as Ag, Au, and even Pt. It is usual for Rare Earth Elements to exist in unison due to similarities in properties. The progression from one element to another in succeeding fashion causes contraction of radii of these elements because of reducing the atomic radius. The higher charge of (+3) has a knock-on effect on the formation of ores from parental magma. REEs, therefore, tend to crystalize last after mainstream elements crystalize, leaving the magma saturated with

lanthanides. This theory best explains the reason why 60% of the rare earth elements are present in the study area, with a closer focus on SMP-25 which has its uniqueness. This fractionation phenomenon also affects the individual optical mineralogy and magnetism of the elements. This circumstance labels the REE as discordant elements. (Van Gosen *et al.*, 2017) have given more examples of discordant elements such as Th, Hf, U, Zr, Ta, Sc, Nb, Ti, and P which we have taken note of in the XRD results of the Kithiori study area. SMP-25 has the most occurrences of rare earth elements. The geology of the area in which it was sampled is interesting to some extent. Whereas the above mechanism of the formation of the rare earth elements is postulated, it is important to note that there is obvious evidence of tectonism within the region of SMP-10 and SMP-25. The rocks were subjected to strain and suffered brittle fracture. This is thought to have occurred post-formation as the brittle fractured boulders cross-cut the host rocks.

### 4.5.5 Gold Occurrence

XRD analysis of sample 01 from SMP-01 shows occurrences of Gold in the following mineral assemblage: $Au_5$ $Zn_8$. Sample 01 is gabbroic. XRF on the other hand shows traces of Gold in the following samples, all of which are ores of iron or contain traces of iron. SMP-02, SMP-03, SMP-05, SMP-06, SMP-07, SMP-08, SMP-13 and SMP-14. A general observation is that the occurrences of Au are structurally controlled. SMP-01 is in an area that shows evidence of shear / ductile movement in the North-South direction and mm-size strained zones.

# CHAPTER 5 CONCLUSIONS AND RECOMMENDATIONS

## 5.1 Conclusions

The study area is a complex geological setting as the findings of the study reveal the occurrence of many different processes, possibly, at different episodes. The episodical and lithological margins are also very fine in terms of the manifestation of the intrusives, the iron ore, REE, and the other associated minerals. The petrology and mineralogy of the area can best be defined based on the major rock units that have been mapped. The main rock units include pockets of iron ore, gabbro, anorthosite, dolerite, pyroxenite, quartzite, quartzofeldspathic pegmatite, and quartz diorite.

It is imperative to note that close to half of the study area has varying concentrations of iron ore mineralization which also contain quantities of REE and other associated metals. Two main hypotheses have been suggested as possible causes for the mineralization of the iron ore deposits. The first one is fractional crystalization due to elemental incompatibility and the second one is through alteration of minerals. In both hypotheses, the study notes that temperature and pressure may have had an important role in the mineralization of the iron ore, REE, and the associated minerals. What has been noted through field relations in the study, is that some of the iron ore mineralization is structurally affiliated. For instance, some of the iron mineralization was noted to occur alongside pyroxenite pegmatites and quartzites which had specific structural dimensions in terms of orientation. This said, it is important to note that the dolerite dyke intrusions have not been associated with the iron ore mineralization.

Based on petrographical, XRD, and XRF analysis, the gabbroic units (the combination of gabbro, dolerite, and anorthosite) contain in excess of 70% plagioclase feldspar mineralization. The entire plagioclase group of minerals was confirmed from the sodium-rich Albite to oligoclase, andesine, labradorite, bytownite, and the calcium-rich anorthite. The dominance of these feldspar minerals makes the rock units almost monomineralic. Further, of the six plagioclase minerals the dominant ones are oligoclase, labradorite, and anorthite, mapped at SMP-01, SMP-10, SMP-11, SMP-15, SMP-16, SMP-21, SMP-22. This was confirmed for both XRD and petrographic results where the 2θ results/peaks and optical properties perfectly integrate. These rocks are of magmatic origin with the gabbro having ophiolitic signatures.

Two major anorthositic suites (Type 1 Kithiori Anorthositic Suite and Type 2 Kithiori Anorthositic Suite) have been suggested based on various degrees of similarity in mineralogy

but slightly different texture and coloration. Many indicator minerals form part of the gabbro indicating hydrothermal action. Some of these minerals include titanite and klockmannite among others. The gabbroic rocks have been cut across in a discordant manner, by dolerite dykes and this is not unique to gabbro because the same is seen to occur across the pyroxenite rocks.

The pyroxenite rocks on the other hand contain clinopyroxene minerals such as augite and diopside ferrian in considerable quantities and a similar case, making the rocks almost mono-mineralic. The accessory minerals include platinum oxide, antimony vanadate, and stannites. It was noted that the pyroxenite rocks correlate with the iron ore mineralization through alteration of iron-rich pyroxene minerals into iron ores, SMP-03 and SMP-12. This, however, as indicated earlier, is complemented by hydrothermal among other processes.

Further East of the study area, it is evident that the lithological units exhibit metamorphic fabric in form of mineralogy, mineral lineation, boudin, pinch, swell structures, and elongated crystal shapes as seen in the quartzofeldspathic pegmatites. This was further confirmed through the geology reported at the control sampling point SMP-09 which is a quartzofeldspathic gneiss. The quartzofeldspathic pegmatites and gneisses contain minerals such as quartz, feldspars, accessory minerals such as sellaite, hawleyite, permingeatite among others. These minerals give a different dimension of the processes that occurred in the study area.

The dolerite dykes form a major part of the geology of the area where the mafic dykes of varying widths were seen to cut across host units. Following analysis carried out on the dolerite, it was noted that the mineralogy is similar to that of gabbro and anorthosite. This study concludes that filter pressing phenomena may have played a role in the formation of the dolerites, similar in chemistry with the gabbro/anorthosites but with different grain sizes and therefore different textures.

The rocks originated from multi-phased magmatic deposition and crystallization and crystallized under varied temperature/pressure conditions. Crystal fractionation played an important role in the development of various units based on their respective properties.

## 5.2 Recommendations

i. Several samples such as SMP-18 have radioactive elements such as Strontium whereas SMP-01 has Uranium. Future researchers could subject the rocks to various dating methods to determine the ages of the rocks.

ii. The area is seen to have undergone various processes that may have altered the mineral species. Detailed elemental transitional studies need to be conducted to document the possible transitional phases of the minerals and possible mechanisms of alteration.

iii. Extensive geophysical studies need to be conducted in the study area to complement the petrographic and geochemical methods used in this study.

iv. Many popular settings globally such as the Stillwater Complex in the United States and the Bushveld Complex of South Africa are known to have layered intrusions in which the PGE occurs. To ascertain the similarities in lithology and structures, it is recommended that future studies should incorporate the results of core samples from drill holes. This will be able to produce stratigraphic columns showing the vertical extent of the units/ores and will also help in correlation to determine the thickness and horizontal spread of the intrusives and ores. This way ore economics shall also be conducted and it shall be possible to calculate possible tonnages of the ores.

v. Due to vast occurrences of PGE and REE in what would seem to be anomalous quantities, future research should document the actual abundance of the elements in Kithiori compared to the actual abundance on the earth's crust.

# REFERENCES


Abuga, V., Moustapha, K., Migwi, C., Ambusso, W., and Muthakia, G. (2013). Geophysical Exploration of Iron Ore Deposit in Kimachia Area in Meru County in Kenya, Using Gravity and Magnetic Techniques. *International Journal of Science and Research (IJSR)* **2(11)**: 104-108.

Anderson, A., Swihart, G., Artioli, G., and Geiger, C. (1984). Segregation Vesicles, Gas Filter-Pressing, and Igneous Differentiation. *The Journal of Geology* **92(1)**: 55-72.

Ashwal, L., Morrison, D., Phinney, W., and Wood, J. (1983). Origin of Archean Anorthosites: Evidence from the Bad Vermilion Lake Anorthosite Complex, Ontario. *Contributions to Mineralogy and Petrology* ***82*****(2–3)**: 259–273.

Ashwal, L. (1993). Anorthosites. *Springer-Verlag Berlin Heidelberg* **21(1)**: pp. 422.

Ashwal, L. (2010). The Temporality of Anorthosites. *The Canadian Mineralogist* **48(4)**: 711-728.

Bea, F., Fershtater, G., Montero, P., Smirnov, V., and Molina, J. (2005). Deformation-Driven Differentiation of Granitic Magma: The Stepninsk Pluton of the Uralides, Russia. *Lithos* **81(1–4)**: 209–233.

Berry, L., Dietrich, R., and Mason, B. (1985). *Mineralogy*. CBS Publishers & Distributors, Delhi, pp.551.

Bett, A., Onyango, J., Maranga, S., and Rop, B. (2019). Quality of Iron Ores in Kenya; Tharaka Nithi and Samia. *International Journal Of Engineering Technology And Scientific Innovation* **4(5)**: 227-233.

Bogdan P., and Herta S. (2007). Re-examination of Berlinite ($AlPO_4$) from the Cioclovina Cave, Romania. *American Mineralogist* **92 (11-12)**: 1998 2001.

Castillo-Oliver M., Galí, S., Melgarejo, J., Griffin, W., Belousova, E., Pearson, N., Watangua, M., and O'Reilly, S. (2016). Trace-Element Geochemistry and U–Pb Dating of Perovskite in Kimberlites of the Lunda Norte Province (NE Angola): Petrogenetic and Tectonic Implications. *Chemical Geology* **426**: 118–134.

Cawthorn, R., Lee, C., Schouwstra, R., and Mellowship, P. (2002). Relationship Between PGE and PGM in the Bushveld Complex. *The Canadian Mineralogist* **40(2)**: 311–328.

Cawthorn, R., (2010). Geological Interpretations from the PGE Distribution in the Bushveld Merensky and UG2 Chromitite Reefs. The 4th International Platinum Conference, Platinum in Transition 'Boom or Bust', *The Southern African Institute of Mining and Metallurgy*. 59-61, 67.

Deloitte CIS Research Centre. (2019). Overview of the Steel and Iron Ore Market H1 2019. Moscow, pp. 6-14.

Dick, H., Natland, J., Alt, J., Bach, W., Bideau, D., Gee, J., Haggas, S., Hertogen, J., Hirth, G., Holm, P., Ildefonse, B., Iturrino, G., John, B., Kelley, D., Kikawa, E., Kingdon, A., LeRoux, P., Maeda, J., Meyer, P., Miller, D., Naslund, H., Niu, Y., Robinson, P., Snow, J., Stephen, R., Trimby, P., Worm, H., and Yoshinobu, A. (2000). A long in situ Section of the Lower Ocean Crust: Results of ODP Leg 176 Drilling at the Southwest Indian Ridge. *Earth and Planetary Science Letters* **179(1)**: 31–51.

Dobrzhinetskaya, L., Wirth, R., Yang, J., Hutcheon, I., Weber, P., and Green, H. (2009). High-Pressure Highly Reduced Nitrides and Oxides from Chromitite of a Tibetan Ophiolite. *Proceedings of the National Academy of Sciences* **106(46)**: 19233-19238.

Dobrzhinetskaya, L., Wirth, R., Yang, J., Green, H., Hutcheon, I., Weber, P., and Grew, E. (2014). Qingsongite, Natural Cubic Boron Nitride: The First Boron Mineral from the Earth's Mantle. *American Mineralogist*, **99(4)**, 764-772.

Giere, R. (1992). Compositional Variation of Metasomatic Titanite from Adamello (Italy). *Schweizerische mineralogische und petrographische Mitteilungen* **72**: 167 - 177.

Gleißner, P. (2010). Petrogenesis of Anorthosites of the Mesoproterozoic Kunene Intrusive Complex, NW Namibia: Evidence from Stable and Radiogenic Isotope and Lithophile and Highly Siderophile Trace Element Composition. Ph.D. Thesis, *University of Berlin*. 178 pp.

Goldfarb, R., Berger, B., George, M., and Seal, R. (2017). Tellurium, chap. R of Schulz, K., DeYoung, J., Jr., Seal, R., and Bradley, D., eds., Critical Mineral Resources of the United States - Economic and Environmental Geology and Prospects for Future Supply: *U.S. Geological Survey Professional Paper* **1802**: p. R1–R27.

Gralik, G., Thomsen, A., Moraes, C., Raupp-Pereira, F., and Hotza, D. (2014). Processing and Characterization of $CaTiO_3$ Perovskite Ceramics. Processing And Application Of Ceramics **8(2)**: 53-57.

Gutzmer, J., and Beukes, N. (1997). Mineralogy and Mineral Chemistry of Oxide-Facies Manganese Ores of the Postmasburg Manganese Field, South Africa. *Mineralogical Magazine* **61(405)**: 213-231.

Harangi, S., Downes, H., Kosa, L., Szabo, C., Thirlwall, M., Mason, P., and Mattey, D. (2001). Almandine Garnet in Calc-alkaline Volcanic Rocks of the Northern Pannonian Basin (Eastern–Central Europe): Geochemistry, Petrogenesis, and Geodynamic Implications. *Journal of Petrology* **42(10)**: 1813–1843.

Hartlaub, R., Böhm, C., Heaman, L., and Simonetti, A. (2005). Northwestern Superior Craton Margin, Manitoba: An Overview of Archean and Proterozoic Episodes of Crustal Growth, Erosion, and Orogenesis (parts of NTS 54D and 64A); in Report of Activities 2005, Manitoba Industry, Economic Development and Mines, *Manitoba Geological Survey*, p. 54–60.

Haymon, R., and Kastner, M. (1986). Caminite: A New Magnesium-Hydroxide-Sulfate-Hydrate Mineral Found in a Submarine Hydrothermal Deposit, East Pacific Rise, 21 °N. Deep-Sea Research Part B. *Oceanographic Literature Review* **33(12)**: 1013.

Hein, J., Koschinsky, A., and Halliday, A. (2003). Global Occurrence of Tellurium-Rich Ferromanganese Crusts and a Model for the Enrichment of Tellurium. *Geochimica Et Cosmochimica Acta* **67(6)**: 1117-1127.

Hoatson, D., and Glaser, L. (1989). Geology and Economics of Platinum-Group Metals in Australia: *Australian Bureau of Mineral Resources*, Geology & Geophysics Resource Report **5**: 81 pp.

Huddleston, A., (1951). Geology of the Kisii District. Degree Sheet 41, S.E. Quadrant. Rep. *Geological Survey of Kenya*, Nairobi. Report Number **18**: 64 pp.

Huddleston, A., (1959). Geology of Kakamega District. Degree Sheet 33, S. E. Quadrant. Rep. *Geological Survey of Kenya*, Nairobi. Report Number **28**: 59pp.

Hudleston, P., and Lan, L. (1995). Rheological Information from Geological Structures. *Pure and Applied Geophysics* **145(3-4)**: 605-620.

Iatan, L. (2009). A New Occurrence of Tellurium Bearing Minerals in the Metaliferi Mountains -Rosia Poieni Porphyry Copper Deposit. Rom. J. *Mineral* **84**: 78-79.

Ichang'i, D. 1983. The Bukura and Mbesa Pyrite Mineralisation of Western Kenya. M.Sc. Thesis, *University of Nairobi*, Kenya, 242 pp.

Ichang'i D. (1990). The Migori Segment of the Archean Nyanza Greenstone Belt, Kenya: Geology, Geochemistry, and Economic Mineral Potential. Ph.D. Thesis, *McGill University, Montreal*, 147 pp.

KMD, (2020). The Weather Outlook for the October-November-December (OND) 2020 Short-Rains Season; September 2020 Weather Outlook; and Review of the June-July-August (JJA) 2020 Rainfall Season. *Kenya Meteorological Department*, pp. 11.

Kenya National Bureau of Statistics (KNBS). (2019). 2019 Kenya Population and Housing Census: Distribution of Population by Administrative Units. *Kenya National Bureau of Statistics (KNBS)*, **2**: 251 pp

Koljonen, T. (1973). Selenium in Certain Igneous Rocks. Bulletin of the Geological Society of Finland, **45(1)**, 9–22.

Lameiras, F., Nunes, E., and Vasconcelos, W., (2009). Infrared and Chemical Characterization of Natural Amethysts and Prasiolites Colored by Irradiation. *Materials Research* **12(3)**: 315–320.

Maier, W., Karykowski, B., and Yang, S. (2016). Formation of Transgressive Anorthosite Seams in the Bushveld Complex via Tectonically Induced Mobilisation of Plagioclase-Rich Crystal Mushes. *Geoscience Frontiers*, **7(6)**, pp.875-889.

Matheson, F. (1966). Geology of the Kajiado Area. Degree Sheet 51, Q. E. Quadrant. Rep. *Geological Survey of Kenya*, Nairobi, Kenya. Report Number **70**: 57pp.

Matthews, P., Akhtar, M., Malik, M., Revaprasadu, N., and O'Brien, P. (2016). Synthetic Routes to Iron Chalcogenide Nanoparticles and Thin Films. *Dalton Transactions*, **45(47)**: 18803-18812.

McCallum, S. (2012). The Stillwater Complex: A Review of the Geology. *Second Conference on the Lunar Highlands Crust Montana*, 42 pp.

Miller, J., and Chandler, V. (1997). Geology, Petrology, and Tectonic Significance of the Beaver Bay Complex, Northeastern Minnesota, in Ojakangas, R.W., Dickas, A.B., and Green, J.C., eds., Middle Proterozoic to Cambrian Rifting, Central North America: *Geological Society of America*. Special Paper **312**, pp. 73- 96.

Mitchell, R., & LIferovich, R. (2004). The Pyrophanite Ecandrewsite Solid-Solution: Crystal Structures of the $Mn_{1-x}Zn_xTiO_3$ Series ($0.1 \leq x \leq 0.8$). *The Canadian Mineralogist* **42(6)**: 1871-1880.

Mrose, M. (1952). Hurlbutite, $CaBe_2(PO_4)_2$, a New Mineral. *American Mineralogist* ; **37 (11-12)**: 931–940.

Niu, Y., Gilmore, T., Mackie, S., Greig, A., and Bach, W. (2002). Mineral Chemistry, Whole-Rock Compositions, and Petrogenesis of Leg 176 Gabbros: Data and discussion. *Proceedings of the Ocean Drilling Program, Scientific Results* **176**: 1-60.

Oberti, R., Boiocchi, M., Hawthorne, F., Pagano, R., and Pagano, A. (2010). Fluoro-potassic-Pargasite, $KCa_2(Mg_4Al)(Si_6Al_2)O_{22}F_2$, from the Tranomaro Area, Madagascar: Mineral Description and Crystal Chemistry. *Mineralogical Magazine* **74(6)**: 961–967.

Onac, B., and White, W. (2003). First Reported Sedimentary Occurrence of Berlinite ($AlPO_4$) in Phosphate-Bearing Sediments from Cioclovina Cave, Romania. *American Mineralogist* **88(8–9)**: 1395–1397.

Paar, W., Putz, H., Topa, D., de Brodtkorb, M., and Sureda, R. (2005). Occurrence and Paragenesis of Tellurium in Mineral Deposits of Argentina. *Springer, Berlin, Heidelberg*. pp1419-1422.

Percival, J., Skulski, T., Sanborn-Barrie, M., Stott, G., Leclair, A., Corkery, M., and Boily, M. (2012). Geology and Tectonic Evolution of the Superior Province, Canada. Chapter 6 In Tectonic Styles in Canada: The Lithoprobe Perspective. *Geological Association of Canada* Special Paper **49**, pp. 321–378.

Pfaff, K., Staude, S., and Markl, G. (2012). On the Origin of Sellaite ($MgF_2$)-Rich Deposits in Mg-Poor Environments. *American Mineralogist* **97(11–12)**: 1987–1997.

Pistone, M., Arzilli, F., Dobson, K., Cordonnier, B., Reusser, E., Ulmer, P., Marone, F., Whittington, A., Mancini, L., Fife, J., and Blundy, J. (2015). Gas-driven filter pressing in magmas: Insights into in-situ Melt Segregation from Crystal Mushes. *Geology*, ***43*(8)**, 699–702.

Polat, A., Longstaffe, F., and Frei, R. (2018). An Overview of Anorthosite-Bearing Layered Intrusions in the Archaean Craton of Southern West Greenland and the Superior Province of Canada: Implications for Archaean Tectonics and the Origin of Megacrystic Plagioclase. *Geodinamica Acta* **30(1)**: pp.84-99.

Pulfrey, W. (1936). Geological Survey of Kenya. Preliminary Report on the Geology of the No. 1 Area, North and Central Kavirondo. Rep. *Mines and Geological Department Kenya*, Report Number **5**: 31pp.

Pulfrey, W., and Walsh, J. (1969). Geological Survey of Kenya. The Geology and Mineral Resources of Kenya. *Mines and Geological Department Kenya*, Bulletin Number **9**: 34pp.

Rajendran, S., and Nasir, S. (2014). Hydrothermal Altered Serpentinized Zone and a Study of Ni-Magnesioferrite–Magnetite–Awaruite Occurrences in Wadi Hibi, Northern Oman Mountain: Discrimination Through Aster Mapping. *Ore Geology Reviews* **62**, 211-226.

Reichl, C., Schatz, M., and Zsak, G. (2018). World Mining Data 2018 Iron and Ferro Alloy Metals Non-Ferrous Metals Precious Metals Industrial Minerals Mineral Fuels. *Federal Ministry of Sustainability and Tourism*, Vienna: pp250.

Rollinson, H., Reid, C., and Windley, B. (2010). Chromitites from the Fiskenæsset Anorthositic Complex, West Greenland: Clues to Late Archaean Mantle Processes. *Geological Society, London, Special Publications*, ***338*(1)**, 197–212.

Ross, N., Hazen, R., Shu, J., & Gasparik, T. (1990). High-Pressure Crystal Chemistry of Stishovite. *American Mineralogist*, **75**: 739-747.

Ruano, S., and Hach-Ali, P. (1996). Hydrothermal Argentopentlandite at El Charcon, Southeastern Spain: Mineral Chemistry and Conditions of Formation. *The Canadian Mineralogist* **34**: 939-94

Schmidt, M., Gao, C., Golubkova, A., Rohrbach, A., and Connolly, J. (2014). Natural Moissanite (SiC) – a Low-Temperature Mineral Formed from Highly Fractionated Ultra-Reducing COH-Fluids. Progress in Earth and Planetary Science **1(1)**: 1-14.

Schmidt, C., Hensen, C., Wallmann, K., Liebetrau, V., Tatzel, M., Schurr, S., Kutterolf, S., Haffert, L., Geilert, S., Hübscher, C., Lebas, E., Heuser, A., Schmidt, M., Strauss, H., Vogl, J., and Hansteen, T. (2019). Origin of High Mg and SO4 Fluids in Sediments of the Terceira Rift, Azores-Indications for Caminite Dissolution in a Waning Hydrothermal System. *Geochemistry, Geophysics, Geosystems*, **20(12)**: 6078–6094.

Schoeman, J. (1951). A Geological Reconnaissance of the Country between Embu and Meru. *Mines and Geological Department, Kenya*, Nairobi. Report Number **17**: 57 pp.

Shackleton, R. (1946). Geology of the Migori Gold Belt and Adjoining Areas. Rep. *Geological Survey of Kenya*, Nairobi. Report Number **10**: 60 pp.

Škácha, P., Sejkora, J., and Plášil, J. (2017). Selenide Mineralization in the Příbram Uranium and Base-Metal District (Czech Republic). *Minerals* ***7*(6)**: 91.

Skála, R., Ondrus, P., Veselovký, F., Táborský, Z., and Ďuda, R. (2007). Vihorlatite, $Bi_{24}Se_{17}Te_4$, a New Mineral of the Tetradymite Group from Vihorlat Mts., Slovakia. *European Journal of Mineralogy* **19(2)**: 255–265.

Sørensen, L., Weatherley, S., Kokfelt, T., and Nielsen, T. (2016). *Geology and Ore: Magmatic Titanium-Vanadium Potential in Greenland*. Geological Survey of Denmark and Greenland (GEUS) **27**: 12pp

Speith, V. (2019). Zechstein Kupferschiefer at Spremberg and Related Sites: Hot Hydrothermal Origin of the Polymetallic Cu-Ag-Au Deposit. Ph.D. Thesis, *University of Stuttgart*, 440 pp.

Sriramadas, A., Rao, K., and Rao, A. (1969). Aluminous Augite in the Pyroxenite of the Charnockite Rocks of Visakhapatnam District, Andhra Pradesh. *Proceedings of the Indian Academy of Sciences - Section B* **70**: 15-27.

St.Clair, S. (1913). Ore Deposits Produced by Magmatic Segregation, with Special Reference to the Nickel Ores of the Sudbury district, Ontario. Masters Thesis, *State University of Iowa*, Iowa, 49pp.

Stendal, H., and Secher, K. (2011). Iron Ore Potential in Greenland. *Geological Survey of Denmark and Greenland (GEUS)* **9**: 12pp.

Stillings, L. (2017). Selenium, chap. Q of Schulz, K., DeYoung, J., Jr., Seal, R., and Bradley, D., eds. Critical Mineral Resources of the United States - Economic and Environmental Geology and Prospects for Future Supply: U.S. Geological Survey Professional Paper **1802** p. Q1–Q55.

Streckeisen, A. (1976). To Each Plutonic Rock its Proper Name. *Earth-Science Reviews*, **12(1)**, pp.1-33.

Stroup, J. (1981). Geologic Investigations in the Cayman Trough and the Nature of the Plutonic Foundation of the Oceanic Crust. Masters Thesis, *University at Albany, State University of New York*, 189pp.

Sugaki, A., Ueno, H., Shimada, N., Kusachi, I., Kitakaze, A., Hayashi, K., Kojima, S., and Sanjines, O. (1983). Geological Study on the Polymetallic Ore Deposits in the Potosi District, Bolivia. Faculty Of Science, Tohoku University, Sendai, Japan. **15**: 409-460.

Traill, R., and Boyle, R. (1955). Hawleyite, Isometric Cadmium Sulphide, A New Mineral. *American Mineralogist*. **40(7&8)**: 555-559

U.S. Geological Survey, (2020). Mineral Commodity Summaries 2020: *U.S. Geological Survey*, 200 p.

Van Gosen, B., Verplanck, P., Seal, R., Long, K., and Gambogi, J. (2017). Rare-Earth Elements, chap. O of Schulz, K., DeYoung, J., Jr., Seal, R., and Bradley, D., eds., Critical Mineral Resources of the United States — Economic and Environmental Geology and Prospects for Future Supply: *U.S. Geological Survey Professional Paper* **1802**, p. O1–O3.

Villanova-de-Benavent, C., Torró, L., Castillo-Oliver, M., Campeny, M., Melgarejo, J., Llovet, X., Galí, S., and Gonçalves, A. (2017). Fe–Ti(–V) Oxide Deposits of the Kunene Anorthosite Complex (SW Angola): Mineralogy and Thermo Oxybarometry. *Minerals*, **7(12)**: pp. 246.

Welch, M., Cooper, M., and Hawthorne, F. (2001). The crystal structure of brunogeierite, $Fe_2GeO_4$ Spinel. *Mineralogical Magazine*, **65(3)**, 441-444.

Yakymchuk, C., and Szilas, K. (2018). Corundum Formation by Metasomatic Reactions in Archean Metapelite, SW Greenland: Exploration Vectors for Ruby Deposits Within High-Grade Greenstone Belts. *Geoscience Frontiers*, **9(3)**, 727–749.

Zaccarini, F., Garuti, G., Ortiz-Suarez, A., and Carugno-Duran, A. (2004). The Paragenesis of Pyrophanite from Sierra De Comechingones, Cordoba, Argentina. *The Canadian Mineralogist* **42(1)**: 155-168.

Zhou, S., Polat, A., Longstaffe, F., Yang, K., Fryer, B., and Weisener, C. (2016). Formation of the Neoarchean Bad Vermilion Lake Anorthosite Complex and spatially associated granitic rocks at a convergent plate margin, Superior Province, Western Ontario, Canada. *Gondwana Research*, **33**, 134–159.

Zientek, M., Loferski, P., Parks, H., Schulte, R., and Seal, R. (2017). Platinum-Group Elements, chap. N of Schulz, K., DeYoung, J., Jr., Seal, R., and Bradley, D., eds., Critical Mineral Resources of the United States— Economic and Environmental Geology and Prospects for Future Supply: *U.S. Geological Survey Professional Paper* **1802**, p. N1–N91.

# APPENDICES

## APPENDIX 1: Sampling Points and their respective coordinates

| | DD MM SS | | | DD MM SS | |
|---|---|---|---|---|---|
| **SAMPLING POINT** | **LATITUDE** | **LONGITUDE** | **SAMPLING POINT** | **LATITUDE** | **LONGITUDE** |
| SMP-01 | 0°10'38.30"S | 37°56'39.40"E | SMP-14 | 0°10'13.00"S | 37°56'16.90"E |
| SMP-02 | 0°10'38.20"S | 37°56'40.20"E | SMP-15 | 0°10'34.40"S | 37°56'43.00"E |
| SMP-03 | 0°10'38.20"S | 37°56'40.50"E | SMP-16 | 0°10'39.20"S | 37°57'20.70"E |
| SMP-04 | 0°10'31.20"S | 37°56'40.30"E | SMP-17 | 0°10'39.20"S | 37°57'20.70"E |
| SMP-05 | 00°10'28.60"S | 37°56'39.50"E | SMP-18 | 0°10'13.10"S | 37°57'41.90"E |
| SMP-06 | 0°10'29.20"S | 37°56'41.80"E | SMP-19 | 0°10'12.70"S | 37°57'43.90"E |
| SMP-07 | 0°10'26.30"S | 37°56'39.20"E | SMP-20 | 0°10'15.10"S | 37°56'34.10"E |
| SMP-08 | 0°10'20.90"S | 37°56'39.10"E | SMP-21 | 0° 9'28.20"S | 37°56'14.70"E |
| SMP-09 | 0°11'2.00"S | 37°57'49.90"E | SMP-22 | 0° 9'6.70"S | 37°55'33.80"E |
| SMP-10 | 0°10'53.00"S | 37°56'49.10"E | SMP-23 | 0° 9'31.00"S | 37°55'19.90"E |
| SMP-11 | 0°10'18.30"S | 37°56'49.80"E | SMP-24 | 0° 9'39.20"S | 37°55'24.40"E |
| SMP-12 | 0° 9'59.00"S | 37°56'43.20"E | SMP-25 | 0°10'52.30"S | 37°56'44.10"E |
| SMP-13 | 0° 9'40.00"S | 37°56'35.60"E | | | |

## APPENDIX 2: Observation Points and their respective coordinates

| | DD MM SS | | | DD MM SS | |
|---|---|---|---|---|---|
| **OBSERVATION POINT** | **LATITUDE** | **LONGITUDE** | **OBSERVATION POINT** | **LATITUDE** | **LONGITUDE** |
| OBP 001 | 0°10'37.80"S | 37°56'40.80"E | OBP 016 | 0°10'4.10"S | 37°56'42.10"E |
| OBP 002 | 0°10'31.70"S | 37°56'44.10"E | OBP 017 | 0°10'0.40"S | 37°56'40.20"E |
| OBP 003 | 0°10'31.60"S | 37°56'41.20"E | OBP 018 | 0° 9'50.20"S | 37°56'41.00"E |
| OBP 004 | 0°10'30.20"S | 37°56'39.60"E | OBP 019 | 0° 9'48.70"S | 37°56'42.90"E |
| OBP 005 | 0°10'30.00"S | 37°56'39.10"E | OBP 020 | 0°10'13.50"S | 37°56'27.80"E |
| OBP 006 | 0°10'30.00"S | 37°56'40.40"E | OBP 021 | 0°10'15.60"S | 37°56'20.40"E |
| OBP 007 | 0°10'26.90"S | 37°56'39.50"E | OBP 022 | 0°10'27.80"S | 37°57'23.40"E |
| OBP 008 | 0°10'23.60"S | 37°56'38.60"E | OBP 023 | 0°10'12.70"S | 37°57'44.20"E |
| OBP 009 | 0°10'52.60"S | 37°56'48.50"E | OBP 024 | 0°10'29.60"S | 37°57'22.00"E |
| OBP 010 | 0°10'29.50"S | 37°56'44.80"E | OBP 025 | 0°10'33.20"S | 37°56'40.20"E |
| OBP 011 | 0°10'26.30"S | 37°56'45.30"E | OBP 026 | 0°10'24.40"S | 37°56'37.60"E |
| OBP 012 | 0°10'20.10"S | 37°56'48.60"E | OBP 027 | 0°10'16.60"S | 37°56'36.80"E |
| OBP 013 | 0°10'19.20"S | 37°56'52.90"E | OBP 028 | 0° 9'29.10"S | 37°56'05.40"E |
| OBP 014 | 0°10'17.50"S | 37°56'57.40"E | OBP 029 | 0° 9'45.40"S | 37°55'26.60"E |
| OBP 015 | 0°10'17.40"S | 37°56'54.70"E | OBP 030 | 0° 9'42.50"S | 37°55'37.70"E |

## APPENDIX 3: Elements of Potential Economic Interest

| S. No. | Sampling Point | Formula | Compound Name | Proportion of Mineral in Sample | Element of Potential Economic Interest |
|---|---|---|---|---|---|
| 1 | SMP-01 | $Cs\ F_3\ Mn\ Mo\ O_3$ | Oxyfluoride of Cesium, Manganese & Molybdenum | 3.5% | Caesium |
| 2 | SMP-01 | $Cs\ F_3\ Mn\ Mo\ O_3$ | Oxyfluoride of Cesium, Manganese & Molybdenum | 3.5% | Molybdenum |
| 3 | SMP-01 | $Cd\ Cu_2\ Se_4\ Sn$ | *-unidentified* | 0.6% | Cadmium |
| 4 | SMP-01 | $Cd\ Cu_2\ Se_4\ Sn$ | *-unidentified* | 0.6% | Selenium |
| 5 | SMP-01 | $Cd\ Cu_2\ Se_4\ Sn$ | *-unidentified* | 0.6% | Tin |
| 6 | SMP-01 | $Ca_{0.925}\ F_{2.15}\ U_{0.075}$ | Calcium uranium fluoride | 7.1% | Uranium |
| 7 | SMP-01 | $Au_5\ Zn_8$ | *-unidentified* | 0.1% | Gold |
| 8 | SMP-03 | $Mn_{0.5}\ Ni_{0.5}\ O_3\ Ti$ | Pyrophanite | 26.5% | Nickel |
| 9 | SMP-03 | $Hg\ Te$ | Coloradoite | 0.5% | Mercury |
| 10 | SMP-03 | $Hg\ Te$ | Coloradoite | 0.5% | Tellurium |
| 11 | SMP-03 | $Cu_{0.86}\ Fe_{2.14}\ O_4$ | Cuprospinel | 17.8% | Copper |
| 12 | SMP-03 | $Cr_2\ Fe\ O_4$ | Chromite | 14.6% | Chromium |
| 13 | SMP-03 | $Ca_{0.4}\ O_3\ Sr_{0.6}\ Ti$ | Tausonite | 18.6% | Strontium |
| 14 | SMP-04 | $O_4\ Sb\ V$ | Antimony Vanadate | 4.6% | Antimony |
| 15 | SMP-04 | $O\ Pt$ | Platinum Oxide | 1.1% | Platinum |
| 16 | SMP-04 | $La_2\ O_2\ Te$ | Dilanthanum Dioxide Telluride | 3.0% | Lanthanum |
| 17 | SMP-04 | $La_2\ O_2\ Te$ | Dilanthanum Dioxide Telluride | 3.0% | Tellurium |
| 18 | SMP-04 | $Cu_{2.2}\ Se_{3.9}\ Sn\ Te_{0.1}\ Zn_{0.78}$ | Chalcogenide Stannite | 0.9% | Selenium |
| 19 | SMP-04 | $Cu_{2.2}\ Se_{3.9}\ Sn\ Te_{0.1}\ Zn_{0.78}$ | Chalcogenide Stannite | 0.9% | Tin |
| 20 | SMP-04 | $Cu_{2.2}\ Se_{3.9}\ Sn\ Te_{0.1}\ Zn_{0.78}$ | Chalcogenide Stannite | 0.9% | Tellurium |
| 21 | SMP-04 | $C\ Ce_3\ In$ | Cerium Carbide Indide | 1.7% | Cerium |

| S. No. | Sampling Point | Formula | Compound Name | Proportion of Mineral in Sample | Element of Potential Economic Interest |
|---|---|---|---|---|---|
| 22 | SMP-04 | $C\ Ce_3\ In$ | Cerium Carbide Indide | 1.7% | Indium |
| 23 | SMP-04 | $Ag\ Sb\ Te_2$ | Silver Antimony Telluride | 2.3% | Silver |
| 24 | SMP-04 | $Ag\ Sb\ Te_2$ | Silver Antimony Telluride | 2.3% | Antimony |
| 25 | SMP-04 | $Ag\ Sb\ Te_2$ | Silver Antimony Telluride | 2.3% | Tellurium |
| 26 | SMP-05 | $In_2\ S_4\ Yb_2$ | Ytterbium(II) Diindium Sulfide | 0.1% | Indium |
| 27 | SMP-05 | $In_2\ S_4\ Yb_2$ | Ytterbium(II) Diindium Sulfide | 0.1% | Ytterbium |
| 28 | SMP-05 | $Fe_{2.05}\ Li_{0.05}\ O_4\ Zn_{0.9}$ | Lithium Zinc Iron Oxide | 18.7% | Lithium |
| 29 | SMP-05 | $Fe_{2.05}\ Li_{0.05}\ O_4\ Zn_{0.9}$ | Lithium Zinc Iron Oxide | 18.7% | Zinc |
| 30 | SMP-05 | $Fe_{1.6}\ Mg_{1.2}\ O_4\ Sn_{0.2}$ | Magnesium Tin Iron(III) Oxide | 10.8% | Tin |
| 31 | SMP-05 | Cu Ge La | Copper Germanium Lanthanum | 6.0% | Copper |
| 32 | SMP-05 | Cu Ge La | Copper Germanium Lanthanum | 6.0% | Germanium |
| 33 | SMP-05 | Cu Ge La | Copper Germanium Lanthanum | 6.0% | Lanthanum |
| 34 | SMP-06 | $N_4\ Ti_4$ | Osbornite | 16.8% | Nitrogen |
| 35 | SMP-06 | $Mn_{0.5}\ Ni_{0.5}\ O_3\ Ti$ | Pyrophanite | 30.0% | Nickel |
| 36 | SMP-08 | $Mn_{0.5}\ Ni_{0.5}\ O_3\ Ti$ | Pyrophanite | 36.2 % | Nickel |
| 37 | SMP-08 | $Fe_2\ Ge\ O_4$ | Brunogeierite | 16.6% | Germanium |
| 38 | SMP-08 | $Ca_{0.13}\ Ce_{0.18}\ La_{0.09}\ Na_{0.46}\ Nb_{0.13}\ Nd_{0.05}\ O_3\ Pr_{0.02}\ Sr_{0.05}\ Ti_{0.87}$ | Loparite-(Ce) | 23.5% | Cerium |
| 39 | SMP-08 | $Ca_{0.13}\ Ce_{0.18}\ La_{0.09}\ Na_{0.46}\ Nb_{0.13}\ Nd_{0.05}\ O_3\ Pr_{0.02}\ Sr_{0.05}\ Ti_{0.87}$ | Loparite-(Ce) | 23.5% | Lanthanum |

| S. No. | Sampling Point | Formula | Compound Name | Proportion of Mineral in Sample | Element of Potential Economic Interest |
|---|---|---|---|---|---|
| 40 | SMP-08 | $Ca_{0.13}$ $Ce_{0.18}$ $La_{0.09}$ $Na_{0.46}$ $Nb_{0.13}$ $Nd_{0.05}$ $O_3$ $Pr_{0.02}$ $Sr_{0.05}$ $Ti_{0.87}$ | Loparite-(Ce) | 23.5% | Niobium |
| 41 | SMP-08 | $Ca_{0.13}$ $Ce_{0.18}$ $La_{0.09}$ $Na_{0.46}$ $Nb_{0.13}$ $Nd_{0.05}$ $O_3$ $Pr_{0.02}$ $Sr_{0.05}$ $Ti_{0.87}$ | Loparite-(Ce) | 23.5% | Neodymium |
| 42 | SMP-08 | $Ca_{0.13}$ $Ce_{0.18}$ $La_{0.09}$ $Na_{0.46}$ $Nb_{0.13}$ $Nd_{0.05}$ $O_3$ $Pr_{0.02}$ $Sr_{0.05}$ $Ti_{0.87}$ | Loparite-(Ce) | 23.5% | Praseodymium |
| 43 | SMP-09 | $H_2$ $Mg_3$ $O_{10}$ $S_2$ | Caminite | 16.6% | Sulphur |
| 44 | SMP-09 | $Al_{1.98}$ Be $Cr_{0.02}$ $O_4$ | Chrysoberyl | 11.9% | Beryllium |
| 45 | SMP-09 | $Ag_{1.486}$ $Pb_{3.436}$ $S_{12}$ $Sb_{5.215}$ | Fizelyite | 2.7% | Silver |
| 46 | SMP-09 | $Ag_{1.486}$ $Pb_{3.436}$ $S_{12}$ $Sb_{5.215}$ | Fizelyite | 2.7% | Lead |
| 47 | SMP-09 | $Ag_{1.486}$ $Pb_{3.436}$ $S_{12}$ $Sb_{5.215}$ | Fizelyite | 2.7% | Antimony |
| 48 | SMP-10 | $Pr_3$ $Te_4$ | Praseodymium Telluride | 0.3% | Praseodymium |
| 49 | SMP-10 | $Pr_3$ $Te_4$ | Praseodymium Telluride | 0.3% | Tellurium |
| 50 | SMP-25 | Ni $O_4$ Te | Imgreite Oxide | 5.9% | Nickel |
| 51 | SMP-25 | Ni $O_4$ Te | Imgreite Oxide | 5.9% | Tellurium |
| 52 | SMP-25 | $La_{0.025}$ Mn $O_{1.5}$ $Sr_{0.975}$ | Lanthanum Strontium Manganite | 10.4% | Strontium |
| 53 | SMP-25 | Hf Ta $V_4$ | Hafnium Tantalum Vanadium | 0.9% | Hafnium |
| 54 | SMP-25 | Hf Ta $V_4$ | Hafnium Tantalum Vanadium | 0.9% | Tantalum |
| 55 | SMP-25 | $Cu_2$ $Fe_{0.4}$ $Se_4$ Sn $Zn_{0.6}$ | Stannite | 2.6% | Selenium |
| 56 | SMP-25 | $Cu_2$ $Fe_{0.4}$ $Se_4$ Sn $Zn_{0.6}$ | Stannite | 2.6% | Tin |
| 57 | SMP-25 | Co Mo $O_6$ $Sr_2$ | Distrontium Cobalt Hexaoxomolybdate | 2.2% | Cobalt |
| 58 | SMP-25 | Co Mo $O_6$ $Sr_2$ | Distrontium Cobalt Hexaoxomolybdate | 2.2% | Molybdenum |

| S. No. | Sampling Point | Formula | Compound Name | Proportion of Mineral in Sample | Element of Potential Economic Interest |
|---|---|---|---|---|---|
| 59 | SMP-25 | $Ce_{0.9}\ O_{1.95}\ Y_{0.1}$ | Yttrium Cerium(IV) Oxide | 18.9% | Cerium |
| 60 | SMP-25 | $Ce_{0.4}\ Gd_{0.6}\ O_{1.7}$ | Gadolinium Cerium Oxide | 6.8% | Cerium |
| 61 | SMP-25 | $Ce_{0.4}\ Gd_{0.6}\ O_{1.7}$ | Gadolinium Cerium Oxide | 6.8% | Gadolinium |
| 62 | SMP-25 | $Ce\ O_2$ | Cerianite | 14.1% | Cerium |
| 63 | SMP-25 | $Cd_{0.9}\ F_{2.1}\ Nd_{0.1}$ | | 10.2% | Cadmium |
| 64 | SMP-25 | $Cd_{0.05}\ S_{0.05}\ Sn_{0.95}\ Te_{0.95}$ | Cadmium Tin Sulfide Telluride | 7.7% | Cadmium |
| 65 | SMP-25 | $Cd_{0.05}\ S_{0.05}\ Sn_{0.95}\ Te_{0.95}$ | Cadmium Tin Sulfide Telluride | 7.7% | Tin |
| 66 | SMP-25 | $Cd_{0.05}\ S_{0.05}\ Sn_{0.95}\ Te_{0.95}$ | Cadmium Tin Sulfide Telluride | 7.7% | Tellurium |
| 67 | SMP-25 | $Ba_8\ Dy_{1.6}\ Fe_{3.72}\ O_{24}\ U_{2.68}$ | Iron(III) Dysprosium Uranium Oxide | 0.2% | Uranium |
| 68 | SMP-25 | $Ba\ O_{12}\ Sr_2\ Tm_6$ | Barium Strontium Thulium Oxide | 2.7% | Thulium |
| 69 | SMP-25 | $Ag_2\ Ho$ | Silver Holmium | 1.5% | Silver |
| 70 | SMP-25 | $Ag_2\ Ho$ | Silver Holmium | 1.5% | Holmium |
| 71 | SMP-11 | $Cu\ O_6\ Sr_2\ Te$ | Distrontium copper tellurate | 0.4% | Tellurium |
| 72 | SMP-11 | $Cs\ F_3\ Mn\ Mo\ O_3$ | Oxyfluorides of Cesium, Manganese and Molybdenum | 2.9% | Caesium |
| 73 | SMP-11 | $Cs\ F_3\ Mn\ Mo\ O_3$ | Oxyfluorides of Cesium, Manganese and Molybdenum | 2.9% | Molybdenum |
| 74 | SMP-11 | $Ce_{0.368}\ O_{8.937}\ U_{3.632}$ | Uranium cerium oxide | 0.2% | Uranium |
| 75 | SMP-12 | $Ti_{0.89}\ V_{0.11}$ | *-unidentified* | 15.4% | Vanadium |

| S. No. | Sampling Point | Formula | Compound Name | Proportion of Mineral in Sample | Element of Potential Economic Interest |
|---|---|---|---|---|---|
| 76 | SMP-12 | $Fe_{1.2}\ O_3\ Ti_{0.8}$ | Ilmenite Species | 32.8% | Iron |
| 77 | SMP-12 | $Fe_{0.5}\ Pt_{0.5}$ | Ferro-platinum | 5.4% | Platinum |
| 78 | SMP-12 | $Cd_2\ Pr$ | Cadmium praseodymium | 5.9% | Cadmium |
| 79 | SMP-12 | $Cd_2\ Pr$ | Cadmium praseodymium | 5.9% | Praseodymium |
| 80 | SMP-13 | $Mn_{0.3}\ O_3\ Ti\ Zn_{0.7}$ | Ecandrewsite | 23.9% | Zinc |
| 81 | SMP-13 | $Fe\ S_{0.5}\ Se_{0.5}$ | Achavalite | 5.5% | Selenium |
| 82 | SMP-14 | Mn Se | Manganese Selenide | 25.6% | Manganese |
| 83 | SMP-14 | Mn Se | Manganese Selenide | 25.6% | Selenium |
| 84 | SMP-15 | $O_3\ W$ | Krasnogorite | 0.2% | Tungsten |
| 85 | SMP-15 | $N\ Na\ O_3$ | Nitratine | 3.5% | Nitrogen |
| 86 | SMP-15 | $Ge_{0.75}\ Sb_2\ Sn_{0.25}\ Te_4$ | Germanium Tin Antimony Telluride | 0.9% | Germanium |
| 87 | SMP-15 | $Ge_{0.75}\ Sb_2\ Sn_{0.25}\ Te_4$ | Germanium Tin Antimony Telluride | 0.9% | Tin |
| 88 | SMP-15 | $Ge_{0.75}\ Sb_2\ Sn_{0.25}\ Te_4$ | Germanium Tin Antimony Telluride | 0.9% | Tellurium |
| 89 | SMP-15 | $Ge_{0.75}\ Sb_2\ Sn_{0.25}\ Te_4$ | Germanium Tin Antimony Telluride | 0.9% | Antimony |
| 90 | SMP-15 | Cu Se | Klockmannite | 10% | Copper |
| 91 | SMP-15 | Cu Se | Klockmannite | 10% | Selenium |
| 92 | SMP-15 | $Cs\ Cu\ F_6\ Mn$ | *-unidentified* | 1.1% | Caesium |
| 93 | SMP-16 | $Nd\ Rh_2\ Si_2$ | *-unidentified* | 0.4% | Rhodium |
| 94 | SMP-16 | $Hf\ O_3\ Sr$ | *-unidentified* | 0.1% | Hafnium |
| 95 | SMP-16 | $Ca_{1.8}\ F_2\ Ga_{1.28}\ Mg_{4.82}\ Na_{0.46}\ O_{22}\ Si_{7.04}$ | Pargasite | 12.1% | Gallium |
| 96 | SMP-16 | $Bi_2\ O_3$ | Sphaerobismoite | 0.9% | Bismuth |
| 97 | SMP-16 | $Bi_2\ Hf_2\ O_7$ | *-unidentified* | 0.2% | Bismuth |
| 98 | SMP-16 | $Bi_2\ Hf_2\ O_7$ | *-unidentified* | 0.2% | Hafnium |
| 99 | SMP-16 | $Bi\ Li_{2.44}\ Zr_{0.14}$ | *-unidentified* | 0.2% | Bismuth |
| 100 | SMP-16 | $Bi\ Li_{2.44}\ Zr_{0.14}$ | *-unidentified* | 0.2% | Lithium |

| S. No. | Sampling Point | Formula | Compound Name | Proportion of Mineral in Sample | Element of Potential Economic Interest |
|---|---|---|---|---|---|
| 101 | SMP-16 | $Bi\ Li_{2.44}\ Zr_{0.14}$ | *-unidentified* | 0.2% | Zirconium |
| 102 | SMP-16 | $Bi\ La\ O\ Pb\ S_3$ | *-unidentified* | 0.1% | Bismuth |
| 103 | SMP-16 | $Ba\ F_6\ Pd\ Sr$ | *-unidentified* | 0.3% | Palladium |
| 104 | SMP-16 | $Ag_2\ Ho$ | *-unidentified* | 0.2% | Silver |
| 105 | SMP-16 | $Ag_2\ Ho$ | *-unidentified* | 0.2% | Holmium |
| 106 | SMP-17 | Si C | Moissanite 3C | 28.0% | Carbon |
| 107 | SMP-17 | $Mn_{0.5}\ Ni_{0.5}\ O_3\ Ti$ | Pyrophanite | 21.6% | Nickel |
| 108 | SMP-17 | $Mn_{0.3}\ O_3\ Ti\ Zn_{0.7}$ | Ecandrewsite | 16.8% | Zinc |
| 109 | SMP-17 | As | Arsenolamprite | 7.1% | Arsenic |
| 110 | SMP-18 | Sr Te | Strontium Telluride | 0.7% | Tellurium |
| 111 | SMP-19 | $Pb\ Sn\ Te_2$ | Lead Tin Telluride | 1.8% | Lead |
| 112 | SMP-19 | $Pb\ Sn\ Te_2$ | Lead Tin Telluride | 1.8% | Tin |
| 113 | SMP-19 | $Pb\ Sn\ Te_2$ | Lead Tin Telluride | 1.8% | Tellurium |
| 114 | SMP-19 | $F_2\ Mg$ | Sellaite | 30.0% | Fluorine |
| 115 | SMP-19 | $Cu_3\ Sb\ Se_4$ | Permingeatite | 1.0% | Antimony |
| 116 | SMP-19 | $Cu_3\ Sb\ Se_4$ | Permingeatite | 1.0% | Selenium |
| 117 | SMP-19 | $Cs_8\ Sn_{44}$ | Ceasium Stannide | 2.9% | Caesium |
| 118 | SMP-19 | $Cs_8\ Sn_{44}$ | Ceasium Stannide | 2.9% | Tin |
| 119 | SMP-19 | Cd S | Hawleyite | 4.9% | Cadmium |
| 120 | SMP-20 | $O_3\ Sm_2$ | Disamarium Trioxide | 2.2% | Samarium |
| 121 | SMP-20 | $Lu\ Si_{1.8}$ | Lutetium Silicide | 2.6% | Lutetium |
| 122 | SMP-20 | $Fe_{0.11}\ S_{0.99}\ Zn_{0.9}$ | Sphalerite | 7.1% | Zinc |
| 123 | SMP-20 | $Cu_3\ Sb\ Se_4$ | Permingeatite | 1.2% | Antimony |
| 124 | SMP-20 | $Cu_3\ Sb\ Se_4$ | Permingeatite | 1.2% | Selenium |
| 125 | SMP-20 | $Cr_{1.37}\ Se_{0.75}\ Te_{1.25}$ | Chromium Chalcogenide Spinel | 9.1% | Chromium |
| 126 | SMP-20 | $Cr_{1.37}\ Se_{0.75}\ Te_{1.25}$ | Chromium Chalcogenide Spinel | 9.1% | Selenium |
| 127 | SMP-20 | $Cr_{1.37}\ Se_{0.75}\ Te_{1.25}$ | Chromium Chalcogenide Spinel | 9.1% | Tellurium |

| S. No. | Sampling Point | Formula | Compound Name | Proportion of Mineral in Sample | Element of Potential Economic Interest |
|---|---|---|---|---|---|
| 128 | SMP-20 | $Co_{2.5}$ $Cu_{2.5}$ Pr | Cobalt Copper Praseodymium | 7.1% | Cobalt |
| 129 | SMP-20 | $Co_{2.5}$ $Cu_{2.5}$ Pr | Cobalt Copper Praseodymium | 7.1% | Copper |
| 130 | SMP-20 | $Co_{2.5}$ $Cu_{2.5}$ Pr | Cobalt Copper Praseodymium | 7.1% | Praseodymium |
| 131 | SMP-20 | Ba Ca $Cu_3$ La $O_{7.06}$ | Lanthanum Barium Calcium Copper Oxide | 6.0% | Copper |
| 132 | SMP-20 | Ba Ca $Cu_3$ La $O_{7.06}$ | Lanthanum Barium Calcium Copper Oxide | 6.0% | Lanthanum |
| 133 | SMP-20 | Ag Ga $S_2$ | Silver Gallium Sulfide | 18.8% | Silver |
| 134 | SMP-20 | Ag Ga $S_2$ | Silver Gallium Sulfide | 18.8% | Gallium |
| 135 | SMP-21 | Sb $Te_2$ Tl | Thallium Antimony Telluride | 0.5% | Antimony |
| 136 | SMP-21 | Sb $Te_2$ Tl | Thallium Antimony Telluride | 0.5% | Tellurium |
| 137 | SMP-21 | Sb $Te_2$ Tl | Thallium Antimony Telluride | 0.5% | Thallium |
| 138 | SMP-21 | Hg Te | Mercury Tellurium | 1.4% | Mercury |
| 139 | SMP-21 | Hg Te | Mercury Tellurium | 1.4% | Tellurium |
| 140 | SMP-21 | $Ge_6$ Pd $Yb_2$ | Diytterbium Palladium Hexagermanide | 0.3% | Germanium |
| 141 | SMP-21 | $Ge_6$ Pd $Yb_2$ | Diytterbium Palladium Hexagermanide | 0.3% | Palladium |
| 142 | SMP-21 | $Ge_6$ Pd $Yb_2$ | Diytterbium Palladium Hexagermanide | 0.3% | Ytterbium |
| 143 | SMP-21 | Gd Ni | Gadolinium Nickel | 0.2% | Gadolinium |
| 144 | SMP-21 | C $Cd_{0.45}$ $Mg_{0.55}$ $O_3$ | Magnesite | 0.9% | Cadmium |
| 145 | SMP-21 | Be $F_2$ | Beryllium Fluoride | 1.2% | Beryllium |

| S. No. | Sampling Point | Formula | Compound Name | Proportion of Mineral in Sample | Element of Potential Economic Interest |
|---|---|---|---|---|---|
| 146 | SMP-21 | $As_5 Pr_4 Zn_{1.68}$ | Praseodymium Zinc Arsenide | 0.9% | Arsenic |
| 147 | SMP-21 | $As_5 Pr_4 Zn_{1.68}$ | Praseodymium Zinc Arsenide | 0.9% | Praseodymium |
| 148 | SMP-21 | As Cu Se | Copper Arsenide Selenide | 4.9% | Arsenic |
| 149 | SMP-21 | As Cu Se | Copper Arsenide Selenide | 4.9% | Copper |
| 150 | SMP-21 | As Cu Se | Copper Arsenide Selenide | 4.9% | Selenium |
| 151 | SMP-22 | Cl Cu | Nantokite | 2.3% | Copper |
| 152 | SMP-22 | $Bi_{21.68} S_{1.7} Se_{15.3} Te_{6.32}$ | Vihorlatite | 0.5% | Bismuth |
| 153 | SMP-22 | $Bi_{21.68} S_{1.7} Se_{15.3} Te_{6.32}$ | Vihorlatite | 0.5% | Selenium |
| 154 | SMP-22 | $Bi_{21.68} S_{1.7} Se_{15.3} Te_{6.32}$ | Vihorlatite | 0.5% | Tellurium |
| 155 | SMP-22 | $Be_2 Ca O_8 P_2$ | Hurlbutite | 6.9% | Beryllium |
| 156 | SMP-23 | Te | Tellurium | 0.6% | Tellurium |
| 157 | SMP-23 | $Ni_5 Sc$ | Nickel Scandium | 4.4% | Nickel |
| 158 | SMP-23 | $Ni_5 Sc$ | Nickel Scandium | 4.4% | Scandium |
| 159 | SMP-23 | $Ge_{0.5} Sb_2 Sn_{0.5} Te_4$ | Sn-Doped GST Mineral (Germanium Antimony Telluride) | 0.9% | Germanium |
| 160 | SMP-23 | $Ge_{0.5} Sb_2 Sn_{0.5} Te_4$ | Sn-Doped GST Mineral (Germanium Antimony Telluride) | 0.9% | Antimony |
| 161 | SMP-23 | $Ge_{0.5} Sb_2 Sn_{0.5} Te_4$ | Sn-Doped GST Mineral (Germanium Antimony Telluride) | 0.9% | Tin |

| S. No. | Sampling Point | Formula | Compound Name | Proportion of Mineral in Sample | Element of Potential Economic Interest |
|---|---|---|---|---|---|
| 162 | SMP-23 | $Ge_{0.5}$ $Sb_2$ $Sn_{0.5}$ $Te_4$ | Sn-Doped GST Mineral (Germanium Antimony Telluride) | 0.9% | Tellurium |
| 163 | SMP-23 | Eu Ga Sn | --*unidentified* | 0.5% | Europium |
| 164 | SMP-23 | Eu Ga Sn | --*unidentified* | 0.5% | Tin |
| 165 | SMP-23 | $C_2$ $B_2$ Tm | Thulium Boride Carbide | 1.2% | Boron |
| 166 | SMP-23 | $C_2$ $B_2$ Tm | Thulium Boride Carbide | 1.2% | Thulium |
| 167 | SMP-23 | $Bi_{7.68}$ $O_{12.16}$ $Ti_{0.32}$ | Bismuth Titanium Oxide | 2.1% | Bismuth |
| 168 | SMP-23 | $Be_6$ $Fe_8$ $O_{24}$ $S_2$ $Si_6$ | Danalite | 4.9% | Beryllium |
| 169 | SMP-23 | $Ag_3$ $Ba_4$ $Ge_{20}$ | Silver Barium Germanium | 2.0% | Silver |
| 170 | SMP-23 | $Ag_3$ $Ba_4$ $Ge_{20}$ | Silver Barium Germanium | 2.0% | Germanium |
| 171 | SMP-24 | Ag $Fe_{4.8}$ $Ni_{3.2}$ $S_8$ | Argentopentlandite | 1.7% | Silver |